FSTC-HT-23-1041-72
10 August 72

ARMY MATERIEL COMMAND

U.S. ARMY
FOREIGN SCIENCE AND TECHNOLOGY CENTER

HIGH-VELOCITY DEFORMATION AND STRUCTURE OF METALS

by

G. N. Epshteyn and O. A. Kaybyshev

USSR

This document is a rendition of the original foreign text without any analytical or editorial comment.

SI72-57 099

UNCLASSIFIED
Security Classification

DOCUMENT CONTROL DATA - R & D

(Security classification of title, body of abstract and indexing annotation must be entered when the overall report is classified)

1. ORIGINATING ACTIVITY (Corporate author) Foreign Science and Technology Center US Army Materiel Command Department of the Army	2a. REPORT SECURITY CLASSIFICATION Unclassified 2b. GROUP

3. REPORT TITLE

High-velocity Deformation and Structure of Metals

4. DESCRIPTIVE NOTES (Type of report and inclusive dates)

Translation

5. AUTHOR(S) (First name, middle initial, last name)

G. N. Epshteyn and O. A. Kaybyshev

6. REPORT DATE	7a. TOTAL NO. OF PAGES	7b. NO. OF REFS
10 August 72	231	N/A

8a. CONTRACT OR GRANT NO. b. PROJECT NO. c. T702301 2301 d. Requester AMXST-SD Mr. Ely	9a. ORIGINATOR'S REPORT NUMBER(S) FSTC-HT-23- 1041-72 9b. OTHER REPORT NO(S) (Any other numbers that may be assigned this report) ACSI K-1583

10. DISTRIBUTION STATEMENT

Approved for public release; distribution unlimited.

11. SUPPLEMENTARY NOTES	12. SPONSORING MILITARY ACTIVITY
	US Army Foreign Science and Technology Center

13. ABSTRACT

This book describes modern methods for the high-velocity deformation of metals and alloys and examines the characteristics of the deformation mechanism under a pulsed load application, as well as the structural characteristics of strengthening by deformation. The book is intended for metal research engineers and scientists concerned with the field of plastic deformation of metals. It may also be useful to students preparing for work in the field of "Physics of Metals". 128 figures, 32 tables, and 273 bibliographic entries.

DD FORM 1473 (1 NOV 68) REPLACES DD FORM 1473, 1 JAN 64, WHICH IS OBSOLETE FOR ARMY USE

UNCLASSIFIED
Security Classification

14. KEY WORDS	LINK A		LINK B		LINK C	
	ROLE	WT	ROLE	WT	ROLE	WT
Metal Deformation						
Physical Metallurgy						
Plastic Deformation						
Shock Wave						
High Strength Alloy						
Metallography						
Solid Mechanical Property						
Shock Wave Interaction						
Shock Wave Velocity						
Detonation						
Magnetic Pulse Deformation						
Twinning						
Crystallography						
Phase Tra. sition						
COSATI Subject Code:						
COUNTRY CODE:						

TECHNICAL TRANSLATION

FSTC-HT-23- 1041-72

ENGLISH TITLE: High-velocity Deformation and Structure of Metals

FOREIGN TITLE: Vysokoskorostnaya Deformatsiya i Struktura Metallov

AUTHOR: G. N. Epshteyn and O. A. Kaybyshev

SOURCE: Moscow, Metallurgiya Publishing House, 1971

This translation was accomplished from a xerox manuscript. The graphics were not reproducible. An attempt to obtain the original graphics yielded negative results. Thus, this document was published as is, in order to make it available on a timely basis.

Translated for FSTC by ACSI K-1583

NOTICE

GRAPHICS NOT REPRODUCIBLE

UDC 539.374

HIGH-VELOCITY DEFORMATION AND STRUCTURE OF METALS

[Complete translation of Russian-language book by G.N. Eshtein and O.A. Kaybyshev: Vysokoskorostnaya Deformatsiya i Struktura Metallov, Moscow, Metallurgiya Publishing House, 1971, signed to press 28 September 1970, 199 pp]

CONTENTS

	PAGE
ANNOTATION	1
FOREWORD	2
CHAPTER 1. MODERN METHODS OF HIGH-VELOCITY DEFORMATION	6
1. Interaction of Shock Waves With Metals	6
2. Deformation by Explosion Through a Transmitting Medium	14
3. Pulsed Deformation Using Magnetic Field Energy	22
4. Electrohydraulic Deformation	27
5. Pulsed Deformation at Superhigh Pressures	28
CHAPTER 2. GLIDING UNDER CONDITIONS OF HIGH-VELOCITY DEFORMATION	31
1. Characteristics of the Behavior of Crystal Lattice Defects During Pulsed Loading	31
2. Methods of Studying Glide in Metals	48
3. Geometry of Glide	57
4. Critical Displacement Stress	66
5. Experimental Study of Gliding	71
6. Boundary Glide	92

CONTENTS PAGE

CHAPTER 3. TWINNING UNDER CONDITIONS OF HIGH-VELOCITY DEFORMATION---------- 105

1. Crystallography and Dislocation Twinning Models- 105
2. Deformation by Twinning---------- 118

CHAPTER 4. STRENGTHENING OF METALS BY HIGH-VELOCITY DEFORMATION---------- 152

1. Basic Concepts of the Strengthening Mechanism--- 152
2. Strength Properties of Metals---------- 163
3. Plastic Properties of Metals---------- 198

CHAPTER 5. HIGH-VELOCITY DEFORMATION AND PHASE TRANSITIONS IN METALS---------- 202

BIBLIOGRAPHY---------- 214

ANNOTATION

This book describes modern methods for the high-velocity deformation of metals and alloys and examines the characteristics of the deformation mechanism under a pulsed load application, as well as the structural characteristics of strengthening by deformation. The book is intended for metal research engineers and scientists concerned with the field of plastic deformation of metals. It may also be useful to students preparing for work in the field of "Physics of Metals". 128 figures, 32 tables, and 273 bibliographic entries.

FOREWORD

High-velocity deformation of metals occupies a very important place in contemporary progressive technological processes. The first patents on explosive deformation were obtained more than seventy years ago, but it has only been for the past ten to fifteen years that the number of products manufactured and treated by the methods of high-velocity deformation has grown sharply.

Technologists, who are primarily interested in practical utilization of the process, very quickly became convinced of the perceivable successes to be attained by using the various types of pulsed operation for the treatment of metals. The punching of large-scale parts from high-strength alloys, the creation of new composite materials, the strengthening of large parts of complex shape, and many other complex and important operations became possible as a result of using the energy from high-pressure shock waves.

Unfortunately, solution to the essentially important problems in metallography, involving study of the mechanism of high-velocity deformation and the properties of metals, obtained as a result of the effect from shock waves, is still not sufficiently developed to permit introduction of these methods into industrial use.

The major problem obviously involves whether it is possible to combine a favorable technological process with the production of optimal properties. To solve this particular problem it is first of all necessary to know the mechanism of high-velocity deformation. It is important to study the possibility of combining high-velocity deformation with other methods used for the strengthening of metals, since it is these complex methods of treatment primarily that permit assurance of the best results. Finally it is important to limit the region in which the use of high-velocity treatment methods is rational.

The attitude of researchers and practical workers to the metallographic aspects of high-velocity deformation has not been constant even for the brief period of time in which this comparatively young branch of science has developed. The first forecasts pertaining to the possibility of obtaining the best properties by shock loading sounded optimistic. It seemed that the difference in the structure produced, and in particular, in the deformation strengthening in comparison with quasi-static deformation would be quite large and could be detected with the "naked eye". However these forecasts were not justified and the first results were found to be more than modest. And, as often happens, in place of the unjustified optimism a certain disappointment came to pass. But at the same time these disappointments stimulated more profound research, as a result of which many interesting and important characteristics were discovered for the behavior of metals during high-velocity deformation, both in the practical and in the theoretical sense.

At the present time investigations involving high-velocity deformation are being conducted in many directions. Almost all metals and alloys of practical interest have been tested under conditions of high-velocity loading. It is true that these results do not always find the necessary explanation. The data obtained have been successfully generalized to an even lesser degree. Without pretending by any means to an exhaustive list of the various directions, we assume that the major ones may be those shown on the diagram given in the FOREWORD.

Each of the questions outlined on the diagram undoubtedly contain several independent significant problems. For example, study of gliding during high-velocity deformation must answer questions concerning change in the number of effective glide systems, the possibility of non-octahedral gliding under the effect of high-pressure shock waves in face-centered cubic crystals, etcetera.

It is also impossible to examine the various sides of the behavior of metals during high-velocity deformation independently. The mechanical properties, produced in components after high-velocity deformation, are determined by the forming microstructure which in turn depends on the deformation mechanism.

This book does not even encompass all those questions shown on the diagram. The main emphasis is on examination of the deformation mechanism and strengthening, formation of the structure of metals, and the mechanical properties under conditions of high-velocity loading (Chapters 2 - 4). Several related questions to a greater or lesser degree have found reflec-

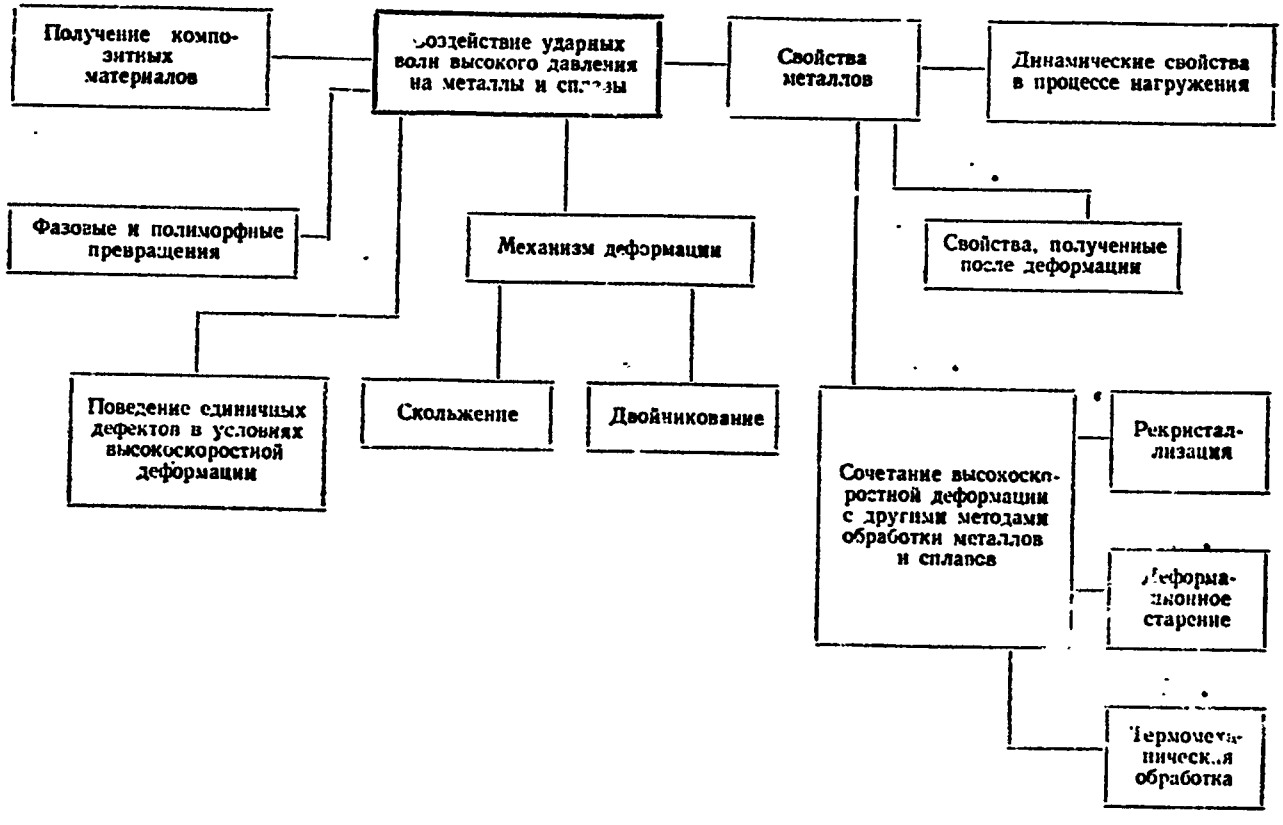

1. Production of composite materials
2. Effect of high-pressure shock waves on metals and alloys
3. Properties of metals
4. Dynamic properties in the loading process
5. Phase and polymorphous transitions
6. Deformation mechanism
7. Properties obtained after deformation
8. Behavior of individual defects under conditions of high-velocity deformation
9. Gliding
10. Twinning
11. Combination of high-velocity deformation with other methods of treating metals and alloys
12. Recrystallization
13. Deformation aging
14. Thermomechanical treatment

tion on the pages of this book. Chapter 5 is concerned with the phase transition under conditions of high-velocity deformation.

The metallographic aspect predominates in Chapters 2-5. These chapters are preceded by Chapter 1 where a description is given of several methods for high-velocity deformation. This description does not entirely encompass the technological side of the processes but gives some idea to the reader of those parameters that influence the properties of the treated materials.

Sections 2-6 in Chapter 2 and Chapter 5 were written by O.A. Kaybyshev, the remainder of the book was written by G.N. Epshteyn.

The authors wish to express their appreciation to Professor Doctor of Technical Sciences M.L. Bernshteyn, Candidate of Technical Sciences R.L. Novobratskiy, Professor Doctor of Technical Sciences V.M. Rozenberg, Professor Doctor of Technical Sciences Yu.A. Skakov, and to the reviewer Professor Doctor of Technical Sciences V.N. Finkel' for his useful comments, which he made in discussing the manuscript.

CHAPTER 1

MODERN METHODS OF HIGH-VELOCITY DEFORMATION

In this chapter we examine a limited number of questions involved with the methods of high-velocity deformation. As concerns the problems discussed in this book, these are first of all the parameters that determine the structure of the metal in the process of high-velocity loading: the deformation rate, the amount of pressure developed, and the temperature of the most widely-used processes.

It is fully possible that such an approach may be objected to since the quite complex interaction of shock waves with metals is of course not exhausted by these characteristics. However the greatest amount of experimental material on the influence of a pulsed load on the structure and properties of metals has been compiled mainly with respect to these parameters.

1. Interaction of Shock Waves With Metals

No matter what means is employed for formation of the high-pressure front (detonation of explosives in contact with the deformed material or separated by some medium, by collision of the sample with a rapidly flying object, by a short magnetic pulse or by pulsed discharge of a battery array), certain general premises allow us to place all methods of high-velocity deformation into a single series, where the difference of one method from another will only be a quantitative one.

High-velocity (or as it is often called, pulsed) deformation is a result of the extremely rapid propagation of a pressure front, the amplitude of which may exceed the yield stress of the material by tens and even hundreds of times. Since the individual displacements (deformation) in the solid state are assumed to be small, we then speak of the propagation

of elastic oscillations or waves in a solid [1]. In investigating the state of metals and alloys acted on by shock waves with a pressure up to hundreds of kilobars, as the basic parameters that characterize the state of the thermodynamic equilibrium, we take the pressure P, the change in volume ΔV, and the change in intrinsic energy ΔE. But since the expanse of the pressure front is very small, it is necessary that the thermodynamic equilibrium be established for a time of about 10^{-7} to 10^{-6} seconds, this being determined by the processes taking place in a compressed sample. However, we can never state that this time in all cases is sufficient for establishment of equilibrium, and this then leads to a disruption in the usually accepted relationships between these quantities.

The second assumption is that the compression acted on by a shock wave, with a pressure P_{max}, will be the same as under hydrostatic stress of the same magnitude. This condition can not be satisfied with sufficient accuracy since first of all the relaxation processes also take place in time and furthermore, under the influence of hydrostatic stress, the stressed state is near the hydrostatic stress, and under the influence of the shock wave it may differ greatly from the hydrostatic stress and even correspond to uniaxial stress.

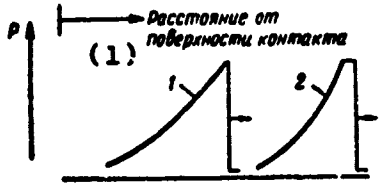

Figure 1. Pressure distribution during the direct contact of an explosive with a metal 1 and during the collision of metal with a flying plate 2. The arrows show the direction of movement of the shock wave front.

1. Distance from contact surface

From Figure 1 it is clear that the front of the shock wave is terminated very abruptly. The metal placed before this front is still found in the original state, and the metal located behind the line of pressure termination undergoes stress at pressure P. The amplitude of the shock wave varies with time. If at some moment of time t_1 (Figure 2) at a given point the pressure reaches P_{max}, then at the moment t_2 it drops to P following the law

$$P_t = P_{max} e^{-t/\theta}, \qquad (1)$$

where P_t is the pressure through the time interval t after reaching P_{max}; P_{max} is the maximal peak pressure at a given distance from the site of the explosion; θ is a time constant that depends on type and mass of the charge, as well as on its placement.

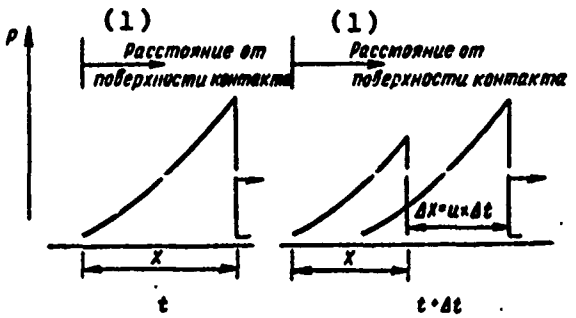

Figure 2. Amount of pressure at point x at moment of time t, corresponding to maximal amplitude, and at moment t+ t. The wave front shifted by $\Delta x = u \times \Delta t$.

1. Distance from contact surface

The intensity in pressure drop, i.e., the difference between P_{max} and P_t after some predetermined time interval t, will depend on the value of θ.

The effect of an elastic wave may in fact be treated as the propagation of two independent waves. In one of them the displacement of particles of the material is directed along the propagation of the wave itself. Such a wave is called longitudinal and is propagated at a velocity of c_1. This wave involves change in volume, which takes place during the interaction between metal and shock waves. Here the normal stress along the shock wave will be:

$$\sigma = \rho c_1 u, \qquad (2)$$

where ρ is the density of the material; u is the displacement rate of the particles of the material acted on by the shock wave.

The second wave is a transverse one. The displacement here lies in the plane perpendicular to the direction of propagation of this wave, and the rate of its propagation c_t is approximately two to three times smaller than c_ℓ. Travel of the transverse waves leads to the formation of tangential stresses γ, producing a relative shift in the individual masses of the metal:

$$\tau \quad \rho c_t u. \tag{3}$$

The methods of high-velocity deformation are actually distinguished by the velocity u which they impart to the particles of the metal. Table 1 shows the values of the tangential and normal stresses for different metals at a 1 m/sec displacement rate of the particles.

Table 1. Stresses Arising in Different Metals at a Particle Displacement Rate of 1 m/sec

(1) Материал	(7) σ, Мн/м² (кГ/мм²)	(8) τ, Мн/м² (кГ/мм²)	(1) Материал	σ, (7) Мн/м² (кГ/мм²)	τ, (8) Мн/м² (кГ/мм²)
(2) Алюминий	17,1 (1,74)	9,3 (0,95)	(5) Свинец	24,4 (2,49)	8,8 (0,9)
(3) Латунь	36,4 (3,71)	17,2 (1,76)	Сталь	45,1 (4,6)	24,2 (2,47)
(4) Медь	40,4 (4,12)	20,0 (2,04)	(6)		

1. Material
2. Aluminum
3. Brass
4. Copper
5. Lead
6. Steel
7. σ, $Mn/m^2 (kpf/mm^2)$
8. τ, $Mn/m^2 (kpf/mm^2)$

The travel rate of the shock wave front U and the particle displacement rate u differ significantly from one another. The state of the metal before the shock wave front is characterized by the pressure P_0 and the specific volume v_0, but directly behind the front this will be P and v, respectively.

Change in the state of the metal in the process of the shock wave influence on it may be characterized by the curve in the coordinates P-v (Figure 3). Each of the points on the curve 0A characterizes the state of the metal for some value of U and u. For a uniform material, not undergoing transitions associated with change in the specific volume, the curve has a continuous character. If phase transitions take place in the metal in the pressure range up to P_{max} then the

curve has a break, but within the state of each phase it is continuous.

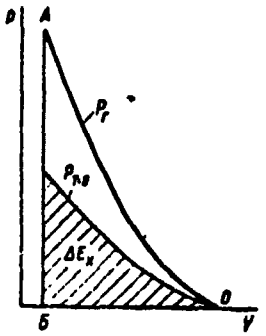

Figure 3. P-V-diagram of shock stress: P_H is the impact adiabatic curve of Hugoniot; $P_{T=0}$ is the curve of "cold" contraction at $T = 0^\circ$ K.

Table 2. Evaluation of Temperature Produced by a Shock Wave in the Deformation of Various Metals [3]

Давление, кбар (1)	Металл (2)	Относительное изменение объема v/v_0 (3)	t_n, °C (7)
100	(4) Свинец	0,865	231
	(5) Медь	0,940	61
	(6) Вольфрам	0,970	35
200	(4) Свинец	0,796	628
	(5) Медь	0,897	118
	(6) Вольфрам	0,944	56
500	(4) Свинец	0,693	2450
	(5) Медь	0,814	446
	(6) Вольфрам	0,882	199
1000	(4) Свинец	0,619	8990
	(5) Медь	0,737	1480
	(6) Вольфрам	0,812	761

1. Pressure, kbar
2. Metal
3. Relative change in volume, v/v_0
4. Lead
5. Copper
6. Tungsten
7. t_n, °C

The total increase in intrinsic energy E during the process is characterized by the region bounded by the curve OA [2]. Part of this energy ΔE_x, bounded by the curve of

cold contraction $P_{T=0}(v)$, is the elastic component and is not associated with the change in temperature of the metal. The difference $\Delta E-\Delta E_x$ characterizes the heat energy of the process and is expended in heating the metal under conditions of adiabatic contraction. The amount of this energy grows strongly with increase in P_{max}, thus making it difficult to compare temperature conditions of the various processes which differ by the amount of the maximally attainable pressure. But even at one and the same pressure, the temperature of the process will depend on the metal found under conditions of adiabatic contraction. Table 2 shows values of the temperature developing in various metals under conditions of adiabatic contraction acted on by a shock wave. The temperature was computed from the Hugionot curve [3]. A pressure of 100-200 kbar, which has a catastrophic effect on lead, produces completely moderate heating of tungsten and copper. However, for the structural investigations it is almost always not the temperature t_n, found by computation, that is the more significant one and is retained in the metal for a period of several microseconds, but rather it is the temperature of the metal t_0 directly after unloading at atmospheric pressure. The difference between these temperatures is quite substantial, especially at a pressure greater than 100-200 kbar (Table 3). This temperature may exert a great influence on the structure of the metal. According to the data of the authors in reference [3], a sample of iron after impact at a pressure of 750 kbar cools to room temperature in about five minutes.

Table 3. Temperature of Iron Under Conditions of Adiabatic Contraction (t_n) and After Unloading (t_0) [3]

Давление, кбар (1)	$t_н$, °C (2)	t_0, °C	Давление, кбар (1)	$t_н$, °C (2)	t_0, °C
130	60	30	500	550	250
350	350	150	750	1050	400

1. Pressure, kbar; 2. t_n, °C

According to Karman and Taylor there must be a critical rate of impact U_{cr}, by the attainment of which the contact surface receiving the impact is fractured:

$$U_{cr}=\int_0^{\varepsilon_m}\sqrt{\frac{d\sigma/d\varepsilon}{\rho}}\,d\varepsilon, \qquad (4)$$

where ε is the degree of instantaneous deformation; ε_m is the degree of deformation corresponding to the yield stress; $d\sigma/d\varepsilon$ is the slope of the curve σ-ε under static tension.

If we substitute the value U_{cr} into formula (2), we can then determine the amount of normal pressure of the shock wave at which surface fracturing or partial cracking of the body receiving the shock must take place at a velocity greater than or equal to U_{cr}.

To evaluate the deformation velocity we usually employ either the absolute rate of movement of the sample v or the relative deformation velocity $\dot{\varepsilon}$, which additionally depends on the length or thickness of the sample in the direction of the effective force. This characteristic has great significance not only for comparing the properties obtained by different methods of deformation and differing in velocity by several orders of magnitude, but also for standard mechanical tests.

The concept of deformation velocity is easiest to introduce after looking at uniaxial tension. The linear deformation velocity $\dot{e}$ is defined as

$$\dot{e}=\frac{de}{dt}=\frac{d(l-l_0)}{dt}=\frac{1}{l_0}\cdot\frac{dl}{dt}=\frac{v}{l_0}, \qquad (5)$$

where l_0 is the initial length of the stretched sample; l is the length of the sample after the time t, v is the rate of movement of the sample determined by the tension at the displacement velocity of the test machine clamps.

This equation is valid only as long as no local deformation develops during stretching, that is, as long as no neck is formed. If we evaluate the true amount of deformation in this case, the relative deformation rate will be:

$$\dot{\varepsilon}=\frac{de}{dt}=\frac{d\ln(l/l_0)}{dt}=\frac{1}{l}\cdot\frac{dl}{dt}=\frac{v}{l}. \qquad (6)$$

To retain the constant true relative deformation velocity when the displacement velocity is increased, it is necessary to increase the length of the sample.

The relationship between the relative true and the linear deformation velocities can be found from the two previous equations:

$$\dot{\varepsilon} = \frac{v}{l} = \frac{l_0}{l} \cdot \frac{dl}{dt} = \frac{1}{1+e} \cdot \frac{de}{dt} = \frac{\dot{e}}{1+e}.$$

In analogy with equation (6), for contraction the relative deformation velocity will be

$$\dot{\varepsilon} = \frac{1}{h} \cdot \frac{dh}{dt} = \frac{v}{h} \quad \text{sec}^{-1}, \qquad (7)$$

where h is the amount of the displacement; for thin sheets of billets it is commensurate with the thickness; for thick ones it corresponds to the layer of the shock wave effect.

The quantity $\dot{\varepsilon}$ is convenient to use for studying pulsed deformation. However it can be reliably determined only if the deformation diagram and the direction of the deforming stress is known and if it is possible to estimate h.

Many papers have mentioned the dependence of yield stress and other strength characteristics on velocity, which has made it necessary to establish the conditions for measuring them during static, or more precisely, quasi-static tests. In the standard quasi-static tests it has been assumed that the rate of movement of a sample, or the displacement rate of the clamps must not exceed 4 mm/min.

However, such a formal approach is inapplicable for distinguishing dynamic deformation from quasi-static.

Chapter 4 will show that the deformation velocity at which the yield stress is sharply increased, and which is different for the various materials and even for one and the same material, depends on its microstructure. So this is the threshold of deformation above which a sharp increase begins in the yield stress of a given material and serves as the boundary between the quasi-static and dynamic deformations.

Table 4 gives the deformation velocities during different loading procedures. In the traditional methods of treating metals with pressure such as the drawing of a wire, and the rolling of thin sheets, the relative deformation velocity may reach about 10^2 to 10^4 sec^{-1}. But these methods differ from the high-velocity deformation in that the high deformation velocity here is reached by localizing the deformation in a small volume, and not by increasing the velocity of sample

displacement. Here such processes as rolling and drawing should be treated as stable or quasi-static processes, whereas in a pulsed treatment we are concerned with the propagation of a stress wave over the volume.

Table 4. Typical Deformation Rates for Various Processes of Treating Metals

(1) Процесс	Абсолютная скорость деформации v, м/сек (10)	Порядок величины l, м (11)	Относительная скорость деформации $\dot{\varepsilon}$, $сек^{-1}$ (12)
(2) Испытание на растяжение	0,00001—0,01	0,03	$3 \cdot 10^{-4}$—$3 \cdot 10^{-1}$
(3) Протяжка труб	0,05—0,5	0,01	5—50
(4) Глубокая вытяжка листа	0,05—1	0,01	5—100
(5) Листовая прокатка . .	0,25—25	0,001	250—25 000
(6) Ковка на молотах . . .	2,5—10	0,1	25—100
(7) Испытание на копре . .	6	0,01	$6 \cdot 10^2$
(8) Протяжка тонкой проволоки	5—40	0,0001	$5 \cdot 10^4$—$4 \cdot 10^5$
(9) Импульсная деформация	30—150	0,001	$3 \cdot 10^4$—$1{,}5 \cdot 10^5$

1. Process
2. Tensile test
3. Drawing of pipes
4. Deep-seated drawing of a sheet
5. Sheet rolling
6. Hammer forging
7. Ram impact machine test
8. Drawing of a fine wire
9. Pulsed deformation
10. Absolute deformation velocity v, m/sec
11. Order of magnitude of ℓ, m
12. Relative deformation velocity $\dot{\varepsilon}$, sec^{-1}

Of the other factors associated with the formation of a structure in the process of high-velocity deformation, we should mention the directionality of the shock wave with respect to the surface of the sample. Ferbrak showed that the structure of iron will depend on whether it was formed under the effect of a plane incident wave or under the effect of an unloading wave. The influence of directionality and structure of the shock wave has been studied in greater detail in the book by Pashkov and Gelunova [4].

2. Deformation by Explosion Through a Transmitting Medium

The first patents on using explosives for the deformation of metals were issued in England and in the USA in 1897 and 1901. However, only several decades later when the problems of utilizing high-strength low-plastic materials were posed to machine builders did this method receive broad recognition. By increasing the strength of the charge its possibilities are practically unlimited, this being especially

important for punching large-scale finished parts. For example, the Japanese firm Japan Steel Works [5] prepared spherical gas containers, 1.6 m in diameter, from a 1.58-mm thick steel having a yield stress of 500-600 Mn/m^2(50-60 kgf/mm^2).

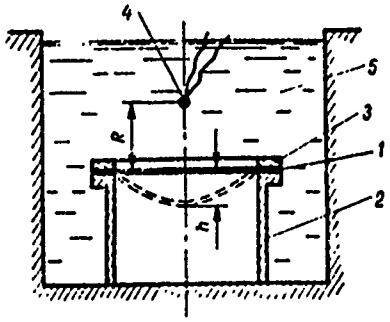

Figure 4. Diagram of explosive deformation of a sheet billet through a transmitting medium.

Explosive deformation and several metallographic aspects of this process have been described in detail in a monograph by Reichardt and Pierson [6]. One of the diagrams of explosive deformation is shown on Figure 4. The sheet billet 1 is placed between the matrices 2 with a spring 3. During explosion of the charge 4, having a mass G and placed above the billet at a height R, a detonation wave is first formed that is propagated over the volume of the charge at a velocity from 3000 to 7000 m/sec depending on the type of explosive used. This velocity determines the amount of the peak pressure. At the moment the detonation wave enters the charge-water boundary, i.e., at that moment when all the charge in transformed into gas, being under a high pressure, an operational (shock) wave forms that is transmitted through the medium filling the reservoir 5, toward the billet. The rate of propagation of the shock wave in the liquid is significantly greater than the rate of motion of a compressed gas. This rate is in fact determined by the rate of propagation of sound in the liquid, i.e., by the rate at which any abrupt change in pressure is transmitted from one part of the liquid to another. The rate of propagation of sound in water (this medium is most often used for explosive deformation) is 1460 m/sec.

If no special measures are taken (setting up a shaping matrix), then following the explosion the component has the shape of a bowl with the bending magnitude h.

Table 5. Parameters of the Explosive Deformation Modes

Номер режима (1)	G, г (2)	R, мм	Величина импульса, 10^5 н·сек/м² (кГ·сек/см²) (3)	P_{max}, кбар (4)
		Сталь с 0,28% С (5)		
1	5,0	36,5	0,0040	3,0
2	10,0	60,0	0,0040	2,4
3	13,2	67,6	0,0041	2,2
4	15,0	80,0	0,0040	1,9
5	20,0	95,0	0,0041	1,8
6	25,0	111,0	0,0041	1,6
		Сплав ОТ-4 (6)		
1	5,0	46,8	0,0032	2,4
2	13,2	95,0	0,0031	1,5
3	15,0	102,0	0,0032	1,4
4	20,0	124,0	0,0034	1,4
5	25,0	146,0	0,0032	1,2

1. Mode number
2. G, g
3. Magnitude of pulse, 10^5 n.sec/m^2(kgf.sec/cm^2)
4. P_{max}, kbar
5. Steel with 0.28% C
6. OT-4 alloy

In studying the explosive method of deformation we should distinguish the two groups of parameters of the process. The first group includes the technological parameters associated with dimensions and shape of the component, required depth of drawing, and number of successive transitions; here the type and mass of the explosive, the height of the placement of the charge above the billet, the transmitting medium, the size of the container, etcetera, are all varied. However, of themselves the parameters do not influence the deformation mechanism and the character of the strengthening. In reference [7] the deformation of sheet billets was done with various groups of placement and mass of the charge, but chosen such that the magnitude of the pulse and the pressure had practically identical values (Table 5). Testing of samples, cut from deformed components, showed that by retaining the magnitude of the pulse and the peak pressure the mechanical properties are found to be at a single level (Table 6). Only zonal stresses, measured in the center of the half-sphere, drop with increase in the height of the charge placement (Figure 5). The influence of the technological parameters on the results of explosive deformation has been studied in detail in special papers [8-10].

Table 6. Mechanical Properties of a Metal After Deformation

Номер режима (1)	$\sigma_{0,2}$, (2) Мн/м² (кГ/мм²)	σ_b, (3) Мн/м² (кГ/мм²)	δ, %
Сталь с 0,28% С (4)			
1	698 (71,3)	748 (76,3)	9,4
2	698 (71,3)	764 (78,0)	10,1
3	704 (71,8)	787 (80,4)	9,6
4	715 (73,0)	776 (79,2)	9,8
5	732 (74,7)	789 (80,5)	8,7
6	710 (72,5)	781 (79,8)	10,0
Сплав ОТ-4 (5)			
1	810 (82,6)	932 (95,3)	7,6
2	765 (78,0)	831 (84,8)	8,0
3	773 (78,9)	900 (91,9)	7,2
4	819 (83,6)	891 (91,0)	6,4
5	735 (75,0)	825 (84,3)	8,0

1. Mode number
2. $\sigma_{0.2}$, Mn/m^2(kgf/mm^2)
3. σ_b, Mn/m^2(kgf/mm^2)
4. Steel with 0.28% C
5. OT-4 alloy

The second group of parameters which permit evaluating the physical characteristics of the process include the amount of pressure (or pulse) of the shock wave, the deformation velocity (duration of the process), and the temperature. Change in the pressure in time is described by equation (1), which is valid only in the initial period, until $P \gg 0.3\ P_{max}$ [10]. In turn, the peak pressure along the shock wave front during detonation of the explosive can be determined from the formula

$$P_{max} = K\left(\frac{G^{1/3}}{R}\right)^{\alpha} \qquad (8)$$

where G is the mass of the charge, kg; R is the distance from the center of the charge to the point where the pressure is measured (in this case the height of placing the charge above the billet), m; K, α are coefficients which depend on the properties of the explosive and the transmitting medium; with the detonation of TNT in water, K = 533, and α = 1/3.

Small charges with a mass of several tens of grams create a pressure along the shock wave front of several kilobars, and powerful charges with a mass up to 3 kg create a pressure up to about 50 kbar.

During detonation, in addition to the basic shock wave, secondary and reflected waves arise, however the magnitude of their pressure does not exceed $(0.1\text{-}0.2)P_{max}$ [9].

Experimental measurements showed that the rate of displacement of the billet during detonation is 200-300 m/sec [11]. If the sheet billet has a thickness of 1 mm, then the relative rate of deformation $\dot{\varepsilon} = (2\text{-}3)\cdot 10^5$ sec^{-1}. The rate of propagation of the high-pressure front here is near the speed of sound.

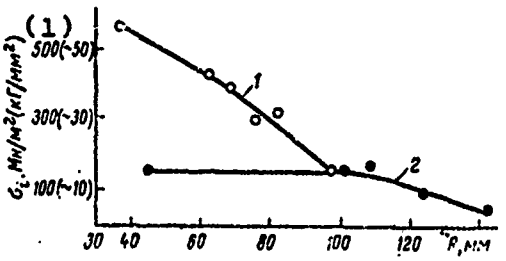

Figure 5. Change in zoneal stresses ($_i$) in medium-carbon steel (1) and the OT-4 alloy (2) as a function of height of placing the charge with a constant pulse magnitude.

1. σ_i, Mn/m^2(kgf/mm^2)

The greatest complexity is represented by evaluating the temperature during explosive deformation. This is explained on the one hand by the purely experimental problems and on the other by the sharp dependence of temperature on deformation mode, which makes it practically impossible to "evaluate the temperature by analogy". Several methods of determining the temperature have been described in the review article [12]. As a rule the experimental and computational methods permit only indirectly establishing the temperature region for the deformation. In reference [10] the temperature of the sample under a dynamic load at a deformation velocity of about 10 sec^{-1} was measured by a low-inertia thermocouple. In deforming the sample, prior to fracture the temperature was raised to 100° C.

Below we shall attempt to evaluate the temperature of a sample during hydroexplosive loading, based on the following premises.

The sources for elevating the temperature may be:

(1) Plastic deformation of the metal;

(2) The effect of high pressure on the metal and the change in volume associated with it;

(3) Heating under the effect of light radiation;

(4) The direct interaction of combustion products with the billet.

The interaction of combustion products and light radiation can not have independent significance during explosive deformation. We can judge as to the influence of high pressure on the basis of reference [2] in which contact detonation was carried out on nickel. It was shown that at a pressure of 100 kbar, when the relative change in volume was 0.954, the temperature did not exceed 321° K. But with further increase in pressure up to 500 and 1000 kbar, the temperature grew, respectively, up to 550 and 1100° K. Consequently, with explosive deformation through a transmitting medium where the pressure comprises a maximum of tens of kilobars, this source of heat also can not be attributed to the elevation in temperature that is essential for structural changes. Then there remains only to evaluate the increase in temperature associated with the plastic deformation itself of the metal.

Eliminating such extraneous factors as heating of the water, scattering of the energy flux (which may only lower the temperature of the billet), we assume that the energy flux of the detonation pulse through unit of surface, arranged normal to the direction of wave propagation, will be equal to:

$$E = E_d + E_Q, \tag{9}$$

where E_d is the energy required for deformation of the component; E_Q is the energy going into heating of the billet.

In reference [10] it was given that E is equal to:

$$E = cG^{1/3}\left(\frac{G^{1/3}}{R}\right)^{\gamma}, \tag{10}$$

where c and γ are constants; for TNT they are equal, respectively, to 0.843 and 2.05.

The energy flux of the detonation pulse per unit of surface is expressed as

$$E = 2\frac{G}{R^2}. \tag{11}$$

The energy of deformation during the drawing of a sheet billet with rigidly restrained flanges will be

$$E_d = \frac{2,4B}{1+\alpha}\left[4/3\left(\frac{h}{r_0}\right)^2\right]^{1+\alpha}\delta, \tag{12}$$

where h is the maximal bending (see Figure 4); δ is the thickness of the sheet; r_0 is the radius of the billet; B and α are coefficients which depend on the material; for low-carbon steel they are equal, respectively, to 590 Mn/m^2 (about 59 kgf/mm^2) and 0.23 [9].

From formulas (9), (11), and (12) we find that the energy going into heating of the component is equal to

$$E_Q = 2\frac{G}{R^2} - \frac{2,4B}{1+\alpha}\left[4/3\left(\frac{h}{r_0}\right)^2\right]^{1+\alpha}\cdot\delta. \tag{13}$$

Assuming the specific heat of the material to be constant in the temperature range ΔT, we have

$$E_Q = m\cdot\bar{c}\cdot\Delta T,$$

where $\bar{c}$ is the mean specific heat of the material; m is the mass of the billet.

Then the elevation in temperature will be

$$\Delta T = \frac{2\frac{G}{R} - \frac{2,4B}{1+\alpha}\left[4/3\left(\frac{h}{r_0}\right)^2\right]^{1+\alpha}\cdot\delta}{m\cdot\bar{c}}. \tag{14}$$

Assuming the conditions of detonation punching for the billet of low-carbon steel type St 3, with a thickness of 0.3 cm, for which G = 20 g, R = 0.04, and h/r_0 = 0.4, we find that the temperature is increased by no more than 100 degrees.

Furthermore, the evaluation of increase in temperature of the billet during detonation was proven experimentally. By electrodeposition we coated a 10-15 μm thick film of low-melting metals -- zinc and tin -- on the surface of the component, and made fine rectangular lines on the films. After detonating a 50-g charge in the water container at a distance

of 30 mm from the billet, on none of the components were there found traces of fusion either in the structure nor on the edges of the lines.

Radiograms taken from the deformed samples (Figure 6) showed that recrystallization occured only in the film of tin. The temperature of recrystallization for tin was equal approximately to 20° C, and for zinc -- approximately 40° C.

Thus we can assume that under the conditions of detonation punching through a transmitting medium using charges whose mass does not exceed several tens of grams, the temperature is not raised to values that would influence the state of the structure. It is probable however that for contact detonation such a conclusion would be incorrect.

The sequence of displacement of the individual segments of the component was studied by Gouforz [13] (Figure 7) under the pulsed effect of a shock wave. At the initial moment a deformation takes place of the peripheral segments, located near the edges of the matrix and the clamp. On these segments the diagram of the deformation is quite complex -- it involves bending, the effect of the clamped end, and other factors. But in the central deformation zone a biaxial tension takes place.

In the general case the magnitude of the deformation at any point is determined from the formula

$$\varepsilon_i = \frac{\sqrt{2}}{3}\sqrt{(\varepsilon_1-\varepsilon_2)^2+(\varepsilon_1-\varepsilon_3)^2+(\varepsilon_2-\varepsilon_3)^2}, \qquad (15)$$

where ε_1, ε_2, and ε_3 are the displacements along the three mutually perpendicular directions.

Under biaxial tension $\varepsilon_1 = \varepsilon_2$. Expanding formula (15) under this condition we find that $\varepsilon_i = \varepsilon_3$, i.e., we can judge as to the degree of deformation of the half-sphere made of sheet billet by using a shock wave based on tapering the material in the direction of the effect of this wave (ε_3). Reference [14] also mentions the diagram of biaxial tension during pulsed deformation "into an open matrix".

The characteristic distribution of tapering along the profile of the half-sphere is shown on Figure 8. Such a distribution of tapering and hardness was found in the deformation of nickel, Nichrome (NKh7), Kh18N10T steel [15], and other materials [16, 17]. Leaving to one side the different

Figure 6. Radiograms taken from thin films of tin (a) and zinc (b) after detonation deformation. Recrystallization took place only in the tin.

technological arguments, we must mention that to study the questions involved in the deformation mechanism or the characteristics of strengthening during pulsed treatment, it is necessary to investigate only the central part of the component in which the biaxial tension takes place.

3. Pulsed Deformation Using Magnetic Field Energy

If the energy accumulated in the condensors is discharged in a period of fractions of a second through the coil-solenoid, then the forming high-strength magnetic field develops a pressure of several tens of kolobars. If the specific pressure here exceeds the yield stress of the material in the zone where the magnetic field has an effect, then plastic deformation will occur. This principle is used as the method of pulsed deformation along with others. In comparison with detonation deformation, electromagnetic punching makes it possible to obtain a well-reproducible stable pulsed load that can be regulated in a large range of velocities and strength.

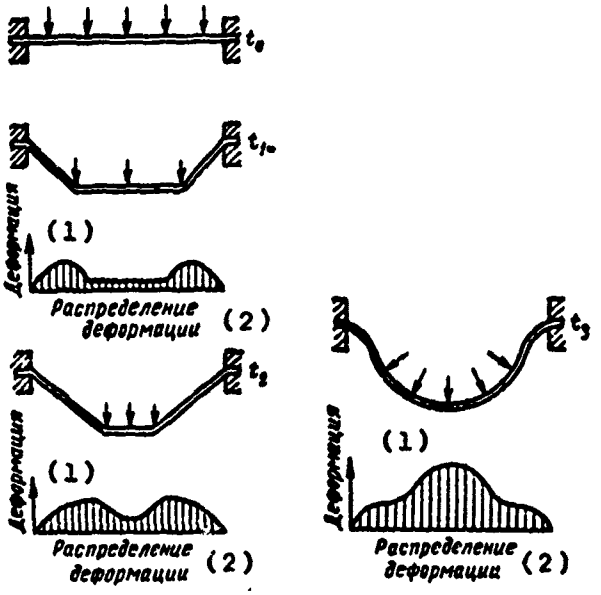

Figure 7. Diagram of the successive displacement of a sheet billet under the effect of a shock wave in time $t_3 > t_2 > t_1 > t_0$.

1. Deformation

2. Distribution of deformation

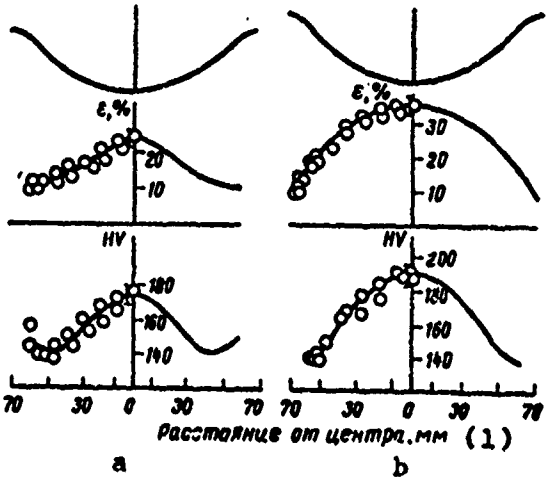

Figure 8. Distribution of degree of deformation and hardness over the profile of the half-sphere after detonation (b) and quasi-static (a) deformation.

1. Distance from center, mm

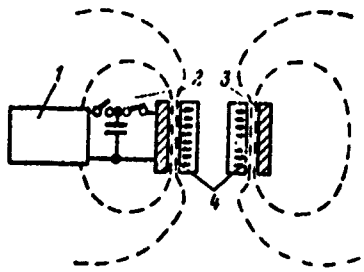

Figure 9. Diagram of the deformation of a tubular billet in an electromagnetic field.

One of the widely-used diagrams of deformation by the energy of the electromagnetic field is shown on Figure 9. The sample 4 in the form of a tube of a material with a good electrical conductivity is placed inside the coils-solenoid 3. According to the data in [18], the specific electrical resistance of the material must be $\leqslant 0.0015$ ohm.m. By discharging the condensor 1, located under high stress, through the discharger 2, a magnetic field is formed between the coil and the sample which develops a high radial pressure (as shown by the arrows on Figure 9). The diameter of the 1-mm thick tube can be decreased in this case by 20-25% [19]. The described diagram has great practical significance, however its disadvantage is the non-uniformity of deformation along the length and throughout the thickness of the sample. In this sense it is more advantageous to use the diagram of electromagnetic deformation of a flat sample. An improved instrument was developed by Svistunov and Bernshteyn [20] for studying the characteristics of the deformation mechanism and strengthening under a pulsed load (Figure 10).

The sample 1 is placed between the support 2 and the plate 3, which in the non-operating state presses down on the sample. The coil-solenoid 4 is placed in such a manner that its axis 0-0 was located at an equal distance from the plate and the lower support 5. The battery array is discharged into the coil using a trigotron which ensures an individual pulse. During the pulse the load grows from zero to P_{max}, as shown on Figure 1. At first the forces P_2 and P_1, acting on different sides of the coil, are equal, but at some moment the force P_2 exceeds the yield stress of the sample and becomes less than P_1. Then the plate is shifted by a distance $\Delta\ell$; the coil is raised to the position of the axis 0_1-0_1 and remains there until the condition $P_2 = P_1$ is recovered.

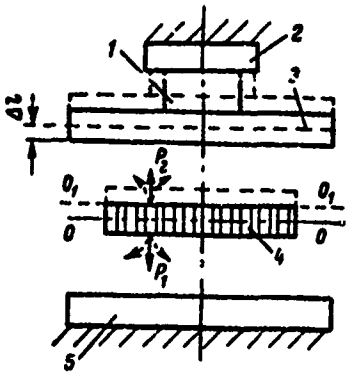

Figure 10. Diagram of the deformation of a flat sample in an electromagnetic field.

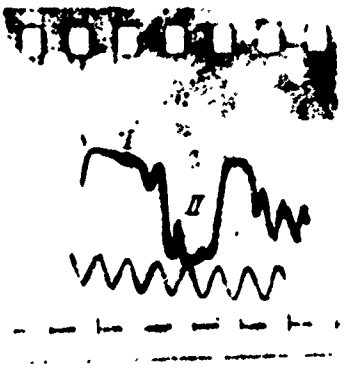

Figure 11. Oscillogram of the process of deformation in an electromagnetic field: I. segment of energy accumulation; II. period of plastic flow of the sample of about 50 usec.

Then the cycle is repeated as long as the forces of the magnetic field are sufficient for deformation of the sample. The oscillogram (Figure 11) permitted determining the time of the process and the displacement rate (100-200 m/sec).

Here the relative deformation velocity will be on the order of 10^4-10^5 sec^{-1}, i.e., near the deformation velocity in detonation punching. For copper and brass the displacement rate during deformation using the diagram shown on Figure 9 is estimated to be, respectively, 130 and 86 m/sec [19]. The authors assume that the maximal rate which can be reached in modern equipment does not exceed 300 m/sec.

The pressure of the magnetic field is determined [21] from the formula

$$P = \mu \left(\frac{H_0}{5000}\right)^2 \cdot 10^{-1} \text{ Mn/m}^2, \qquad (16)$$

where H_0 is the magnetic field strength, oersted; μ is the magnetic permeability of the material; in high-strength magnetic fields the value of μ for practically all of the materials used can be assumed equal to unity.

In turn the magnetic field strength can be obtained from the following formula:

$$H_0 = \left(\frac{40c}{l}\right)^{1/2} \frac{v}{a_1} \cdot K, \qquad (17)$$

where c is the capacitance of the battery array, μF; v is the voltage on the capacitor plates, V; l is the length of the coil, cm; a_1 is the radius of the coil, cm; K is a coefficient which depends on the form of the solenoid and the rate of damping of the oscillations in the circuit, equal to 0.3 [1].

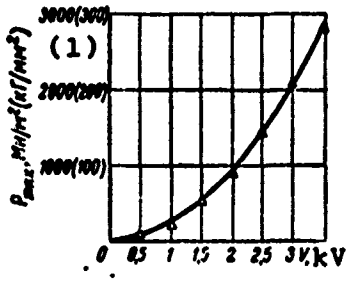

Figure 12. Dependence of pressure developing by the magnetic field on voltage applied on the condensor (C = 4000 μF).

1. P_{max}, Mn/m^2 (kgf/mm^2)

[1] For a more detailed definition of K see: Karasik, V.R., Fizika i Tekhnika Sil'nykh Magnitnykh Poley. (Physics and Technology of Strong Magnetic Fields), USSR Academy of Sciences Publishing House, 1964.

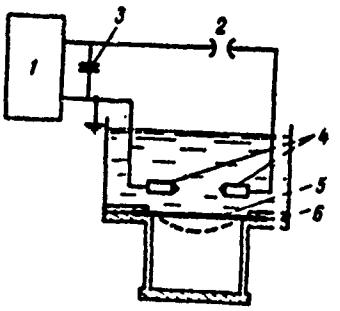

Figure 13. Diagram of the set-up for electrospark pulsed deformation: 1. high-voltage generator; 2. discharge gap; 3. battery array; 4. electrodes; 5. sample; 6. matrix.

With a battery array capacitance of 4000 μF, a voltage of 3000 V, and a coil length of 0.9 cm, the field strength will be equal to 360 kOe. Then from formula (16) the pressure will be 207,000 Mn/m^2 (about 20,700 kgf/mm^2).

Thus, the amount of pressure developed during electromagnetic punching is of the same order of magnitude as during detonation deformation, but can be easily regulated by varying the voltage but with the same condensor capacitance (Figure 12).

4. Electrohydraulic Deformation

A high pressure is developed in carrying out spark discharge under water in the space between the two electrodes for a short period of time. The liquid which washes the electrodes converts into vapor which is rapidly spread, as a result of which a high-pressure zone is generated that creates a shock wave. The method based on this principle, just as the method of electromagnetic punching, is used for the deformation of tubular billets and for the manufacture of components such as half-spheres from a sheet. The theoretical diagram of the electrospark equipment is shown on Figure 13. Reference [22] shows that during electrospark punching the same stages of flow of the metal are retained as during detonation deformation of sheet material (see Figure 7).

The deformation rate during electrospark discharge is slightly lower than during detonation and electromagnetic punching; the pressure developed is 2-5 kbar.

5. Pulsed Deformation at Superhigh Pressures

The methods of pulsed deformation described above are connected by one common condition: the sources of the shock wave and the sample are separated by an intermediate medium. In spite of the broad possibilities of these methods, their use is limited by the rate of propagation of the shock waves, and consequently by the amount of pressure developed.

We know the methods of pulsed deformation which permit increasing the deformation rate and the magnitude of P_{max} by tens and hundreds of times. The use of these methods has permitted obtaining much interesting data on phase transitions at high pressures [23-26].

Here we shall look at two methods of deformation at superhigh pressures: contact detonation and the casting of thin plates.

Contact Detonation

In detonating a charge located in direct contact with the metal, the amount of pressure will depend on the characteristics of the explosive, the density of the metal, the rate of propagation of sound in the given metal, and on other factors. With this type of loading, regions of localized stresses are created in the material that determine the process of fracture. If a high-power stress wave acts along the axis of the sample, then an unloading wave acts in the perpendicular direction that may significantly exceed the yield stress of the material and therefore facilitate its fracture.

The pressure developed on the surface of the metal P_{max} is determined by the formula

$$P_{max} = \frac{2P_x\rho_m c_l}{\rho_m c_l + \rho_x D_x}, \qquad (18)$$

where P_x is the detonation pressure of the explosive; ρ_m is the initial density of the metal; ρ_x is the initial density of the explosive; D_x is the rate of detonating the explosive.

In detonating TNT the pressure on the surface of aluminum is equal to 234 kbar, and on the surface of iron 312 kbar.

The contact placement of the charge with a directed effect from the shock wave is used for strengthening large-scale products and producing multi-layer composite materials [27].

Casting of Thin Plates at High Velocities

The greatest value of the peak pressure along the front of the shock wave may be obtained by using the energy of a thin plate, flying at high velocity. Various devices based on this principle are being used with increasing frequency at the present time for research as well as for practical purposes.

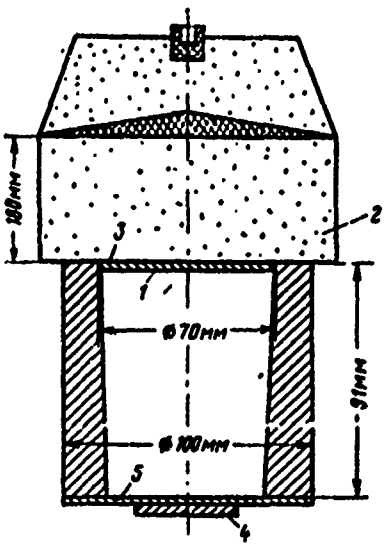

Figure 14. Diagram of the deformation using thin steel plates accelerated by products of detonation [2].

The diagram of one such device is shown on Figure 14. A steel disk 1, (1-1.5 mm thick) under the effect of the detonation products assumes a velocity of several thousand km/sec. At such an initial velocity the disk flies a distance of about 90 mm inside the control nozzle. In order to decrease heating of the disk itself, a thin spacer of plastic 3 is placed between the explosive charge 2 and the disk.

Two waves are generated and propagated on both sides of the impact surface by the collision between the striker 1 and the sample 4. If the speed of the striker prior to the moment of impact were W_y, then after impact the speed of the material behind the wave front will be U, and that of the striker will be W_y-U [2]. If the accelerating disk and the

sample are made of one and the same material, then $U = 1/2\ W_v$. A screen 5 made from a material with a known Hugoniot adiabatic curve is often placed between the sample and the flying plate.

In several papers it is shown that the speed of the flying plate prior to slowing down may reach 9 or even 14 km/sec. This process has been described in greater detail in the survey report [2].

CHAPTER 2

GLIDING UNDER CONDITIONS OF HIGH-VELOCITY DEFORMATION

By applying an external load, processes are realized in metals that diminish or eliminate the stress generated.

Elastic and plastic deformation, as well as fracture, are basic types of reaction of a metal to an external load; they may be studied as different procedures for the relaxation of external stresses. The specific type of relaxation of external stresses is determined by many factors, mainly such as the type of crystal lattice of the metal, the degree of purity, the pressure, and the velocity and temperature of deformation.

Two basic mechanisms of deformation are known: gliding and twinning.

In the present chapter we shall examine the characteristics of gliding during the pulsed loading of metals. However we must first briefly describe the behavior of individual defects in the process of high-velocity deformation and the methods by whose use we can experimentally study the process of gliding. Sections 1 and 2 are concerned with these questions.

1. Characteristics of the Behavior of Crystal Lattice Defects During Pulsed Loading

The different behavior of crystal lattice defects during high-velocity and quasi-static deformation has been mentioned in many experiments. There are several theoretical bases for this effect [28-31]. The change in concentration of any kind of defects C_i in the process of plastic deformation can be evaluated from the following formula:

$$C_i = C_{i(0)} e^{-\frac{t}{t_{ri}}}, \qquad (19)$$

where $C_{i(0)}$ is the original concentration of defects; t is the duration of the process; t_{ri} is the relaxation time for the given process.

The quantity t_{ri} may be either the time of effect of the dislocations source or the time of the interaction between the defects, or the time necessary for migration of the boundaries, etcetera. It is obvious that only those processes will enter into the deformation for which $t_{ri} < t$. If $t < t_{ri}$, then under the given deformation conditions, this process can not take place.

Consequently with high-velocity deformation there must be a redistribution of the contributions from the various processes which in turn will determine the change in properties of the materials. Furthermore, any significant change in the properties must be associated with some definite deformation velocity and will not be the same in any of the velocity ranges.

Let us look only at several of the more important aspects involving the effect of high-velocity deformation on the individual crystal lattice defects.

Rate of Motion of Dislocations and the Forces of Friction During Their Displacement

The displacement of dislocations along the glide plane is one of the determining operations in the process of plastic deformation. To increase the strength properti4s ofthe metal it is not absolutely necessary to have a large number of dislocations (or maximally small); it is important only to create conditions which make their displacement difficult for any density of dislocations.

When the theory of solid-state defects was created, dislocations were treated as mobile linear defects in an isotropic medium, actually not associated with the crystal lattice or asscciated purely geometrically through the shift vector (Burgers vector) b and the direction of the axis or the line of the dislocation $\vec{l}$.

Later Pauerls and Nabarro [32, 33] studied the influence of the periodic structure of the crystal lattice on the conditions of displacement of the dislocation through the crystal.

They determined the force of friction which the dislocations had to overcome in the transition from one equilibrium state to another:

$$\tau = \frac{2G}{K} \exp\left[-\frac{2\pi}{K}\left(\frac{\lambda}{b}\right)\right], \qquad (20)$$

where G is the modulus shift; K is a constant near unity; b is the distance between the atoms in the direction perpendicular tothe shift plane; λ is the width of the dislocation which characterizes the extent of the deformed segment around the dislocation (Figure 15).

The width of the dislocation depends strongly on the type of interatomic bond and on the temperature of deformation and can be figured only approximately. The error may be quite substantial moreover since the rate of motion of the dislocation along the plane also exerts an influence on the width of the dislocation. Taking into account that the quantity λ appears in the exponent, the shearing stress necessary to overcome the force of friction from the side of the crystal, is determined only approximately. It was found that, for pure crystals with a metallic bond, these forces are quite insignificant. For example, in metals with an fcc lattice in the plane of dense packing (111) $\tau \approx 10^{-3}$ G for the edge dislocation and $\tau \approx 10^{-2}$ for the Burgers dislocation. During the displacement of a dislocation in a crystal with a directed bond of ion or covalent type the force of friction is increased by 10 times [34] in comparison with that computed from formula (20) on the basis of the Peierls model.

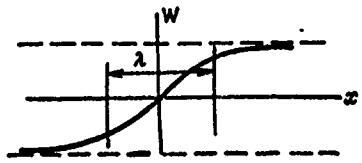

Figure 15. Distribution of dislocation energy W as a function of distance x from the dislocation center. The effective width of the dislocation λ may be figured only approximately.

The forces of friction may grow abruptly during the motion of the dislocations if the deformation conditions are changed. A substantial change in the friction force should be expected by changing the temperature and the deformation velocity, as well as the magnitude of the shock wave pulse. The changes may be rather large. The dependence of friction force

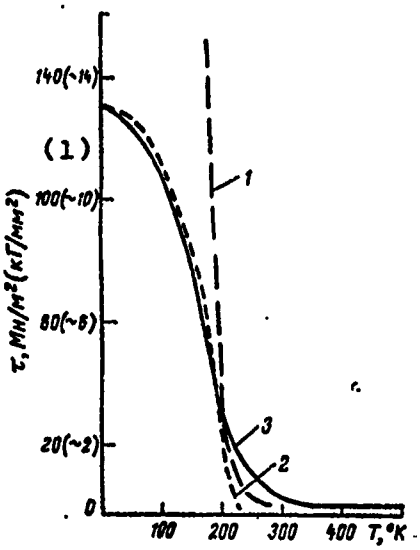

Figure 16. Comparison of the experimental and theoretically computed dependences of shift stress on temperature in iron: 1. computed from the Lot-Hirsh equation on the basis of the Peierls forces; 2. computed according to Fridel, on the basis of the Peierls forces; 3. experimental data.

1. τ, $Mn/m^2(kgf/mm^2)$.

on temperature has been investigated in the greatest detail. For the temprature dependence there are computational formulas and sufficiently reliable experiments. As is clear from Figure 16 [35] when the temperature is lowered the friction force may grow by an order of magnitude. There is a certain critical temperature (or narrow temperature range) at which the Peierls force is abruptly increased. We should mention the rather good agreement between the computed (after Fridel) and the experimental data, in any case, in the temperature range for which a large friction force is characteristic.

For the present it is still impossible to determine the dependence of friction force on the rate of displacement of the dislocations in the crystal with the same degree of reliability since the necessary experimental data and analytical formulas are lacking to do so. The dependence on velocity can be figured only qualitatively by varying the energy of the moving dislocation.

The energy derivative over the parameter a (in the direction of the glide plane) $\partial w/\partial a$ represents a force which may be written as the product $b.\tau_{cr}$, where τ_{cr} is the critical

stress necessary for motion of the dislocation which can be treated as a force that inhibits motion of the dislocations, i.e., the force of friction.

In accordance with the theory of the motion of dislocations, formulated in general form by Frank and Eshelby [36, 37] the motion of the dislocations is similar to the motion of the particles described by the special theory of relativity. Then

$$W_v = \frac{W_0}{\sqrt{1 - \frac{v_d^2}{c_t^2}}}, \qquad (21)$$

where v_d is the rate of displacement of the dislocations in the glide plane; W_v is the energy of dislocation being displaced at a rate V_d; W_0 is the energy of dislocation in the state of rest; c_t is the rate of propagation of transverse sonic waves in the metal.

From formula (31) it follows first of all that by increasing the rate of displacement of the dislocation its energy grows and when it reaches the value c_t the dislocation energy tends to infinity.

The width of the dislocation also depends on the rate of its displacement:

$$\lambda = \lambda_0 \sqrt{1 - \frac{v_d^2}{c_t^2}}, \qquad (22)$$

where λ_0 is the width of the stationary dislocation.

From comparison of formulas (20) and (22) and also from formula (21) it follows that increasing the rate of displacement of the dislocations will lead to an increase in the friction force, as a result of which an additional strengthening of the metal will take place during high-velocity deformation.

From these premises the deformation under conditions of pulsed loading should be treated as the effect of a very large cleavage stress along the glide plane at the displacement rate of the dislocation, since in Chapter 1 we showed that the peak pressure during high-velocity deformation may grow by several orders of magnitude.

The numerous experimental data giveing the dependence of the rate of displacement of the dislocation on the amount of stress applied, obtained by various researchers [38-46], can be described quite well by the formula

$$v_d = c_i \left(\frac{\tau - \tau_i}{\tau_0}\right)^m, \qquad (23)$$

where τ is the amount of cleavage stress in the glide plane; τ_i is the stress of resistance of the lattice to motion of the dislocations; τ_0 is the constant amount of stress necessary to apply in order for v_d = 1 cm/sec; m is an exponent which depends on the type of crystal.

Table 7. Value of the Index m Which Characterizes the Mobility of the Dislocations in Various Crystals

Материал (1)	Температура испытания, °С (2)	m	Литературный источник (3)
Si	600—900	1,4	[38]
Ge	420—700	1,4—1,9	[38—40]
InSb	218	1,87	[38]
GaSb	450	2,0	[38]
W	20	5,0	[40]
W	—196	14,0	[40]
Mo	23	6,4	[41]
Fe + 3,25% Si *	—77	38—42	[42, 43]
	20	34—35	
	—40	43	
	100	41	
LiF	20	14,5	[44]
Cu	—	~200	[45]
Ag	—	~300	[45]

* Скольжение идет по плоскости {110}. (4)

1. Material
2. Test temperature, °C
3. Literature source
4. *Gliding takes place along the plane {110}.

Table 7 gives the value of the index m for several crystals. We must first pay attention to the sharp dependence of m on type of crystal lattice. The lowest exponent

in crystals with a directed covalent bond is in silicon and germanium, which are the most sensitive to increase in deformation velocity. The maximal exponents in crystals with an fcc lattice are those which are most plastic under conditions of high-velocity deformation. The exponent m in metals with a bcc lattice differs by more than an order of magnitude in comparison with the fcc metals; the bcc lattices, as we know, possess a more abrupt temperature and velocity dependence of the strengthening characteristics.

As yet we have insufficient data for a categorical judgement of the influence exerted by type of lattice on behavior of the dislocations during pulsed deformation, but the cited results permit us to mention certain laws.

However, formula (23) is valid only in certain limits of deformation velocity since in principle γ and m may be sufficiently large and then we can show that $v_d \gg c_t$.

Gilman [29, 47] suggested the following formula for describing the dependnece of rate of motion of the dislocations on the magnitude of the cleavage stresses

$$v_d = v_0 e^{-\frac{\tau_0}{\tau}}. \qquad (24)$$

Gilman assumes that this is the simplest function that will describe the experimental data sufficiently well, although the setting up of the experiment itself is complex and the results obtained have a large amount of scatter.

Figure 17 shows the curves of the dependence of the logarithm of dislocation velocity on the amount of pressure applied for various crystals. For each crystal there is some critical value of the cleavage stress, which will lead to a sharp growth in the dislocation velocity. Lavrent'yev and Salita [48] studied the mobility of dislocations in the pyramidal plane $\{11\bar{2}2\}$ of zinc single crystals during impact loading. They also established an exponential dependence of the velocity of dislocation displacement on stress, although they distinguished two segments: the first when the dependence is very acute, and the second when a four-fold increase in stress raises the dislocation velocity by only 10 times. For NaCl crystals doped with bivalent strontium, two values are determined for the index m: for low and high values of γ [46].

In one of his later works [49] Gilman showed that for a number of crystals the bremsstahlung of moving dislocations is simply proportional to ξ^2.

Thus, during high-velocity deformation characterizing extremely high values of applied stress, the rate of dislocation displacement grows sharply along the glide plane, which in turn is associated with an increase in the resistance of the lattice to dislocation displacement. The described phenomenon is undoubtedly one of the important causes for the additional increase in strength during high-velocity deformation in comparison with quasi-static deformation strengthening.

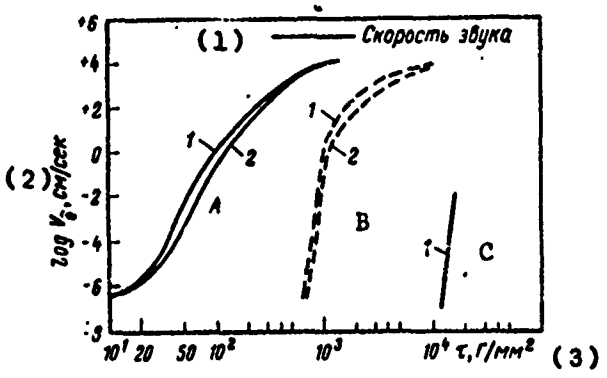

Figure 17. Dependence of rate of motion of dislocations on applied stress at room temperature: 1. edge dislocations; 2. Burgers dislocations; A. for NaCl according to the data in [30]; B. for LiF according to the data in [44]; C. for Fe + 30% Si according to the data in [42].

1. Speed of sound
2. log v_d, cm/sec
3. τ, gf/mm^2

Furthermore it is completely possible that the difference in additional strengthening of the different metals is determined to a significant degree by the index m in equation (23).

Campbell and Harding [50] studied the influence of deformation and neutron irradiation on the lower yield stress σ_y of iron and low-carbon steel, by determining the values of the coefficients in the familiar Petch equation:

$$\sigma_y = \sigma_i + k_y d^{-1/2},$$

where σ_i is the stress necessary for displacement of the dislocations through the crystals; k_y is the strength of blocking of the dislocations; d is the diameter of the grain.

The data in Table 8 show that both with irradiation and without neutron irradiation, the value of σ_i grows abruptly with increase in deformation velocity, the degree of the increase in resistance of the lattice in the selected velocity range virtually not varying as a function of the irradiation dose, although the absolute of σ_i does increase.

Table 8. Influence of Deformation Velocity and Neutron Bombardment on the Values of the Coefficients in the Petch Equation [50]

Доза облучения нейтронами $\frac{нейтрон}{см^2} \cdot 10^{18}$ (1)	Скорость деформации, $сек^{-1}$ (2)	Железо (3)		Сталь (4)	
		σ_i, $Мн/м^2$ (5)	k_y, $Мн/(м^2 \cdot мм^{1/2})$ (6)	σ_i, $Мн/м^2$ (5)	k_y $Мн/(м^2 \cdot мм^{1/2})$ (6)
0	10^{-3}	0,048	1,86	0,08	1,8
	10^3	0,800	1,88	1,04	1,23
	$2,6 \cdot 10^3$	0,910	1,86	1,16	1,21
0,8	10^{-3}	0,30	0,81	0,21	0,8
	10^3	1,07	0,61	1,05	1,5
	$2,6 \cdot 10^3$	1,20	0,20	1,09	1,5
5	10^{-3}	0,37	0,25	0,26	1,0
	10^3	1,20	0,15	1,10	1,1
	$2,6 \cdot 10^3$	1,30	—0,05	1,21	1,1

1. Neutron bombardment dose, neutron.10^{18}
2. Deformation velocity, sec^{-1}
3. Iron
4. Steel
5. σ_i, Mn/m^2
6. $Mn/(m^2 \cdot mm^{1/2})$

The value of k_y remains virtually constant with increase in deformation velocity but drops abruptly during bombardment due to the formation of point defects.

According to the data in [30] and [44] there is a difference in displacement velocity of the edge and Burgers dislocations with one and the same stress value. Here the displacement velocity of the edge dislocations is approximately 10 times greater, this obviously being due to the ability of the edge dislocations to remain in the limits of one glide plane.

The limits of change in the velocity of the edge and Burgers dislocations are also different. The velocity of the first may vary from zero to the propagation velocity of Rayleigh waves (c_r), and the velocity of the second -- from zero to c_i. The propagation velocity of the Rayleigh surface waves is less than the transverse speed of sound propagation by 5-13%, depending on the material. For materials with Poisson coefficients $\mu = 1/2$, $c_r = 0.95\ c_t$; when $\mu = 1/3$, $c_r = 0.93\ c_t$; and for a material with $\mu = 0$, $c_r = 0.87\ c_t$.

It should be mentioned that the change in temperature of deformation does not change the character of the dependence of dislocation velocity on the magnitude of the stress applied (Figure 18). In logarithmic coordinates the lines are shifted only along the abscissa axis.

Formation of Dislocations of Several Spherical Types

In accordance with the general theory of dislocations the velocity of the dislocations must be limited by the velocity of the transverse sonic waves. However the theoretical works on the motion of dislocations by Eshelby and other researchers [28, 51, 52] showed that this limitation is not a general one, and in particular that the edge dislocations have a finite energy value at supersonic displacement velocities.

Another limitation on the dislocation velocity follows from equation (22) according to which the width of the dislocation is equal to zero when a velocity of c_i is reached. If by width of the dislocation we mean the number of vertical curved planes along both sides of the excessive half-plane, then the possibility of forming supersonic dislocations may be explained in the following manner [28]. Let us assume we have the positive dislocation shown on Figure 19, a. With increase in displacement velocity its width is decreased and for c_t reaches zero (Figure 19 b). But with further increase in velocity a dislocation of opposite sign is formed (Figure 19 c). Since the presence of a dislocation leads to a bending of the glide plane itself, by increasing the displacement velocity of the dislocation of the opposite sign, the angle of bending will be constantly increased.

A diagram of the supersonic edge dislocation was given by Eshelby (Figure 20). The atoms arranged above the glide plane may occupy two positions. To the right of the dislocation A the position is unstable, and to the left it is stable. The position of the atoms to the right of A may vary if they are shifted to the left and occupy a stable position. This movement will be equivalent to the dislocation being

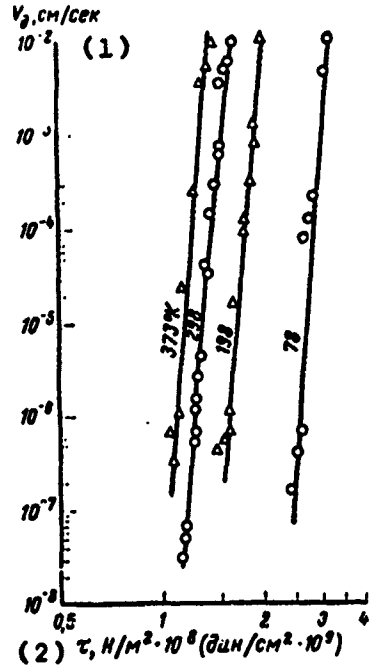

Figure 18. Influence of temperature of deformation on the displacement velocity of edge dislocations versus the amount of stress [42].

1. v_d, cm/sec 2. τ, n/m^2.10^8(dyn/cm^2.10^9)

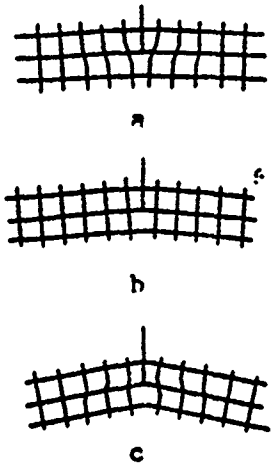

Figure 19. Conversion of the positive edge dislocation to a negative one through the intermediate state at which the width of the dislocation is equal to zero (after Weertman).

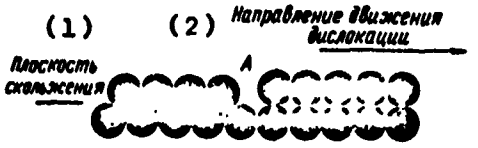

Figure 20. Formation of a supersonic dislocation after Eshelby.

1. Glide plane
2. Direction of dislocation motion

shifted to the right in the direction shown by the arrow. The energy of the unstable position also creates that driving force which determines the motion of the dislocation. If all theatoms located to the right of A are displaced simultaneously from their unstable positions to a stable position, the dislocation will be displaced at an infinitely high velocity.

The displacement velocity of the dislocation is first of all a function of the effective stress. Reference [51] shows that to reach a velocity near that of sound the stress in the sample must be G/75, i.e., for iron approximately 10 kbar. In pulsed deformation (see Chapter 1) the peak pressure may far exceed this value.

On the other hand, according to Eshelby, the formation of supersonic dislocations must be accompanied by the presence of an interface, similar to the surface forming during diffusionless processes. When a shock wave exerts an effect on the metal, such an interface will be narrow and not exceed several microns; the band in which the pressure drop is comprises hundreds of kilobars.

However for the present there are no experimental data which would confirm the existence of supersonic dislocations. Even in studying the motion of dislocations in the subsonic range the investigated velocities fail to reach the speed of sound by at least an order of magnitude.

Short-Term Effect of a Large-Amplitude Pulse on Dislocation Sources

The Frank-Reed diagram is one of the most common for explaining the mechanism of multiplication of dislocations under the influence of an externally applied load. In this case the potential sources of the dislocations may be the individual segments of the dislocation line, consisting of a grid of dislocations affixed between the point defects and inclusions and located inside the grain and at the boundary.

There are certain conditions which must be energetically satisfied in order for one or another segment of the dislocation line to be converted into a Frank-Reed source. If we treat this line independently in an elastic medium, then for multiplication of the dislocations we must apply a critical stress.

$$\tau_{cr} \geqslant \frac{Gb}{l}, \qquad (25)$$

where l is the length of the dislocation line; G is the modulus of shift; $\bar{b}$ is the Burgers vector.

In addition to the Frank-Reed source found in a real crystal, for the production of dislocations it is necessary to overcome the resistance of the stress fields σ_c created by the various barriers; grain boundaries, vacancy clusters, dislocation forest, etcetera. Here the value of the stress σ_c acting on the source depends on the position of the dislocation line in the crystal and may also vary in wide limits. Hart [53] shows that even a small liberated loop may act as a Frank-Reed source with a stress $\tau < \tau_{cr}$ if it moves at a velocity near the speed of sound, since with motion it possesses a high kinetic energy. Thus, in a crystal there is a wide spectrum of potential dislocation sources, which begin to act under quite different conditions. One thing is clear, increasing the effective pressure will facilitate the formation of new sources as a result of realizing sources with small l and overcoming of the resistance σ_c. Simple computation shows that if take for iron G = 84,000 Mn/m^2 (8400 kgf/mm^2), $\bar{b} \approx 0.1$ nm (1 Å), then with quasi-static deformation when the pressure does not exceed 2000 Mn/m^2 (200 kgf/mm^2), and consequently τ does not exceed 1000 Mn/m^2 (100 kgf/mm^2) [1], only those sources may act for which l is no less than 8 nm (80 Å).

During pulsed deformation with a pressure of 100 kbar the dislocation sources are found to be lines with a length of about 1.5 nm (15 Å).

According to the data in reference [54] the time necessary for operation of the Frank-Reed source is 5.10^{-5} sec

[1] The Schmid orientation factor is taken as maximal -- 0.5.

with a stress on the order of 10^{-4} gf. This time is at least an order of magnitude less than the time of effect of a shock wave, and by increasing the load (during pulsed deformation it is far greater than 10^{-4}) it is reduced even more.

Formation of Point Defects

The formation of point defects during the motion of dislocations was first examined by Seitz [55]. As a result he suggested several mechanisms for this process, including the formation of point defects during the displacement of dislocations with thresholds.

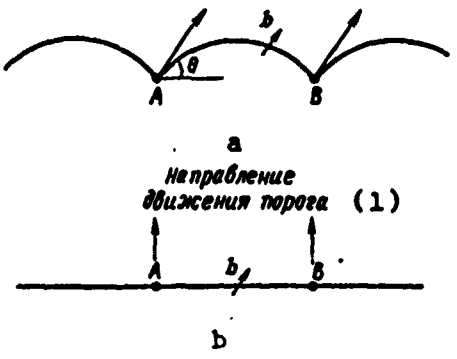

Figure 21. Diagram of the motion of low-velocity (a) and high-velocity (b) dislocation loops, bounded by the the thresholds A and B [28].

1. Direction of threshold motion

If a dislocation having thresholds A and B (Figure 21 a) moves through the crystal at subsonic velocity, then a segment of the dislocation line is formed between the thresholds that is perpendicular to the glide plane of the dislocation coinciding with the plane of the drawing.

In this case the purely edge thresholds have the vector $\bar{b}$ with the same direction as the Burgers vector of the basic part of the dislocation line. Such a conservative motion of the thresholds in the glide plane does not lead to the formation of new point defects [28, 55] and the character of the threshold displacement does not depend on the type of dislocation.

During motion of the dislocations at velocities near the sonic, the stress acting on the dislocation line tends to

infinity and the number of kinks to zero (Figure 21) [28]. Under these conditions, both conservative and noncons. .vative motion of the thresholds is possible. The force component of the conservative motion is proportional to the angle θ. At high velocities of displacement, when the angle θ is small, a nonconservative motion of the thresholds A and B sets in for which point defects are formed. The concentration of defects is greater as the dislocation displacement velocity is higher.

Interaction of Dislocations

The interaction of dislocations has great significance for final formation of the dislocation structure. The formation of thresholds, annihilations, alignment of dislocations at the wall, the formation of point defects -- all these processes are determined to a large degree by the interaction of the dislocations.

If there are two parallel Burgers dislocations located at a distance r from one another, then the force of the interaction between them may be defined similar to the force acting between two point electric charges:

$$F = \frac{G\bar{b}_1\bar{b}_2}{2\pi} \cdot \frac{1}{r}, \qquad (26)$$

where G is the modulus of shift.

The force acts along the radius connecting the two dislocation lines, and if $\bar{b}_1\bar{b}_2 > 0$, then it will be repulsive (+); if $\bar{b}_1\bar{b}_2 < 0$ then it will be attractive (-). This simple interaction of the Burgers dislocations does not depend on the dislocation displacement velocity, and consequently is retained during high-velocity deformation.

The interaction of two edge dislocations is more complex. If two edge dislocations are arranged in parallel glide planes (on Figure 22 the dislocations are conventionally denoted by the points), then the effect of one of them (placed at the origin) on the second is determined by two forces: the radial F_r and the tangential F_θ:

$$F_r = \frac{G\bar{b}_1\bar{b}_2}{2\pi(1-\mu)} \cdot \frac{1}{r}, \qquad (26a)$$

$$F_0 = \frac{G\bar{b}_1\bar{b}_2}{2\pi(1-\mu)} \frac{\sin 2\theta}{r}. \qquad (27)$$

Taking into account the major properties of the edge dislocations -- the conservativeness of the motion in the

primary glide plane, we can determine the resultant force acting on the dislocation in this plane from the equation

$$\tau_{xy} = F_r - F_0 = \frac{G\bar{b}_1\bar{b}_2}{2\pi(1-\mu)}\frac{1}{2}\cos\theta\cos 2\theta. \qquad (28)$$

Formula (28) in the x-y coordinates will have the form:

$$\tau_{xy} = \frac{G\bar{b}_1\bar{b}_2}{2\pi(1-\mu)}\frac{x(x^2-y^2)}{(x^2+y^2)^2}. \qquad (29)$$

The stressed state produced by the presence of an edge dislocation is one-dimensional and does not depend on the third coordinate. From formula (29) it is easy to see that the sign of the stress will depend on where the dislocations in the neighboring planes are located (that is, what are the coordinates of x and y) with respect to the dislocation found at the origin. Figure 23 shows the regions of mutual attraction and repulsion of the edge dislocations having identical sign ($\bar{b}_1\bar{b}_2 > 0$). For dislocations with different sign ($\bar{b}_1\bar{b}_2 < 0$) the picture will be the reverse.

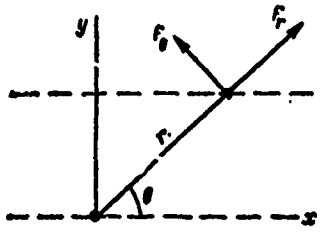

Figure 22. Radial F_r and tangential F_θ forces, acting between two edge dislocations located in parallel glide planes.

As shown by Weertman [28] the angle of slope α of the lines dividing the fields of different interaction of two edge dislocations depends on the velocity of their displacement. If the dislocations are found in a state of rest or are being displaced at a low velocity, the angle α is equal

---

[2] The first index shows the direction of the effect of the stress component, and the second -- the direction of the normal to the area on which this stress acts.

to 45°; by increasing the velocity of the dislocation motion this angle is decreased.

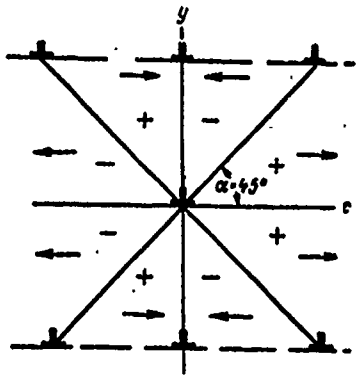

Figure 23. Signs of stress fields for uniform edge dislocations ($\bar{b}_1\bar{b}_2 > 0$) as a function of their mutual arrangement.

Figure 24 a shows the fields of interaction of two dislocations. The dislocation displacement velocity here is rather high, however it is less than the propagation velocity of the Rayleigh waves in a given material. If the velocity of the edge dislocation exceeds c_r, then in one and the same glide plane the two unlike dislocations will be attracted rather than repelled (Figure 24 b).

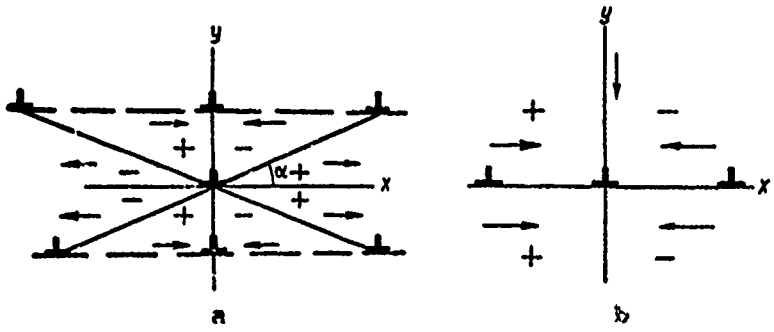

Figure 24. Fields of interaction of two uniform dislocations ($\bar{b}_1\bar{b}_2 > 0$) when $v_d < c_r$ (a) and $v_d > c_r$ (b).

The mechanism suggested by Weertman for the interaction of high-velocity dislocations has as yet no direct confirmation, but we do know that there are differences in the ultimately formed dislocation structures obtained at various deformation velocities. In particular we can mention the

anomalously high mobility of edge components of the dislocation loops in bcc metals during high-velocity deformation. This will be discussed in detail in Chapter 4.

2. Methods of Studying Glide in Metals

Different methods are used to determine the elements of glide and to study the development of glide deformation; these can be divided into two basic groups:

Direct methods of metallographic, radiographic, and electron-microscopic research;

Indirect methods based, for example, on analysis of the changes in crystal orientation or texture of a polycrystalline sample in the deformation process.

Let us examine several of these methods in more detail.

Investigation of Glide Tracks

Glide tracks are generated on the polished surface of a deformed crystal when the yield stress is reached; these are lines of intersection of the glide plane with the outer surface of the crystal. If no special reagents are used the glide lines can then be distinguished from the deformation tracks of another type in that after polishing and etching they are clear in the field of the thin section. In a number of cases the glide lines are caused by etching [3]. With a low dislocation density the glide lines may be observed along the etching holes. We know that a glide track is a step with a given shift, the size of which can be established by using an interference microscope. By using an electron microscope [57, 58] it was established that the glide track has a complex structure: it consists of bundles of glide lines remaining at a distance of 20-25 nm (200-250 Å) from one another. Each such line is a track of the elementary step on the glide plane. To denote the glide elements we use the terminology used in reference [58]. Glide bands are such tracks in which individual glide lines can be detected by using electron microscopic analysis of the images. Such lines create a step. Still finer glide tracks, distinguished only in an electron microscope, are called microglide. The definitions used are illustrated on Figure 25.

By studying the appearance of glide lines in the process of crystal deformation, we can also obtain extensive

---

[3] The compositions of the reagents for the most widely used metals and alloys are given, for example, in reference [56].

information on the mechanism of the process. Analysis of the glide tracks permits determining the indices of the glide planes. For this purpose, using x-ray or metallographic data, we can establish the crystal orientation in space and the position of the axis of the sample relative to the major axes of the crystal. As an example let us look at an interpretation of the effective glide plane for fcc metals [59].

Figure 25. Diagram of glide tracks.

1. Glide band
2. Glide line
3. Glide step
4. Microglide

Figure 26 shows the orientation of the axis of tension of a crystal inside a standard triangle.

As metallographic investigations have shown, the angle between the glide track and the direction of the axis of the sample on two mutually perpendicular planes is 43 and 46.5°. Based on these angles we have constructed a stereographic projection of the glide plane. The projection of the crystal and the glid plane are plotted with solid lines. The projection of the crystal agrees with the plane ABCD of the sample (see the diagram of the sample). The dotted lines are used to plot the standard projection of the crystal. By combining the projection of the crystal with the standard projection the normal to the glide plane N coincides with the normal to the plane N', determined analytically. From Figure 26 it is clear that the plane determined from the metallographic data agrees with the plane $(1\bar{1}1)$ with an accuracy up to two degrees, and the direction of glide with the direction $\langle 110 \rangle$.

The indices of the glide plane can be easily established if we know the angle λ between the glide plane and the surface of the crystal, as well as the crystallographic orientation of the crystal. By investigating the glide tracks in an electron microscope, where their fine structure is well resolved, using the method of a latex globe

[60] the height of each individual line is determined. Knowing the height and the width of the glide line, we can measure the angle λ. These statements are valid if we assume that the glide track is the result of displacement along one plane. Proof of the individual glide as yet has been found only for alpha-brass [61] and alloys of Al-Mg [62].

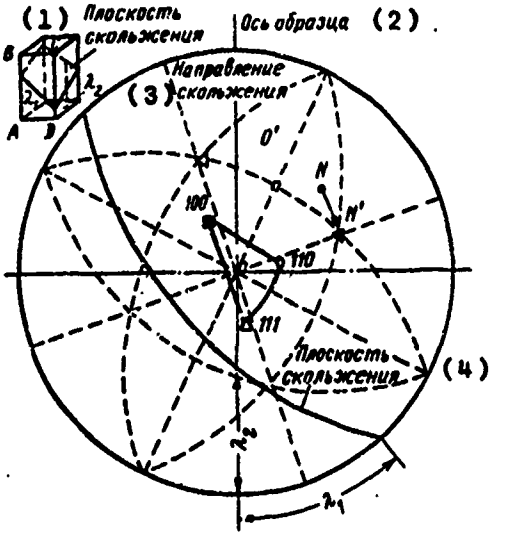

Figure 26. Determination of the indices of the glide plane according to the known crystal orientation with respect to the axis of tension.

1. Glide plane
2. Axis of sample
3. Direction of glide
4. Glide plane

In aluminum and a number of alloys, gliding in the track takes place in a bundle of planes [63]. Moreover, from reference [64] it follows that the distribution of displacements in the planes of the glide bundle may be both uniform and non-uniform.

The general-purpose method for studying glide tracks using images and for observing them in an electron microscope was suggested in reference [65]. In this method, to establish the distribution of displacement over the width of the glide track and to study the plastic deformation inside the crystal, we can use either coherent separation from the matrices, or the edge of the etching hole, or scratches drawn on the surface.

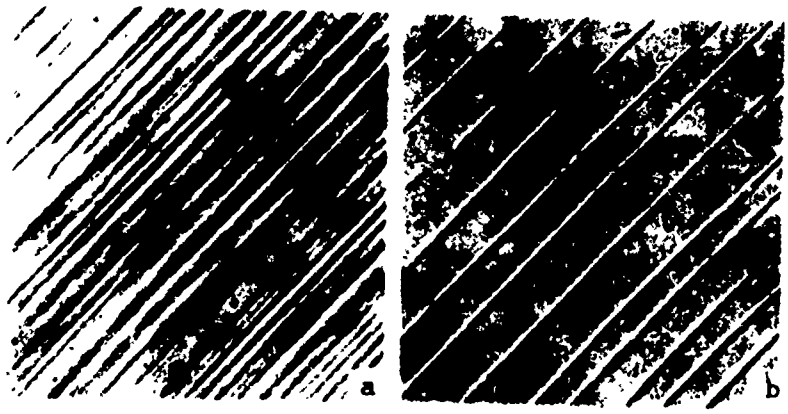

Figure 27. Glide lines on the surface of an aluminum single crystal [67]: a. after high-velocity deformation; b. after quasi-static deformation.

After measuring the relative displacement of the individual amounts of separation, arranged on different sides of the glide track, as well as the width of the track, we can quantitatively evaluate the total displacement in the glide track, determine the thickness of the glide bundle, and establish where the glide takes place -- in one atomic plane or in a bundle of planes.

Simple crystallographic analysis on the basis of the known direction of the glide track permits determining the crystallographic indices of the direction of glide.

It is quite important that by studying the glide lines at different degrees of deformation we can not only judge as to the effective glide systems, but also trace the stages of the deformation process.

As Mader and Seger [63] showed, the glide lines have a different structure at different stages of deformation. At the first stage of deformation when one glide plane is effective, the height of the steps is increased and the length of the glide lines actually remains constant. At the second stage the length of the newly generated glide lines is decreased with increase in the degree of deformation. At the third stage the development of transverse glide is observed; in this case the glide bands are slightly widened, and the glide between bands practically ceases.

Change in the temperature and velocity of the process at one and the same degree of deformation changes the character of the glide tracks. Brawn [66] showed that by in-

creasing the temperature or reducing the deformation velocity, the number of elementary planes in the glide tracks increases. Ioshida and Nagata [67] found that a deformation velocity of 10^2-10^3 sec^{-1} the density of the glide lines in single crystals of aluminum is significantly increased (Figure 27), this being associated with growth in the number of effective dislocation sources. According to the data of these authors, the type of the glide tracks in zinc and copper does not change at high deformation velocities [68].

By analyzing the character of the distribution of glide lines, we can judge as to the change in the dislocation structure. The length of the glide lines characterizes the length of the dislocation path and its change as a function of stress or deformation. The height of the step, forming on the glide line, is porportional to the number of dislocations based on the Frank-Reed source, i.e., proportional to the number of the dislocation groups of one sign [69]. Investigations of the structure of glide lines by transillumination confirmed that the steps are generated during deformation as a result of the precipitation of dislocations onto the surface of the metal [70].

In metals with a high energy of the packing defects, after high- and low-velocity deformation, metallographic analysis reveals straight glide lines and electron microscopic analysis reveals a cellular structure in the glide track [61].

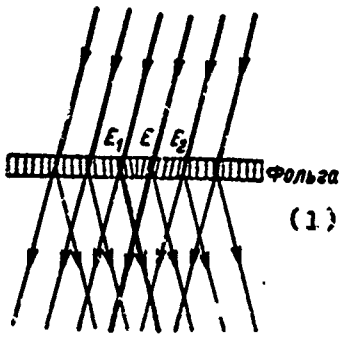

Figure 28. Diffraction of electrons on foil containing one edge dislocation at point E: E_1 is the diffraction bundle from the region containing the dislocation; E_2 is the same, from the region not containing the dislocation.

1. Foil

Method of Electron Microscopy

In recent years this method has been used to produce considerable interesting data which characterize the process of glide in crystals [71-73].

Let us look at the principle involved in this method.

Let us assume that the foil examined in an electron microscope contains one edge dislocation (Figure 28). If the crystal is found in some random position, not precisely corresponding to the reflecting one (Wulff-Bragg), then the deformation results under the Wulff-Braff condition near the dislocation are satisfied better than in the entire crystal, and consequently the intensity of the diffracted bundle E_1 on this segment is greater. Since in the microscope the diffracted ray is intercepted by the objective aperture and only the straight ray passes through, on the segment corresponding to the image of the dislocation the intensity is less, i.e., a dark line is visible. From Figure 29 it is clear that the existence of contrast depends also on the position of the dislocation with respect to the primary bundle. The planes of the lattice, parallel to the Burgers vector, are not distorted, and therefore can not alter the intensity of the diffracted rays. Mathematically this con-

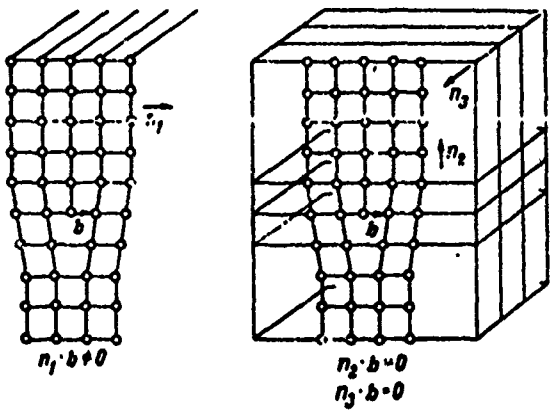

Figure 29. Mutual arrangement of the diffraction vectors ($\bar{n}$) and the Burgers vector of the dislocation ($\bar{b}$). The contrast from the dislocation arises when $\bar{n}\bar{b} \neq 0$.

dition corresponds to $(\bar{n}\bar{b}) = 0$, where $\bar{n}$ is the vector perpendicular to the plane of the crystal, and $\bar{b}$ is the Burgers vector of the dislocation. The Burgers vector can be determ-

ined from this condition by knowing the indices of the planes, upon reflection from which the image of the dislocation disappears.

The Burgers vector can be determined in practice from the slope of the sample using a goniometric device.

This method permits not only determining the effective glide system, but also individually computing the density of the dislocations having different Burgers vectors. A substantial disadvantage in this method is that it may be used only for small degrees of deformation (5-10%).

X-Ray Methods

This method is most often used to determine the glide elements [74].

When it is possible to direct the x-ray perpendicular to the glide plane, the indices of this plane can be established on a Laue diffraction pattern. The indices of the glide direction are determined by a rotating-crystal x-ray photograph.

Based on the change in orientation of single crystals in the process of plastic deformation we can recognize the glide elements. The direction in the glide plane toward which the longitudinal axis of the sample approaches in the process of tension, is the direction of glide.

In metals with fcc and hexagonal close-packed lattices the glide planes can be judged by rotating the lattice in the process of contraction -- in this case the direction of the normal to the glide plane is changed, approaching the direction of the effect of the force.

However the simultaneous effect of many glide systems, for example of bcc metals, makes analysis difficult.

The glide elements are also determined by asterism. We assume that asterism is caused by rotation of the glide plane, in this case the axis of asterism during tension is found in the glide plane and perpendicular to the direction of glide [75]. Consequently, by finding the axes of the clearly expressed asterism, we can also establish the plane and the direction of glide.

Usually to find the axis of asterism we use the registration of reflections involving a photographic method, however it permits obtaining reliable results only at small degrees of deformation (less than 10%) due to the weak intensity of the

reflections. More promising is the diffractometric method which permits finding the various reflections of the single crystal in the reflecting position and using a counter to determine the fine form of the reflection in various cross sections of inverse space. In analyzing polycrystalline materials by x-ray methods it is impossible to determine uniquely the effective glide system, however we can make a choice among several systems.

Indirect Methods of Evaluating the Glide Elements

In the process of plastic deformation, when a plastic displacement takes place, the orientation of the individual crystals is altered in space. If in the original sample prior to deformation there was already an orientation, then under the influence of such a displacement a fracture takes place of the old orientation and a new orientation is formed [76]. Plastic deformation of the individual grains of the oriented polycrystalline sample can be compared with the plastic deformation of a single crystal having the same orientation (grain-boundary effects are not taken into account in this case). Then the stress σ, at which fracture of the old orientation begins, can be determined from the criticcal stress τ_{cr} corresponding to the onset of glide in the different glide planes of the single crystal with a given orientation:

$$\tau_{cr} = \sigma \cdot \cos\varphi \cos\lambda, \qquad (30)$$

where φ is the angle between the normal to the glide plane and the force; λ is the angle between the direction of glide and the force.

If prior to deformation there were several orientation maxima in the sample, corresponding to the different orientations, then in order of their fracture we can establish whether the suggested glide system is effective in the given case.

If we know the direction of the effective stress we can compute the Schmid orientation factor ($\cos\varphi \cos\lambda$) for the different systems of glide, and then the displacement of the orientation maximum as a result of glide in the given system. Here we take into account that glide in the plane along the determined direction is equivalent to rotating the crystal around the normal to the plane and the direction of glide. Thus, we can determine the possible glide systems for a given orientation of the crystals and compare the theoretically computed change in form of the pole figure with that found experimentally.

Of the indirect methods permitting us to find the characteristics of the fine structure of metals after deformation, and also give a qualitative picture of the change in the deformation mechanism, it follows to mention the x-ray methods that permit us to determine the intragranular disorientation of regions of coherent scattering. Rovinskiy and Rybakova [77] suggested for measuring the disorientation to use the method of measuring the magnitude of the reflection obtained from an individual crystallite of a fixed sample. Further development of this method [78] permitted finding the computational formulas which connect the radial and the azimuthal broadening of the reflection with the parameters of the internal structure of the crystallite and the geometry of the photograph. In these works it was shown that the most favorable geometry that will ensure a high resolution is that at which bundles with a small angle of convergence are used in the azimuthal direction and a large angle in the radial direction. Determination of the disorientation based on azimuthal broadening is more precise.

Hirsh [79] suggested a method for studying the subgranular disorientation using a microbundle. Such conditions for the photographing permit connecting the azimuthal broadening of the reflection with the angular characteristics of the substructure.

In reference [80] for determining the substructure the method of an oscillating curve was suggested by using the diagram of a double crystal-spectrometer. Monochromatism of the primary bundle is used to reach a decrease in the angle of convergence and removal of the heterogeneity in radiation, which facilitates a high resolution. However in this case the intensity of the reflected ray is sharply diminished.

All these methods require the photographic registration of the reflection and are quite time-consuming. By increasing the angle of disorientation the magnitude of the reflection grows, its intensity drops, and measurement of the dimensions becomes only slightly reliable. Furthermore, the overlapping of reflections from different crystallites also decreases the resolving power of the methods. In references [81, 82] it was shown that a substantial disadvantage of the photographic methods of determining the subgranular disorientation is that the individual crystallite, the reflection from which is being studied, is not brought to the maximally reflecting position. Therefore in an unoriented sample the amount of the orientation is determined that is decreased in comparison with the maximal by approximately 20%. In an oriented material this error is still higher and depends on the conditions of the photography, the

sharpness of the orientation, etcetera. In these references for determination of sufficiently large disorientations ($\varphi > 20'$) it is recommended to use the diffractometric method, and for increasing the resolution by retaining a sufficient intensity of the bundle, it is recommended to set up a narrow slit on the x-ray tube.

3. Geometry of Glide

Glide is accomplished by the parallel displacement of one volume of the crystal relative to the other along predetermined planes and directions. The directions of the glide are always such that they are most densely packed with atoms, and the planes of glide, as a rule, are the planes with the greatest reticular density. This also follows from the formula [20], which can be rewritten in the form:

$$\tau = \frac{2G}{K} e^{-\frac{2\pi}{K}\left(\frac{a}{b}\right)}, \qquad (31)$$

where a is the interplanar spacing; $\bar{b}$ is the Burgers vector of complete dislocation.

From expression (31) it follows that the resistance to displacement is minimal in the planes with the densest packing of atoms (maximal value of a) in the direction of minimal displacement of the atoms. One exception to this rule involves the ion crystals with an NaCl-type lattice in which the glide occurs along the direction of least atomic density (110), and the glide plane (110) is not the plane of the densest packing. This is because in these crystals the electrostatic forces exert a resistance to glide along the planes (100). However at elevated temperatures and in ion crystals, as was shown on MgO in reference [83], gliding is observed along the densely packed plane (100).

As follows from Table 9 the effect of these or other glide systems in the general case depends on the type of crystal lattice, temperature, and deformation velocity.

In fcc metals the glide takes place as a rule along twelve different systems of $\{111\}\langle 110\rangle$. Only in aluminum, other than the octahedral, was there also observe glide along the systems $(100)\langle 011\rangle$. Data do exist which indicate that in polycrystalline copper with significant degrees of deformation gliding develops along the non-octahedral planes [76].

Table 9. Elements of Glide in Different Metals

Тип кристаллической решетки (1)	Металл (2)	Системы скольжения: при нормальных и низких температурах (4) (3)		дополнительные системы (5): при высокотемпературной деформации (6)		при высокоскоростной деформации (7)		Литература (8)
(9) Гранецентрированная кубическая	Al	(111)	$\langle 10\bar{1}\rangle$	(100)	$\langle 001\rangle$	—		[85]
	Cu	(111)	$\langle 10\bar{1}\rangle$	(100)	$\langle 011\rangle$	(100)	$\langle 001\rangle$	[101]
	Ni	(111)	$\langle 10\bar{1}\rangle$	—		—		
	Ag	(111)	$\langle 10\bar{1}\rangle$	—		—		
(10) Объемноцентрированная кубическая	α-Fe	(110)	$\langle 1\bar{1}1\rangle$	(110)	$\langle 1\bar{1}1\rangle$	(110)	$\langle \bar{1}\bar{1}1\rangle$	[105]
		(112)	$\langle 1\bar{1}1\rangle$	—		—		[85]
		(123)	$\langle 1\bar{1}1\rangle$	—		—		
	Mo	(112)	$\langle 1\bar{1}1\rangle$	(110)	$\langle 1\bar{1}1\rangle$	—		
	W	(112)	$\langle 1\bar{1}1\rangle$	—		—		
	Fe—Si	(110)	$\langle 1\bar{1}1\rangle$	—		—		
(11) Гексагональная плотноупакованная	Mg	(0001)	$\langle 11\bar{2}0\rangle$	$(10\bar{1}1)$ $(10\bar{1}0)$	$\langle 11\bar{2}0\rangle$ $\langle 12\bar{2}0\rangle$	$(10\bar{1}1)$ $(10\bar{1}0)$	$\langle 11\bar{2}0\rangle$ $\langle 11\bar{2}0\rangle$	[108; 109]
	Zn	(0001) (1122)	$\langle 11\bar{2}0\rangle$ $\langle 11\bar{2}3\rangle$	$(10\bar{1}0)$	$\langle 12\bar{1}0\rangle$	—		[33]

[Continued on next page]

[Continued from previous page]

Cd	(0001) (1122)	⟨11$\bar{2}$0⟩ ⟨11$\bar{2}$3⟩	(10$\bar{1}$0) (10$\bar{1}$1)	⟨1$\bar{2}$10⟩ ⟨1$\bar{2}$10⟩	— —	[94]
α-Ti	(10$\bar{1}$0) (0001) (10$\bar{1}$1)	⟨11$\bar{2}$0⟩ ⟨11$\bar{2}$0⟩ ⟨11$\bar{2}$0⟩	— — —		— — —	[95]
Zr	(10$\bar{1}$0) (10$\bar{1}$3)	⟨11$\bar{2}$0⟩	— —		— —	[272]
Be	(0001) (10$\bar{1}$0)	⟨11$\bar{2}$0⟩ ⟨11$\bar{2}$0⟩	(10$\bar{1}$0) (10$\bar{1}$1) (10$\bar{1}$2) (10$\bar{1}$3) (10$\bar{1}$4) (11$\bar{2}$1)	⟨11$\bar{2}$0⟩ ⟨11$\bar{2}$0⟩ ⟨11$\bar{2}$0⟩ ⟨11$\bar{2}$0⟩ ⟨11$\bar{2}$0⟩	— — — — —	[92]
Co	(0001)	⟨11$\bar{2}$0⟩	—		—	—

1. Type of crystal lattice
2. Metal
3. At normal and low temperatures
4. Glide systems
5. Additional systems
6. During high-temperature deformation
7. During high-velocity deformation
8. Literature
9. Face-centered cubic
10. Body-centered cubic
11. Hexagonal densely-packed

In order to examine the sequence of the development of glide in an fcc crystal during quasi-static deformation, we use a stereographic projection of the crystal (Figure 30). The axis of tension or contraction of the crystal may always be represented on this projection in the form of a point, the apexes of which are the projections of planes of the type (100), (110), and (111).

Let us assume that the axis of tension agrees with the projection of the direction [531] in a given crystal. Using the known expression for determining the cosine of the angle between the two crystallographic directions in a cubic crystal, we can determine the Schmid coefficient for different glide systems.

The respective computations for the case when the axis of tension coincided with the direction [531], are shown on Table 10.

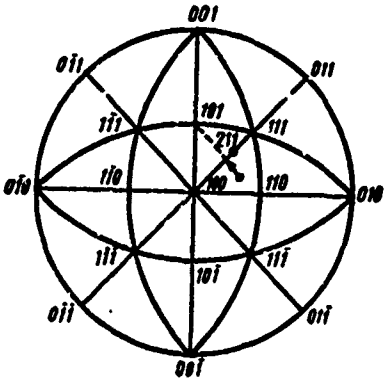

Figure 30. Stereographic projection of a crystal. The arrow shows the change in orientation of the sample during tension.

With the orientation of the crystal given on Figure 30 for all glide systems the Schmid factor is non-zero. However, glide in this crystal begins in the primary system, since the Schmid factor has a maximal value for it and here for the first time the stresses of the displacement exceed the critical value. Then the critical and conjugate systems enter into the effect. Glide along any of the systems [111]⟨110⟩ may be represented as the rotation around one of the axes ⟨112⟩. Thus, glide along the primary system leads to the rotation of the crystal and to change in the primary Schmid coefficients. As a result of this, after the primary one the glide begins along the conjugate plane.

Table 10. Computation of the Schmid Coefficients for Glide Systems During Orientation of the Crystal [531]

Элементы системы скольжения (1)		cos φ	cos λ	cos φ cos λ	Система (4)
плоскость (2)	направление (3)				
$11\bar{1}$	101	0,654	0,717	0,468	Первичная (5)
	011		0,479	0,313	
	$1\bar{1}0$		0,239	0,156	
$1\bar{1}1$	110	0,280	0,959	0,268	Сопряженная (6)
	011		0,479	0,134	
	$10\bar{1}$		0,479	0,134	
111	$10\bar{1}$	0,842	0,479	0,403	Критическая (7)
	$1\bar{1}0$		0,239	0,201	
	$01\bar{1}$		0,239	0,201	
$1\bar{1}\bar{1}$	101	0,093	0,717	0,067	Поперечная (8)
	$0\bar{1}1$		0,239	0,022	
	110		0,959	0,089	

1. Elements of the glide system
2. Plane
3. Direction
4. System
5. Primary
6. Conjugate
7. Critical
8. Transverse

If the glide takes place in one system, then the pole of the axis of tension moves in a great circle, approaching the direction of the glide. The displacement generated in this case is shown by the arrow; the change in orientation in this case is a function of the deformation.

However the direction of glide ⟨101⟩ will not be reached since the axis of tension at some stage of the deformation intersects the side (100)-(111) of the triangle and the stresses become equal to the primary and conjugate systems.

In this case the glide begins along both systems and the stage of multiple glide sets in. Multiple glide also changes the orientation of the axis of tension, by shifting it along the side of the triangle [100] and [111] in the direction of the axis ⟨211⟩.

It is significantly more complex to establish the effective glide systems in metals with a body-centered cubic lattice. Cox et al [84] assume that glide in alpha-iron may take place in any plane of the zone with the direction ⟨111⟩. But Burret et al [85] and Allen et al [86], observing the glide lines, came to the conclusion that glide takes place only along the planes (110), (112), and (123). Many researchers mention that there is a tendency to gliding along the planes (110) when the temperature is lowered below room temperature and the deformation velocity is increased. Such a discrepancy in the indexing is explained by the undulation in the glide lines (non-crystallographic type) in alpha-iron.

If the glide takes place strictly in one series of planes, then the glide lines are rectilinear. In the general case, the complex glide surface can be represented as consisting of a series of rectilinear segments, on each of which the glide takes place along a determined plane, and the direction of glide remains constant. Such glide is reminescent of the longitudinal shift in bundle of pencils, therefore it is called "pencil" glide. It takes place in the presence of several systems of glide having a common shift vector.

The appearance of undulating glide tracks is associated with the characteristics of dislocation in the alpha-zone. Fridel [87] showed that in pure bcc metals the dislocations are not split into partial ones and give no packing defects as in fcc crystals. The unsplit Burgers dislocations in first approximation have no primary plane for glide, therefore we can expect that they will be displaced in the planes with maximal effective shearing stresses independent of whether the given plane is more densely packed or not.

This was experimentally shown by Low and Guard on single crystals of an Fe-Si alloy [88]. They proceeded from the fact that the glide line is formed during the emergence of the dislocation loop to the surface of the crystal, here however they somehow took into account t. it the surface of the crystal is oriented with respect to to the Burgers dislocation vector. If the Burgers vector of the edge dislocation is perpendicular to the plane, then a step is generated -- the glide line; if it is parallel, then no step appears. The method of etching permitted finding the difference in motion of the edge and the Burgers dislocations in the bcc lattice. They found that on the surface perpendicular to the edge component of the dislocation, the glide lines are straight and correspond to the glide along the planes (011), and on the surface parallel to the edge com-

ponent the glide lines are undulating and here it is impossible to determine the preferred glide plane. On this surface the glide track may be formed only as a result of the emergence of the Burgers dislocations onto the surface. In this respect the authors came to the conclusion that the edge dislocations in bcc crystals are displaced only in certain crystallographic planes. The glide surface has an irregular shape and is not crystallographic because the Burgers dislocations may be displaced along any plane in the direction of the dense packing.

In hexagonal metals in addition to glide along the basal plane $(0001)\langle 11\bar{2}0\rangle$ glide is possible along the non-basal planes. Figure 31 schematically shows the possible planes and directions for glide for hexagonal densely-packed crystals. Under one and the same conditions of deformation in individual hexagonal densely-packed metals the preferred plane of glide is the basal plane (0001); in others it is the prismatic plane $(10\bar{1}0)$.

Table 11 gives the preferred planes of glide, experimentally determined critical stresses of displacement for the hexagonal densely-packed metals [89, 90], as well as the theoretically computed ones taking formula (31) into account and the values of the elastic constants of the ratio of stresses necessary for motion of the edge dislocation in the basal and prismatic planes [91].

The difference in the deformation characteristics of hexagonal densely-packed metals is usually associated with the change in the ratio c/a of the crystal lattice. If the lattice is stretched along the hexagonal axis in zinc and cadmium, then in beryllium, titanium, and zirconium, it is contracted. This contraction leads to a decrease in the distance between the basal planes, therefore in metals from cadmium to uranium the possibility of glide appears along the prismatic plane. One exception is beryllium [92], this not involving the influence of the impurities -- the purer the beryllium the more preferred is the basal plane.

The computed and experimentally determined ratios of the displacement stresses in the different planes do not coincide. In particular, computation shows that the Peierls stress in zirconium along the basal plane is less, however in practice glide along this plane is observed very rarely. Probably here the determinant role is played by the width of the split dislocations in the various glide planes, but because of the absence of reliable experimental data it is impossible to make any final conclusions at the present time.

It should be mentioned that in hexagonal densely-packed metals the effect is observed from a number of other

glide systems. At elevated temperatures glide may take place along the pyramidal plane $(10\bar{1}1)$ [90]. At low temperatures in zinc [93] the glide takes place along the plane $(11\bar{2}2)$ in the direction of non-dense packing $\langle 11\bar{2}3\rangle$; the effect of this system is also detected in cadmium [94].

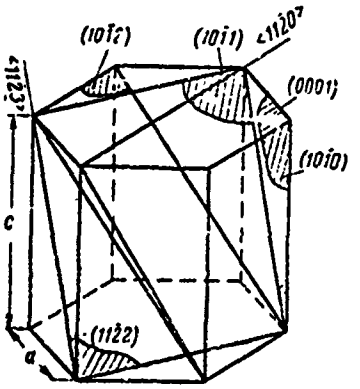

Figure 31. Most frequently encountered glide planes in metals with hexagonal densely-packed lattice.

Realization of these or other glide systems depends on the deformation conditions. The velocity and the diagram of the loading and the temperature of deformation may alter the effective glide planes (see Table 9).

Schmid showed that gliding in the crystal begins when the shearing stresses reach a certain critical value (τ_{cr}) along the direction of the glide for a given plane of the crystal. Hence it follows that if there are several crystallographically equivalent planes in the crystal, then the glide begins in the plane for which the shearing component of the stress is maximal. On the other hand, the effect of the determined planes of glide is associated with the fact that the critical displacement stresses for the various planes are different, as for example in hexagonal metals.

New systems of gliding by pulsed loading appear either as a result of increasing the critical displacement stress for several systems or as a result of change in the relationship between τ_{cr} for the various glide systems. Hence it follows that for understanding the mechanism of high-velocity deformation of metals we must examine the change in τ_{cr} by varying the conditions of the deformation and the physical nature of the critical displacement stress.

Table 11. Critical Displacement Stresses Along Different Planes of Several Metals With a Hexagonal Densely-Packed Lattice

(1) Металл	$\frac{c}{a}$	(2) Преимущественная плоскость скольжения	(3) Другие плоскости скольжения	(4) $\tau_{кр}$, Мн/м² (кгс/мм²)	(5) $\frac{\tau_{кр.\ баз}}{\tau_{кр.\ призм}}$ (эксп.)	(6) $\frac{\tau_{баз}}{\tau_{призм}}$ (теор.)
Cd	1,886	(0001)	(0001) (10$\bar{1}$0)	—	—	3 152
Zn	1,856	(0001)	(0001) (10$\bar{1}$1)	0,34 (0,0347) 9,81÷14,7 (1—1,5)	— 0,035÷0,023	0 305
Co	1,628	(0001)	(0001) (10$\bar{1}$0)	—	—	1,10
Mg	1,624	(0001)	(0001) (10$\bar{1}$1) (10$\bar{1}$0)	4,51 (0,46) 5,1 (0,52) 39,2 (4,0)	— 0,884 0,115	1,006
Re	1,615	(0001)	(0001) (10$\bar{1}$0)	— —	— —	0 978
Tl	1,598	—	—	—	—	5,58
Zr	1,593	(10$\bar{1}$0)	(0001) (10$\bar{1}$0)	— —	— —	0 902
α-Ti	1,587	(10$\bar{1}$0)	(0001) (10$\bar{1}$0)	62,0 (6,33) 13,8 (1,41)	4,5	1,35
Hf	1,581	(10$\bar{1}$0)	(0001) (10$\bar{1}$0)	— —	— —	,55
Y	1,571	(10$\bar{1}$0)	(0001) (10$\bar{1}$0)	— —	— —	1 288
Be	1,568	(0001)	(0001) (10$\bar{1}$0) (10$\bar{1}$1)	0,14 (0,0143) 56,4 (5,74) 194,5 (19,85)	0,038 0,001 —	2 001

1. Metal
2. Preferred plane of glide
3. Other glide planes
4. τ_{cr}, Mn/m^2 (kgf/mm^2)
5. $\frac{\tau_{cr\ bas}}{\tau_{cr\ prism}}$ (exp)
6. $\frac{\tau_{bas}}{\tau_{prism}}$ (theor)

4. Critical Displacement Stress

Experiments have shown that critical cleavage stresses depend on the impurities, and this dependence is due to the interaction between the components of the alloy in the solid state. In the formation of solid solutions the strengthening effect is significantly greater than in the case when the components are not soluble in one another.

It is interesting to note that the impurities influence the critical displacement stresses differently in the different planes. Churchman [95] showed that by increasing the amount of oxygen and nitrogen in titanium up to 0.1%, glide becomes possible along the planes $(10\bar{1}0)$, $(10\bar{1}1)$, and (0001) since the critical displacement stresses over all these planes become practically identical. Apparently the influence of the impurities on the magnitude of the critical cleavage stresses can be explained by the fact that the different researchers cite different values of this magnitude for one and the same metal.

Experiments have shown that the magnitude of the critical cleavage stress depends also on temperature, velocity and degree of deformation.

With increase in temperature the critical displacement stress, as a rule, is decreased, but not monotonically. There are temperature ranges, where τ_{cr} is lowered quite significantly and where this magnitude is practically constant. For example, at the melting point the critical displacement stress drops practically to zero, and at a temperature near absolute zero, it remains the same as at room temperature. The change in resistance to displacement as a function of temperature of deformation velocity is not identical for all planes of the crystal lattice.

Increasing the deformation velocity, as a rule, increases the critical displacement stress. Here for the non-basal plane the growth in τ_{cr} takes significantly more intensely than for the basal plane (Figure 32). In reference [90] a rather sharp dependence is noted of τ_{cr} on temperature for the non-basal plane and a weaker one for the basal plane.

The velocity dependence of the critical displacement stresses for a number of metals was investigated by the Japanese scientists Ioshida and Nagata [68, 96]. The magnitude of the critical displacement stress was determined by extrapolating the curve $\tau = f(\varepsilon)$, obtained during dynamic tests, to the zero degree of deformation. For single crystals

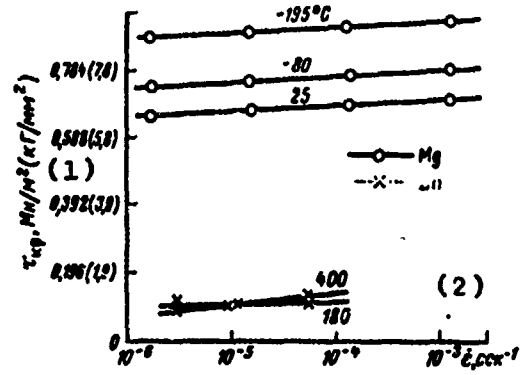

Figure 32. Dependence of critical displacement stress on velocity and temperature of deformation for several hexagonal densely-packed metals [127]: a. for the basal plane; b. for the prismatic plane.

1. τ_{cr}, Mn/m^2 (kgf/mm^2) 2. $\dot{\varepsilon}$, sec^{-1}

of aluminum τ_{cr} was found to equal 2.5-5 Mn/m^2 (0.25-0.5 kgf/mm^2); in the quasi-static tests τ_{cr} was 0.5-1 Mn/m^2 (0.05-0.1 kgf/mm^2). Interesting results were obtained on zinc crystal crystals. In the range of deformation velocities $\dot{\varepsilon} = 10^{-4}$-$10^{-1}$ sec^{-1} the critical displacement stress is practically independent of the deformation velocity. In the limits investigated by the authors the change in temperature exerts no influence on the critical displacement stress when $\dot{\varepsilon} < 10^{2}$ sec^{-1}, but it increases noticeably with growth in temperature at a deformation velocity $\dot{\varepsilon} = 10^{3}$ sec^{-1}.

Dependences which are analogous in character were obtained for pure copper and its alloys with 0.1, 0.5, and 1.1% Mn. In all cases during high-velocity deformation the critical stresses were greater than during quasi-static.

These experimental data can be explained after examining the processes of deformation carried out in the microvolumes. Glide, according to modern concepts, is the result of the displacement of dislocations under the influence of an external load, and the critical displacement stress is the stress required to overcome the dislocations in the glide plane in order that movement can begin. The effectiveness of the influence of the various factors on the resistance to displacement of the dislocations may be expressed in the following manner:

$$\tau_{cr} = \tau_1 + \tau_2 + \ldots + \tau_n, \qquad (33)$$

where $\tau_1, \ldots, \tau_n$ is the stress which should be applied for accomplishing any elementary process; each such process is determined by the conditions of the deformation and is characterized by the relaxation time in accordance with formula (19).

Let us cite the most important terms of the critical displacement stress that appear in expression (33), and the tendency to change of these quantities under conditions of a pulsed load application:

1. High-velocity deformation is accomplished by larger external forces than the usual quasi-static. Therefore we should expect that under these conditions of loading the number of effective sources in accordance with formula (25) will grow, since sources act here with a smaller initial length. Such a result, as mentioned above, was found by Ioshida and Nagata on aluminum single crystals. However the experiments of these same authors with zinc and copper indicate that the increase in critical displacement stresses during high-velocity deformation can never be explained only by the action of this effect.

2. The displacement of the dislocation is hindered by the force of friction (Peierls force) which may be figured from formula (31).

3. Probably one of the basic reasons for the change in critical displacement stress should be assumed as the increase in velocity of the mobile dislocations, and also their interaction with other dislocations and defects of the crystal lattice.

Increasing the applied stress, as already mentioned, increases the velocity of displacement of the dislocations.

Lyubov and Chernizer [31] theoretically computed the magnitude of the scattering of dislocation energy on heavy impurity atoms with increase in the dislocation displacement velocity. According to their data, the resistance of the lattice has a maximum at a certain sufficiently large velocity of motion of the dislocations. However, an increase in dynamic friction was observed also in quite pure metals.

Seger et al [98] assume that one of the basic factors determining the velocity and temperature dependence of the critical displacement stress is the interaction of the moving dislocations with a "forest" of dislocations. Thresholds are formed on the constrictions of the stretched dislocations as a result of which point defects are generated. For overcoming these barriers we must have either a thermal fluctuation or significant external stresses. Consequently, the magnitude of the displacement stresses is equal to

$$\tau = \tau_0 + \tau_s, \tag{34}$$

where τ_G is the stress counteracting the moving dislocation; it is caused by the long-range interaction of the field of stresses with the dislocations of the same system of glide on different glide planes; τ_s are the stresses necessary to overcome the moving dislocation of the local barriers.

Since the stress τ_s is connected with the thermally activating processes, it depends on temperature and velocity of deformation. The component τ_G does not depend on these parameters.

The relationship between the stress τ_s, temperature of deformation, and velocity $\dot{\varepsilon}$ is given by the following expression:

$$\dot{\varepsilon} = NA\bar{b}\nu_0 \exp\left\{\frac{U_0 - v\tau_s}{kT}\right\}, \tag{35}$$

where N is the density of forest dislocations, intersected by the moving dislocation; A is the mean area of propagation of the moving dislocation; $\bar{b}$ is the Burgers vector of the intersecting dislocation; ν_0 is the frequency of oscillations of the dislocation; U_0 is the activation energy; v is the activating volume; k is the Boltzmann constant.

Taking into account the interaction of the dislocations with the point defects, the processes of formation of the constrictions of the dislocations, and thresholds of intersection, reference [98] gives the following expression for τ_s:

$$\tau_s = \frac{U_0 - kT \ln \frac{\dot{\varepsilon}_0}{\dot{\varepsilon}}}{\frac{3}{2} bd \sqrt[3]{G \frac{b}{N}}}, \qquad (36)$$

where $\dot{\varepsilon}$ is the deformation velocity; d is the mean effective diameter of the "barrier", which is overcome with the aid of the combined effect of thermal fluctuations and applied stresses.

At temperatures of $T > T_0$, where

$$T_0 = \frac{U_0}{k \ln \frac{\dot{\varepsilon}_0}{\dot{\varepsilon}}},$$

the magnitude of τ_s is small and the flow stress $\tau = \tau_G$.

Seger et al cite a series of experiments with magnesium, aluminum, and silver, the results of which agree with their theory. Other experimental data are contradictory and do not permit accurately determining the regions of applicability of formula (36). Probably this model is applicable to flow stresses during large deformations, where the role of interaction between dislocations is signifantly increased.

Thus, at the present time there is no common theory which satisfactorily explains the change in critical displacement stresses with increase in deformation velocity. At the same time we can apparently state that the significant amount of increase in displacement stress during high-velocity deformation is associated with change in the dynamic resistance of the lattice during increase in the dislocation velocity. Thus the experiments of Ferguson et al [99] showed that the displacement stress along the basal plane of zinc grows linearly with increase in dislocation velocity in the range $\dot{\varepsilon} = 5.10^3$-$10^4$ sec^{-1}. Along with this, it is still not clear as to the quantitative contribution from the various factors to the velocity dependence of the

critical cleavage stress, and also the reasons for the different change in τ_{cr} under the influence of velocity for the various systems.

5. Experimental Study of Gliding

Glide in crystals having an fcc lattic[illegible]s been studied most fully. As shown above the amount of the critical cleavage stress is identical for all planes (111) usually participating in the deformation, therefore the glide begins in the plane that is most favorably oriented with respect to the effective stress.

Change in orientation of single crystals of nickel under conditions of quasi-static and high-velocity deformation was studied by Epshteyn and Kazachkov [100]. The deformation of samples was accomplished on a 5-ton press at a velocity of $\dot{\varepsilon} = 10^{-2}$ sec^{-1} and by the method of electromagnetic punching [20] at $\dot{\varepsilon} = 10^{3}$-$10^{4}$ sec^{-1}. The axis of contraction of the samples corresponded to t[illegible]e directions ⟨110⟩, ⟨111⟩, and ⟨112⟩.

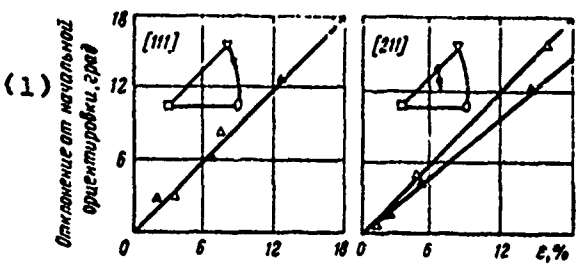

Figure 33. Change in orientation of nickel single crystals after quasi-static (Δ) and high-velocity (▲) deformation.

1. Deviation from initial orientation, deg

Orientation of the crystals ⟨111⟩ and ⟨112⟩ under conditions of high-velocity deformation varies differently (Figure 33): for orientation of ⟨111⟩ if the rotation of the crystal lattice with increase in the degree of deformation does not depend on the type of load, then for ⟨112⟩ during high-velocity deformation this rotation is less than during the quasi-static. Such a difference in the change in orientation involves the glide characteristics. During the deformation of a single crystal with the axis of contraction ⟨111⟩ there are six equivalent glide systems with the Schmid factor equal to 0.27 (Table 12). For the other systems

it is equal to zero. Thus, for a crystal with such orientation the glide is begun immediately over all systems and therefore the change in orientation with increase in degree of deformation does not depend on the type of load. If the axis of contraction corresponds to the direction ⟨112⟩, then the Schmid factor is maximal for the primary and the conjugate systems and is equal to 0,409; for four of the systems it comprises 0,273, and for two -- 0.137.

If we assume that during quasi-static deformation the glide takes place along the primary and conjugate systems, then the decrease in rotation of the crystal under a dynamic load must be associated with the increase in number of effective systems of glide. Probably, in the dynamics of glide, the other planes in which the Schmid factor is nonzero are also involved.

Table 12. Values of the Schmid Orientation Factor for Crystals Oriented Differently to the External Load

(1) Системы скольжения	cos φ cos λ для ориентировки кристаллов (2)			(1) Системы скольжения	cos φ cos λ для ориентировки кристаллов (2)		
	[110]	[111]	[112]		[110]	[111]	[112]
$(11\bar{1})$ $[101]$	0,41	0,27	0,406	$(1\bar{1}1)$ $[\bar{1}\bar{1}0]$	0	0,27	0,406
$(11\bar{1})$ $[\bar{1}\bar{1}0]$	0	0	0,136	$(1\bar{1}1)$ $[\bar{1}01]$	0	0	0,136
$(11\bar{1})$ $[011]$	0,41	0,27	0,273	(111) $[011]$	0	0,27	0,273
(111) $[\bar{1}\bar{1}0]$	0	0	0,273	$(1\bar{1}\bar{1})$ $[\bar{1}\bar{1}0]$	0	0,27	0
(111) $[10\bar{1}]$	0,41	0	0,273	$(1\bar{1}\bar{1})$ $[101]$	0	0,27	0
(111) $[01\bar{1}]$	0,41	0	0	$(1\bar{1}\bar{1})$ $[01\bar{1}]$	0	0	0

1. Glide system
2. cos φ cos λ for orientation of the crystals

Reference [100] showed also that the change in width of the x-ray line, the subgranular disorientation, and the microhardness of crystals for these two orientations also differs depending on the deformation method (Figure 34). For a crystal contracted in the direction ⟨112⟩, these characteristics after pulsed deformation are higher than after the quasi-static, and for a crystal contracted in the direction ⟨111⟩ they are virtually the same as those obtained after quasi-static deformation. These results also involve the mechanism of glide which in the given case produces the formation of a substructure.

The effect of these or other glide systems depends on the orientation of the single crystal with respect to the

shock wave. Thus in single crystals of copper [101] under a load by a shock wave of 200 kbar in the direction ⟨110⟩ multiple gliding takes place in the plane (111), and under a load by a shock of the same intensity in the direction ⟨111⟩ along with the octahedral planes the non-octahedral planes (100) participate in the glide. Reference [75] showed the possibility of non-octahedral glide in copper with high degrees of deformation.

In reference [102] the mechanism of high-velocity deformation was studied by detonation punching (see Figure 4). Under these conditions a pressure is developed up to several kilobars and at the same time no significant heating occurs. On polycrystalline samples having different grain orientation, the geometric interpretation of glide was made difficult by the simultaneous effect in one grain of many glide planes of one and the same type. In copper after rolling and subsequent recrystallization it was found to be possible to obtain a grain with dimensions of about 150 μm and a sharp orientation. The maximal angle of scattering of the orientation, figured from the pole figure, was ±8°, but the difference in orientation between neighboring grains, determined from the etching holes, was no more than 5°. Such orientation of the crystals permits us to treat the boundaries between them as boundaries of the slope. The existence of a sharp orientation and large grain with a small sheet thickness (in cross section, five-six grains) indicates that the deformation of such polycrystalline samples is similar to the deformation of single crystals of the same orientation.

Investigations showed that both during quasi-static and during pulsed deformation the glide is accomplished along the planes (111). The glide lines are oriented parallel to the diagonal of the square of the etching hole, which corresponds to the intersection of the glide plane (111) with the surface of the sample, corresponding to the plane (100). After hydrostatic punching prior to deformation of 12% an optical and interference microscopic investigation showed that the glide goes only in one plane (Figure 35). It is characterized by long straight bands, common for several grains. The glide bands pass through the grain boundary, only slightly changing its direction in accordance with the orientation of the neighboring grain. The grain boundaries are not a place where the glide bands preferentially begin or end, i.e., the deformation is easily transmitted from one grain to another. The boundaries of the slope, which in the given case are grain boundaries, present a less effective barrier for the moving dislocation than for the individual slowed-down dislocation in the glide plane. This was confirmed experimentally in reference [103].

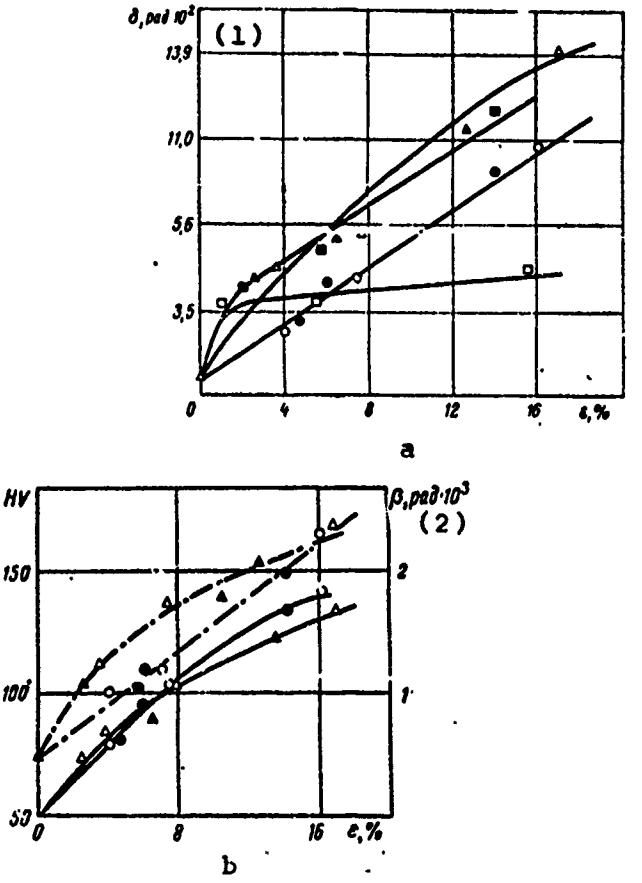

Figure 34. Dependence of the subgranular disorientation (a), hardness -- the dotted lines -- and broadening of the x-ray lines (222) -- the solid lines (b) of single crystals of nickel ▲△[111]; ■□[112]; ●○ [110]. The light circles represent quasi-static deformation and the dark ones represent high-velocity deformation.

1. δ, rad.10^2 2. β, rad.10^3

The density of the glide bands and the height of the step grow with increase in the degree of deformation, whereas the length of the glide bands changes insignificantly (Table 13). Consequently, the increase in deformation is determined not only by the increase in the step on the existing bands, but also by the generation of new glide bands.

Figure 35. Glide lines in copper after hydrostatic loading ε = 12%. X 500.

Electron microscopic investigations of the images show that between the glide bands there is always a microglide which is not resolvable in the optical microscope.

Study of the images obtained after hydrostatic deformation of copper confirmed the fact that up to 6-7% deformation only one glide system has an influence (Figure 36 a). However when $\varepsilon > 7\%$ this method permitted clarifying the effect of the second glide system, buts contribution to the overall deformation is still insignificant. Even when ε = 13%, when the glide tracks in the primary plane are grouped into bands with a sufficiently large height of the step, in the second plane only individual microglide tracks are observed (Figure 36 b). The results of the electron microscopic investigations and the measurement of the glide parameters (see Table 13) permit us to assume that a hydrostatic deformation up to 7% corresponds to the first stage of the deformation of single crystals of copper.

During hydrodetonation and electromagnetic punching of copper the deformation begins with glide, immediately in at least two systems. Even with the very smallest degrees of deformation when the glide lines are not visible in an optical microscope, the electron microscopic investigation reveals two systems (Figure 37 a). When ε = 5-6% the two systems of glide tracks are detected already by metallographic investigation (Figure 37 b). The glide bands after hydrodetonation and electromagnetic deformation are shorter than during the hydrostatic, and their mean length is decreased with increase inthe degree of deformation, which is undoubtedly associated with the effect of the secondary glide systems (see Table 13). The density

Table 13. Quantitative Characteristics of Glide Tracks in Copper Deformed at Different Velocities

Деформация (1)	$\dot{\varepsilon}$, $сек^{-1}$ (5)	ε, %	Высота ступеньки, мкм (6)		Расстояние между полосами скольжения, мм (9)		Длина полос скольжения, мкм (12)	(13) Расстояние между линиями скольжения в электронном микроскопе, нм (Å)
			I плоскость (7)	II плоскость (8)	I плоскость (10)	II плоскость (11)		
Гидростатическая (2)	10^{-3}	3	0,03	—	0,048	—	275	53 (530)
		5	0,03	—	0,032	—	300	40 (400)
		9	0,048	—	0,0016	—	275	27 (270)
		11	0,081	—	0,0015	—	270	27 (270)
Гидровзрывная (3)	10^{4}	3	0,03	0,03	0,07	(,080	160	62 (620)
		5	0,03	0,03	0,052	(,070	170	—
		9	0,04	0,032	0,0021	(,0036	120	—
		12	0,10	0,082	0,0015	(,0027	90	—
Электромагнитная (4)	10^{6}	6	0,40	0,03	0,06	(,072	115	—
		9	0,62	0,05	0,002	0,003	100	—
		13	0,120	0,09	0,0014	(,0024	85	—

1. Deformation
2. Hydrostatic
3. Hydrodetonation
4. Electromagnetic
5. $\dot{\varepsilon}.sec^{-1}$
6. Height of step, μm
7. Plane I
8. Plane II
9. Distance between glide bands, mm
10. Plane I
11. Plane II
12. Length of glide bands, μm
13. Distance between glide lines in the electron microscope, nm (Å)

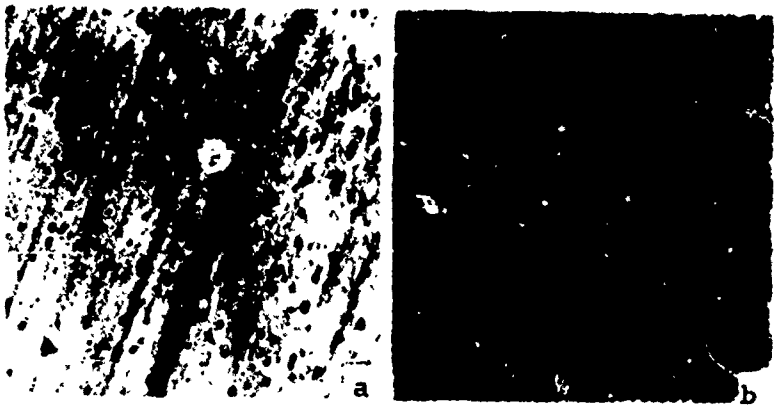

Figure 36. Glide tracks in copper after hydrostatic loading, revealed by electron microscope: a. ε = 6%; b. ε = 13%; X 25,000.

of the glide bands and the height of the step grow with increase in the degree of deformation. Since there is a slight difference in the height of the steps and the distance between individual bands for the two glide systems, it is then obvious that they are not equal in value and make a different contribution to the overall deformation. Between the bands there is always a microglide, which is easy to see on the interferograms and the electron microscopic photographs.

On the surface of the sample corresponding to the plane (100), we can observe glide tracks over all four planes. Two groups of these tracks must be parallel to each other, and two groups perpendicular to them. However with a slight deviation from the strict orientation (100) the parallelness of the glide tracks is disrupted, which permits us to accurately determine the number of effective glide systems. During hydrodetonation and electromagnetic punching deviations were often observed from the parallelness of glide tracks within a single grain (see Figure 37 b). From this it follows obviously that during pulsed deformation all four glide planes are activated.

As we know, transition from the first deformation stage of single crystals to the second involves the effect of secondary glide planes. If during quasi-static loading up to ε = 5-6% the deformation is similar to the first deformation stage of the single crystals, then we can assume that during pulsed deformation the first stage is suppressed and the second stage begins immediately. Under the effect of the secondary glide systems, which is usually noted during the transition from the first to the second deformation stage,

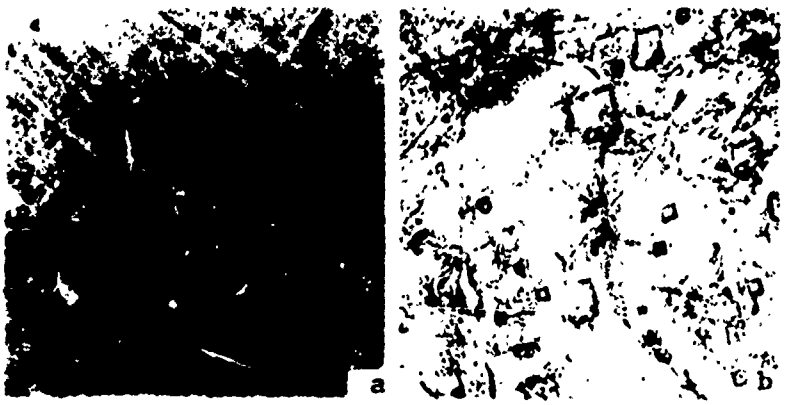

Figure 37. Glide tracks in copper after high-velocity deformation. a. ε = 2%. X 25,000; b. ε = 5%. X 500.

as a result of the interaction of dislocations of the primary and secondary systems, barriers are generated at which pile-up of the dislocations of the primary glide system is possible. Therefore transition to the secondary deformation stage is accompanied by a sharp increase in the coefficient of strengthening.

The glide parameters given on Table 13 for various conditions of deformation should be treated as the results of the dislocation processes. By analyzing these data, we can get some idea as to the characteristics of these processes during quasi-static and dynamic deformation.

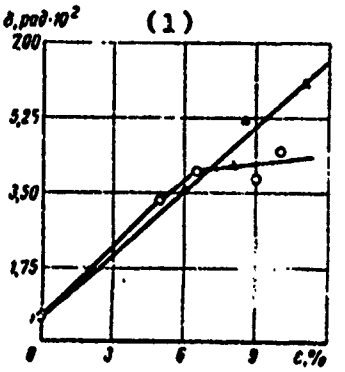

Figure 38. Change in the subgranular disorientation in polycrystalline copper after hydrostatic ▲ and detonation (o) loading.

1. δ, rad.10^2

During pulsed loading with increase in the degree of deformation the length of the glide bands is decreased. Consequently, the mean length of the free path of the dislocations during pulsed deformation is two-three times less than during quasi-static. Probably this is involved with the fact that during pulsed loading of copper the number of barriers which inhibit motion of the dislocations is increased, and they are arranged at a smaller distance from one another.

The density of the glide tracks during pulsed deformation is higher than during the quasi-static; this means that the density of the dislocations may be greater, especially if we take into account that during pulsed deformation the glide takes place immediately over several planes.

Ioshida and Nagata studied the mechanism of deformation by contraction on single crystals of aluminum, 99.999% pure. The deformation velocity was about 10^2 sec^{-1}. In crystals oriented favorably for individual gliding, the critical displacement stress during dynamic deformation was greater than during quasi-static, and at the same time the region of easy glide was more extended. At this stage of increase in the deformation velocity only the number of dislocations of the given system which participate in the deformation is increased, as a result of which the density of the glide tracks grows and the height of the step is decreased.

Simultaneously with the metallographic investigation we conducted a radiographic determination of the subgranular disorientation $\bar{\delta}$ with ionization registration of the reflections using the method described in reference [82].

Figure 38 shows the results of the experiment. During hydrodetonation deformation the disorientation is increased linearly with increase in the degree of deformation, and during quasi-static deformation the linear growth in disorientation takes place only up to $\varepsilon = 7\%$, and then the rate of this growth is significantly lowered. Such a change in the disorientation agrees well with the metallographic data on the mechanism of deformation of copper. The bend in the lattice in the process of deformation may be represented as a process of pile-up of dislocations on one sign. During detonation deformation several planes participate directly in the glide; the number of these planes does not vary with increase in ε; this also leads to a monotonic dependence of the disorientation on the degree of deformation in the entire investigated range. During static deformation up to $\varepsilon = 6\%$, as shown above, one glide plane exerts influence; here dislocations of one sign are generated. As a result the total bend in the lattice grows linearly with ε,

and the amount of disorientation is even slightly higher than after hydrodetonation deformation in spite of the large total density of dislocations after pulsed punching. When $\varepsilon > 7\%$ secondary planes are involved in the quasi-static deformation, in which dislocations of the other sign may be generated. As a result the rate of growth in the total bend of the lattice is decreased and correspondingly the character of the change in subgranular disorientation changes.

Thus, both analysis of the x-ray data and the direct metallographic observations confirm the conclusion as to an increase in the number of effective glide systems in copper during pulsed deformation in comparison with the quasi-static.

The formation of orientation of a material is directly connected with glide and twinning. In those cases when no twinning is accomplished, we can assume that the formation of an orientation, change and smearing of the orientation maxima are determined by gliding. All this refers completely to copper deformed under the conditions examined. Since at a pressure of 3-5 kbar, no twinned layers are formed, the authors studied the change in initial orientation of the sheets as a result of detonation and hydrostatic deformation.

Figure 39 shows the pole figure of samples in the initial state (prior to punching) on which two components of orientation are visible: (001) $\langle 100 \rangle$ and (123) $\langle 1\bar{2}1 \rangle$, the component (001) $\langle 100 \rangle$ being the preferred one. Such a type of orientation is characteristic of recrystallized copper, since at the first stage of recrystallization part of the grains retain their orientation near the rolling orientation.

In the process both of hydrostatic and dynamic deformation the form of the pole figure changes.

We undertook an experiment to figure the number of effective glide systems based on change in orientation in the deformation process. We can assume that in the original samples the stress acts in the direction $\langle 001 \rangle$ and then we can compute the Schmid factor for the various glide systems and the displacement of the orientation factor as a result of glide in the given system. Here we must take into account that gliding in the plane along the predetermined direction is equivalent to rotating the crystal around the normal to the plane and to the direction of glide. Then glide over systems $\{111\} \langle 1\bar{1}0 \rangle$ can be represented as the rotation of a crystallite around the direction $\langle 112 \rangle$.

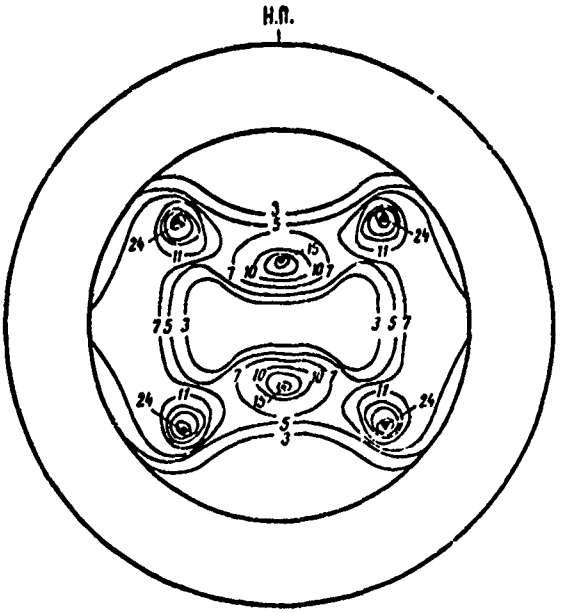

Figure 39. Pole figure (111) of sheet copper in the original state.

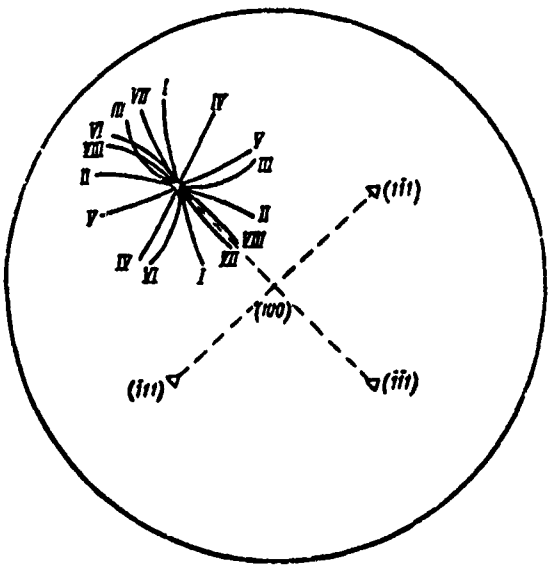

Figure 40. Great circle of the stereographic projection; displacement of the orientation maximum (111) as a result of glide over different systems (111) $\langle 1\bar{1}0 \rangle$. The number on the drawing corresponds to the glide systems given in Table 14.

Table 14 gives the result of such an analysis for the original cubic orientation.

Figure 40 shows a diagram that indicates the direction of displacement of the orientation maximum (111) as a result of glide over the cited systems. From the pole figures taken from the original and the deformed samples (Figures 39 and 41), it is clear that the resulting displacement is directed toward the center of the pole figure. This permits determining the probable glide systems. The preferred effect of one glide system, for example $(\bar{1}11)\langle 0\bar{1}1\rangle$ -- VII, or $(\bar{1}\bar{1}1)\langle 101\rangle$ -- VIII, produces a rapid disruption of the original orientation and the creation of a new one. In the presence of multiple glide the change in the pole figure will be less directed and the rate of the creation of a new orientation will be less since the resulting displacement with identical ε is not high. Analysis of the change in the pole figures showed that during quasi-static and pulsed deformation the glide in copper takes place over the systems $\{111\}\ \langle 1\bar{1}0\rangle$, but during pulsed deformation in each individual grain a large number of uniform glide systems has influence.

Table 14. Schmid Coefficients for Various Glide Systems in Copper Under the Effect of Loading in the Direction $\langle 001\rangle$

Система (1)	Плоскость скольжения (2)	Направление скольжения (3)	Исходная ось вращения (4)	$\cos\psi\cos\lambda$ (5)
—	(111)	$1\bar{1}0$	$\bar{1}\bar{1}2$	0
I		$10\bar{1}$	121	0,405
II		$01\bar{1}$	211	0,405
—	$(\bar{1}11)$	110	$1\bar{1}2$	0
III		$0\bar{1}1$	211	0,405
IV		101	$12\bar{1}$	0,405
V	$(1\bar{1}1)$	011	$21\bar{1}$	0,405
VI		$10\bar{1}$	121	0,405
—		110	$\bar{1}12$	0
VII	$(\bar{1}\bar{1}1)$	011	$2\bar{1}1$	0,405
VIII		101	$\bar{1}21$	0,405
—		$1\bar{1}0$	112	0

1. System
2. Glide plane
3. Direction of glide
4. Original axis of rotation
5. $\cos\psi\cos\lambda$

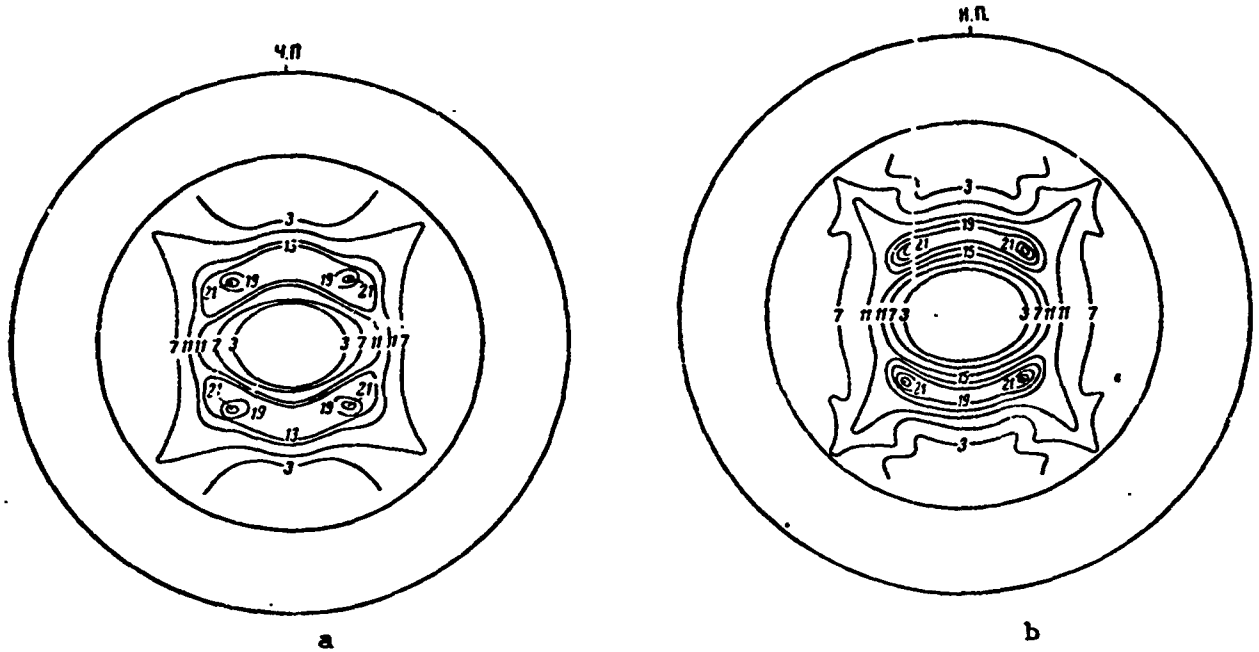

Figure 41. Pole figures of the line (111) of copper. a. after hydrostatic deformation; b. after detonation deformation.

Reference [104] mentions the sharp change in the pole figure during dynamic deformation of the alloy Fe-Si in comparison with the quasi-static and the formation of a new type of orientation (001) ⟨210⟩. This difference, in the opinion of the authors, involves a decrease in the number of glide systems during dynamic deformation.

However, as analysis shows, changing only the number of effective glide systems may lead to more or less intense smearing of the orientation maxima and almost never leads to formation of a new orientation. The change observed in reference [104] in the pole figure of the iron-silicon alloy, as a result of pulsed deformation, is primarily associated with the development of twinning.

In studying the mechanism of deformation of medium-carbon steel, Campbell [105] detected multiple glide in a sample deformed at a low velocity. During impact loading he noticed only a fine gliding along several systems, analogous to the gliding in samples deformed quasi-statically at low temperatures. According to these data the glide lines during impact loading become rectilinear.

Leslie [106] showed that the configuration of dislocations in alpha-iron after detonation deformatio is similar to that which is generated after rolling at low temperature. The dislocation lines are straight and uniformly distributed.

Odinokova and Bogachev [107] observed a sharp change in the plasticity of beta-titanium during high-velocity deformation. At ordinary deformation velocities the glide lines in beta-titanium are undulating, they appear in several directions with the preferred development of one direction. The basic mechanism of deformation of the alloy under these conditions is pencil gliding along many planes.

Under the conditions of dynamic tension in beta-titanium the density of the glide tracks is reduced significantly and their form is changed. The glide tracks become rectilinear in each grain and go only in one direction. Only on individual grains does the glide take place along two systems.

Based on these results, the authors come to the conclusion that during dynamic loading the number of active glide planes for metals with a bcc lattice is decreased.

As we shall show in Chapter 5, the dislocation structure of metals and alloys with a bcc lattice after impact loading differs substantially from the structure of metals

with an fcc lattice. In metals with a bcc lattice the dislocations are distributed uniformly and in metals and alloys with an fcc lattice a cellular structure is formed.

The lack of undulation in the glide tracks in metals with a bcc lattice during pulsed loading probably is due to the difference in the velocity of dislocation displacement of the various types. It is mainly the Burgers dislocations which produce the appearance of undulating glide tracks in the bcc lattice. During pulsed loading a large part of the deformation takes place as a result of the motion of the edge dislocations, therefore the displacement producing the formation of glide tracks is the result of displacement of the edge dislocations. The emergence of the edge dislocation onto the surface also leads to the onset of rectilinear glide lines.

Thus, the lack of undulating glide tracks during high-velocity deformation of metals with a bcc lattice still does not indicate a decrease in the number of effective active glide planes.

During impact loading the deformation mechanism of metals with a hexagonal densely-packed lattice changes significantly [97, 108], however, the conditions for this change for the various metals may be different.

In tests with technical titanium type VT-1 we used deformation velocities of 10^{-3} and 10 sec^{-1} [97]. When $\dot{\varepsilon} = 10^{-3}$ sec^{-1} the glide is developed in one plane, when the degree of deformation is 4-5%, with increase in this same ε up to 15-17% the glide begins to take place in three-four planes, here in several of the grains twinning is observed. In samples deformed at a velocity of 10 sec^{-1}, the glide also takes place along many planes and twinning is greatly facilitated in them. During hydrodetonation punching in alpha-titanium, no intragranular glide in general appears and the deformation is basically accomplished as a result of twinning.

Investigation of alpha-titanium showed that during deformation at low velocities the glide takes place preferentially along the prismatic planes. However already under these conditions of loading the development of multiple glide is observed. Undulating glide tracks appear, intersecting at an angle of 60°, which corresponds to gliding over the prismatic and pyramidal planes simultaneously. There are glide tracks that intersect at an angle of 90°, which is possible by the combined effect of the prismatic and basal glide. The multiple glide takes place at comparatively large degrees of deformation.

Odinakova and Bogachev [107] observed twinning during the dynamic deformation of alpha-titanium ($\dot{\varepsilon} = 10^2$ sec^{-1}), but the form of the glide tracks were practically the same as during quasi-static deformation. At the same deformation velocity in an alloy on a base of alpha-titanium no twinning was developed, and the glide takes place over many planes. However the density of the glide tracks during dynamic loading is decreased in comparison with the quasi-static, and the relief over the grain boundaries is revealed better. The authors also mention that during the impact loading of alpha-titanium the deformation is accomplished preferentially by twinning.

Figure 42. Microstructure of the alloy MA-8: a. after quasi-static deformation ($\dot{\varepsilon} \approx 10^{-3}$ sec^{-1}). X 600; b. after high-velocity deformation ($\dot{\varepsilon} \approx 10^4$ sec^{-1}). X 1200.

The behavior of magnesium and its alloys is interesting during high-velocity deformation [108, 109]. The fact is that under normal deformation conditions in magnesium (unlike titanium) the glide takes place along the basal plane (0001). But with hydrostatic punching of sheets of polycrystalline magnesium and its alloy MA-8 the intragranular glide is expressed very weakly. Only when $\varepsilon > 4\%$ can the glide tracks be seen along the basal plane, and no intragranular glide along the nonbasal planes appears (Figure 42 a).

During hydrodetonation punching of these same materials the deformation mechanism becomes quite different -- the role of the intragranular gliding and twinning grows. Intragranular glide appears as multiple, and within one grain the glide takes place both along the basal and the non-basal planes. The tracks of the non-basal glide are

expressed very sharply (Figure 42 b) and correspond to the glide over the pyramidal planes of the system $(1\bar{1}01)\langle 11\bar{2}0\rangle$. The tracks of the prismatic glide are often arranged in the boundary region or at the junction of several grains (Figure 43). Probably the appearance of prismatic glide stimulates the local concentration of stress at the grain boundaries. The lines of prismatic glide, as a rule, have the form of pencil gliding. With large increases it is possible to detect that they consist of short tracks of alternate glide along the basal and pyramidal planes, as is shown schematically on Figure 43. The height of the steps on the glide lines of different planes is different. This also explains the difficulty of their simultaneous focusing during photographing.

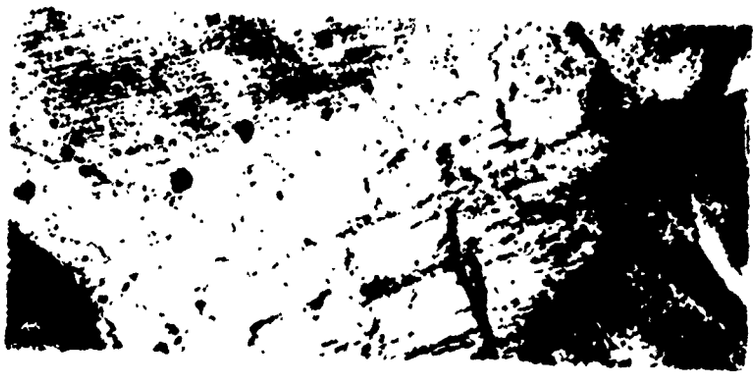

Figure 43. Prismatic glide in the MA-8 alloy after high-velocity deformation. X 600.

Figure 44. Hultiple intragranular glide in the MA-8 alloy along the basal and non-basal planes during detonation deformation. X 600.

On Figure 44 we can clearly see the glide over all three planes. In the body of the grain the gliding takes place over the basal and pyramidal planes, and in the boundary region it is still over the prismatic planes. In this same grain we can see the deformation twins which intersect with the glide lines.

Thus, unlike alpha-titanium, in the MA-8 alloy after dynamic loading the undulation of the glide tracks does not disappear, but rather appears. Consequently, under one and the same regimes of dynamic loading, the deformation mechanism changes differently.

Interesting results were obtained in reference [110] by studying the pulsed deformation of single crystals of MgO. Just as in ion crystals with an NaCl-type lattice,

Figure 45. Hultiple glide in MgO by pulsed deformation [110]. The plane (110) corresponds to the plane of the thin section.

glide in these crystals under ordinary deformation conditions is accomplished along the densely packed direction ⟨110⟩ and along the planes $(1\bar{1}0)$. Klien and Edington investigated the deformation of MgO crystals after contact detonation. The single crystals were cut along the planes (100), (110), and (111) and deformed between lead sheets so that the plane of the shock wave with a pressure of 47-80 kbar was approximately parallel to the directions ⟨100⟩, ⟨110⟩, and ⟨111⟩. To identify the effective glide planes they used an electron microscopic investigation of the thin foils by transillumination.

It was found that in the direction ⟨100⟩, in addition to the ordinary glide along the planes (110), an effect

from additional planes of the set (111) is observed. The authors mention that in this case the glide along (110) is still preferential. The shearing stresses acting in the system (110) $\langle 1\bar{1}0\rangle$ may be significantly decreased by changing the orientation of the crystal with respect to the effective force. For crystals oriented with the direction $\langle 100\rangle$, $\langle 110\rangle$, and $\langle 111\rangle$ along the front of the shock wave, the shearing displacement stresses in the system (110) $\langle 1\bar{1}0\rangle$ comprise 0.56σ, 0.25σ, and 0, respectively, where σ characterizes the amount of stress applied.

Consequently, the potentially possible glide systems may be revealed by the effect of the shock wave in the directions $\langle 110\rangle$ and $\langle 111\rangle$ of the crystal. In fact, application of a load along these directions permitted finding still another series of planes acting under the conditions of pulsed loading.

Figure 45 shows the form of the glide tracks on the plane (110) for MgO crystals subjected to impact loading along the direction $\langle 110\rangle$. Identification of the glide tracks showed that in pulsed loading of the MgO crystals the glide is developed along the planes (100), (110), and (112). For crystals deformed in the direction $\langle 111\rangle$ glide was also detected along the plane (112). Regardless of the effective glide plane, the direction of the glide remained as $\langle 110\rangle$. Glide over the system (110) $\langle 1\bar{1}0\rangle$ was observed even when the shock wave acted along the $\langle 111\rangle$, although in this case the critical displacement stress for the plane (110) was equal to zero. The authors associate this with the action of the reflected shock wave.

Thus, by high-velocity loading of the MgO crystals a tendency appears quite distinctly to multiple glide.

In general form any metal can be characterized [111] by a set of glide planes $(h_1k_1\ell_1)$, $h_2k_2\ell_2)$,..., $(h_nk_n\ell_n)$ with the corresponding values of the critical cleavage stresses

$$\tau_1, \tau_2, \ldots, \tau_n, \tag{37}$$

and also with the twinning planes

$$(h_1'k_1'l_1'), (h_2'k_2'l_2') \ldots (h_m'k_m'l_m')$$

and the critical stresses for twinning corresponding to them

$$\tau_1', \tau_2' \ldots \tau_m'. \qquad (38)$$

Then the deformation can be treated as a relaxation process, accomplished successively along those glide and twinning planes for which the value of τ_{cr} is reached at a given moment. If we know (37) and (38), we can compile the series:

$$\tau_1, \tau_2 \ldots \tau_n, \tau_1', \tau_2' \ldots \tau_m' \qquad (39)$$

where

$$\tau_1 < \tau_2 < \tau_n < \tau_1' < \tau_2' < \ldots \tau_m'.$$

From (39) we can represent the character of the change in the deformation mechanism of a metal with increase in the effective stress. The diagram on Figure 46 shows that in the general case there may be four stages in the change of the deformation mechanism with growth in velocity deformation. The extent of each stage is determined by the relationships between the previous and subsequent terms of the series (39). On the basis of such an approach we can examine the possible change in the deformation mechanism during pulsed loading of metals of different types of lattices.

In metals with an fcc lattice the glide planes of the set (111) are active, therefore in them the transition from single glide to multiple takes place easily. In these metals τ_1 and τ_2, τ_3, and τ_4 are identical and the development of multiple glide is determined by the increase in the effective forces of the value of τ_{cr} allowing for the Schmid factor. Thus, in the case of deformation of polycrystals with an fcc lattice at low velocities (P_2 is small) the glide takes place over many octahedral planes. With increase in the pressure during transition to pulsed loads in a significant range of deformation velocities the deformation mechanism is actually unchanged, since the relaxation of stresses as a result of gliding along the planes (111) is high, and the difference between τ_{cr} for the octahedral and the non-octahedral planes is significant. These metals have little sensitivity to increase in the deformation velocity in a significant range of deformation velocities. In principle also in these metals, beginning from a certain value of P_2 the glide must take place along the non-

octahedral planes. However if $\tau_{cr}^{non\text{-}oct}$ is found to be larger than τ_{cr}^{twin} for a given fcc metal, then the development of relaxation of stresses as a result of twinning may lead to the non-octahedral planes not participating in the deformation.

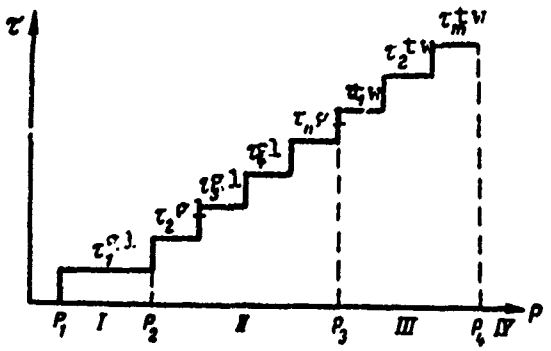

Figure 46. Diagram of the change in deformation mechanism with increase in deformation velocity: I. single glide; II. multiple glide; III. twinning; IV. fracture.

Non-octahedral glide is observed in metals with a large energy of packing defects, but with large values of pressure of the shock wave ($P > 100$ kbar) it may take place also in crystals of copper [99, 112]. However by pulsed deformation of metals with an fcc lattice along with the glide, twinning is observed and the threshold P_3 from which the twinning begins (see Figure 46) in these metals is determined by the energy of the packing defects.

Let us look at the mechanism of high-velocity deformation of metals with a hexagonal densely-packed lattice.

From Table 11, for example, it follows that in magnesium the critical displacement stress is minimal for the basal plane. For accomplishment of multiple glide in magnesium it is necessary to increase the effective stresses by several times. In this case the glide takes place both along the basal plane and the prismatic and pyramidal planes, which in fact also takes place during hydrodetonation deformation. Simultaneously we observe twinning along the planes $(10\bar{1}2)$. Probably in magnesium and in the MA-8 alloy $\tau_{2,3}^{gl} \leqslant \tau_{cr}^{twin}$, therefore the development of multiple glide here appears sufficiently distinctly. For these same metals it was established that with values of the maximal pressure

up to 200 kbar the deformation is developed both by gliding along multiple planes and by twinning. However by increasing the effective pressure up to 400 kbar, at which the samples are already fracturing, the basic mechanism of deformation becomes twinning.

In contrast to magnesium, in alpha-titanium the multiple glide exists already at ordinary deformation velocities. Increasing the effective stress during pulsed deformation leads first of all to the critical displacement stresses increasing with increase in deformation velocity, this being especially strong for the non-basal planes (see Figure 32 b), and secondly by increasing the effective stress different systems of twinning begin to act and this mechanism becomes basic in the process of stress relaxation. Such a mechanism is possible in that case if $\tau_{2,3}^{gl}$ becomes greater than τ_{cr}^{twin}. However, if we alter the relationship between τ_{cr}^{gl} and τ_{cr}^{twin} in alpha-titanium, we can also see the development of multiple glide during high-velocity deformation. For example, by increasing the temperature and correspondingly reducing the value of the critical displacement stresses, over all the glide planes we can create such conditions for which τ_{cr}^{gl} becomes less than τ_{cr}^{twin}.

Thus, it is obvious that during high-velocity loading in metals with any type of crystal lattice a larger number of deformation elements is realized (glide or twinning) than during quasi-static loading. It is obvious that under the conditions of multiple glide the plasticity of the metals will be the greatest. However any specific change in the deformation mechanism will depend on the relationship between τ_{cr}^{gl} and τ_{cr}^{twin}.

6. Boundary Glide

The Role of Boundaries in the Process of Deformation of Polycrystals

The presence of boundaries produces a difference in the deformation mechanism in single crystals and in polycrystalline aggregates. For a polycrystal it is characteristic to have a complex deformation as a result of the development of boundary deformation and twinning in the boundary region.

By boundary deformation we must understand the plastic flow by gliding in the boundary band, when a relative displacement takes place of the two grains when a stress is ap-

plied over their total surface. This deformation may take place in the zone, bounded by the width of the boundary or may lead to a displacement completely over the surface of the boundaries. This latter is more often observed at elevated temperatures ($T \sim 0.4T_{melt}$). Already in earlier metallographic investigations there has been observed the formation of steps along the grain boundaries [113], and an anomalously large tension (2000%) of the alloys of eutectoid composition of the binary systems Pb-Sn and Sn-Bi almost fully as a result of the boundary deformation [114].

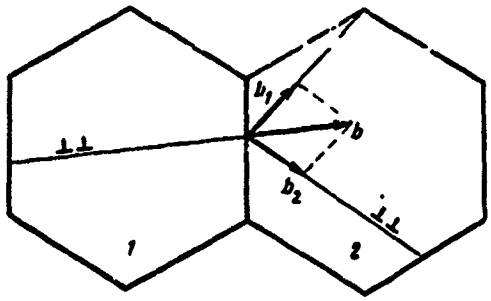

Figure 47. Possible diagram of the relay glide through the grain boundary.

This mechanism also plays a very important role in the deformation of metals with a limited number of glide systems. In metals with a hexagonal densely-packed lattice, the boundary deformation takes place even at a temperature of 4.2° K [115]. Polycrystalline magnesium fractures at 5-10% deformation, whereas single crystals of magnesium may be deformed by 250% or more by gliding. The basic reason for the low plasticity in polycrystalline magnesium is the development of a boundary deformation. In significant temperature and deformation velocity ranges, magnesium and its alloys fracture along the grain boundaries [116]. Consequently, the plasticity of these metals may be increased by such deformation regimes in which the development of boundary deformation is suppressed.

Let us examine the deformation of two neighboring grains in a polycrystal (Figure 47). Let us assume that in grain 1 a uniform glide takes place over one plane. Then in order that no disruption in continuity between grains 1 and 2 take place, the deformation in grain 2 must take place over several planes. The displacement vector $\bar{b}$ is expanded into the components $\bar{b}_1$ and $\bar{b}_2$. Here the deformation conditions in the first and in the second grain are equal to each

other. According to the condition of compatibility of the deformation determined by Mises [117] and Taylor [119], to retain the relationship between the individual grains and to prevent cavities at the boundaries, in each grain it is necessary that there be an effect from no less than five glide systems. This conclusion follows from the fact that the total deformation includes six components, but the sum of three of the normal deformation components is equal to zero, since the volume remains constant. Consequently only five of the independent deformation mechanisms are required to obtain five independent deformation components.

Taylor suggested that to retain the continuity of deformation through the grain boundaries, all grains of the polycrystal must be subjected to the same macroscopic deformation. In deriving his relationship, Taylor assumed a constancy in the law of critical shearing stresses in the case of multiple glide. Chalmers' experiments [119] on symmetrically disoriented bicrystals of tin showed that for the deformation to be transmitted from one crystal to another by increasing the disorientation between crystals the external stresses must be increased. This confirms that the grain boundary itself does not influence the plastic properties.

Nevertheless, if we know the law of deformation of individual crystals, oriented arbitrarily in space, we still can not describe the behavior of a polycrystal. In particular, on the basis of the orientation of the crystallites in space and the diagram of tension of the single crystals, by computation we constructed a diagram of the tension of the polycrystal; however, these results did not coincide with the experimental ones. Such an approach can not explain the well-known fact of increase in friction with decrease in the grain size.

In fact the grain is deformed non-uniformly. At the grain boundary there is always a stress gradient. This is due particularly to the fact that the moduli in the various directions in the crystal do not have spherical symmetry. As a result the field of stresses generated during the application of an external load is non-uniform. This can be detected by the methods of photoelasticity even in the elastic region [119].

The transfer of deformation from one grain to another may be accomplished either as shown on Figure 47 or according to the following mechanism. The dislocations, moving along the glide planes, reach the grain boundary and are piled up, not having any suitable glide plane. At the boundary of the neighboring grain the concentration of

stresses is increased and, if their value is sufficiently high, they then induce glide in the neighboring grain up to the amount when the shearing stresses acting in them reach values of the critical displacement stress.

In reference [103] the transfer of glide between two grains was observed experimentally on bicrystals of NaCl and LiF. The generation of dislocations and their displacement under the action of an external stress was determined from the etching holes, and the value of the external stresses was determined by photoelastic methods. It was found that at small angles of disorientation ($\delta < 5°$(the deformation was transmitted by relay by means of a direct break in the boundary between the grains. Here the stresses necessary for the break grew linearly with increase in the angle of disorientation between the grains. At larger angles of disorientation, in spite of the fact that the stresses grew by several times, a break in the boundary became impossible and the deformation was transferred by means of inducing dislocations in the neighboring grain.

The existence of a stress gradient in the boundary region may lead to the development of deformation mechanisms that are not characteristic of single crystals. Hence the basic role of the grain boundaries during the deformation of metals with a limited number of glide systems, as well as during high-temperature deformation, is clear.

In the first case the significant stresses generated at the grain boundaries may be relaxed by means of deformation in the boundary region, and in the second case -- the deformation as a result of the boundary glide is greatly facilitated due to the heat activation of the process.

In metals with an fcc lattice having a sufficient number of different glide systems, the condition for compatibility is satisfied rather easily. Therefore during ordinary deformation at the grain boundaries the stress gradient is not high and the boundary deformation plays no great role. In metals with a hexagonal densely-packed lattice the condition for compatibility is virtually unsatisfied, therefore then the role of the boundary deformation is rather high. In the process of deformation of polycrystalline magnesium at the temperature of liquid nitrogen glide is developed in the boundary region along the prismatic plane, although here the displacement stresses are several times higher than along the basal plane [103]. Due to concentration stresses in the boundary region, twinning appears in magnesium, traveling from the grain boundaries along the planes [10$\bar{1}$2] even with small degrees of deformation.

In spite of the numerous investigations, the mechanism of boundary deformation is still not clear. Ke [120] assumes that the existence of internal friction in polycrystals is due to relaxation of the cleavage stresses at the boundaries by means of ductile glide. However the velocity of the displacement, computed on the basis of data concerning internal friction, exceeds the actually observable ones in the bicrystals by five-eight orders of magnitude. The experiments of Voloshina and Rozenberg [121] with bicrystals, as well as those of Rhines et al [122], indicate that glide exists in a wide zone around the boundary and that intragranular glide takes place up to the onset of boundary deformation. Thus, the hypothesis of ductile glide received no experimental confirmation.

Reference [123] suggests a dislocation mechanism of the boundary glide: in the plane of the boundary the dislocations are split into several partial ones and the boundary deformation takes place as a result of the motion of these partial dislocations parallel to the plane of the boundary. Leak [24] assumes that the relaxation of stresses during boundary deformation is accomplished by means of migration of the grain boundaries. It is possible that this mechanism is also realized in individual cases at elevated temperatures.

The best agreement with experiment is given by the theory of Fazon et al [125], in which the relaxation of stresses takes place at triple points and other defects of the boundary and any further displacements are controlled by deformation of these barriers. In view of the local increase in effective stresses in the boundary region, glide is possible along systems which are absent in other segments of the grain, even under the influence of a moderate displacement stress less than the macroscopic yield stress.

Reference [126] mentions the predominant role of boundary deformation during the quasi-static loading of polycrystalline magnesium and its alloys with change in deformation velocity from 10^{-6} to 4 m/sec. In the velocity range investigated by them the fracture took place at the grain boundaries as a result of the development of boundary deformation.

However at significantly higher loading velocities (100-200 m/sec) the plasticity of magnesium and the MA-8 alloy grows [108], due to the redistribution of the contribution from the various deformation mechanisms.

Let us examine the methods of quantitative evaluation of the contribution from the various mechanisms to the overall deformation.

Expansion Produced by Gliding

Quantitative evaluation of the deformation based on coarse glide tracks was done in reference [128]. Let us assume that the grain is chaotically arranged in space and has many glide systems. Then the glide begins along the plane arranged at an angle of 45° to the direction of the tension (Figure 48). As a result of glide along such a plane the expansion of the sample is determined by:

$$\varepsilon_{gl} = \frac{a - a_0}{a_0}. \tag{40}$$

(The quantities a and a_0 are denoted on Figure 48). If we denote the displacement in the direction of glide by p_{gl}, then

$$a = \sqrt{a_0^2 + p_{gl}^2 + 2a_0 p_{gl} \cos\gamma}, \tag{41}$$

where $a_0 = 1/n$, and n is the number of glide lines per unit of initial length.

Taking (40) and (41) into account, we obtain

$$\varepsilon_{gl} = \frac{\sqrt{\frac{1}{n^2} + p_{gl}^2 + 2\frac{p_{gl}}{n}\cos\gamma} - \frac{1}{n}}{\frac{1}{n}} = \sqrt{1 + p_{gl}^2 n^2 + 2p_{gl}\cos\gamma} - 1. \tag{42}$$

Assuming the angle γ to be constant, and also $pn \ll 1$, we obtain

$$\varepsilon_{gl} = \frac{np_{gl}}{\sqrt{2}} \cdot 100\%. \tag{43}$$

To obtain a more precise expression for ε_{gl} it is necessary to carry out integration in the range of possible angles determining the position of the glide plane with respect to the effective stress.

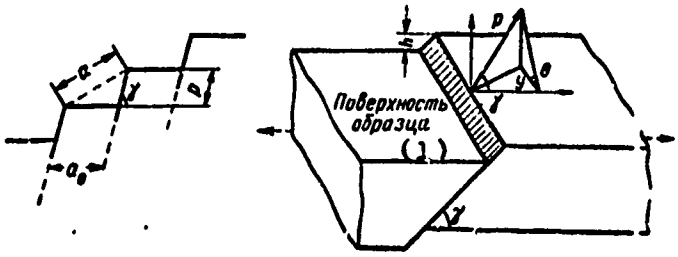

Figure 48. Diagram explaining the method of determining the amount of displacement in the glide tracks.

1. Surface of sample

It is difficult to experimentally measure the amount of displacement p_{gl}, therefore we determine the height of the step h of the glide line. From Figure 48 it follows that

$$p_{gl} \sin \gamma \sin \theta = h.$$

Assuming γ equal to $\pi/4$, we find

$$h = p_{gl} \frac{\sqrt{2}}{2} \sin \theta. \qquad (44)$$

Differentiating (44), we will have

$$dh = \frac{\sqrt{2}}{2} p_{gl} \cos \theta d\theta.$$

Then the mean value of the height of the step will be:

$$h_{av} = \frac{\int_0^{\infty} dh}{\int_0^{\pi/2} d\theta} = \frac{\frac{\sqrt{2}}{2} p_0 \int_0^{\pi/2} \cos \theta d\theta}{\int_0^{\pi/2} d\theta} = \frac{\sqrt{2}}{\pi} \cdot p_{gl}. \qquad (45)$$

or

$$p_{av} = \frac{\pi h}{\sqrt{2}} av = 2{,}22 h_{av}. \qquad (46)$$

In the general the general case we must allow for the fact that the displacement in the track depends on the magnitude of the shearing displacement stress τ. If we assume that the displacement is proportional to τ, then it is easy to show that

$$p_{av} = 2{,}3\, h_{av}, \tag{46a}$$

The magnitude of h is measured on the surface of the deformed sample. Because of the overall expansion the height of the step is decreased by $\sqrt{1+\varepsilon_{tot}}$ times. Then

$$p_{av} = 2{,}3 h_{av} \sqrt{1+\varepsilon_{tot}}. \tag{47}$$

Substituting (47) into formula (43), we find the final expression for computing the deformation caused by the coarse glide tracks

$$\varepsilon_{gl} = \frac{2{,}3 h_{av} \beta \sqrt{1+\varepsilon_{tot}}}{\sqrt{2}} \cdot 100\% = 1{,}62 h_{av} \beta \sqrt{1+\varepsilon_{tot}}. \tag{48}$$

Thus, after determining the number of glide lines and measuring the height of the step on the tracks, we can compute the deformation introduced by the glide tracks.

The height of the steps can be measured using an MII-4 Linnik interferometer, which permits determining the height of irregularities on the surface, beginning from 50 μm. The error here comprises 3-5%.

In those cases when the height of the step is small, we use a multibeam interferometer, the sensitivity of which is one order of magnitude higher. The quite fine relief can be investigated in an optical microscope by the phase contrast method [56].

Expansion Caused by Boundary Deformation

Two methods exist for evaluating the amount of boundary deformation. The first is based on a quantitative measurement of the displacements in the boundary region (method of MacLean), the second is based on comparison of the deformation of individual grains and that of the entire sample as a whole (the method of Rachinger [129]).

Just as in intragranular glide, the displacement of grains takes place not only in the longitudinal direction but also in the direction perpendicular to the surface. Here the amount of the boundary deformation depends on orientation of the boundary with respect to the effective force, i.e., on the size of the angle β. This can be explained by the fact that boundary deformation, just as intragranular glide, is accomplished under the effect of shearing stresses which are maximal when $\beta = 45°$.

Having made the assumption as in the case of intragranular glide, we find an expression for evaluating the amount of the boundary deformation:

$$\varepsilon_{gb} = \left[\left(\sqrt{1 + p_b^2 n^2 + \sqrt{2 p_b^2 n^2}} - 1\right)\right] \cdot 100\%,$$

and under the condition that $pn \ll 1$

$$\varepsilon_{gb} = \frac{100 p_b n}{\sqrt{2}} \%. \qquad (49)$$

where p_b is the mean displacement along the grain boundary; n is the number of boundaries per unit of length of the sample.

By measuring the mean vertical displacement component along the boundary h_{av}, we find

$$\varepsilon_{av} = 1{,}62 h_{av} n \sqrt{1 + \varepsilon_{tot}}. \qquad (50)$$

The procedure described was used by Rozenberg [59] for evaluating the amount of displacement in the glide tracks during creep.

In Rachinger's method [129], which may be used only for uniaxial tension, it is assumed that the mean grain size prior to deformation is the same both in the longitudinal and transverse directions. The mean diameter of the grain is equal to 1/n, where n is the number of grains per unit of length of the sample.

During uniaxial tension the grain is expanded in the longitudinal direction and is contracted in the transverse. If the grain were expanded in the longitudinal direction by a magnitude of ε_3, then its mean diameter would be increased by $(1+\varepsilon_g)$ times, and in the transverse -- it is increased by

$\sqrt{1+\varepsilon_g}$ times. This leads to a change in the number of grains per unit of length of the sample in the longitudinal and transverse directions:

$$N_{long} = \frac{n}{1+\varepsilon_g} \cdot \frac{1}{k},$$
$$N_{trans} = n\sqrt{1+\varepsilon_g} \cdot \frac{1}{k}. \qquad (51)$$

The coefficient 1/k takes into account the possible growth in grains at elevated temperatures. In the absence of growth in the grains it may be assumed equal to unity and then

$$\varepsilon_g = \left(\frac{N_{trans}}{N_{long}}\right)^{2/3} - 1. \qquad (52)$$

The deformation produced by the grain boundaries can be computed as the difference:

$$\varepsilon_{gb} = \varepsilon_{tot} - \varepsilon_g.$$

Thus, in Rachinger's method, determination of the mean deformation of the grain is reduced to measuring the grain diameters in the longitudinal and transverse directions.

The complexity of this method involves the fact that to reach the required accuracy it is necessary to measure the diameters of 1000 to 3000 grains. The number of required measurements may be decreased if we determine the ratio of the longitudinal and transverse diameters of each grain; the accuracy of the method increases in such case.

References [108, 109] studied the contribution of the various mechanisms to the deformation of magnesium and the MA-8 alloy during quasi-static and high-velocity deformation.

Under the conditions of quasi-static loading ($\dot{\varepsilon} = 10^{-3}$ sec^{-1}) the plastic flow is basically accomplished by means of boundary deformation and twinning. Even with a degree of deformation less than 1% a relief appears on the grain boundaries. With growth in the degree of deformation the displacements in the boundary region reach 2-3 μm. The greatest value is that of the junction of several grains (Figure 49), where the condition of compatibility of the grain deformation

is especially hard to satisfy. The development of a boundary deformation produces the appearance of microcracks, which produce fracture of the magnesium and the MA-8 alloy.

Figure 49. Quasi-static deformation of the MA-8 alloy. Interference lines are concentrated in the boundary zone and at the junctions of the grains $\bar{\varepsilon}$ = 2%.

Intragranular glide is expressed very weakly; even with degrees of deformation near 10% the glide tracks give a quite fine relief that can be detected only with the aid of an interference microscope. Here the displacement does not exceed 0.03 μm.

Such a character for the development of plastic deformation involves both the limited number of possible glide systems and their their characteristics of the orientation of the sheet material. As is clear from the pole figure (Figure 50), the grain distribution in the MA-8 alloy is such that the basal plane (0001) deviates no more than 35° from the sheet plane. Here in the overwhelming majority of grains the deviation does not exceed 15°. Thus, the grain is oriented unfavorably for basal glide. In pure magnesium the orientation is still sharper.

Under conditions of pulsed loading the deformation mechanism of these metals changes sharply. The quantitative contribution of the various mechanisms to the overall deformation also changes substantially. The density of the glide lines and twins over the body of the grain is sharply increased and the displacement in the boundary region is decreased.

Quantitative evaluation of the amount of the various types of deformation under hydrostatic and pulsed loading was done in [108] by the MacLean method.

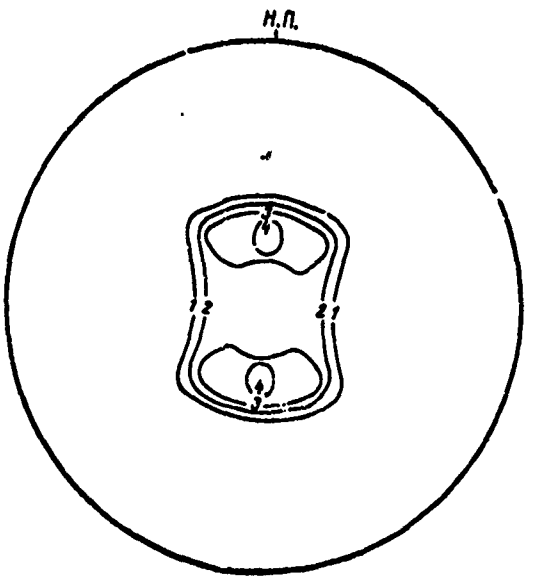

Figure 50. Pole figure (0001) of sheets of the MA-8 alloy in the original state.

The contribution of twinning was computed using the same formulas that were used to determine the amount of intragranular glide and boundary deformation. Here we measured the density of the twins per unit of length of the sample and the height of the step on the twin. The total deformation was assumed equal to 100%.

The results obtained for magnesium and the MA-8 alloy are shown on Table 15.

If the basic contribution belongs to boundary deformation (more than 80%) in the hydrostatic loading of magnesium and the MA-8 alloy, then by detonation loading the basic part of the deformation is accomplished by means of intragranular glide (45%) and twinning (40%), and the amount of the boundary deformation is reduced to 10%.

The effect of redistribution of the contribution of the various mechanisms is so high it greatly exceeds possible error. Thus, the density of the glide tracks during pulsed deformation increases by 30-40 times, and the density of the twins increases by 3-4 times.

Table 15. Contribution of the Various Mechanisms to the Overall Deformation of Magnesium and the MA-8 Alloy

Материал (1)	ε, %	Метод нагружения (4)	Доля в общей деформации, % (7)		
			внутризеренное скольжение (8)	двойникование (9)	межзеренная деформация (10)
Магний (2)	2,0	(5) Гидростатический	1	16	83
		(6) Взрывной	45	40	15
Сплав МА-8 (3)	2,0	(5) Гидростатический	1	13	86
		(6) Взрывной	60	30	10
	3,0	(5) Гидростатический	1	15	84
		(6) Взрывной	55	34	11
	4,0	(5) Гидростатический	1	16	83
		(6) Взрывной	55	36	9

1. Material
2. Magnesium
3. MA-8 alloy
4. Method of loading
5. Hydrostatic
6. Detonation
7. Contribution to total deformation, %
8. Intragranular glide
9. Twinning
10. Boundary deformation

Decreasing the amount of boundary deformation favorably influences the plastic properties of magnesium and its alloy -- their plasticity more than doubles.

Such a redistribution of the contribution from the various mechanisms to the overall deformation can be explained by the characteristics of the intragranular glide during pulsed deformation. As mentioned above, during pulsed deformation of these alloys multiple glide is carried out over the planes (0001), $(10\bar{1}0)$, and $(10\bar{1}1)$. The development of multiple glide favors satisfaction of the condition of compatibility of deformation of the individual grains, which leads to a decrease in the stress gradient at the grain boundaries, as a result of which the development of boundary deformation is slowed down and its contribution to the overall deformation is reduced.

CHAPTER 3

TWINNING UNDER CONDITIONS OF HIGH-VELOCITY DEFORMATION

Twinning is a process which competes with gliding in the relaxation of externally applied stress. Just as the gliding process, it is associated with restructuring of the crystal lattice. In each specific case relaxation may take place by one or another means or simultaneously by the two mechanisms, if there are the proper premises for this both from the viewpoint of geometry of the process and from the energetic viewpoint.

1. Crystallography and Dislocation Twinning Models

Twinning can be represented as the uniform displacement of one part of a crystal with respect to another, parallel in some way to the rational crystallographic plane. The spherical volume of radius R, separated from the crystal as a result of the twinning displacement, is converted into an ellipsoid. If one of the twinning planes coincides with the twin-original crystal boundary, then the displacement as a result of such shift will be that shown on Figure 51. The twinning process can be described by any pair of components (K_1 and η_2 or K_2 and η_1) and by the magnitude of the shift S (for a single radius of the sphere) or the size of the angle 2ψ associated with it.

If the twinning plane is K_1, then the shift S must lead to the formation of a rational crystallographic direction η_2 (usually with small indices). By twinning along the plane K_2 the rational indices must have the direction η_1.

For highly symmetrical crystal lattices such as face-centered cubic, body-centered cubic, and hexagonal densely-packed, the twinning process can be represented schematically

as a shift of planes lying to one side of a certain zero plane, taken for the twinning plane K_1 (Figure 52).

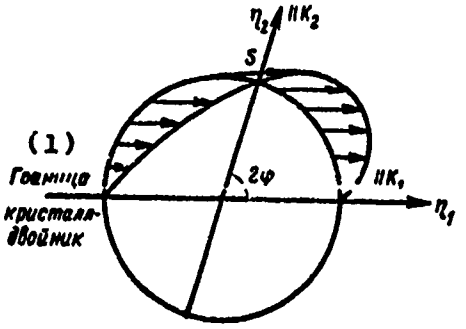

Figure 51. Deformation of the spherical volume of a crystal as a result of twinning. K_1 and K_2 are the possible planes of twinning, that are common for the ellipsoid of deformation and of the original sphere; η_1 and η_2 are the directions of the twinning displacement lying, respectively, in the planes K_1 and K_2. The plane K_1 coincides with the boundary twin-original crystal.

1. Crystal-twin boundary

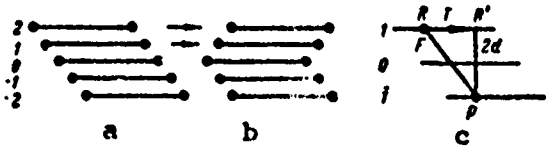

Figure 52. Diagram of the twinning process by means of a simple displacement: a. original state; b. twins; c. relationship between the amount of the displacement S and the parameters ξ and d for the simple lattice.

The displacement as a result of twinning will be such that the position of the atoms in the plane 1, 2, etcetera, will become a mirror of the respective atoms in the planes -1, -2, etcetera, arranged below the plane of symmetry, which is the plane of twinning. Since the planes and the directions of twinning may have only simple crystallographic indices, from Figure 52 c it follows that the amount of the displacement T will be

$$T^2 = F^2 - 4d^2, \qquad (53)$$

where F is the modulus of the arbitrarily selected direction in the crystal lattice, connecting the two atoms in the planes -1 and 1; d is the interplanar spacing of the selected system of parallel planes.

The amount of the single displacement S then will be S = T/d, whence

$$S^2 = \frac{F^2 - 4d^2}{d^2}. \qquad (54)$$

Replacing F by a shorter vector of the lattice b, using the extreme value of S = 1, and solving equation (54) relative to d, we find the inequality

$$\frac{1}{d^2} \leqslant \frac{5}{b^2}. \qquad (55)$$

Inequality (55), as well as the diagram shown on Figure 52 c, permit predicting the possible crystallographic indices of the plane and direction of twinning for simple crystal structures [130].

Treating the twinning process as a uniform displacement, Schmid and Boas [131] showed that twinning is associated with change in the size of the sample in the direction of applied stress. The change $\varepsilon = \ell_1/\ell_0$ (where ℓ_0 and ℓ_1 represent the distance between the two boundary planes of twinning, respectively, before and after deformation) depends on the amount of displacement S. During tension the maximal expansion is

$$\varepsilon_{\max}^{\text{ten}} = \frac{S}{2} + \sqrt{\frac{S^2}{4} + 1}, \qquad (56)$$

and during contraction the maximal shortening will be equal to

$$\varepsilon_{\max}^{\text{cont}} = -\frac{S}{2} + \sqrt{\frac{S^2}{4} + 1}. \qquad (57)$$

If the direction of the applied stress lies in the plane of twinning K_1 or K_2, then the twinning does not lead to change in dimensions. Thus, the sign of the deformation will depend on the crystallographic orientation of the sample.

Figure 53 shows the axis of the deformed sample on a sphere of projection. Here we can distinguish the regions in which the sign of deformation as a result of twinning will be positive (the unshaded part) or negative (the shaded part). Such a conclusion follows from purely geometric treatment of twinning as a process of displacement determined by the plane and the direction of the displacement.

However we know that the final sign of the deformation is determined by the directionality of the external stress. If a tensile stress is applied to the sample, then regardless of its crystallographic orientation the sample is increased in the direction of the effective stress and decreased in cross section. During contracting stress the picture will be the opposite.

In all metal crystals possessing a high symmetry of the crystal lattice there are about ten adequate twinning systems from the crystallographic viewpoint, but differently oriented with respect to the effective stress. Therefore it is obvious that if a tensile stress is applied to the sample, those systems of twinning will act which give a positive deformation, and during contraction -- those which give a negative deformation.

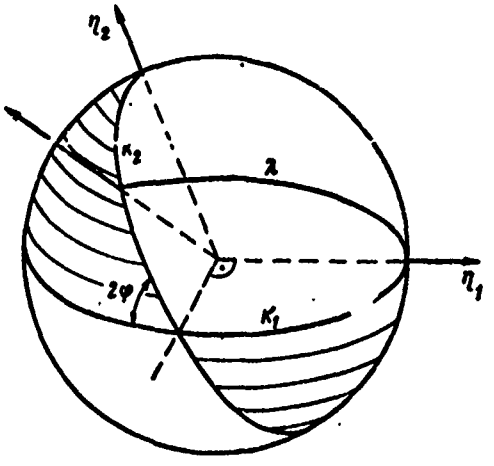

Figure 53. Regions of possible orientations for twinning on a sphere of projection.

The onset of twinning of a layer in a crystal is associated with the reorientation of the metal found between the two extreme planes of twinning in comparison with the matrix. Let HKL be the indices of the twinning plane K_1 or K_2,

and [UVW] be the indices of the direction η_2 or η_1. Then if some plane of the crystal prior to twinning had the indices (hkℓ), then following twinning the indices of this plane be (h'k'ℓ') [131]:

$$\left.\begin{aligned} h' &= h(HU + KV + LW) - 2H(Uh + Vk + Wl), \\ k' &= k(HU + KV + LW) - 2K(Uh + Vk + Wl), \\ l' &= l(HU + KV + LW) - 2L(Uh + Vk + Wl). \end{aligned}\right\} \qquad (58)$$

The crystallographic direction [uvw] after twinning will have the indices [u'v'w']:

$$\left.\begin{aligned} u' &= u(HU + KV + LW) - 2U(Hu + Kv + Lw), \\ v' &= v(HU + KV + LW) - 2V(Hu + Kv + Lu) \\ w' &= w(HU + KV + LW) - 2W(Hu + Kv + Lu) \end{aligned}\right\} \qquad (59)$$

Equations (58) and (59) may be very useful for analyzing changes in the pole figure. After experimentally determining the displacement of the orientation maxima, we can compute the twinning systems associated with this orientation transition.

The dislocation twinning mechanism was described by Cottrell and Bilby [132]; later this theory was further developed by Venables [133, 134]. In accordance with the dislocation mechanism, which in the literature is often termed a polar mechanism, twinning of the layer is generated under certain conditions:

1. The twinning dislocation must be formed by displacement in the plane which becomes the twinning plane.

2. The Burgers vector of the polar dislocation must have a component that is perpendicular to the twinning plane or, what amounts to the same thing, equal to the interplanar spacing for the twinning plane.

3. Polar dislocation must be sufficiently well secure in order to resist stresses moving o the twinning dislocation. The most reliable assurance is in the case if the polar dislocation is a sessile-type dislocation.

4. Twinning and polar dislocations along with the total dislocation line must form a site which is the pole. Twinning dislocation must have the possibility o moving in the twinning plane relative to the pole.

Twinning Elements of Crystals With a Body-Centered Cubic Lattice

After taking $\bar{b} = 1/2\ [111]\ a$, in inequality (55) for crystals with a bcc lattice, we will have:

$$\frac{a^2}{d^2} \leqslant \frac{5.4}{3}.$$

Since $a^2/d^2 = H^2+K^2+L^2$, then the sum of the squares of the indices of the twinning plane must be no more than six. To select the twinning plane there are a number of limitations: such a plane for example can not be the plane of symmetry (for more detail see [130]). In crystals with a bcc lattice the twinning plane is the planes of the set {112}. The minimal displacement leading to symmetrical arrangement of the sites relative to such plane will be 1/6 [111] a.

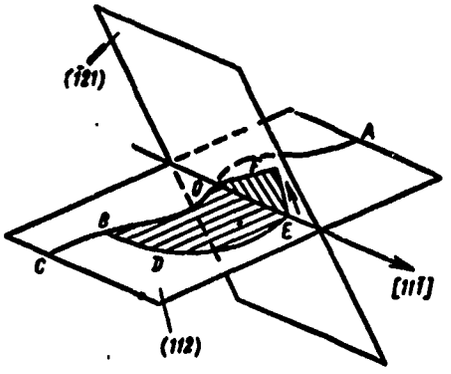

Figure 54. Diagram of twinning according to the polar mechanism in a bcc lattice [132]: OA is the single dislocation in the plane (112) with a Burgers vector a/2 [111]; OB is the sessile dislocation with the Burgers vector a/3 [112]; OFEDB is the twinning dislocation with the vector a/b [111].

If the single dislocation OA is found in the plane (112) (Figure 54), then at point O it is split into two partial dislocations according to the reaction

$$\frac{a}{2}[111] \rightarrow \frac{a}{3}[112] + \frac{a}{6}[111].$$

Then OB -- the sessile dislocation a/3 [112] -- remains immobile, and the loops OEDB may be displaced to the plane (112). The Burgers vector for the dislocations in the plane (112) and

$(\bar{1}21)$ is one and the same. The segment of the mobile loop OE may freely convert to the plane $(\bar{1}21)$, forming a contour, which twins the dislocation OFEDB and is equal to a/6 $[11\bar{1}]$.

With complete rotation for one turn of the vector OF around the point O a single-layer twin is formed with displacement along OB by a magnitude of a/6 $[\bar{1}21]$. For twinning according to the described mechanism it is necessary to have a dissociation of the complete dislocations and consequently the formation of a segment with a packing defect. The stress which is necessary for the formation of such a segment is proportional to $\gamma/\bar{b}$ (where γ is the energy of the packing defect and $\bar{b}$ is the Burgers single dislocation OA). With a value of $\gamma \approx 100$ erg/cm^2 for the formation of a twin according to the described mechanism in the bcc lattice there must be a stress that is near the theoretical strength.

Reorientation of the crystal lattice as a result of twinning is shown on Figure 55. The displacement of the atoms led to their symmetrical arrangement relative to the twinning plane (112), which is the interface matrix-twin. S is the amount of the single displacement obtained by one rotation of the twinning dislocation. The displacement in the other planes is a multiple of this value.

In cubic crystals there are twelve systems $\{112\}\langle 111\rangle$, by which twinning may take place. Realization of one or another system depends on the amount of the cleavage stress proportional to the Schmid coefficient. In the standard triangle it is difficult to determine the orientation of crystals, for which only the twinning system will be effective. However it has been proven that this is such an orientation for which the ratio of cleavage stresses (or what amounts to the same thing, the Schmid coefficients) for two of the most heavily loaded systems [135] is the greatest. Figure 56 shows the contours of such a ratio for different orientations in the triangle during tension and contraction. From these data in particular it follows that the minimal number of twinning systems is realized during contraction in that case if the stress is applied in the direction [355], lying on the line [111]-[110], and during tension this direction deviates by 6° toward the center of the triangle.

In reference [130] single crystals of silicon iron were deformed in various crystallographic directions. The results are given on Table 16. Under the influence of a shock wave in the direction [111] during contraction three twinning systems may be realized. Of the other nine systems, three have an orientation factor equal to zero, and the other six systems appear only under tension.

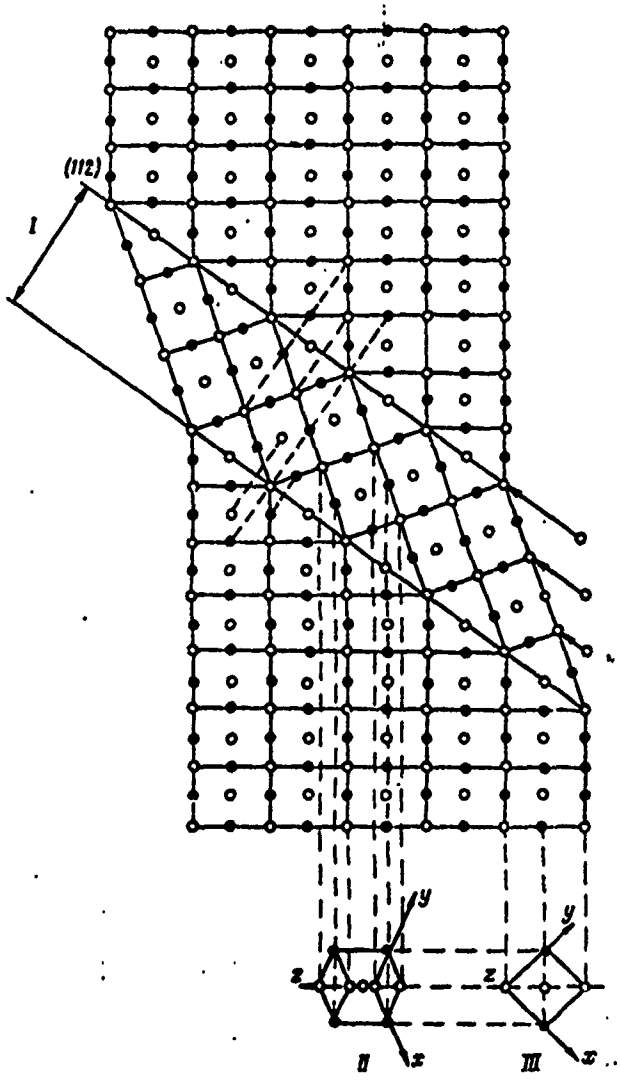

Figure 55. Projection on the plane $(1\bar{1}0)$ of the matrix and the twinned layer of a bcc lattice. The twinning plane is (112), direction of twinning is $[\bar{1}\bar{1}1]$: I. twinned layer; II. projection of the twin; III. projection of the matrix; O = atoms lying in the plane of the drawing; O = atoms displaced relative to the plane of the drawing above or below by a value of $a\sqrt{2}/2$.

In the direction [112] the shock wave may induce four systems, for which the orientation factor is equal to 0.39 and 0.16. Of these four systems three were determined metallographically in the form of tracks on the plane $(1\bar{1}1)$. Of the other eight, three have a displacement stress equal to zero and five may act only under tension.

Table 16. Twinning in Single Crystals of Silicon Iron, Deformed in Different Crystallographic Directions [136]

Направление ударной волны (1)	Плоскость наблюдения двойников (2)	Номер двойникующей системы (3)	Система двойникования (4)		Ориентационный фактор (5)	Наличие двойникования в системе (6)
[$\bar{1}$11]	(211)	1	($\bar{1}$12)	[1$\bar{1}$1]	0,32	(7) Двойникование обнаружено
		3	(2$\bar{1}$1)	[111]	0,32	(8) То же
		5	($\bar{1}$21)	[11$\bar{1}$]	0,32	»
[$\bar{1}\bar{1}$2]	(1$\bar{1}$1)	3	(2$\bar{1}$1)	[111]	0,39	(7) Двойникование обнаружено
		4	(211)	[$\bar{1}$11]	0,39	(8) То же
		5	(12$\bar{1}$)	[$\bar{1}\bar{1}$1]	0,16	(9) Двойникование не обнаружено
		11	($\bar{1}$21)	[$\bar{1}$11]	0,16	(9) Двойникование не обнаружено
[001]	(110)	1*	($\bar{1}$12)	[1$\bar{1}$1]	0,47	(9) Двойникование не обнаружено
		2*	(112)	[11$\bar{1}$]	0,47	(10) То же
		7*	(11$\bar{2}$)	[$\bar{1}$11]	0,47	»
		8*	(1$\bar{1}$2)	[111]	0,47	»
		3*	(2$\bar{1}\bar{1}$)	[$\bar{1}$11]	0,24	(7) Двойникование обнаружено
		5	($\bar{1}$21)	[111]	0,24	(8) То же
		6	(121)	[1$\bar{1}$1]	0,24	»
		9	(21$\bar{1}$)	[111]	0,24	»
		4	(211)	[$\bar{1}$11]	0,24	»
		11	($\bar{1}$2$\bar{1}$)	[$\bar{1}$11]	0,24	»
		10	(2$\bar{1}$1)	[111]	0,24	»
		12	(121)	[111]	0,24	»

(11*) Двойникование по этим системам возможно только при растяжении

1. Direction of shock wave
2. Plane of observation of the twins
3. Number of the twinning system
4. System of twinning
5. Orientation factor
6. Existence of twins in the system
7. Twinning detected
8. Same
9. Twinning not detected
10. Same
11. * Twinning over these systems possible only under tension

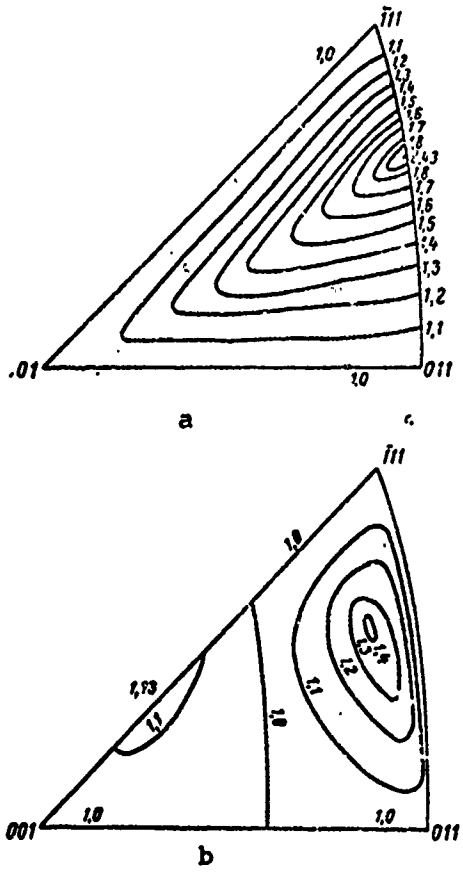

Figure 56. Contours of the ratio of Schmid coefficients for two of the most heavily loaded twinning systems {112} ⟨111⟩ under contraction (a) and tension (b) [135].

In the deformation by contraction in the direction [001] eight twinning systems appear. But on the plane (110) they are detected in the form of four systems of tracks. The largest number of twins is found along the planes {113}.

Twinning Elements of Crystals With a Face-Centered Cubic Lattice

Taking the minimal displacement in the fcc lattice in inequality (55) as $\vec{b} = 1/2\ [110]\ a$, we find that the twinning plane may be {111} with a displacement in the direction ⟨112⟩. The correctness of this statement has been proven in numerous experiments.

A necessary premise for the formation of a twin in an fcc lattice, according to Venables, is the formation of long

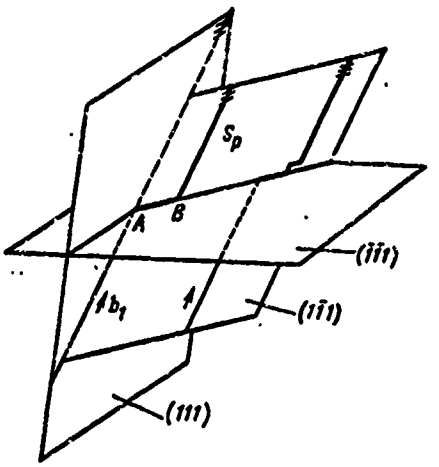

Figure 57. Diagram of twinning according to the polar mechanism in an fcc lattice [137]: $(\bar{1}\bar{1}1)$ is the conjugate plane; $(1\bar{1}1)$ is the transverse plane; (111) is the primary glide plane.

thresholds in the plane adjoint to the primary glide plane. These thresholds are generated when the dislocation S_p, moving in the transverse plane $(1\bar{1}1)$, meets a dislocation forest in its path, that is located in the conjugate plane $(\bar{1}\bar{1}1)$ (see Figure 57). Then the segment of the dislocation AB under certain conditions may dissociate according to the equation:

$$\frac{a}{2}[\bar{1}01] = \frac{a}{3}[\bar{1}\bar{1}1] + \frac{a}{6}[\bar{1}21]$$

with the formation of the twinning dislocation a/6 [121] and the polar dislocation a/3 $[\bar{1}\bar{1}1]$. As a result of the full rotation of the polar dislocation the segment of the dislocation in the primary plane b_1 is shifted to the transverse plane by a value AB with formation of the defect along (111). The new splitting will still give one jump similar to AB, etcetera.

Reorientation of the fcc matrix as a result of twinning was examined in Figure 58, where the projection of the crystal on the plane $(1\bar{1}0)$ is given. The boundaries of the twins represent a track of the plane (111). In the plane of the drawing $(1\bar{1}0)$ we see the atoms with coordinates of the type [[000]] and [[1/2, 1/2, 0]]. The atoms with coordinates

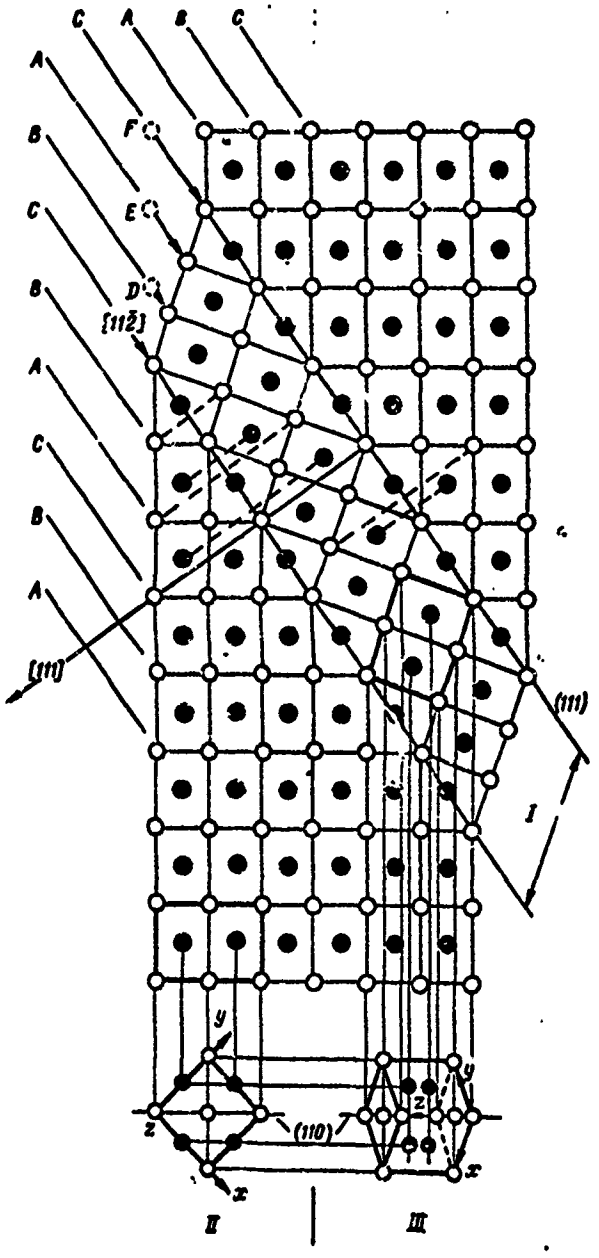

Figure 58. Projection on the plane (1$\bar{1}$0) of the matrix and twin in an fcc lattice [138]. The twinning plane is (111), the displacement direction is [11$\bar{2}$]. The white circles represent atoms arranged in the plane of the drawing. The black ones are shifted upward and downward with respect to the plane of the drawing by $\frac{a\sqrt{2}}{4}$. I is the twinned layer; II is the projection of the matrix; III is the twin projection.

[[1/2 0 1/2]] and [[0 1/2 1/2]] are shifted above and below relative to the plane $(1\bar{1}0)$ by a value of $\frac{a\sqrt{2}}{4}$.

As is obvious from the diagram shown, twinning changes the order of arrangement of the atomic layers, in the direction perpendicular to the plane $(1\bar{1}1)$. The usual order of arrangement for fcc metals ABCABC is restructured into the order ABC [BAC] ABC. The segment of the crystal included in the brackets is a twinned layer with mirror arrangement of the atoms relative to the twinning plane.

Twinning Elements of Crystals With a Hexagonal Densely-Packed Lattice

Twinning in hexagonal crystals has no such uniformity as in cubic crystals. The planes and even the direction of twinning may vary as a function of the temperature and velocity of the deformation, the degree of doping of the alloy, and the orientation of the grain.

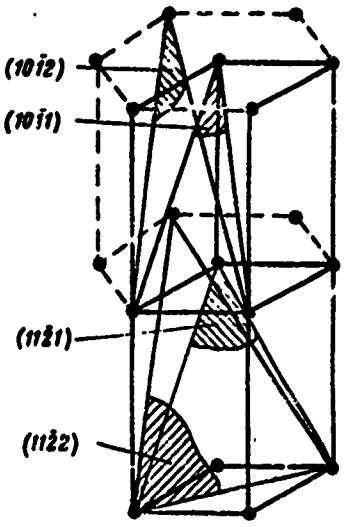

Figure 59. Planes of twinning in a hexagonal densely-packed lattice.

As yet we are unable to systematize and explain one or another system of twinning in each specific case.

Numerous attempts have been made to associate the behavior of hexagonal metals during deformation with the ratio of the lattice constants c/a. However here also no orderly system has been found. Twinning along the plane $\{10\bar{1}2\}$ in

the direction $[10\bar{1}1]$, which is encountered most often, was found in cadmium (c/a = 1.886), magnesium (c/a = 1.623), and in beryllium (c/a = 1.568). At the same time, as will be shown later, titanium (c/a = 1.587) during static deformation is twinned along the plane $\{10\bar{1}2\}$, and during high-velocity deformation furthermore along the planes $\{11\bar{2}1\}$ and $\{11\bar{2}2\}$. Table 17 shows the twinning systems for the various metals with a hexagonal densely-packed lattice. The twinning planes shown on Figure 59 are the ones most often encountered.

Reorientation of the twinned segment with respect to the matrix during twinning along the plane $(10\bar{1}2)$ is shown on Figure 60. Here the projection is given for both segments of the crystal on the plane $(\bar{1}2\bar{1}0)$. If we take the hexagonal prism for the unit cell, then one of the atoms with the base [[000]] and one of the three atoms with a base of the type [[1/3 2/3 1/2]] will enter the plane. The other atoms, as is clear from Figure 62, are found above or below the plane of the drawing. Analogously we can also construct the twinning diagrams along the other planes [139].

2. Deformation by Twinning

Twinning in Metals With a Hexagonal Densely-Packed Lattice

Mechanical twinning in metals and alloys with a hexagonal densely-packed lattice has been studied numerous times in connection with the different conditions of plastic deformation. For example, twinning has been detected during tension, pressing, rolling, and detonation punching of polycrystalline crystals of magnesium and its alloys. Twinning exerts a substantial influence on the properties of metals. The stresses concentrated at the boundary of the twin or at the point of intersection of two twins, may be the reason for the formation of microcracks, and it may alter the level of the microstresses. As will be shown, the formation of twins substanially influences the strengthening process.

Reed-Hill [140] found a complex twinning in single crystals of magnesium under tension parallel to the plane (0001). It was experimentally shown that the part of the twins forming first along the planes $(10\bar{1}1)$ and $(10\bar{1}3)$ are retwinned along the plane $(10\bar{1}2)$ in the process of plastic deformation.

In the investigations of Couling et al [141] a significant twinning was observed during rolling of an Mg-Th alloy. Here the authors showed that when the degree of deformation per operation does not exceed 2%, repeated rolling

permits obtaining sufficiently large total degrees of deformation without fracturing the metal.

Table 17. Twinning Systems in Hexagonal Densely-Packed Metals

(1) Металл	c/a	Плоскости двойникования {hkil} (2)	Направление сдвига [uvtw] (3)
Cd	1,886	$\{10\bar{1}2\}$	$\langle 10\bar{1}1\rangle$
Zn	1,856	$\{10\bar{1}2\}$	$\langle 10\bar{1}1\rangle$
Mg	1,623	$\{10\bar{1}2\}$ $\{10\bar{1}1\}$ $\{10\bar{1}3\}$ $\{11\bar{2}1\}$	$\langle 10\bar{1}1\rangle$ $\langle 10\bar{1}2\rangle$ $\langle\bar{3}032\rangle$ $\langle\bar{1}\bar{1}26\rangle$
Zr	1,592	$\{10\bar{1}2\}$ $\{11\bar{2}1\}$ $\{11\bar{2}2\}$ $\{11\bar{2}3\}$	$\langle 10\bar{1}1\rangle$ $\langle 11\bar{2}6\rangle$ $\langle\bar{1}\bar{1}23\rangle$
α-Ti	1,587	$\{10\bar{1}2\}$ $\{11\bar{2}1\}$ $\{11\bar{2}2\}$ $\{11\bar{2}3\}$	$\langle 10\bar{1}1\rangle$ $\langle 11\bar{2}6\rangle$ $\langle\bar{1}\bar{1}23\rangle$
Be.	1,568	$\{10\bar{1}2\}$	$\langle 10\bar{1}1\rangle$
Re	1,614	$\{11\bar{2}1\}$ $\{10\bar{1}2\}$ $\{11\bar{2}2\}$	$\langle 11\bar{2}6\rangle$ $\langle 10\bar{1}1\rangle$ $\langle\bar{1}\bar{1}23\rangle$
Co	1,623	$\{10\bar{1}2\}$ $\{11\bar{2}1\}$	$\langle 10\bar{1}1\rangle$ $\langle 11\bar{2}6\rangle$

1. Metal
2. Twinning plane {hkil}
3. Direction of displacement [uvtw]

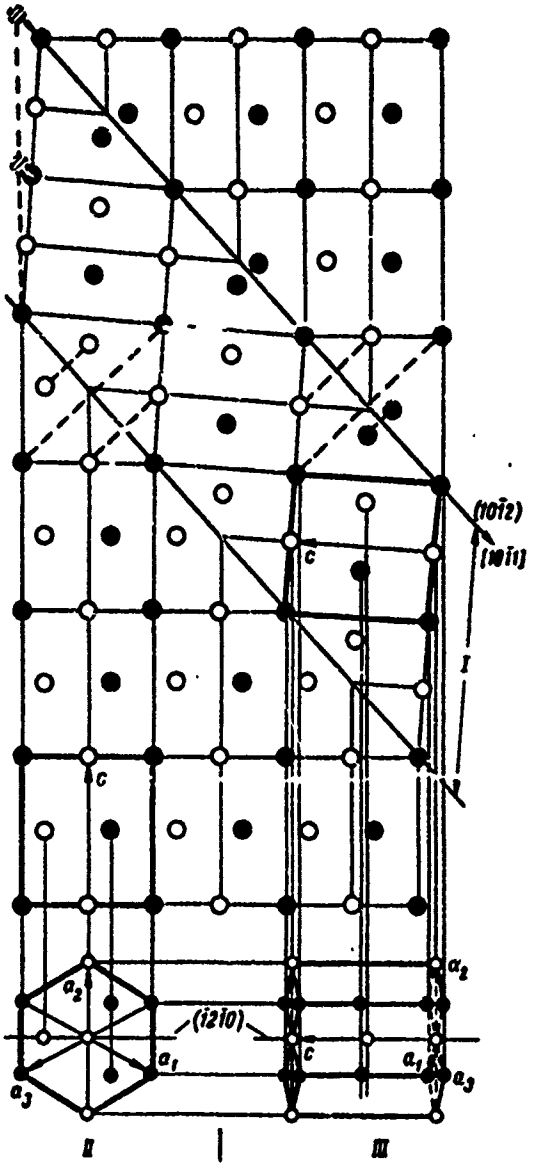

Figure 60. Projection of the matrix and twin in an hexagonal densely-packed lattice on the plane (1$\bar{2}$10). The twinning plane is (10$\bar{1}$0) and the direction of the displacement is [10$\bar{1}$1]: I is the layer of the twin; II is the projection of the matrix; III is the projection of the twin.

Mechanical twinning takes place at stresses much less than the theoretical strength of an ideal crystal. Nevertheless, for the onset of twinning the stresses must be considerably greater than for gliding, and further development of the process may take place even at lower stresses. Unlike gliding, for twinning it is difficult to establish the magnitude of the critical displacement stress. The values which have been derived for the actual twinning stress by various authors sometimes differ by 100 times [14]. Such scatter is caused both by methodical errors and because twinning during static deformation depends strongly on the presence of stress concentrators. Local stresses may be formed, for example, by the pile-up of dislocations. Price [143], during the deformation of zinc whiskers, found that the critical twinning stress is equal to 100 Mn/m^2 (10 kgf/mm^2) during favorable orientation and 600 Mn/m^2 (60 kgf/mm^2) in individual samples. If we eliminate the influence of the concentrators, then the necessary stress is 400-650 Mn/m^2 (40-65 kgf/mm^2). According to the data in [144], for the onset of twinning in zinc whiskers there must be a stress of 500 Mn/m^2 (50 kgf/mm^2) and for growth of the already existing twin it is less than 5 Mn/m^2 (0.5 kgf/mm^2).

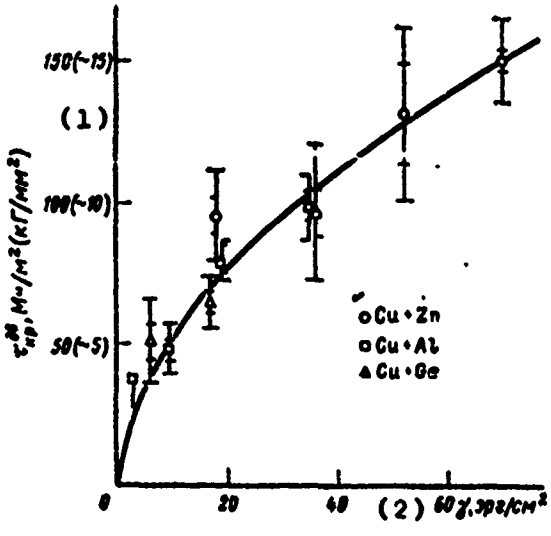

Figure 61. Dependence of stress necessary for formation of twins on energy of packing defects of copper alloys doped with zinc, aluminum, and germanium [134].

1. τ_{cr}^{tw}, Mn/m^2(kgf/mm^2)

2. γ, erg/cm^2

Reference [145] showed that by lowering the deformation temperature the resistance to twinning in zinc is increased by four-five times. In titanium by lowering the temperature and pulsed load the twinning planes are modified. All this indicates that determination of a critical twinning stress involves considerable experimental difficulty.

By investigating transition metals and alloys on their base, in reference [146] it was found that the moment of appearance of twins depends on the magnitude of the effective stress. Twins are generated under loads which exceed a certain given magnitude of twinning stress τ_{cr}^{tw}, which is determined basically by the energy of the packing defects of the alloy and depends on its chemical composition. The dependence of twinning stress on energy of the packing defects γ was also mentioned in reference [134], where copper, doped with various elements that lower γ, was investigated (Figure 61). The magnitude of the stress at which the twins are generated depends on the purity of the crystal. Bochvar et al [147] established that the stress necessary for onset of twins in zone-refined bismuth is almost half that of technical bismuth.

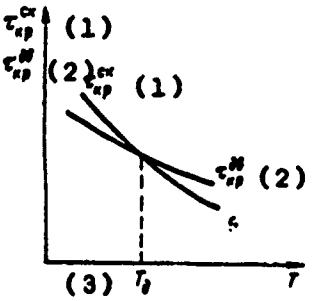

Figure 62. Schematic dependence of the critical cleavage stress of gliding and twinning on deformation temperature.

1. τ_{cr}^{gl}
2. τ_{cr}^{tw}
3. T_d

Decreasing the temperature and increasing the deformation velocity facilitates the development of twinning. With decrease in temperature a transition is observed from gliding to twinning. This involves a different temperature dependence of the critical gliding stresses (τ_{cr}^{gl}) and twinning stresses (τ_{cr}^{tw}) (Figure 62). The equation $\tau_{cr}^{gl} = \tau_{cr}^{tw}$ is satis-

fied at a certain temperature T_d. When $T < T_d$-$\tau_{cr}^{gl} > \tau_{cr}^{tw}$, plastic deformation begins by twinning. For metals with an fcc lattice, for example, τ_{cr}^{tw} must be less than the critical cleavage stress along the plane {111}. When $T > T_d$ gliding is preferred. Since τ_{cr}^{tw} varies more weakly with deformation velocity than τ_{cr}^{gl} [148, 149], increasing $\dot{\varepsilon}$ shifts T_d to the region of higher temperatures.

Just as in all similar cases, in the shaping of new formations it is interesting to examine the origin and the propagation velocity of the twin. The secondary velocity may be represented, for example, as the rate of displacement of the twinning dislocation along the line OB (see Figure 54). However it is extremely difficult to obtain such data experimentally. In reference [150] an attempt was made to evaluate the linear density of twins, i.e., their number, or rate of formation per unit of time as a function of the amount of deformation. According to the data in [150], the linear density grows only up to 2% of the deformation, then remains constant. These results, however, are contradicted by numerous experiments according to which a high stress is necessary for the onset of twinning. Furthermore, direct metallographic investigations show that it is mainly the number of twins that grows with development of the deformation. Takenchi [151] estimated the rate of propagation of the apex of the twin in iron in the direction parallel to the shift ⟨111⟩. The value of 2.5 mm/μsec, which he found, is near the rate of propagation of transverse waves. In the perpendicular direction the velocity was 6 mm/μsec.

In this case it is more proper to evaluate, as is done in the majority of works, the rate of propagation of the twin by experimentally determining the time of its propagation. Bunshah [152] studied the rate of propagation of twins in bismuth, zinc, and iron at various temperatures. In all cases this rate comprises a significant part of the rate of propagation of the elastic transverse wave. For bismuth it almost reaches this latter (1800 m/sec), and for zinc and iron it comprises approximately half. The reason for the rapid propagation of twins is the large difference in the formation stresses and growth of the layer. It is interesting that in the deformation of bismuth in the range from +20 to -195° C, the rate of propagation of the twin is practically identical. Analogous results were also found on iron in the temperature range of -196 ° C to +123° C at a deformation velocity of 10^{-4} sec^{-1} [151]. Thus, growth in twins is obviously not a thermally activating process.

At the present time there are no directly experimental data that determine the influence of deformation velocity on the rate of propagation of the twins. But, as has been shown, the rate of propagation is near the velocity of the elastic wave. At the same time, from Chapter 2 it follows that the velocity of dislocation displacement by increasing the external stress approaches those same values but does not exceed them [1]. Consequently, we can expect that the increase in deformation velocity, just as the change in temperature, is not substantially expressed in the rate of propagation of the twins.

If we take on the average the rate of twin propagation to be equal to approximately 2000 m/sec, and the length of the twin to be commensurate with a grain size of 20 μm, then we find that the time of the formation of the twinned layer is about 10^{-8} sec. This time is certainly less than the time of application of the pulsed load. More important, for the formation of a twin, we nevertheless do not require a stress in the hundreds or even in the tens of kilobars.

The twinning characteristics in magnesium and the MA-8 alloy on a magnesium base (1.32% Mn, 1.2% Zn, 0.32% Ce) were studied bu us [108, 109] in the detonation and hydrostatic punching of half-spheres, having a radius of about 150 mm. In the billets we grew a grain of about 500 um in size; the surface of the samples prior to deformation was polished in 15% HNO_3.

The twins during quasi-static deformation of magnesium and the MA-8 alloy are usually developed from the grain boundaries (Figure 63). They have a lenticular loop and within a single grain they are propagated in one or two directions. Analogous twins were also detected in reference [126] and identified as $\{10\bar{1}2\}\langle 10\bar{1}1\rangle$. Although in the general case twinning may be accomplished in all six pyramidal planes, in static deformation it takes place only along those for which the magnitude of the shearing stresses reaches a certain value of τ_{cr} for the given twinning plane. Reaching τ_{cr} is facilitated by the presence of stress concentrators, which in the given case are the grain boundaries. During pulsed loading the role of twinning grows significantly both in magnesium and in the MA-8 alloy. Under these conditions the twinning takes place along a greater number of planes; the number of twins grows by two to three times and they are ar-

[1] Supersonic dislocations in this case do not have to be examined since for the movement of such dislocations we assume the lack of barriers in the glide plane and for the formation of twinning dislocations there must be a fixed pole.

ranged in three to four directions (Figure 64). Here the deformation twins appear both in the boundary region and directly in the body of the grain, i.e., their generation depends to a lesser degree on the stress concentration at the grain boundaries than during quasi-static deformation. The density of the twins n_{tw}, i.e., the number of twins intersecting the straight line in one field of the thin section, during pulsed deformation is increased by almost three times. If during the quasi-static deformation up to $\varepsilon = 4\%$, $n_{tw} = 2.9$, then during pulsed deformation with the same degree of deformation, $n_{tw} = 6.6$.

Figure 63. Twinning in magnesium by static deformation. The individual twins come from the grain boundaries. Within a single grain the twins are parallel, thus indicating a single twinning system. X 300.

Twinning progresses with increase in the degree of deformation regardless of the loading velocity, but this process takes place more abruptly by detonation punching.

Joshinaga and Horinchi [153] observed a pile-up and subsequent slow-down of the dislocations in the displacement plane $\{11\bar{2}0\}$ in the deformation of magnesium. Rather high stresses were generated in the plane that were partially relaxed by bending the crystal along this plane and partially by extensive twinning along the $\{10\bar{1}2\}$ under conditions which are completely uncharacteristic of twinning. This led to a significant strengthening of the magnesium crystal, similar to the strengthening of metals with an fcc lattice at the second stage, although the strengthening for magnesium was G/1000, which is several times lower than for the fcc metals [154].

Figure 64. Twins in magnesium during detonation deformation, arranged along four different planes.

In addition to the magnitude of the critical cleavage stress, one or another twinning system is determined by the orientation factor. Reed-Hill [155] studied twinning in zirconium, whose grains had a different orientation of the basal plane with respect to the applied load. Computation shows that the maximum of the orientation factor for the various twinning systems is found at different angles to the basal plane (Figure 65 a). The identification of twins made by the authors in the variously oriented grains, is shown in the form of histograms on Figure 65 b. The results agree well with the computed coefficients.

If the twinned layer is oriented such that the glide planes are favorably arranged to the effective stress, it is possible to have a gliding process inside the twin. Such an example is shown on Figure 66. Inside the forming twins we can see traces of base gliding. Probably this may be an illustration of a specific case when, in spite of the past twinning, a stress level was retained that is sufficient for gliding along the basal plane by favorable orientation of the plane with respect to the applied stress.

The dependence of the width of the x-ray lines of the MA-8 alloy on the degree and type of deformation (Figure 67) has a slightly unusual form. Even with small degrees of quasi-static and pulsed deformation ($\varepsilon \approx 2\%$) the width of the line (0006) grows by almost three times in comparison with the original value and then practically grows no more. At the same time the width of the line (0002) is monotonically increased in the entire range of the degrees of deformation.

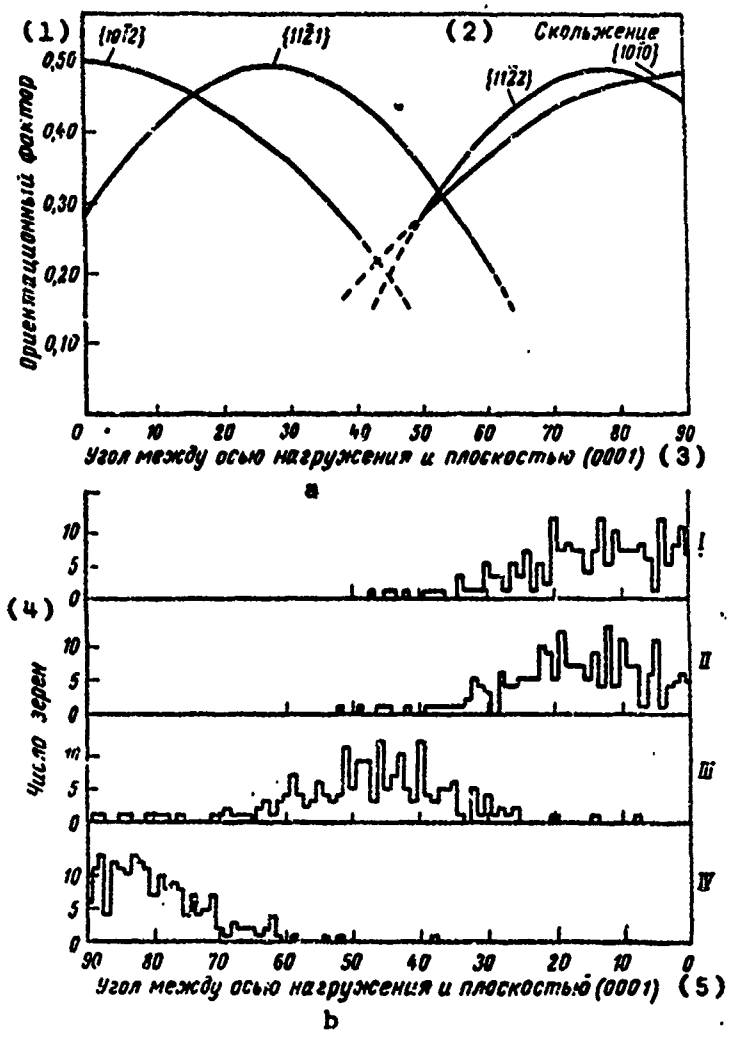

Figure 65. Change in the orientation factor (a) for the various twinning and gliding systems along $\{10\bar{1}0\}$ and distribution of the number of grains with different systems of twins (b) as a function of the angle of slope of the basal plane [155]: I. grains without twins with gliding along $\{10\bar{1}0\}$; II. twins along the plane $\{11\bar{2}2\}$; III. twins along the plane $\{11\bar{2}1\}$; IV. twins along the plane $\{10\bar{1}2\}$.

1. Orientation factor
2. Gliding
3. Angle between the axis of the load and the plane (0001)
4. Number of grains
5. Angle between the axis of the load and the plane (0001)

Figure 66. Pulsed deformation of magnesium. Visible are tracks of the base glide and twins. Inside the twinned layers is seen the base glide of a lower density than in the matrix. X 600.

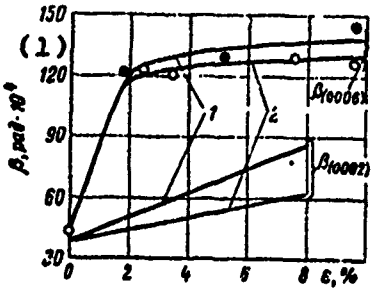

Figure 67. Dependence of the width of the x-ray lines (0006) and (0002) of the MA-8 alloy on the degree and type of deformation: 1. dynamic deformation; 2. quasi-static deformation.

1. β, rad.10^4

The results of harmonic analysis on the shape of the line showed that the size of the blocks of coherent scattering is decreased with increase in the degree of deformation (Figure 68). Such a dependence was found repeatedly on many materials. But the size of the microdeformations (Figure 69) is also decreased, and its drop is more sharply expressed during high-velocity deformation. This somewhat unusual result can be understood by examining it in connection with the deformation mechanism at the various stages of the process. With small degrees of deformation, although the critical cleavage stress of twinning is not yet reached, all the

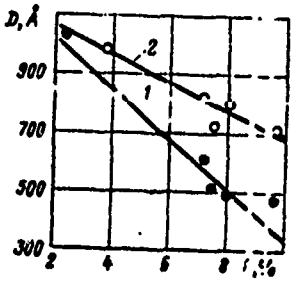

Figure 68. Change in the size of the experimental MA-8 alloy as a function of type and degree of deformation: 1. dynamic deformation; 2. quasi-static deformation.

deformation takes place by gliding along some single system that is most favorably oriented with respect to the external stress. During this period, in the absence of a sufficient amount of the relaxation processes, the microdeformations grow rapidly. But after reaching a given magnitude the stresses are relaxed as a result of the developing process of twinning. As is clear from Table 15, with an increase in the degree of deformation, the twinning role is increased, which also leads to the dependence shown on Figure 69. This is manifested especially sharply during high-velocity deformation. Iohari and Thomas [156] mentioned that the density of the dislocations is lowered by the appearance of twins.

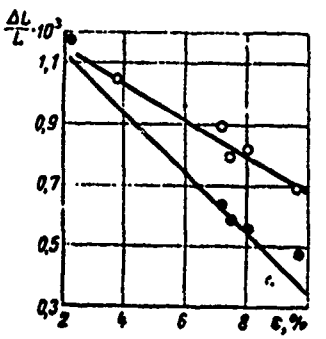

Figure 69. Change in the magnitude of microdeformations in the MA-8 alloy as a result of the type and degree of deformation. The symbols are the same as in Figure 68.

Titanium is very sensitive to the loading procedure. The mechanism of its deformation varies as a function of the diagram of the stressed state [157, 158], the velocity [159],

and the deformation temperature [160]. If the deformation is accomplished by gliding in the process of tension at room temperature, then a large number of twins is observed during twisting. Increasing the rate of the tension from 0.8 to 24 mm/min significantly intensifies the twinning process [159].

In our work we investigated type VT-1 technically pure titanium. The billets were subjected to quasi-static deformation at a velocity of about 10^{-3} sec^{-1} on a hydraulic testing press or on a 1000-ton hydraulic press.

High-velocity deformation was done either according to the detonation diagram (see Figure 4) or by the electromagnetic method described in Chapter 1. In both cases the deformation velocity was about 10^4 sec^{-1}.

For the intermediate deformation velocity (about 10 sec^{-1}) we used plastomere, whose design was described in reference [161].

We grew a grain of about 200 μm in size in the billets with the aid of two-fold and three-fold deformation up to a critical degree of 7-8% and subsequent annealing at 800° C. The surface on which we studied the glide and twin tracks was first polished in an electrolyte with a composition of 80% H_2SO_4, 10% HF and 10% H_2O, at a current density of 15 A/cm^2.

Quasi-static deformation, as already mentioned, begins from gliding (Figure 70 a). With increase in the degree of deformation the number of systems included in the gliding is increased, and only when ε = 15-18% (Figure 70 c) do individual twins appear in a single direction.

The mechanism varies sharply in deformation by detonation and during electromagnetic punching. The deformation is almost completely accomplished by twinning (Figure 71). Depending on the orientation of the grain with respect to the effective stress, the twins have a different shape, which apparently is already due to the rate of growth rather than to the conditions of twin origin. But in either case quite a few twinning systems are detected. In grains with wide twins we can observe any interaction between them within the framework of the classification suggested by Startsev, Kosevich, and Tomlenov [162].

Ul'yanov and Moskalenko [160] assume that the shape of the twins in alpha-titanium depends on the twinning system. But they made no identification. A different shape of the twins under impact tension was also detected in reference [163]. These authors assume that the shape of the twins is

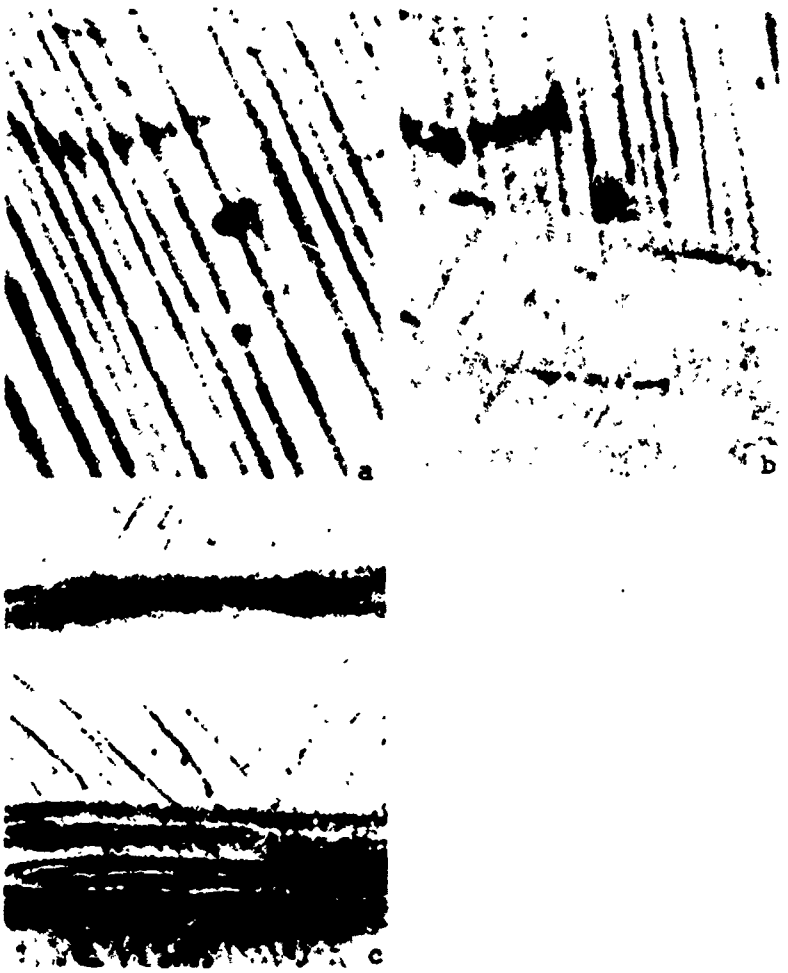

Figure 70. Deformation tracks in technically pure titanium type VT-1 after quasi-static deformation: a. ε = 5%; visible are tracks of prismatic gliding; b. ε = 10%; basal and prismatic gliding are developed; c. ε = 18%; twins appear arranged in one direction. X 500.

determined by the deformation velocity, assuming that at small velocities the time of applying the load is greater and this facilitates growth of the twin. Such an opinion is not correct, since it is known that for the development of twinning we need a significantly lower stress level than for the onset, and the time of application of this stress is undoubtedly greater then the time of the non-diffusion displacement.

The explanation suggested in reference [163] is not confirmed by our experiments either. The twins shown on the two photographs on Figure 71 have been produced in various grains on one and the same sample deformed by 12% detonation.

By carefully preparing the surface of the thin section in samples of alpha-titanium it is possible to produce etching holes which permit identifying the twins and the glide lines in the individual grains. Depending on the orientation of the grain of alpha-titanium to the plane of the thin section the shape of the etching holes, as shown on Figure 72 a may be different. For identification on a great circle of projections (Figure 73) from the microphotographs the etching holes (shaded triangle in the center of the circle) and the twin tracks oriented toward them are shifted. Since the sides of the isosceles triangle are tracks of the intersection of the plane of the thin section with the planes of the set $\{10\bar{1}0\}$, then the gnomonic projections of these planes must lie on the normals to the sides of the triangle (the thin dotted lines on Figure 73 b). Then we can determine the position of the gnomonic projection of the basal plane (0001), which is 90° away from $(01\bar{1}0)$ and from $(10\bar{1}0)$. Thus the grain orientation has been determined.

Possible twinning planes, as we know, depend on the type of crystal lattice. Therefore on the great circle of projections in accordance with the grain orientation we plot the projections of the planes which may be the twinning planes. For titanium it is feasible to plot the projections of the planes $\{10\bar{1}2\}$, $\{11\bar{2}1\}$, $\{11\bar{2}2\}$, and $\{11\bar{2}3\}$.

At the same time the stereographic projection of the twinning plane plotted from the microphotograph must lie on the normal drawn toward this plane and passing through the center of the great circle of projections. On Figure 75 the twinning planes are identified as $(\bar{1}2\bar{1}2)$ and $(10\bar{1}2)$. The glide tracks may be identified analogously.

Identification of a large number of thin sections showed that during quasi-static deformation in alpha-titanium the twinning takes place only along planes of the set $\{10\bar{1}2\}$, for which obviously τ_{cr}^{tw} is minimal. During high-velocity deformation titanium in addition is twinned along the planes $\{11\bar{2}1\}$ and $\{11\bar{2}2\}$. Fine twins, analogous to those shown on Figure 71, were produced by Reed-Hill and Buchman [164] in zirconium and called "zig-zag" twins. Interpretation determined the twinning planes as $\{10\bar{1}2\}$ and $\{11\bar{2}1\}$.

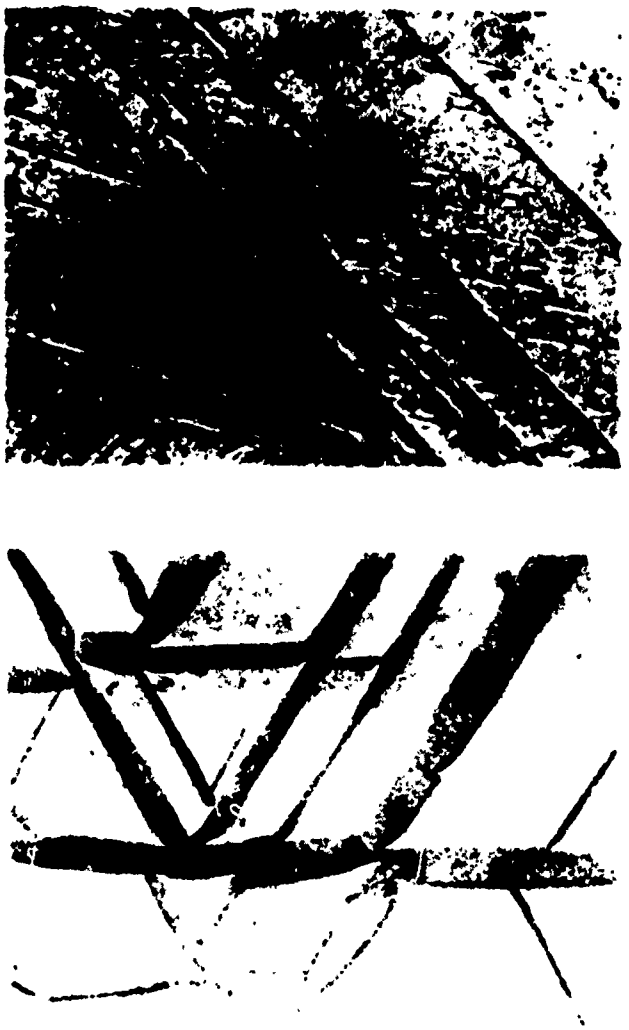

Figure 71. Microstructure of type VT-1 titanium after high-velocity deformation. In one grain the twins are arranged along several crystallographic planes. ε = 12%. Depending on the orientation of the grain the twins have a different shape. X 500.

Twinning in the VT-1 titanium and the OT-4 alloy (2.92% Al and 1.4% Mn) at various deformation velocities was studied by Knizhnik [165]. For identification of the twins in single-phase alpha-titanium type VT-1 the method described in reference [166] was used also for the identification of twins in the OT-4 alloy and an assumption of crystallographic correspondence was made, according to which the particles of beta-titanium are arranged along the

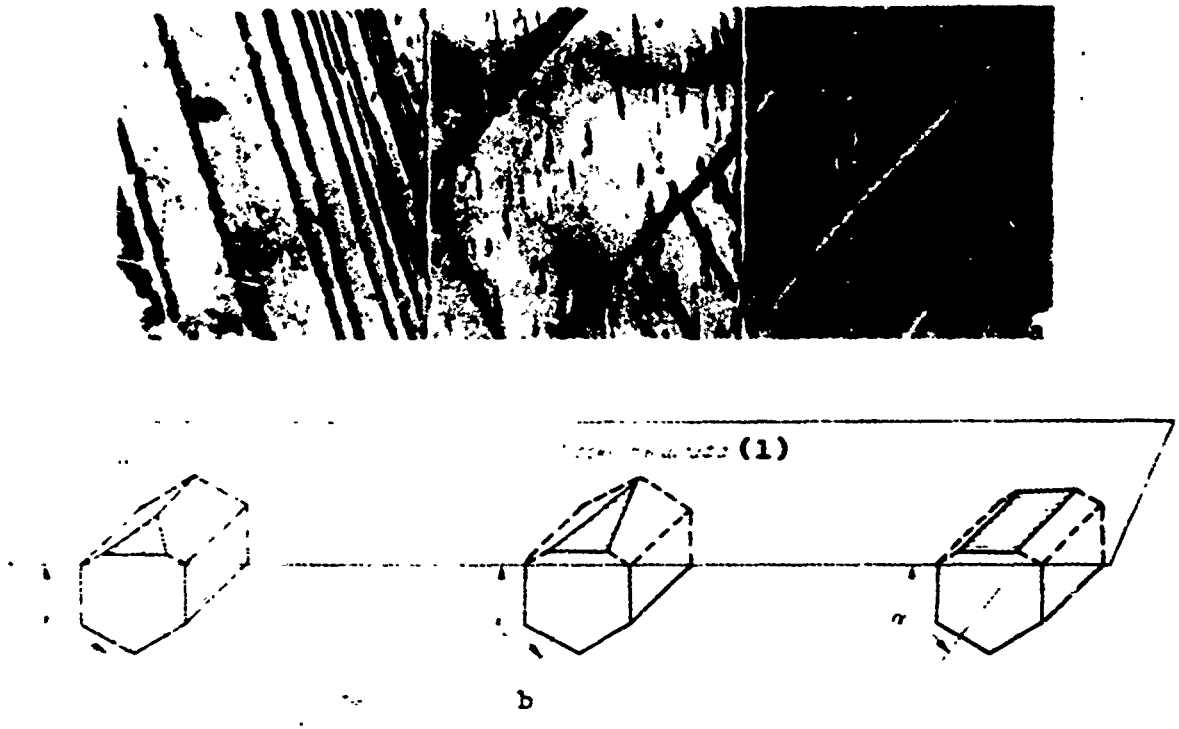

Figure 72. Shape of the etching holes in grains of alpha-titanium as a function of grain orientation to the plane of the thin section (a) and the respective arrangement of the crystal (b). The alpha-angle between the plane of the thin section and the axis Z, $\alpha_1 > \alpha_2 > \alpha_3$.

1. Plane of the thin section.

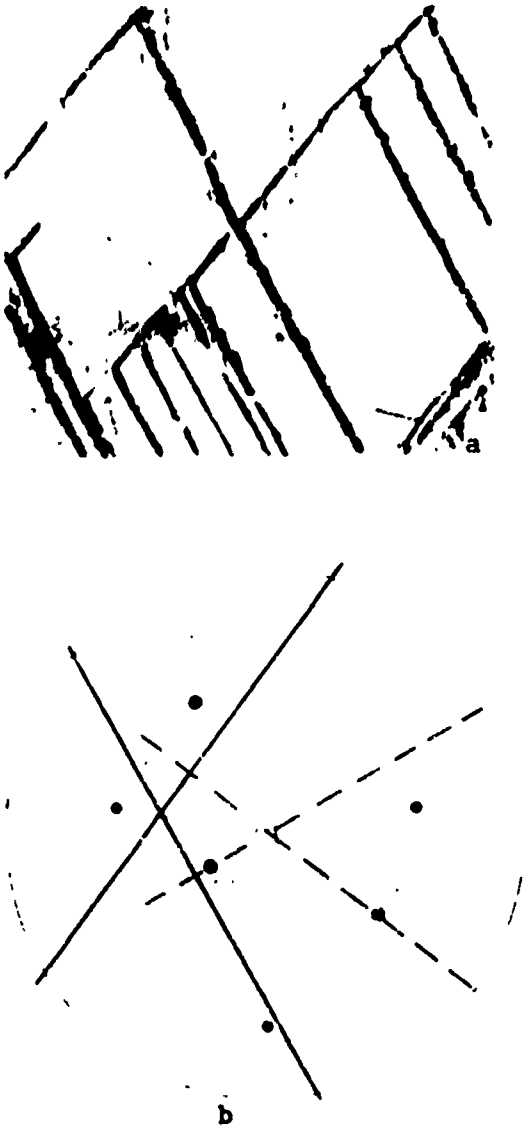

Figure 73. Identification of twins from the etching holes: a. twins and etching holes in alpha-titanium; b. great circle of projections; triangle in the center is similar to the etching hole; the heavy solid lines are tracks of the twins; the heavy dotted lines are the normals to the twinning planes; o are the possible twinning planes; ● are the indices of the twinning planes visible on the microphotograph.

planes $\{10\bar{1}0\}$ of the alpha-phase. The deformation velocity varied from 0,00167 to 600 m/sec. The author assumes that by increasing the deformation velocity the number of twinning systems is decreased and the twinning systems $\{1\bar{1}01\}$ and

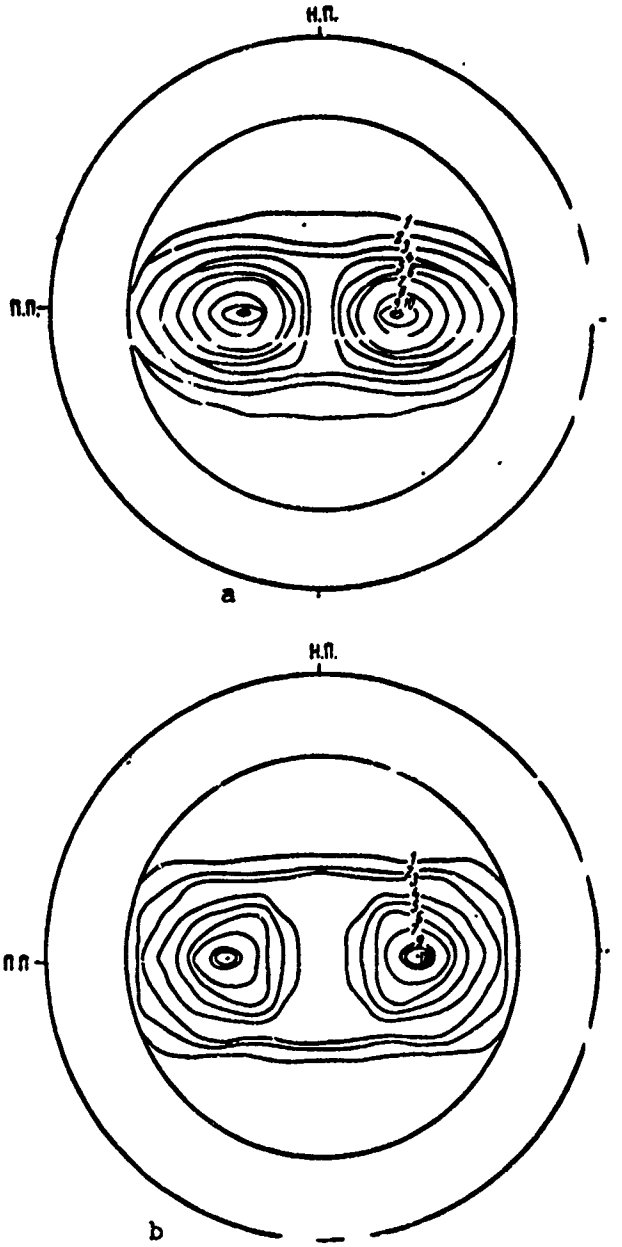

[Continued on next page]

[Continued from previous page]

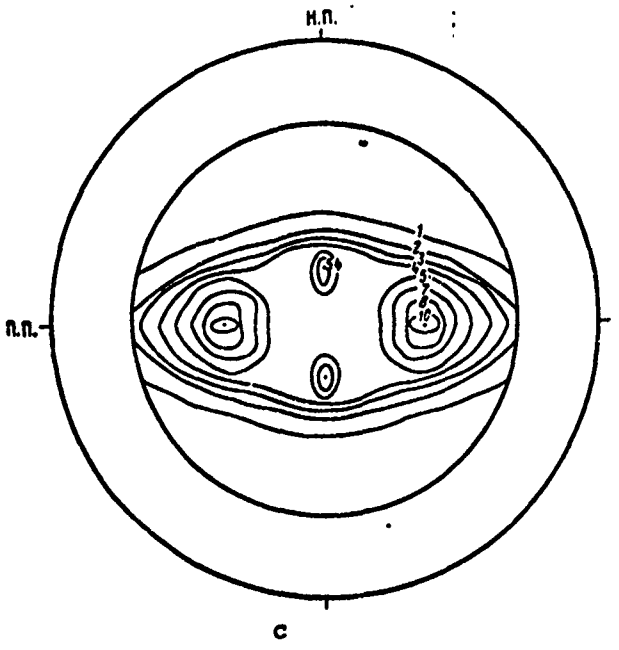

Figure 74. Pole figures (0001) of the VT-1 alloy: a. after rolling; b. after quasi-static deformation; c. after pulsed deformation.

$\{1\bar{1}02\}$, appearing statically are changed after detonation into $\{11\bar{2}1\}$ and $\{11\bar{2}2\}$ for the VT-1 alloy and into $\{2\bar{2}01\}$ and $\{2\bar{2}03\}$ for the OT-4 alloy.

Twinning along the planes with such large indices is encountered very seldom, and as a rule, is not confirmed by further investigations. In magnesium the twins which first were identified as $(30\bar{3}4)$ [167] were found to be twins $(10\bar{1}1)$ and $(10\bar{1}3)$ which are then retwinned along $(10\bar{1}2)$ [140]. In reference [165] it would probably be necessary to confirm the structural correspondence of beta- and alpha-titanium by electron diffraction, which may change under pulsed loading conditions.

In recent years analysis of the orientation has been made not only as a method of describing the isotropicity of the properties of metals, but also as a method of investigating the elements of gliding and twinning [146]. Such a relationship undoubtedly has proper structural premises, but as yet no overall diagram exists which permits making any quantitative evaluation in each individual case.

The original sheets of the VT-1 alloy, which we deformed by detonation and quasi-statically, had an orientation that is characteristic of many metals with a hexagonal densely-packed lattice. The basal plane (0001) was turned by approximately 30° around the direction of rolling (Figure 74). During quasi-static and hydrodetonation deformation the change in orientation has a common trend. With increase in the degree of deformation a secondary orientation maximum (0001) appears that forms an angle of about 20° with the plane of the rolling. But, as we can see from Figure 74 b and c, during detonation deformation the secondary maximum appears significantly earlier. An analogous change in the orientation was mentioned in references [168, 169] by doping titanium with zirconium. The authors associate the appearance of supplementary maxima with change in the effective twinning systems.

Twinning in Metals With an fcc Lattice

Twinning in metals and alloys with an fcc lattice is not such a common mechanism for the relaxation of stresses as in hexagonal densely-packed metals. Analysis of references [156, 170-172] shows that the onset of twinning in metals and alloys with an fcc lattice depends mainly on the following factors:

(1) The amount of energy of the packing defects in the metal or alloy and correspondingly the degree of doping of the alloy;

(2) Temperature of deformation;

(3) Velocity of deformation;

(4) Original crystallographic orientation with respect to the effective stress.

The curve for the tension of metals with an fcc lattice at low temperatures has a characteristic shape with a segment of the broken line where twinning is actively developed (Figure 75). The formation of twins is accompanied by characteristic cracking and propagation of Neumann bands over the entire deformed volume. Deformation curves analogous to those shown on Figure 75 were obtained for the tension of copper [171] and of alloys of copper with gallium and germanium [172].

With increase in the deformation velocity in several metals, and especially in alloys, twins appear along the plane of the octahedron at room temperature and even at elevated temperature [173, 156, 101] and from a certain value of the velocity (or value of the peak pressure) this process pro-

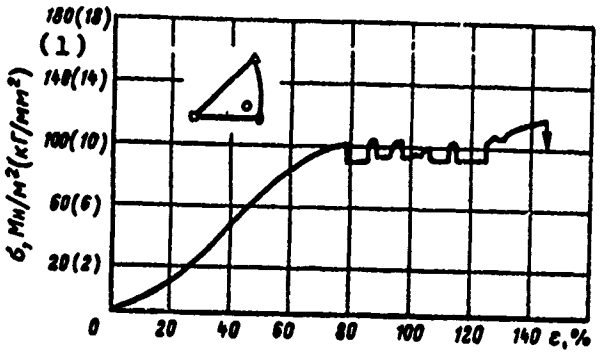

Figure 75. Stress-strain curve for the Au+10% Ag alloy at 77.3° K [172].

1. σ, $Mn/m^2(kgf/mm^2)$

gresses: the contribution of twinning to the overall deformation grows. The pressure, at which twinning begins, varies in wide ranges for the various metals and alloys. A definite relationship is seen between this pressure and the energy of the packing defects (Table 18). On the Cu-Al alloy [156] it is shown that the density of the twins is increased with increase in pressure, and the thickness of the twinned layer is decreased.

Table 18. Critical Pressure Corresponding to the Onset of Twins During Pulsed Deformation for Alloys With Different Packing Defect Energy

Металл или сплав (1)	γ, эрг/см² (2)	$P_{крит}$ для появления двойников, кбар (3)	Литературный источник (4)
Ni	~180	350	[173]
Fe + 29% Ni	~100	220	[101]
Cu	70	16—28	[156]
Cu + 1,1% Al	50	12—25	
Cu + 2,2% Al	35	6—12	
Cu + 8,19% Al	2,5	<6	

1. Metal or alloy
2. γ, erg/cm^2
3. P_{cr} for onset of twins, kbar
4. Literature source

In accordance with the twinning model of Venables [133, 134] the critical cleavage stress of displacement during twinning τ_{cr}^{tw} depends on the energy of the packing defects γ, the Burgers vector of the partial dislocation $\bar{b}_1$, the coefficient of the stress concentration n and on the radius of the half-loop of the packing defect a_0:

$$n\tau_{cr}^{tw} = \frac{\gamma}{\bar{b}} + \frac{G\bar{b}_1}{2a_0}. \qquad (60)$$

But the value of $2a_0$ may be equated to the length of the dislocation line ℓ, the motion of which under the effect of the applied stress is determined by the familiar relationship $\tau = G\bar{b}/\ell$. Substituting this value into formula (60), we have

$$\tau_{cr}^{tw} = \frac{\gamma\bar{b}}{\bar{b}_1(n\bar{b} - \bar{b}_1)}. \qquad (61)$$

The presence of the concentration factor explains why, in the individual regions of the crystal, twinning is observed and in others with the same density of dislocations there are no twins. For quasi-static deformation Venables assumes $n \geqslant 3$ wherein n may vary as a function of γ. During pulsed deformation [156], even assuming n = 1, the computational data are found to be slightly lower than the experimental data (see Figure 76). In other words, under conditions of pulsed loading, the role of the stress concentrators is significantly reduced.

As follows from the dislocation twinning model, the formation of twins in an fcc lattice is directly related to the activation of transverse gliding. Table 19 shows data [137] on twinning in metals with an fcc lattice as a function of the quantity $G\bar{b}^3/A$ (where A is the energy of activation of transverse gliding).

It is still difficult to establish from which of the values the better correlation is established for the critical twinning stress: with the energy of the packing defects or with the energy of activation of the transverse gliding. But we do know that these values are interrelated.

For single crystals the pressure necessary for twinning depends to a significant degree on the crystallographic direction. According to the data of DeAngelies and Cohen

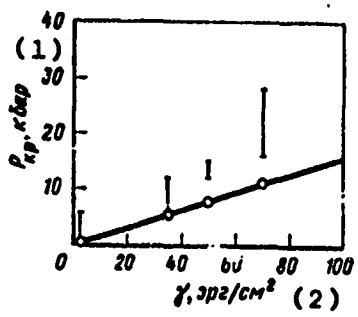

Figure 76. Dependence of the critical impact pressure, necessary for the appearance of twins, on the energy of packing defects; the vertical segments are plotted from the experimental data [156]; the points on the line are computed from formula (61).

1. P_{cr}, kbar 2. γ, erg/cm^2

Table 19. Dependence of Twinning on the Value of Gb^3/A

Металл или сплав (1)	Gb^3/A	Образование двойников (2)
Al Ni Pb	32 12 9,4	Не образуются (3)
Ni + 40% Co	8,7	Образуются при низкой температуре (4)
Cu + 1% Ge Ag Cu Ni + 5% Cu Au Cu + 33% Ge	7,5 5,3—7,6 5,3 4,6 4,1 4,0	Легко образуются (5)

1. Metal or alloy
2. Formation of twins
3. None formed
4. Formed at low temperature
5. Easily formed

[174], if the deformation takes place in the direction [100], the twins appear at 145 kbar; if this direction of deformation is [111], then they appear at 200 kbar.

Verbraak [101] deformed copper under a pressure of 220 kbar, applying a load in different crystallographic directions. The largest number of twins, arranged along the octahedral faces, was seen in the deformation of copper in

the direction [113], there were fewer twins and twinning systems by loading along the [100] and no twinning took place under the effect of the shock wave in the direction [110]. Twinning by deformation along [113] is explained mainly by the fact that in this case a maximal effective stress is generated on the octahedral planes.

The opposite result was found by Smith [175, 176], who observed abundant twinning during deformation along [110] and an absence of twins under the effect of the shock wave along [113]. The reason for such contradictory results becomes clear if we examine the conditions of the experiments. In Verbraak's experiments two samples arranged one on the other were subjected to the effect of a shock wave. Under these conditions the interference tension was completely damped in the lower sample, and the upper sample was subjected only to compression. In Smith's experiments the sample was deformed actually under the effect of the expansion wave, and as a result of the polar mechanism of twinning in these tests the opposite result was obtained.

An effective method of studying the twinned layers is analysis of electron-diffraction patterns.

In nickel, because of the high energy of the packing defects, twins are formed only under high pressures, and the twins are so fine that they are not resolved under ordinary optical magnification [177]. Holder and Thomas [173], under the same deformation conditions as in reference [177] at a pressure of about 350 kbar, detected in nickel a system of very fine twins (about 0.05 μm), which they were able to see only with the aid of electron diffraction. The {111} plane was the twinning plane.

In the development of plastic deformation the glide bands or twins must interact with one another or with the barriers existing in the grains. Pogrebnoy and Zhak [178] assume that the twinning is accompanied by more complex and diverse local deformations that gliding. This assumes especially great significance during high-velocity deformation since it is related to the large volume of twinning and to higher peak pressure. The authors of reference [179] observed, in stainless steel during loading at a velocity of 10^3-10^4 sec^{-1}, a transition of the dislocations and the glide lines through the twinned boundaries, and the onset of glide bands in the matrix due to the high concentration of stresses as a result of twinning.

Subsequent deformation by twinning and gliding was observed by Verbraak [101] on an alloy of iron with 29% Ni.

This alloy with an fcc lattice was deformed by a shock wave at a pressure of 220 Kbar in the direction [113]. As is clear from the microphotograph (Figure 77) the twins traveling along the octahedral planes, are intersected by the glide lines, traveling from the twin to the matrix. Such a picture was observed by us in magnesium (see Figure 66). In all probability, the gliding was formed after twinning. At the initial moment of loading the grain was not favorably oriented for gliding. However as a result of twinning the octahedral plane AB is set up such that gliding is found to be possible along [110], and the externally applied stress was partially relaxed, but remained at a level sufficient for gliding. Gliding reaches the twin-matrix boundary and continues in the matrix along the line BC.

Figure 77. Formation of glide bands in twins of the alloy Fe + 29% Ni [101]. As a result of twinning a more favorable orientation for gliding along {111} <110> was formed. X 125.

The reverse picture was observed on silicon iron [180] -- gliding preceded twinning. Theoretically such a sequence is possible at the proper temperature and deformation velocity when $\tau_{cr}^{tw} > \tau_{cr}^{gl}$.

It is interesting to note that the sign of the applied stress (contraction or expansion) may abruptly change the character of the processes taking place in deformation. In the described works of Verbraak the samples were subjected to compression. By expansion in the same Fe-Ni alloy instead of twinning, and consequently gliding, a martensite transformation was observed.

Twinning in Metals With a bcc Lattice

In metals with an fcc lattice, though twinning becomes possible only under sharply limited conditions and is very sensitive to the energy of the packing defects, in metals with a bcc lattice this method of relaxation of stresses is encountered rather often and in a number of instances determines the properties found. Just as in the deformation of metals with hexagonal densely-packed and fcc lattices, increasing the deformation velocity facilitates the development of twinning in metals and alloys having a bcc lattice.

Tardif et al [181] deformed cylindrical samples of iron at a pressure up to 400 kbar. At a length of 5 mm from the site of contact with the cast plate a maximal hardness was produced. Only the surface layer itself had a slightly reduced hardness.

This may be due to the fact that in the contact layer as a result of friction a rather high temperature is developed (according to Schekhtman's [2] data, during impact loading of copper and molybdenum up to 200 kbar in the surface layer with a thickness of about 0.5 mm the temperature of recrystallization is reached).

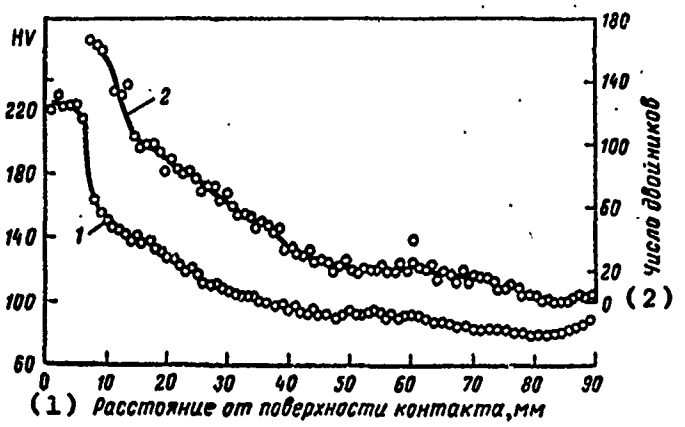

Figure 78. Hardness of iron (1) and number of twins (2) at various distances from the contact surface [181].

1. Distance from contact surface 2. Number of twins

[2] Private communication

The hardness, maximal near the contact surface, drops in proportion to the distance from this surface (Figure 78), and the number of twins in the grains is reduced. Obviously in this case the level of hardness is generally determined by the twinning process.

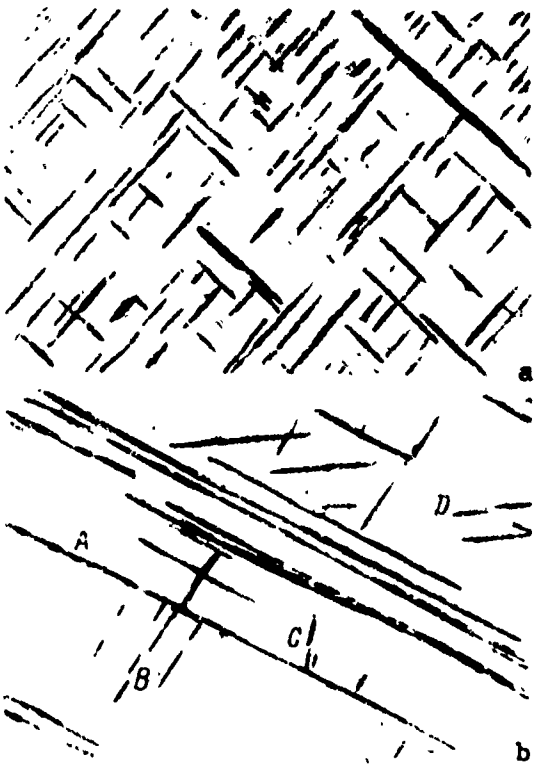

Figure 79. Twinning in single crystals of molybdenum under impact loading at a pressure of 200 kbar; a. in the direction [110]; twinning takes place over two systems; b. in the direction [112]; twins are seen that are arranged along four systems; A, B, C, and D are different twinning systems. X 200.

To realize twinning in crystals with a bcc lattice we must have a significant pile-up of dislocations in the plane {112}. One of the essential results of the effect of the shock wave consists of the creation of a high dislocation density along the twinning plane.

Verbraak [101] deformed single crystals of molybdenum at pressures of 20-30 kbar. The intensity of the twinning

under these conditions to a significant degree depended on the direction of the effective stress, although not a single orientation was detected at which twinning would commonly be absent.

During deformation in the direction [110] in the two twinning systems {112} ⟨111⟩, the coefficients of orientation were equal to 0.47 and in accordance with this the twinning took place along two systems (Figure 79 a). By applying an impact stress along the [112] it is possible to have an effect from seven systems, of which two have an orientation factor of 0.41, three have 0.32, and two have 0.16 (Figure 72 b). We know that the probability of twinning is decreased as the temperature is elevated. This is due not so much to the change in the kinetics of the twinning itself, as to the sharp decrease in τ_{cr}^{gl}. The same dependence is also retained at high deformation velocities. Twinning in molybdenum, which is extensive at room temperature, sharply drops if the deformation is carried out at 300° C, and ceases completely at 500° C. In this case all the deformation takes place by gliding.

In 1958 Davidenkov [183] was the first to show on armco iron that if two deformation operations follow one after the other, then the first to some degree determines the mechanism of the second. Single crystals of molybdenum [101] prior to detonation deformation were loaded quasi-statically with a small degree of deformation for identification of the gliding. During subsequent detonation deformation, at a pressure of 20-40 kbar, gliding was also observed instead of the twinning that is usual for these conditions.

Zukas and Fowler [184] subjected samples of iron to impact loading after annealing and after preliminary rolling with reduction of 10, 20, 30, and 50%. A pressure up to 750 kbar was applied in the direction perpendicular to the direction of rolling. Here regardless of the magnitude of applied pressure the number of grains with twins was decreased with increase in the degree of preliminary deformation (Figure 80). The authors also observed a dependence of the number of grains on the direction of the shock wave, which in our view probably is determined by the orientation produced after rolling.

In the twinning of two-phase materials a number of specific problems arise. On the one hand the influence of the secondary phase is manifested by twinning in the matrix. This is especially noticeable in that case when the secondary phase has a high hardness. On the other hand, the question arises as to succession of the secondary phase of the stress

relaxation mechanism created by the external load, and the stresses generated at the boundary of the two phases as a result of plastic deformation in the first phase.

Figure 80. Influence of preliminary rolling at room temperature on the number of twinning grains of iron during detonation [184]; pressure of the detonation wave: 1. 650 kbar; 2. 500 kbar; 3. 300 kbar; 4. 45 kbar.

1. Number of twinning grains, % 2. Degree of deformation during rolling, %

Bowden and Kelly [185] in the pulsed deformation of steel with 0.99% C at a pressure of 200 kbar observed twins of two types. Part of the twinned layers in the alpha-phase led to a displacement in the neighboring cementite grains (Figure 81 a), and part did not result in such displacement (Figure 81 b). Crystallographic investigation of the orientation showed that succession of the deformation by cementite is possible only with a given crystallographic correspondence. In order that the displacement of the type shown on Figure 81 a take place, it is necessary that the directions $[\bar{1}\bar{1}1]_{\alpha}$ and $[\bar{1}11]_{\alpha}$ correspond to the directions $[0\bar{1}1]_{Fe_3C}$ and $[\bar{1}11]_{Fe_3C}$.

Mehl et al [186], by examining the displacements in cementite of perlite and in hypereutectoid cementite, came to the conclusion concerning the structural correspondence of this phase found in various structural components. Probably the method of dynamic loading with different deformation stress may be used in two-phase materials for evaluation of the structural correspondence. For this purpose it is extremely effective to use electron diffraction identification of the twins by studying the thin twinned layers.

Figure 81. Twinning in steel with 0.99% C [185]: a. twinning in the alpha-phase leads to a shift in the cementite; b. no shift in the cementite.

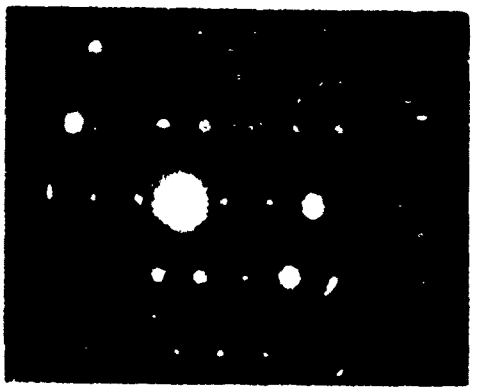

Figure 82. Electron diffraction pattern taken from the matrix and twin in low-carbon martensite. Accelerating voltage of 100 kV.

Figure 82 shows an electron diffraction pattern taken from quenched samples of low-carbon steel. A certain volume of the matrix was incident on the cross section of the electron beam: the alpha-solution of iron and the twinned layer. In accordance with this, on the electron diffraction pattern (Figures 82 and 83) we can discern the cell obtained from reflections from the matrix (solid lines on Figure 83), and the cell produced from the twin. With respect to the fact that one of the twinning planes of the set {112} is common, part of the reflections belongs both to the matrix and to the

twin. A characteristic feature of the electron diffraction pattern taken from the twin is that the reflections from the twin are shifted by a certain distance with respect to the basic reflections (in the first series by 1/3 of the size of the matrix cell, in the second by 2/3, etcetera) and are arranged symmetrically with the reflections from the matrix relative to the track of the twinning plane. The computations of the electron diffraction patterns have been studied in detail in reference [187].

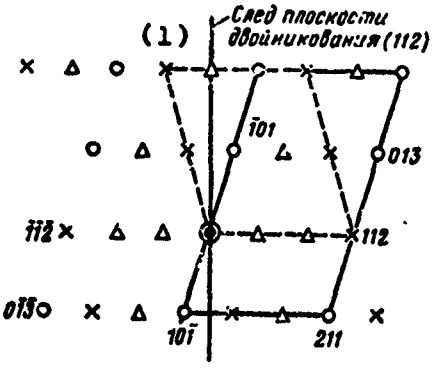

Figure 83. Diagram of the electron diffraction pattern shown on Figure 82. Axis of the zone [$1\bar{3}1$]: o = reflections from the matrix; x = reflections from the twin; Δ = reflections obtained from double diffraction;

1. Track of the twinning plane (112)

At the present time the majority of metals having more or less wide-spread practical use, have been investigated under conditions of high-velocity deformation. Nevertheless it is still difficult to create a classification that will define the groups of metals characterized by identical behavior under conditions of high-velocity deformation. In addition to the type of crystal lattice, the behavior of metals and their alloys during high-temperature deformation is determined by the melting point and the point of recrystallization, the energy of the packing defects, the presence or absence of a phase transition in the range of pressures investigated, and by other factors. An attempt to classify metals based on their behavior under conditions of high-velocity deformation was made by Dieter [188]. However, in recent years much new material has been accumulated. In Table 20 the metals and alloys are distributed in different groups. We stress those which are most characteristic of their "structural behavior" during high-velocity deformation.

Table 20. Behavior of Various Metals Under Conditions of High-Velocity Deformation

Тип кристаллической структуры (1)	Двойникование проходит сравнительно легко (9)	Обнаружено полиморфное превращение чистых элементов (13)		Фазовые превращения в сплаве (17)		(24) Высокоскоростная деформация влияния не оказывает
		превращение необратимо (14)	превращение обратимо (15)	необратимые (18)	обратимые (19)	
Кубическая объемноцентрированная (2)	Fe [181] Сталь (0,1% C) [182] (10) Сталь (0,9% C) [185] (11) Nb [177] Ta [177] Mo [99]		Fe [192]	—	Малоуглеродистые стали, никелевые и хромистые стали [198, 199] (20)	—
Кубическая гранецентрированная (3)	Cu [156] α-латунь [176] (12) Au—Ag [189] Cu—Al [156] Fe+29% Ni [101]	—	—	Fe + 29% Ni [101] Сталь Гадфильда [196] (21) Нержавеющая сталь [197] (22)	Инвар [200] (23)	Al [197] Монель [197] (25) Ni — образуются двойники только при $P > 350$ *кбар* [173] (26)
Кубическая типа алмаза (4)	—	—	Ge [195]	—	—	—
Кубическая сложная (5)	—	Mn [26]	—	—	—	—
Гексагональная компактная (6)	—	Графит → Алмаз [191]	(16)	—	—	—
Гексагональная плотноупакованная (7)	Ti [97] Mg [109] Mg + 1.32% Mn	Co [26; 190]	—	—	—	—
Ромбоэдрическая (8)	—	—	Bi [194] Sb [193]	—	—	—

1. Type of crystal lattice
2. Cubic body-centered
3. Cubic face-centered
4. Cubic diamond-type
5. Cubic complex
6. Hexagonal non-compact
7. Hexagonal densely-packed
8. Rhombohedral
9. Twinning takes place rather easily
10. Steel (0.1% C) [182]
11. Steel (0.9% C) [185]
12. Alpha-brass [176]
13. Polymorphic transformation of pure elements detected
14. Transformation irreversible
15. Transformation reversible
16. Graphite → diamond [191]
17. Phase transformation in alloy
18. Irreversible
19. Reversible
20. Low-carbon steel, nickel, and chrome steels [198, 199]

[Continued on next page]

[Continued from previous page]

21. Fe+29% Ni [101] Hadfield steel [196]
22. Stainless steel [197]
23. Invar
24. High-velocity deformation exerts no influence
25. Monel [197]
26. Ni -- twins are formed only when P > 350 kbar [173]

CHAPTER 4

STRENGTHENING OF METALS BY HIGH-VELOCITY DEFORMATION

The characteristics of the mechanism of high-velocity deformation to a significant degree determine the formation of the structure which to some degree differs from the structure of the metals deformed under conditions of quasi-static loading. These structural differences determine the properties of the metal in the process of high-velocity loading itself (dynamic properties), and also the properties of the deformed material (deformation strengthening). Thus, the data given in the present chapter should be treated in connection with the processes described in Chapters 2 and 3.

1. Basic Concepts of the Strengthening Mechanism

A definite difference exists in the physical and engineering concepts of the strength of metals. The first is defined as the crystal structure of a metal, and in the absence of structural defects (or with a very small concentration of them) leads us to the value of the theoretical strength, determined by the interatomic bonds. With increase in the concentration of defects, capable of being displaced along the crystal, the strength drops. But if the operation of plastic deformation is treated as the displacement of dislocations, then in principle we can represent such a state when the dislocations existing in the crystal will be deprived of the capacity to travel, and in this case we can find as high a strength as we wish, all the way up to the theoretical.

However, such a physical concept of strength (described of course quite schematically for clarity of comparison) is inapplicable in the engineering sense, where by strength we mean the capacity of the material to absorb an external load without significant plastic deformation and fracture. But the total slow down of all the existing dislocations in a

component found in a real stressed state, leads to its brittle fracture and the available reserve of strength is not used. Consequently, it does not follow to attempt to reach a state near the theoretical strength in the majority of real objects.

To estimate the real strength of metals and alloys it is not sufficient to know only the concentration of defects. In a number of instances such characteristics as the distribution of dislocations, the angles of disorientation of the subgrains, the structure of the boundaries and the interaction of the dislocation with the extrinsic atoms determine the real properties of the metals even to a larger degree than does the density of defects.

Mechanical strengthening in the process of plastic deformation is the end result of the relaxation of externally applied stress, i.e., gliding and twinning, and it is manifested in the change in macroscopic properties, in particular, strength.

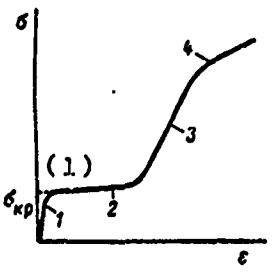

Figure 84. Typical stress-strain curve for single crystals with an fcc lattice: 1. elastic deformation; 2. stage I $\frac{d\sigma}{d\varepsilon} \approx 5 \cdot 10^{-4}$ G; 3. stage II $\frac{d\sigma}{d\varepsilon} \approx 10^{-2}$ G; 4. stage III. 1. σ_{cr}

In describing the process of strengthening it is most convenient to use the well-known curve of deformation in the coordinates σ-ε for single crystals with an fcc lattice (Figure 84). This curve describes three stages of deformation: the stage of easy glide, when the strengthening is minimal, then the stage of linear strengthening when the coefficient of strengthening reaches a maximum, and the stage of parabolic strengthening. However, seldom does the deformation curve for single crystals, let alone the deformation of polycrystals, have the described classical shape. The temperature and speed of the test, the orientation and chemical composition of the single crystals, the state of the surface

of the sample, and other factors may substantially influence the shape of this curve. Nevertheless, the influence of various factors and comparison of the behavior of metals with different types of crystal lattice can be done conveniently in the usual terms of this curve.

Stage I. Two quantities characterize this stage: the extent and the coefficient of strengthening $d\sigma/d\varepsilon$. Numerous structural investigations have shown that this stage of deformation is accompanied by the development of sliding over the primary system with emergence onto the free surface of the crystal of fine parallel slide tracks. The characteristic parameters of sliding at stage I are shown on Table 21.

Table 21. Glide parameters for Stage I of the Deformation of Metals and Alloys With an fcc Lattice [60]

Металл или сплав (1)	Температура деформации, °С (2)	Расстояние между действующими плоскостями скольжения, *нм* (Å) (3)	Длина пробега дислокаций, *мкм* (4)
Ni	—183	80 (800)	10·0
Ni + 20% Co	20	50 (500)	10·0
Ni + 40% Co	20	22 (220)	—
Ni + 50% Co	60	20 (200)	5·0
Cu	—183	38 (380)	7·0

1. Metal or alloy
2. Temperature of deformation, °C
3. Distance between effective glide planes, nm (Å)
4. Length of path of the dislocation, μm

The amount of the shift in the glide tracks is approximately 3-5 nm (30-50 Å). Seger et al [98], using electron microscopic investigations, showed that the length of the glide lines and the distances between them are constant throughout stage I. Here the average size of the loops coming from one source also remains constant. On this basis the conclusion was made that at the stage of easy glide the forming loops can never be treated as a flat pile-up of dislocations. Based on the described model, Seger gives a formula for determining the slope of the curve of strengthening for stage I: this slope represents the strengthening factor:

$$\frac{d\sigma}{d\varepsilon} = \frac{8}{9}\frac{G}{\pi}\left(\frac{d}{L}\right)^{1/4}, \qquad (62)$$

where d is the distance between planes, in which the sources act or the distance between glide tracks on the surface of the crystal; L is the size of the path of the dislocation loops; G is the shift modulus.

For copper the slope of the curve is equal to 0.7-0.75 kgf/mm.

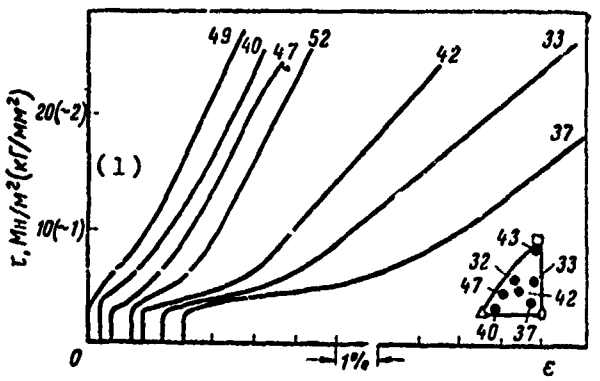

Figure 85. Influence of the orientation of single crystals of silver (99.93%) on the extent of the stage of easy glide [201].

1. τ, Mn/m^2 (kgf/mm^2)

The stress at which the stage of easy glide τ_{cr} begins corresponds to the stress of transition from the elastic deformation to plastic. The conditionality of this transition does not permit uniquely determining the value of τ_{cr}. Usually this value is assumed equal to $(10^{-5}-10^{-4})G$. It is often measured experimentally by extrapolation of the segment of the stage of easy glide on the ordinate axis.

From the above it follows that the necessary conditions for the formation of easy glide is the effect of some single preferential glide system, i.e., the assurance of a relatively barrier-free displacement of the dislocations along the plane. Hence it is obvious that the extent of the stage of easy glide must have a clear dependence on the orientation of the single crystal in the direction to the external applied stress.

Numerous experimental data confirm the validity of these definitions. Figure 85 gives the curves for the deformation of single crystals of silver, oriented differently in a standard stereographic triangle. As is clear from Tables

12 and 14, in the orientations of the crystal [111] and [100], eight glide systems are found under identical conditions with respect to the applied load due to the equal orientation factor. It is natural that in these and similar cases we can never expect any sizable region of easy glide; this is confirmed by the path of curves 40 and 49 on Figure 85. However in the limits of the standard triangle there are fields where the orientation factor is sharply differentiated. For example, for orientations near [110], the orientation factor for the majority of glide systems is equal to zero or very insignificantly differs from zero. In this case (see curves 37 and 33 on Figure 85) the stage of easy glide may be sufficiently large -- it has an extent of 20-30%. On copper, at 93° K, it was possible to increase the easy glide up to 40% [202].

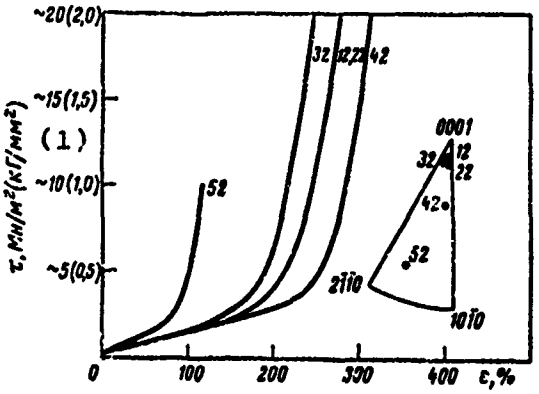

Figure 86. Displacement stress-displacement strain curves for cadmium single crystals (99.9999%) at 77° K [203].

1. τ, Mn/m^2 (kgf/mm^2)

In the majority of hexagonal densely-packed metals for which c/a is greater than or near the value of 1.633 (and also in beryllium with c/a = 1.568) the glide takes place preferentially along the basal plane, as a result of which the stage of easy glide may reach 500%. But also for the hexagonal metals the extent of stage I is determined by the orientation of the crystal (see Figure 86). Most favorable for the basal glide is the deviation of the basal plane from the surface of the sample by 10-20°. For such metals as zinc and cadmium the deformation diagrams are basically similar to the corresponding diagrams for the fcc metals and it may be assumed that the strengthening mechanism here is also identical. The only difference is that in the hexagonal densely-packed crystals the strengthening factor is

significantly smaller than in the fcc crystals. Consequently a larger number of dislocation loops reaches the surface.

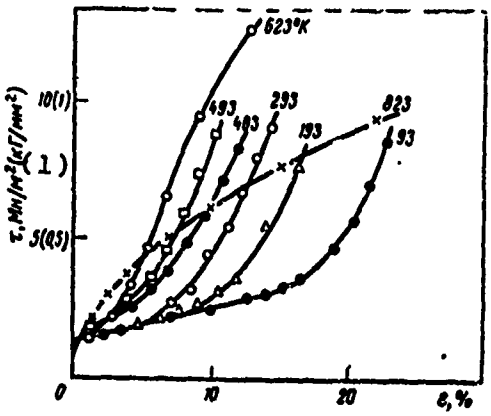

Figure 87. Influence of temperature on the stress-strain curves of copper [202].

1. τ, Mn/m^2 (kgf/mm^2)

Analysis of the influence of deformation temperature on the behavior of metals at the first stage is more complex.

The most convincing data were found in reference [20] on copper single crystals with an orientation near [110], i.e., with a relatively large region of easy glide. From the results shown on Figure 87, it is clear that by lowering of temperature from 823 to 93° K the region of easy glide is greatly increased, but the strengthening factor is not changed. Analogous results were found in other works [205, 206]. They may be explained in the following manner. We know that the critical cleavage stress grows with reduction in temperature. At the same time, although during gliding at the first stage the majority of dislocations emerge on the surface of the crystal, part of them are nevertheless slowed down near the barriers, creating a field of stresses. It is mainly this slowing down which determines the small but final value of the strengthening at the first stage. The stresses generated facilitate reaching the critical stress in the secondary systems, the effect of which is necessary for formation of stable configurations of the Lomer-Cottrell type and for the formation of thresholds. At low temperatures a higher level of stresses must be created because of the temperature dependence of τ_{cr}.

An analogy is usually made between the effect which the reduction in temperature exerts on the deformation and

the increase in deformation velocity. In a number of cases such an analogy is justified and often supported by the identity of the structural changes taking place. However such similarity can not be assumed all the time and always be used.

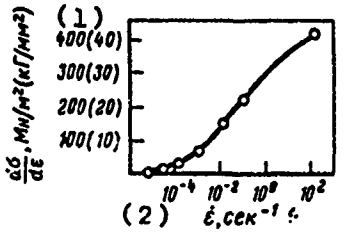

Figure 88. Influence of deformation velocity on the strengthening factor of zinc [204].

1. $d\sigma/d\varepsilon$, Mn/m^2 (kgf/mm^2) 2. $\dot{\varepsilon}$, sec^{-1}

Let us examine the influence of deformation velocity on gliding at stage I. The strengthening factor at stage I depends on deformation velocity. As follows from Figure 88, in the velocity range from 10^{-4} to 10^{-3} sec^{-1}, the strengthening factor of zinc varies significantly less than in the range from 10^{-2} to 10 sec^{-1}.

However the velocity dependence of the strengthening factor is determined not only by the velocity range but also by the orientation of the crystal. In reference [100] it was shown that in nickel single crystals with orientation [110] and [111] in the direction of the effective stress the increase in deformation velocity does not lead to additional strengthening. But with orientations of the type [.12], when the orientation factor has different values for the different glide systems, the influence of deformation velocity is found to be opposite to the effect of reducing the deformation temperature, and namely, for producing the same degree of deformation by high-velocity loading a higher level of stresses is required. In this case the first stage in fact is virtually absent. Thus, increasing the deformation velocity raises the strengthening factor but only in those single crystals in which the orientation factors are different for the different glide systems.

According to the data of Boas and Schmid [207] and LÜcke et al [208], increasing the deformation velocity also increases the strengthening factor in hexagonal metals.

The deformation diagram of metals with a bcc lattice is similar to the deformation diagram of fcc metals only in that case when the bcc metals contain very few impurities. If the injection impurities are present in these bcc metals in amounts that are characteristic of technically pure metals, then the diagram becomes similar to the expansion diagram for polycrystals.

In the deformation of polycrystalline samples the stage of easy glide is almost always absent. For the plastic deformation of grains found in contact with one another without the formation of a band, in each grain, several glide systems must act simultaneously, in the general case no less than five, according to the rule of Taylor-Mieses. Such condition naturally contradicts the mechanism of easy glide.

Stage II. This stage of glide begins at that moment when a large number of systems are included in the gliding and are oriented differently with respect to the applied stress. The interaction of dislocations, belonging to different planes produces the formation of stable configurations (sessile dislocations of Lomer-Cottrell, dipoles, thresholds, etcetera). This involves a decrease in the length of the free path of the dislocation L, which at the second stage, according to Seger, is determined by the formula

$$L = \Lambda (\varepsilon - \varepsilon^*), \tag{63}$$

where Λ is a constant equal to about $4 \cdot 10^{-4}$ cm; ε is the amount of deformation in the limits of stage II; ε^* is the amount of deformation corresponding to the end of stage I.

Although, as Klerboro and Kharrgrivs [58] show, orientation influences the second deformation stage to a lesser degree than the first one; the strengthening factor at the second stage grows noticeably only in that case if the orientation deviates from [110] toward [111] and toward [100] or is near the boundary [111]-[100].

Lindholm and Jeakley [209] studied strengthening of aluminum single crystals having the orientation shown on Figure 89, which also determined the number of effective glide systems. Table 22 shows only such glide planes for which the values of the orientation factor comprises no less than 90% of the maximal value. Figure 90 gives the strain-stress curves, plotted for various deformation velocities, differing from one another by approximately five orders of magnitude. Analysis of these curves shows that in quasi-static deformation ($3.3 \cdot 10^{-3}$ sec^{-1}) the influence of orien-

tation is in fact quite insignificant, the slope of the curve is approximately identical. But at a deformation velocity of about $4.5 \cdot 10^2$ sec^{-1} the difference becomes quite substantial. The greatest effect of velocity is seen in single crystals, in the orientation of which a large number of slide systems act (A7, A17). With orientations of samples A4 and A31, where the number of slide systems is low and the orientation factor differs no more than 0.01 -- the effect of deformation velocity was found to be minimal. Thus, our research on nickel [100] and reference [209] on aluminum define the conditions under which the effect of velocity may give additional strengthening in the deformation of single crystals.

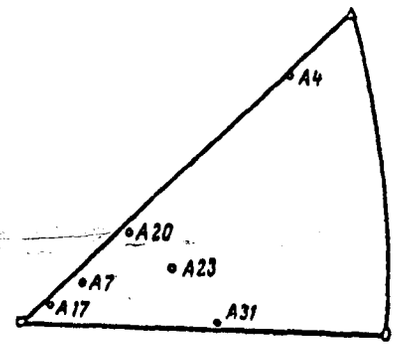

Figure 89. Original orientation of aluminum single crystals [209].

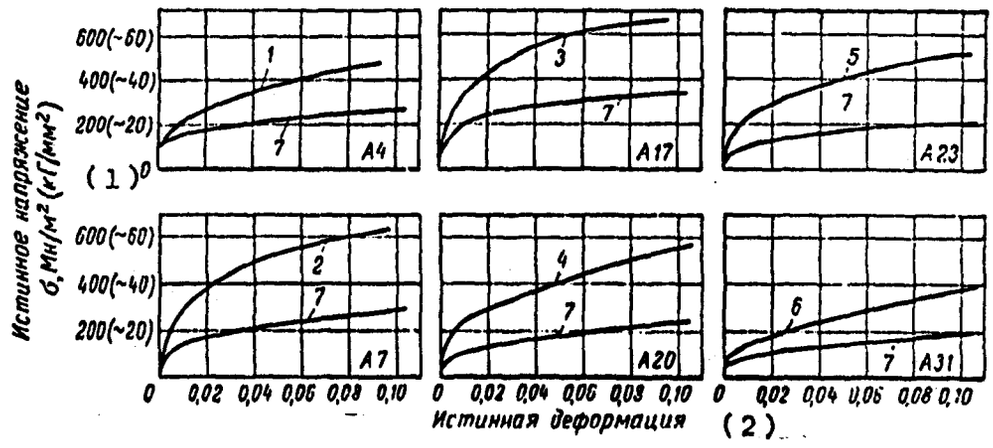

Figure 90. Stress-strain curve for aluminum produced at different loading velocities, sec^{-1}: 1. 425; 2. 435; 3. 450; 4. 465; 5. 475; 6. 500; 7. $3.33 \cdot 10^{-3}$.

1. True stress, σ, Mn/m^2 (kgf/mm^2) 2. True deformation

Table 22. Values of the Orientation Factor for Glide Systems of the Single Crystals Shown on Figure 89

Образец (1)	Плоскость и направление скольжения (2)		θ, град (3)	λ, град (4)	cos θ cos λ
A4	(111)	[$\bar{1}$01]	65	31	0,36
	($\bar{1}\bar{1}$1)	[011]	66	31	0,35
A7	(111)	[$\bar{1}$01]	54	40	0,55
	($\bar{1}$11)	[101]	45	51	0,45
	($\bar{1}$11)	[0$\bar{1}$1]	45	52	0,44
	($\bar{1}\bar{1}$1)	[011]	56	38	0,44
A17	(111)	[$\bar{1}$01]	53	43	0,44
	(111)	[0$\bar{1}$1]	53	48	0,40
	($\bar{1}$11)	[101]	50	47	0,44
	($\bar{1}$11)	[0$\bar{1}$1]	50	48	0,43
	($\bar{1}\bar{1}$1)	[011]	55	42	0,43
	($\bar{1}\bar{1}$1)	[101]	55	47	0,39
	(1$\bar{1}$1)	[011]	58	42	0,39
	(1$\bar{1}$1)	[101]	58	43	0,39
A20	(111)	[$\bar{1}$01]	57	33	0,47
	($\bar{1}$11)	[101]	37	59	0,42
	($\bar{1}\bar{1}$1)	[011]	55	35	0,47
A23	(111)	[$\bar{1}$01]	49	41	0,49
	($\bar{1}$11)	[101]	40	53	0,46
A31	($\bar{1}$11)	[0$\bar{1}$1]	40	50	0,49
	($\bar{1}\bar{1}$1)	[011]	42	48	0,50

1. Sample
2. Plane and direction of glide
3. θ, deg
4. λ, deg

The experimental data cited pertain to crystals with an fcc lattice. A similar analysis may also be made for metals with other crystal lattices. We must only discern in the stereographic triangle those regions in which the orientation factor for the various glide systems has different numerical values.

Stage III. The onset of glide stage III is characterized by the fact that the metal is already found under the influence of a rather high stress with a high dislocation density, accumulated in the course of the second stage. Here a rather intense plastic deformation begins in the metal without further noticeable increase in the external load. The strengthening factor at this stage drops sharply.

It is obvious that the significant increase in plastic deformation must be due to some new mechanism of dislocation displacement. One of the possible explanations of this phenomenon is that under the influence of a high stress the dislocations finally were able to overcome the barriers that prevented their displacement. In this case the value of the dislocation path must be increased. However such an explanation is found to be in contradiction to the experimental data. Many investigators in studying the deformation process showed that at the second and third stages the length of the glide lines is also decreased with the development of plastic deformation. But if the extent of the glide lines is decreased, consequently the path of the individual dislocation is also decreased.

Using direct electron microscopic observations on thin foils, Hirsh [210] and other researchers showed that with the onset of stage III a cellular dislocation structure is formed. Several boundaries of the cells are arranged parallel to the glide planes, and others in the direction perpendicular to the glide plane.

An explanation which satisfies the experiment was given by Seger [211]. According to Seger, at stage III the dislocations do not overcome the resistance of the barriers, but a transverse glide of Burgers dislocations takes place, as a result of which first a cellular structure is formed and second the Burgers component, displaced to the parallel plane, becomes the new Franck-Reed source, if the stress determined by formula (25) exists in this plane.

Thus, at glide stage III under the effect of a high stress there is first of all a redistribution of the dislocations called "dynamic recovery". The stress which is necessary for dynamic recovery depends strongly on temperature. Analogous processes, if they take place after unloading, are called static recovery. Since transverse gliding is a thermally activating process, the amount of the critical stress of transition from the second stage to the third (τ_{III}) has a clearly expressed dependence on temperature (Figure 91) and, as Sokolov [212] showed, increases with increase in deformation velocity.

Furthermore, for metals with an fcc lattice the dependence of this value on the energy of the packing defects is determined:

$$\tau_{III(0)} \quad \frac{2G}{n}\left(0{,}056 - \frac{\gamma}{Gb}\right), \qquad (64)$$

where $\tau_{III(0)}$ is the stress at 0° K; n is the average number of dislocations around the barrier; γ is the energy of the packing defects.

The value of $\tau_{III(0)}$ may be evaluated from the experimental determination of τ_{III} at a given temperature T and the value of the energy of activation of the transverse glide $U(\tau)$, which is connected by the expression:

$$U(\tau) = -A \ln \left[\frac{\tau_{III(T)}}{\tau_{III(0)}} \right]. \qquad (65)$$

Sometimes expressions (64) and (65) are used for evaluating the energy of the packing defects, however this method does not give reliable results. Solokov, using this method [212], obtained an energy of the packing defects for copper equal to about 100 erg/cm^2.

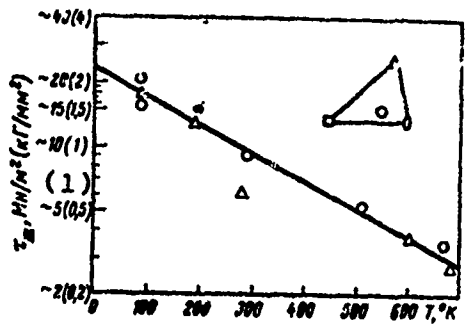

Figure 91. Temperature dependence of the stress necessary for transition from the second stage to the third for gold single crystals [213].

1. τ_{III}, Mn/m^2 (kgf/mm^2)

2. Strength Properties of Metals

There may be two approaches to determining the properties of metals during change in deformation velocity. One of them characterizes the behavior of the metal in the process of deformation itself. In this case we are concerned with the so-called quasi-static or dynamic properties. Obviously we can never draw a sharp boundary, on one side of which would be the quasi-static properties and on the other the dynamic ones. As such a conditional boundary it is feas-

ible to select a velocity of 4 mm/min, which can be assumed to be maximal for the quasi-static yield stress.

The second approach involves evaluating the properties found in the material after the deformation process. The range of deformation velocities determining the post-deformation strengthening is quite wide; from punching on hydraulic presses, where the rates of displacement of the instrument comprise about 1 m/sec, to shaping through the transmitting medium or without it, where the rate of motion of the shock wave front reaches up to several hundreds or even thousands of m/sec.

a b

Figure 92. Radiograms taken from a single crystal of nickel in the initial state (a) and after deformation with a shock wave pressure of 220 kbar (b).

The effect of shock waves alters the physical and mechanical properties of metals and consequently their operational qualities. Figures 92 and 93 show radiograms that indicate substantial structural changes taking place in metals in the process of pulsed deformation.

Because of the intense development in recent years of various methods of pulsed deformation, it is very important to combine in the production the properties of the technological processes and the strengthening of metals as a result of high-velocity deformation. In addition, in individual aspects of contemporary technology, it is necessary to foresee the possibility of the collision of fast-moving ob-

iects and the resultant alteration in their properties. At the present time considerable factual material has been compiled both on the dynamic prope ties of metals and on their properties after high-velocit deformation. And although this material as yet has not been completely classified, these and other properties must be examined jointly, since they appear as a result of the mechanism determined for plastic deformation.

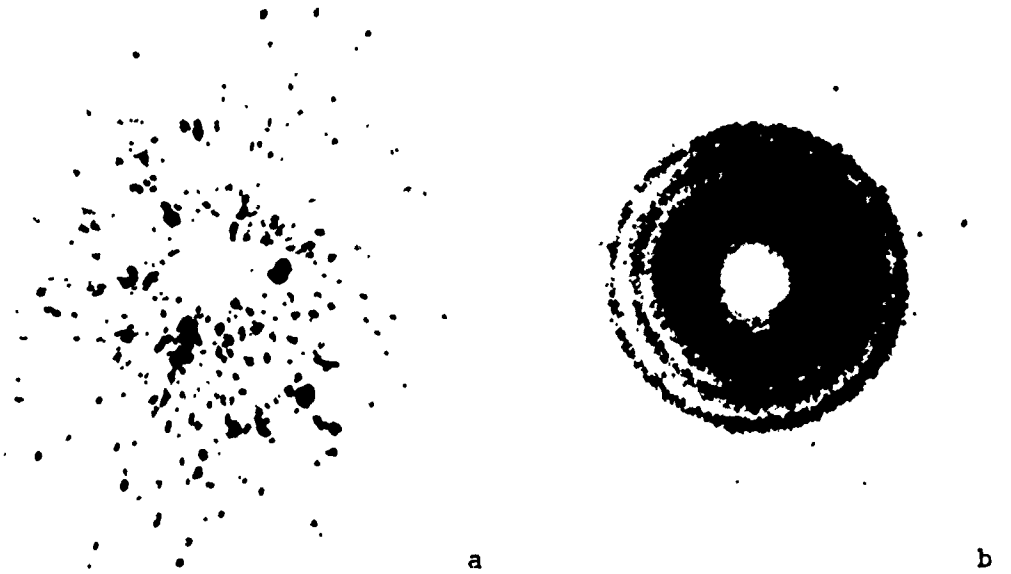

a b

Figure 93. Radiograms taken from large-grained magnesium in the initial state (a) and after deformation with a shock wave pressure of 200 kbar (b).

The authors of reference [214], after generalizing a series of investigations on the influence of deformation velocity on yield stress, assume that the increase in yield stress is caused: (a) by a decrease in the influence of thermal fluctuations, which reduce the yield stress; and (b) by an increase in the resistance of the lattice to motion of the dislocations which in turn is associated with an increase in the rate of displacement of these latter.

The influence of these factors has been repeatedly studied experimentally. Several aspects of this question were discussed by us in Chapter 2.

Table 23. Value of the Dynamic Strength Factor for Various Degrees of Deformation [215]

ε, %	$K = \frac{\sigma_b^{дин}}{\sigma_b^{стат}}$ (1)		ε, %	$K = \frac{\sigma_b^{дин}}{\sigma_b^{стат}}$ (1)	
	медь (2)	никель (3)		медь (2)	никель (3)
10	1,25	1,14	40	1,18	—
20	1,21	1,13	50	1,18	—
30	1,17	1,12			

1. $K = \frac{\sigma_b^{dyn}}{\sigma_b^{stat}}$
2. Copper
3. Nickel

Sokolov assumes [215] that the higher the loading velocity, the lower is the time for occurence of plastic deformation, and consequently the higher is the stress at which the transition takes place from elastic deformation to plastic. Another basis for the effect of dynamic strengthening, in Sokolov's opinion, is "that depending on the duration of the plastic deformation the generated strengthening, to one or another degree, is removed by disordering. As a result the rapid deformation process is represented by a more ordered state of the metal than the slow process, i.e., the stress is again greater as the deformation rate is higher."

The basic disadvantage of the explanations given above is the difficulty in abstracting them by treating one of the most important connecting links, such as the mechanism of deformation. Obviously there is no more sensitive property to the deformation velocity than is the deformation mechanism.

The influence of velocity on change in the deformation mechanism described in previous chapters permits us to explain a series of experimental data. Sokolov [215], for example, found a decrease in the dynamic strength factor $K = \sigma_b^{dyn}/\sigma_b^{stat}$ (where σ_b^{stat} is the tensile strength during the quasi-static test, σ_b^{dyn} is the same during the dynamic test) as a function of the degree of deformation for copper and nickel (Table 23).

In Chapter 2 it was shown that the greatest increase in strength properties during high-velocity deformation, produced by the effect of a large number of glide systems, corresponds to 10-20% of the deformation. With increase in the degree of deformation and with quasi-static deformation the secondary systems come into effect, and with increase in the degree of deformation their specific weight becomes even greater. Here the dynamic strength factor must in fact be decreased; this is confirmed by Sokolov's data.

Not only doe the strength characteristics depend on the deformation velocity range but the dynamic strength factor itself as well. By studying the dynamic coefficient of the yield stress for low-carbon structural steel in the range from $\dot{\varepsilon} = 10^{-4}$ sec^{-1} to $\dot{\varepsilon} = 1.6 \cdot 10^{5}$ sec^{-1}, the authors of reference [216] showed that it may be described by the following equation:

$$K_{0.2} = \frac{\sigma_{0.2}^{dyn}}{\sigma_{0.2}^{stat}} = 1 + k\dot{\varepsilon}n,$$

where k and n are constants for the given material. In narrower limits (from 200 to 1600 sec^{-1}) this dependence is linear

$$\sigma_{0.2}^{dyn} - \sigma_{0.2}^{stat} = 3.2 + 0.001\,\dot{\varepsilon}.$$

All factors which influence the dynamic properties and the properties found in the material after deformation may be divided into two groups.

1. General factors which to a greater or lesser degree appear for all metals. Included in these are the increase in the force of friction during the motion of the dislocations, the increase in dislocation density, and point defects, etcetera.

2. In this group belong those factors whose appearance is determined by the specific conditions of deformation and the material subjected to high-velocity deformation. Hence we include the initiation of new glide systems, the initiation of twinning, the formation of packing defects, the onset of point defects, etcetera. The appearance or non-appearance of these factors depends on the one hand on the conditions of deformation (velocity range, deformation temperature, and deformation diagram), and on the other hand on

the properties of the material (type of crystal lattice, melting point, and recrystallization, and energy of the packing defects).

Yakutovich et al [217], in analyzing the expansion diagrams of polycrystalline cadmium under various temperature conditions, suggested the classification shown on Figure 94.

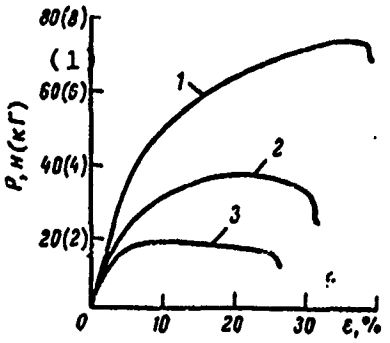

Figure 94. Expansion curves for polycrystalline cadmium at various temperatures [217].

1. P, n (kgf)

In the first belong the curves obtained at low test temperatures (1). For them we find to be characteristic a continuous growth in the deformation stresses, high strength properties of the metal, and a sharp drop in stress after reaching a maximal value. The curves of the second type (curve 3) were obtained during high-temperature deformation; they are distinguished by the large yield region after reaching a maximal stress and then the sharp drop in the deformation stress due to the formation of a neck. Curves of the third type (curve 2) are found in the intermediate temperature range and have a transitional character.

An analogous change in the deformation curve with decrease in temperature was obtained by Wessel [218] on zirconium, nickel, and other metals.

Change in the path of the strain-stress curve with increase in the deformation velocity has been studied on many metals and alloys [219-223]. In spite of the obvious difference in the diagrams produced by the temperature tests, the orientation of the single crystal, the chemical composition of the alloys, the type of crystal lattice, and other

factors, a common trend for change in the curves can be determined: with increase in the deformation velocity the high-temperature shape converts to the low-temperature.

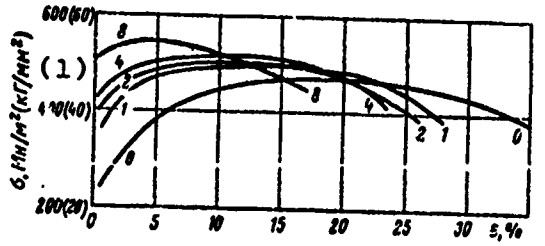

Figure 95. Curves for the deformation of steel 1030 after strengthening by detonation. The numbers show the number of plates of explosive with a thickness of 2.5 mm [223].

1. σ, Mn/m^2 (kgf/mm^2)

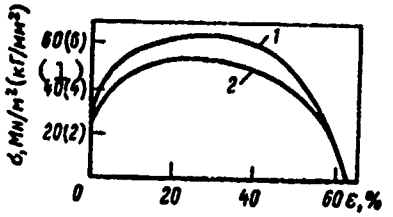

Figure 96. Stress-strain curves for aluminun [221]: 1. $\dot{\varepsilon}$ = 100 sec^{-1}; 2. $\dot{\varepsilon}$ = 2.4·10^{-3} sec^{-1}.

1. σ, Mn/m^2 (kgf/mm^2)

Based on the known power dependence of the rate of motion of the dislocation on the amount of stress applied (23), and taking into account the research of Johnston and Gilman [44], the velocity of plastic deformation $\dot{\varepsilon}$ can be represented as a function of the overall length of the mobile dislocations L with the Burgers vector $\vec{b}$ and the rate of shift v:

$$\dot{\varepsilon} = \Phi L b v, \tag{66}$$

where Φ is an orientation factor not exceeding 0.5.

Cottress [224] determines the influence of deformation velocity on stress by the equation:

$$\sigma = q\varepsilon + \sigma_0 \left[\frac{\dot{\varepsilon}}{\Phi \bar{b} (L_0 + C\varepsilon^{\alpha})} \right]^{1/m}, \qquad (67)$$

where q is the amount of deformation strengthening equal to $d\sigma/d\varepsilon$; σ_0 is the stress necessary for shift of the dislocation at a single velocity; C is the coefficient of proportionality; α is a constant equal to 0.7-1.5.

The stresses computed from this formula gave good agreement with the experimental data obtained on germanium [225]. Let us note that the values of m and L_0 in formula (67) actually determine the shape of the deformation curve. In one case this may be a curve similar to that shown on Figures 95 and 96 for steel and aluminum with no well-expressed yield peak, and in the other it may be similar to that obtained by Campbell and Harding [50] for armco iron (Figure 97).

In the majority of methods involving pulsed deformation the loading diagram corresponds to uniaxial compression. For construction of the diagrams, in the coordinates stress - strain, for low loading velocities as a rule the uniaxial expansion is used. However this does not prevent combined analysis of the obtained properties, with the exception of those processes which are determined by a polar, directed mechanism, for example, twinning (see Chapter 3).

Tests for expansion and contraction have their own disadvantages, which lead to a deviation from the ideal diagram of the uniaxial loading. During contraction forces of friction are generated at the sites of contact between the sample and the transverse component of the test machine. During expansion of the sample the axis is bent since the glide plane tends to decrease in angle with the direction of load application.

Imai and Hashiwara [226] designed a machine in which they were able to carry out expansion during the detonation of an explosive, using the reverse diagram. The expansion diagrams constructed under these conditions for steel and brass are similar to those which were obtained by other authors for pulsed contraction.

The characteristic change in the stress-strain diagram for medium-carbon steel with increase in deformation velocity is shown on Figure 95. The deformation velocity and correspondingly the amount of maximal pressure of the shock wave varied as a function of the number of plates of

explosive, which were applied directly on the sample. With increase in deformation velocity the yield stress and the tensile strength were increased and the plasticity dropped slightly.

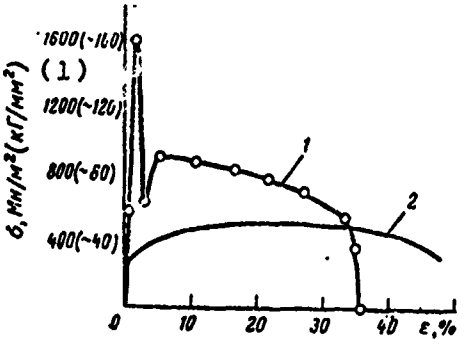

Figure 97. Stress-strain curve for armco iron at a relative velocity of 10^{-3} and $2.6 \cdot 10^{3}$ sec^{-1} [50]: 1. dynamic deformation; 2. quasi-static deformation.

1. σ, Mn/m^2 (kgf/mm^2)

This diagram differs from the low-temperature one in that the difference between the yield stress and the tensile strength is less than in the deformation of cadmium at lowered temperatures. For aluminum [221] in the limits of the deformation velocity from $2.4 \cdot 10^{-3}$ to 10^{2} sec^{-1} (see Figure 96) the diagram has an intermediate character. Baron [227] showed that in the velocity range from 10^{-3} to 10^{2} sec^{-1} in all carbon steels with increase in deformation velocity the upper and lower yield stress appears. The diagram of technically pure copper varies approximately the same as for aluminum (see Figure 96) and for brass and an alloy such as duralumin the expansion diagram varies very insignificantly.

Even within one type of crystal lattice the strengthening as a result of the effect of the shock wave may be substantially different, especially if the effect of the shock waves involves a phase transition in the given pressure range. As is obvious from Figure 98, the strengthening of niobium is significantly less than the strengthening of iron. The strength properties of iron are sharply increased at a pressure on the order of 130 kbar, i.e., at such a pressure which produces a polymorphic transformation.

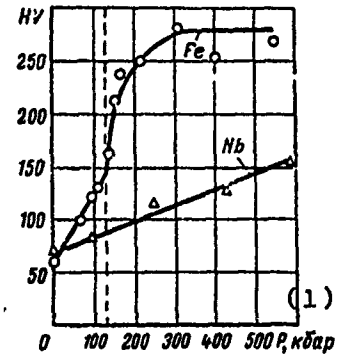

Figure 98. Dependence of hardness on maximal pressure of a shock wave for iron and niobium [177].

1. P, kbar

The effect of sharp change in hardness during phase transitions is also known with respect to the temperature changes. Bowden and Kelly [24] found a jump in hardness at the temperatures of the phase transitions in manganese and in other metals.

The magnitude of the critical pressure of the phase transition and consequently the interval in which the sharp increase for iron is seen (for iron, 130 kbar) depend on the composition and structure of the steel. It was shown in reference [228] that in low-carbon and high-carbon steel, the distance between particles of the cementite influences the value of P_{cr} at which σ_B and $\sigma_{0.1}$ grow.

Figure 99 and Table 24 show the increase in hardness and strength with pulsed strengthening of various metals and alloys at a pressure up to 500 kbar. As is clear from Figure 99, the group of metals and alloys with an fcc lattice is strengthened more strongly than metals with a bcc lattice. One exception is iron and low-carbon steel, where the hardening grows as a result of the phase transition.

Of the group of investigated metals with an fcc lattice, the greatest strengthening is reached in Hadfield steel and in stainless steel; this is obviously due to the energy of the packing defects and to the additional strengthening during twinning.

Strengthening by high-velocity deformation of any metal is determined not only by the amount of pressure from the shock wave. One of the essential factors is the deforma-

tion temperature. As far back as 1947 Gubkin [230] showed that the magnitude of the dynamic strength factor depends on the range of the deformation velocity in which the strengthening is studied and on the deformation temperature (Table 25).

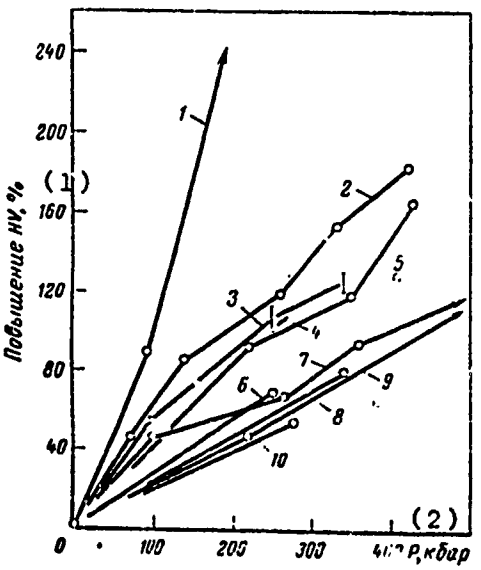

Figure 99. Dependence of growth in hardness on amount of pressure from the shock wave for various metals and alloys [229]: 1. iron and low-carbon steel; 2. Hadfield steel; 3. austenite stainless steel; 4. monel; 5. copper; 6. niobium; 7. nickel; 8. Au+17% Ag; 9. alpha-brass; 10. tantalum.

1. Increase in HV, % 2. P, kbar

Baron [231] cites data on change in yield stress, tensile strength and narrowing of the cross section with increase in deformation velocity from about $4 \cdot 10^{-4}$ to 10^2 sec^{-1} at various test temperatures (Table 26). First of all we should mention that the dynamic coefficient of the yield stress is greater than the dynamic coefficient of the tensile strength. For armco iron and austenite stainless steel this difference is especially high. Although in reference [231] the deformation was not studied, it is obvious that, at velocities of about 10^2 sec^{-1}, the overwhelming amount of the deformation drops to a fraction of the glide.

The authors of reference [221], investigating an alloy of aluminum with 4.65% Mg, found that approximately in the

Table 24. Mechanical Properties of Several bcc Metals After Pulsed Treatment [177]

Металл (1)	Обработка (6)	HV	$\sigma_{0,2}$, Мн/м² (кГ/мм²) (12)	$\sigma_в$, Мн/м² (кГ/мм²) (13)
Железо (2)	Отжиг	64	131 (13,3)	218 (22,2)
	Деформация, (7) P = 220 кбар	250	759 (77,3)	864 (88,3)
Сталь (0,17% C) (3)	Отжиг	85	246 (25,1)	408 (41,7)
	Деформация: (8) P = 95 кбар	160	435 (44,5)	506 (51,6)
	P = 220 кбар	260	808 (82,4)	879 (89,6)
Ф + 3% Si	Отжиг	180	380 (38,8)	520 (52,2
	Деформация: (9) P = 95 кбар	300	583 (59,5)	668 (68,3)
	P = 220 кбар	380	984 (100,2)	1068 (109)
Тантал (4)	Отжиг	120	197 (20,1)	260 (26,6)
	Деформация, (10) P = 275 кбар	185	316 (32,3)	337 (34,6)
Ниобий (5)	Отжиг	68	183 (18,7)	309 (31,6)
	Деформация, (11) P = 250 кбар	115	330 (33,7)	358 (36,6)

1. Metal
2. Iron
3. Steel (0.17% C)
4. Tantalum
5. Niobium
6. Treatment
7. Annealing, deformation, P = 220 kbar
8. Annealing, deformation, P = 95 kbar, P = 220 kbar
9. Annealing, deformation, P = 95 kbar, P = 220 kbar
10. Annealing, deformation, P = 275 kbar
11. Annealing, deformation, P = 250 kbar
12. $\sigma_{0.2}$, Mn/m^2 (kgf/mm^2)
13. σ_u, Mn/m^2 (kgf/mm^2)

same range of deformation velocities the yield stress is increased and the tensile strength is slightly decreased. From analysis of Table 26 it follows that in the range of deformation velocities from $4 \cdot 10^{-4}$ to about 10^2 sec^{-1} the reaction of the various metals is different.

Davidenkov and Chu Wen [232] studied the influence of temperature on the change in yield stress of various metals. ratio $\frac{\sigma_{-196^\circ C} - \sigma_{20^\circ C}}{20^\circ C}$ for metals with a bcc lattice (Ta, Mo, Fe) is 130-250, and for metals with an fcc lattice (Al, Cu, Ni) it is 10-30. Such a sharp difference in the influence

of deformation temperature is still caused apparently by an influence from injection impurities on the strength of the metals with a bcc lattice that was not checked by the authors.

Table 25. Influence of Velocity and Temperature of Deformation on the Value of the Dynamic Strength Factor K = $\sigma_b^{dyn}/\sigma_b^{stat}$ [230]

$\dot{\varepsilon}$, м/сек (1)	(3) K при температуре		
	$< 0{,}5T_{пл}$ (4)	$\sim 0{,}5T_{пл}$ (5)	$> 0{,}5T_{пл}$ (6)
0,1—0,25	1,1	1,4—2,4	1,2—1,3
0,25—0,75	1,15	2,4—3,0	1,6—2,0
1	1,25	3,5	2,.
Ударная деформация (2)	1,5	5,0	4,.

1. $\dot{\varepsilon}$, m/sec
2. Impact deformation
3. K at a temperature of
4. 0.5 T_{melt}
5. about 0.5 T_{melt}
6. > 0.5 T_{melt}

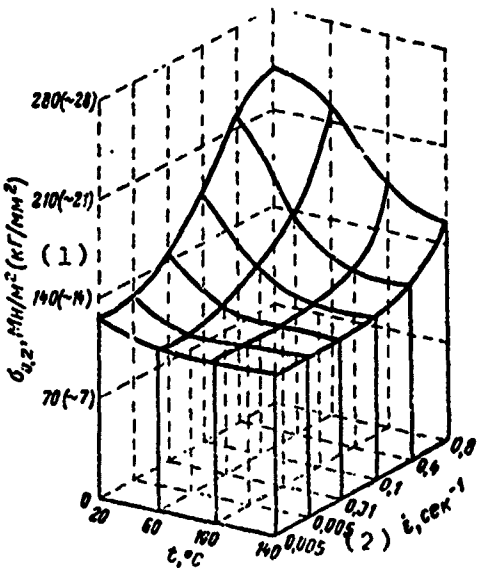

Figure 100. Diagram of the dependence of yield stress of quiet sheet steel on velocity and temperature of deformation.

1. $\sigma_{0,2}$, Mn/m^2 (kgf/mm^2) 2. $\dot{\varepsilon}$, sec^{-1}

Table 26. Static and Dynamic Properties of Various Metals and Alloys During Expansion [231]

Металл (1)	Температура испытаний, °С (8)	$\sigma_{0.2}^{стат}$ (9)	$\sigma_{0.2}^{дин}$ (10)	$K_{\sigma_{0,2}} = \frac{\sigma_{0.2}^{дин}}{\sigma_{0.2}^{стат}}$ (12)	$\sigma_b^{стат}$ (13)	$\sigma_b^{дин}$ (14)	$K_{\sigma_b} = \frac{\sigma_b^{дин}}{\sigma_b^{стат}}$ (16)	$\psi_{стат}$ % (17)	$\psi_{дин}$ % (18)
		$Мн/м^2$ ($кГ/мм^2$) (11)			$Мн/м^2$ ($кГ/мм^2$) (15)				
Армко-железо (2)	20	8,5 (~8,5)	190 (~19,0)	2,2	140 (~14,0)	190 (~19,0)	1,4	70	73
	—78	140 (~14,0)	280 (~28,0)	2,0	175 (~17,5)	231 (~28,1)	1,6	70	67
	—196	—	—	—	35,1 (~35,1)	—	—	31	2
Cr-Ni-Mo сталь (3)	20	422 (~42,2)	478 (~47,8)	1,1	457 (~45,7)	506 (~50,6)	1,1	69	67
	—78	436 (~43,6)	513 (~51,3)	1,2	500 (~50,0)	541 (~54,1)	1,1	68	65
	—196	569 (~56,9)	—	—	618 (~61,8)	668 (~66,8)	1,1	58	58
Аустенитная нержавеющая сталь (4)	20	140 (~14,0)	210 (~21,0)	1,5	350 (~35,1)	373 (~37,3)	1,06	67	63
Дуралюмин (5)	20	175 (~17,5)	190 (~19,0)	1,1	232 (~23,2)	232 (~23,2)	1,0	22	[illegible]
Медь (6)	20	35 (~3,5)	42 (~4,2)	1,2	98 (~9,8)	119 (~11,9)	1,2	[illegible]	75
Бронза 60-40 (7)	20	70 (~7,0)	84 (~8,4)	1,2	197 (~19,7)	211 (~21,1)	1,06	[illegible]	51

1. Metal
2. Armco iron
3. Cr-Ni-Mo steel
4. Austenite stainless steel
5. Duralumin
6. Copper
7. Bronze 60-40
8. Test temperature, °C
9. $\sigma_{0.2}^{stat}$
10. $\sigma_{0.2}^{dyn}$
11. Mn/m^2 (kgf/mm^2)
12. $K_{\sigma_{0.2}} = \frac{\sigma_{0.2}^{dyn}}{\sigma_{0.2}^{stat}}$
13. σ_b^{stat}
14. σ_b^{dyn}
15. Mn/m^2 (kgf/mm^2)
16. $K_{\sigma_b} = \frac{\sigma_b^{dyn}}{\sigma_b^{stat}}$
17. ψ_{stat} %
18. ψ_{dyn} %

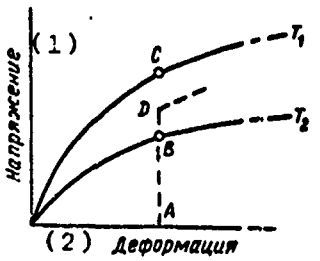

Figure 101. Schematic representation of the expansion diagrams at two different temperatures ($T_2 > T_1$) after Cottrell and Stokes.

1. Stress 2. Strain

MacDonald et al [233] constructed a ternary diagram for quiet sheet steel which illustrates the dependence of yield stress on velocity and temperature of deformation (Figure 100).

In reference [234] it was established that the sensitivity of the yield stress of soft steel (0.14% C) to deformation velocity (from $2 \cdot 10^{-4}$ to $4 \cdot 10^{2}$ sec^{-1}) is decreased with elevation in test temperature and increase in degree of deformation. It will be shown later that the dependence of the properties of metals on deformation velocity is determined by the initial structure to a significant degree.

The large amount of experimental data concerning the influence of deformation velocity on the properties of metals and alloys still does not permit us to establish the factors that determine the production of these properties after high-velocity deformation. For the present, posing this question requires the creation of certain modeling concepts and their experimental proof.

In 1955 a paper was published by Cottrell and Stokes [235] that has become a classic, in which the authors investigated the influence of temperature on the amount of deforming stress at the third gliding stage. The authors showed that if a tensile test is made at two temperatures ($T_2 > T_1$), then one and the same amount of plastic deformation is reached with an equal value of the stress (Figure 101).

The cause of this temperature effect, just as the effect of deformation velocity, requires special study. It was mentioned that the amount of additional stress necessary

for reaching the same amount of deformation is different for the different metals. Thus, the ratio AB/AC for polycrystalline aluminum is 0.4-0.5, for copper 0.6-0.7, with change in the test temperature from 292 to 78° K [236].

The difference in stress (BC) is due to two groups of factors.

Included in the first group are the factors that are associated with the characteristics of shaping the structure of a metal in the deformation process. This includes the density and distribution of dislocations, the concentration of point defects, and other elements of the substructure. The specific weight of the individual elements of the substructure in turn depends on the material and the deformation conditions. Those structural changes which took place during plastic deformation are irreversible if the applied stress is removed.

Included in the second group are the temperature changes in the properties of the crystal itself, and obviously of course the change in the amount of critical cleavage stress τ_{cr}. With a reverse change in temperature τ_{cr} will have prime significance. Those factors which make a contribution to the temperature effect are called reversible.

If we begin the tension at a higher temperature T_2 and, by reducing the deformation to a certain value B, abruptly change the temperature to T_1, then the curve will have the form OBD (see Figure 101). It is necessary only to assure that the change in temperature will not produce any aging of the alloys, phase recrystallization, or other similar phenomena.

The increase in stress BD thus obtained will be determined by the properties of the crystal at various temperatures. According to the data of Dorn et al [236], the ratio AB/BD with change in temperature from 292° to 72° K is equal to 0.7-0.8 for aluminum and 0.8-0.9 for copper. We must mention that this quantitative evaluation has an especially singular character.

Cottrell and Stokes [235] made a test using a slightly different diagram. In a wide range of degrees of deformation they determined the ratio of changes in flow stress by transition from 293 to 90° K and from 90 to 293° K. By varying the test temperature along with the stress and load, they were able to divide the effect from the influence of temperature into change in yield stress and into change in the structure of aluminum for which the experiment was conducted.

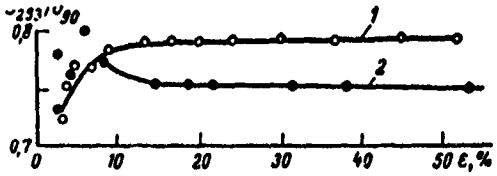

Figure 102. Dependence of the ratio of deforming stresses on degree of deformation with change in deformation temperature: 1. from 293 to 90° K; 2. from 90 to 293° K.

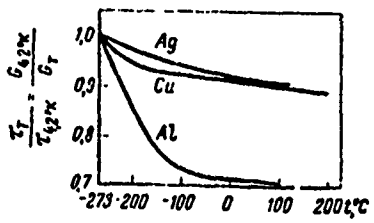

Figure 103. Temperature dependence of the resistance to plastic deformation of several metals with an fcc lattice. The data obtained on single crystals and polycrystals of aluminum lie on a single curve. Only single crystals were investigated for silver and copper [238].

The results are shown on Figure 102. Common to both curves is a weak dependence of the ratio of cleavage stresses on deformation. From the experiment of Cottrell-Stokes it follows that by transition from low temperature to high the increase in strength is basically determined by the stable (irreversible) factors which characterize the substructure of the metal, and the transition from high temperature to low is due to the properties of the lattice, and particularly to the dependence of τ_{cr} on temperature. Cottrell and Stokes showed that the ratio AD/AB remains constant for crystals with different orientation in the stereographic triangle. Thus, this transition from high temperatures to low is found to be structurally insensitive.

McLean [237] shows that such an experiment may be properly treated in that case if the flow stress determined at each temperature is divided into the value of the modulus of elasticity at the same temperature.

In reference [238] the temperature dependence was studied of the resistance to plastic deformation of a number

of metals with an fcc lattice. From the results shown on Figure 103 it follows first of all that generally for all the investigated metals the ratio τ/G varies very little and for metals such as copper and silver, is practically constant. Consequently, the temperature dependence of deformation strengthening is almost completely determined by the structure formed.

In metals with a bcc lattice on the other hand the flow stress changes substantially with temperature [239, 240]. In iron the amount of carbon does not influence this dependence. Consequently the flow stress in bcc metals is much more sensitive to temperature than in fcc metals, and undoubtedly plays a major role in the temperature dependence of deformation strengthening.

Any process involving plastic flow stress may be treated as the overcoming of an energy barrier. Thermal activation which facilitates overcoming this barrier is an operation that is carried out by an externally applied stress, the amount of which is determined by the deformation velocity. Consequently it is theoretically possible to study the velocity dependence of dynamic strengthening from the positions discussed in the work of Cottrell and Stokes. However a quantitative evaluation of the effect of increase in stress $\Delta\sigma$, determined by Cottrell and Stokes in the form $\Delta\sigma/\sigma$ = const, obviously has narrow boundaries of application.

Haasen [241], for example, gives the following expression for the two temperatures T_1 and T_2

$$\sigma_{T_1} - \sigma_{T_2} = a + b\sigma_{T_2},$$

where a and b are constants.

It is assumed that this formula best describes the available data for large stress values. Basinski and Christian [239] assume that with an abrupt change in test temperature the magnitude of is generally constant. The rule of Cottrell and Stokes is valid for pure metals with an fcc lattice.

At the same time, attempts are already being made to evaluate the possible increase in flow stress of a metal with increase in deformation velocity. Wada and Kimura [220], studying the deformation of iron and its alloys with vanadium, found that by changing the deformation velocity by ten fold the following expressions are satisfied:

$$\left.\begin{aligned}\sigma_1-\sigma_2&=A,\\ \sigma_2-\sigma_3&=Ar,\\ &\cdots\cdots\cdots\\ \sigma_{n-1}-\sigma_n&=Ar^{n-2}\end{aligned}\right\} \qquad (68)$$

where A and r are positive coefficients and $r < 1$; σ, σ_2, and σ_n are the magnitudes of the stresses necessary for producing one and the same deformation, and with increase in n per unit of deformation velocity they differ by 10 fold.

Summing the ratios in (68) we can determine the difference in flow stress for the two deformation velocities which differ by a factor of 10:

$$\sigma_1-\sigma_n=\frac{A(1-r^{n-1})}{1-r}.$$

Yamada and Koterazawa [221] produced strain-stress diagrams for aluminum. They not only used different deformation velocities, but also varied the deformation velocity after 20% expansion. Thus, they constructed curves for the transition from a velocity of $2.4\cdot10^{-3}$ to 10^{-2} sec^{-1} (curve C-D on Figure 104) and for the transition from higher velocity to lower (curve D-C). Based on the data in [221] we computed the values of $\sigma_{stat}/\sigma_{dyn}$ and $\sigma_{dyn}/\sigma_{stat}$ in the range from 25 to 50% deformation, which are plotted on Figure 105. Let us turn our attention to the fact that the value of these ratios does not depend on the degree of deformation, just as in the experiment of Cottrell-Stokes. Furthermore, as follows from Figure 105, the ratios $\sigma_{stat}/\sigma_{dyn}$ and $\sigma_{dyn}/\sigma_{stat}$ practically coincide.

It is still difficult to say how general these results are. Probably they belong primarily to metals with an fcc lattice. In metals with a bcc lattice the behavior of the dislocations under conditions of high-velocity loading differs from the behavior of dislocations in crystals with an fcc lattice. Furthermore we must take into account that the role of injection impurities and disperse separations in these metals is rather high. All this may substantially influence the relationship of the reversible and irreversible factors in the dynamic strengthening of metals with a bcc lattice. These conclusions to some degree are confirmed experimentally by references [238, 239]

where it was shown that iron is more sensitive to change in deformation velocity than silver, copper, and aluminum.

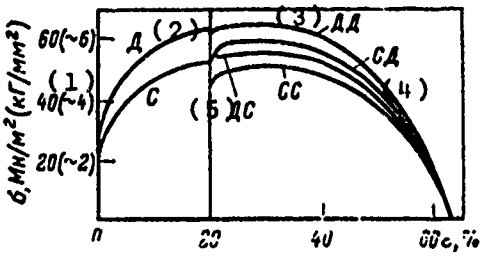

Figure 104. Expansion diagrams of aluminum obtained at a variable deformation velocity after 20% deformation [221]; the sequence: C-C = quasi-static → quasi-static; D-D = dynamic → dynamic; D-C = dynamic → quasi-static; C-D = quasi-static → dynamic; $\dot{\varepsilon}_{stat} = 2.4 \cdot 10^{-3}$ sec^{-1}, $\dot{\varepsilon}_{dyn} = 10^2$ sec^{-1}.

1. σ, Mn/m^2 (kgf/mm^2)
2. D
3. DD
4. CD
5. DC

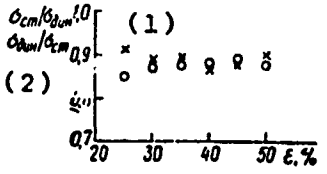

Figure 105. Dependence of the relative change in flow stress on change in deformation velocity in the range from 25 to 50% deformation: computed from the data in [221]: x = transition from quasi-static deformation to dynamic; o = transition from dynamic deformation to quasi-static.

1. $\sigma_{stat}/\sigma_{dyn}$
2. $\sigma_{dyn}/\sigma_{stat}$

The deformation distribution and correspondingly the distribution of deformation strengthening in components is determined by the loading diagram. During the punching of sheet billets through a transmitting medium, according to the diagram shown on Figure 4, the maximal deformation and hardness are found in the center of the half-sphere (see

Figure 8). This distribution is analogous to that which is observed during quasi-static deep drawing, the only difference being that the hardness after high-velocity deformation is slightly greater.

By the contact placement of a charge, the maximal strengthening is reached on the surface (Figure 106). Pierson [242] varied the size of the charge during strengthening by contact detonation of steels with different amounts of carbon and correspondingly with different initial hardness. The increase in hardness during contact detonation strengthening, as would be expected, is greater as the initial hardness is lower, and this value depends little on the size of the charge (in any case for low-carbon steels), but the zone of strengthening grows substantially.

In a collision with a fast-moving plate the size of the deformation zone depends on the material. By varying the collision velocity from several meters per second to 20 m/sec, Udziro and Sindzi [243] produced a deformation zone in aluminum smaller than in copper (Figure 107). Computation shows that with a rate of particle displacement of 1 m/sec, tangential stresses are generated equal to 95 Mn/m^2 (9.5 kgf/mm^2) in aluminum, and 204 Mn/m^2 (20.4 kgf/mm^2) in copper.

The dependence of hardness and mechanical properties of copper on the degree of deformation after various types of punching is shown on Figures 108 and 109. From the results obtained it follows that strengthening at one and the same degree of deformation is maximal after dydrodetonation and electromagnetic punching and minimal after hydrostatic. When ε = 10% the microhardness of copper after deformation under conditions of hydrostatic loading grows to 160 Mn/m^2 (about 16 kgf/mm^2), after electrohydraulic to 240 Mn/m^2 (about 24 kgf/mm^2), and after detonation and electromagnetic punching to 320 Mn/m^2 (about 32 kgf/mm^2). Thus, a significant additional strengthening of copper is observed that is determined by the deformation velocity. The characteristic of this additional strengthening is that it is maximal in the range ε = 10-20%; with a larger degree of deformation the difference is less.

The microhardness of coarse-grain copper is less in absolute value, but the additional strengthening after pulsed deformation remains the same and we can assume that it is independent of the size of the original grain.

orita [17c] showed on copper and armco iron that strengthening by shock waves at a pressure up to 600 kbar gives an increase in hardness that is greater than rolling with a reduction of 60 and 95% (Table 27).

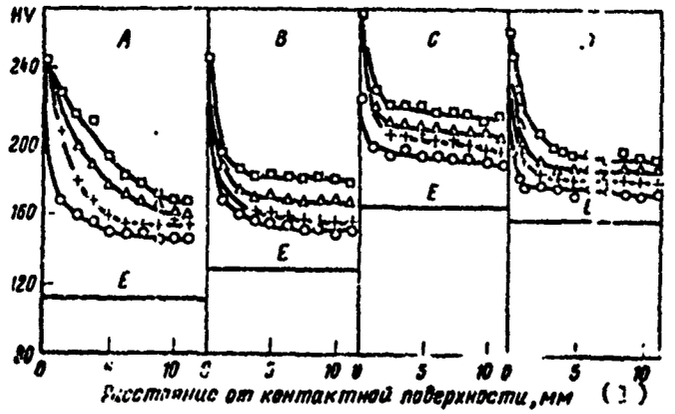

Figure 106. Curves of the change in hardness of steel plates treated by contact detonation [42]: A = 1020 steel; B = 1030 steel; C = 1050 steel; D = 4130 steel; E = initial hardness. Thickness of the charge, mm: o = 2.13; + = 4.25; Δ = 8.5; □ = 17.0.

1. Distance from contact surface, mm

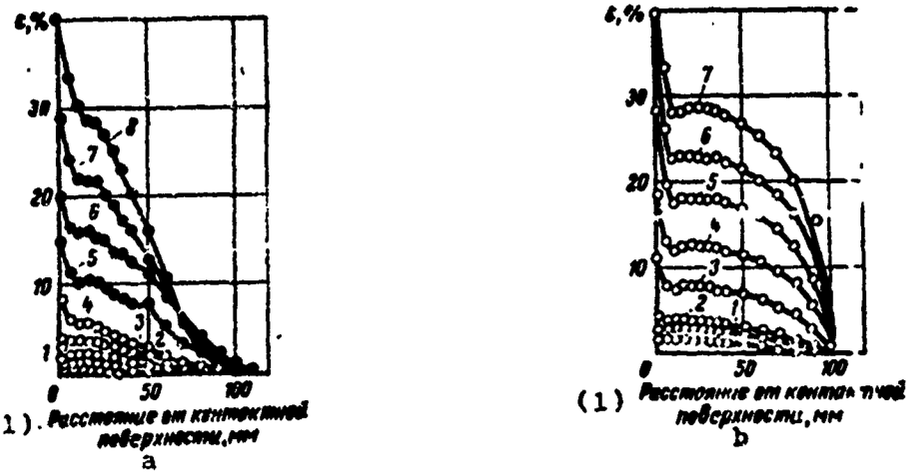

Figure 107. Change in degree of deformation along the length of the sample after collision in aluminum (a) and in copper (b). The degree of deformation in the contact zone grows with increase in collision velocity. The deformation velocity grows with increase in curve number.

1. Distance from contact surface, mm

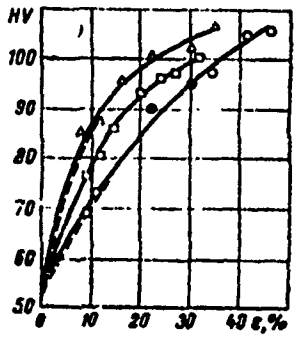

Figure 1 8. Influence of the degree of deformation and type of punching on the microhardness of copper: ——— = samples with 17 μm grain; ----- = 150 μm; Δ = hydrodetonation and electromagnetic punching; o = hydrostatic; □ = electrohydraulic.

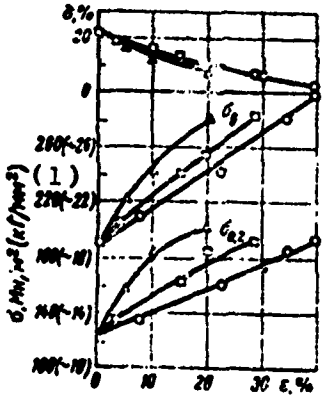

Figure 109. Change in the mechanical properties of copper (grain size 17 um) as a function of type and degree of deformation. The symbols are the same as on Figure 108.

1. σ, Mn/m^2 (kgf/mm^2)

Additional strengthening may be due either to size reduction of the grains or to change in the dislocation structure. Quantitative metallographic analysis showed that the grain size of copper is independent of deformation velocity. It is possible only to detect an increase in the etchability of the grains with increase in the degree of deformation which qualitatively indicates an increase in the grain of the microdeformations. Pashkov et al [273] also mentioned that detonation deformation of armco iron does not lead to grain size reduction.

Table 27. Microhardness of Copper and Armco Iron After Various Types of Treatment

Обработка (1)	Твердость HV (2)	
	медь (3)	армко-железо (4)
Отжиг (5)	54	95
Деформация:		
$P = 225$ кбар (6)	105	—
$P = 250$ »	—	250
$P = 350$ »	109	—
$P = 425$ »	132	—
$P = 600$ »	—	284
Прокатка с деформацией 60%	109	212
» » » 95% (7)	129	259

1. Treatment
2. Hardness HV
3. Copper
4. Armco iron
5. Annealing
6. Deformation, kbar
7. Rolling with deformation of 60% and 95%

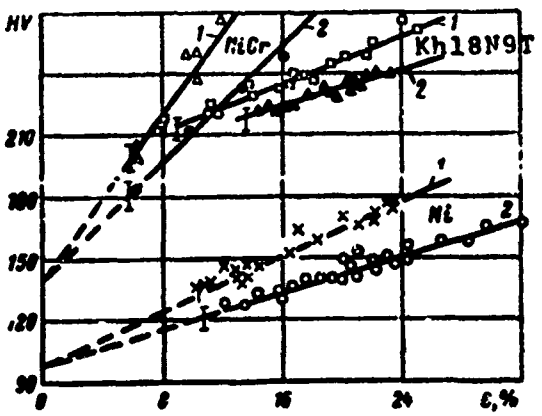

Figure 110. Dependence of hardness of nickel and nickel-base alloys on degree of deformation after detonation (1) and hydrostatic (2) loading.

Our investigations [244] on the hardness and mechanical properties of nickel, nichrome, and 1Kh18N9T steel (Figure 110) also showed the main strengthening after detonation deformation. Nichrome differs from pure nickel and 1Kh18N9T steel in the large gradient of deformation strengthening. This relationship is retained also during quasi-static and hydrodetonation deformation.

The results of studying the fine structure indicate that change in the physical line width (420) of copper as a function of velocity and degree of deformation (Figure 111) agrees well with the change in the strength properties.

The stress necessary for continuation of the plastic deformation is proportional to the concentration of defects, including density of dislocations. However evaluation of the dislocation structure is represented only inadequately by the density, since for any dislocation density such pile-ups are possible which lead to the formation of brittle cracks, and a high strength can not be reached. Therefore not only does the dislocation density have great significance but their distribution by volume of the subgrains and at small-angle boundaries as well.

In references [245, 246] it was shown that the physical broadening of the x-ray lines is due to the presence of defects, the angular dependence of the broadening involves distribution of the dislocations by volume, and the ratio of the physical width of the two lines near the ratio of the tangents may indicate a uniform distribution of dislocations and is most desirable.

The concept of a uniform distribution of dislocations is often not unambiguous. If we are speaking about the dislocation structure, in which no space lattice is formed for the cells, then the difference in number of dislocations in arbitrarily selected volumes will characterize the uniformity of the dislocation distribution.

After the formation of a cellular structure the dislocation distribution is differentiated: large pile-ups are formed at the boundaries of the cells and regions appear that are more or less free of dislocations. In this case the concept of uniformity in dislocation distribution involves the dimensions of the cells. The smaller the cell dimension, the smaller is the stress gradient acting per individual dislocation arranged inside the cell in different directions.

From the data of measuring the width of the x-ray lines given on Table 28, it follows that with increase in the deformation velocity not only does the dislocation density grow, but also their distribution is modified. By hydrodetonation and magnetopulsed deformation the ratio $\frac{\beta_{400}}{\beta_{200}}$ increases and in fact reaches the ratio $\frac{\tan\vartheta_{400}}{\tan\vartheta_{200}}$.

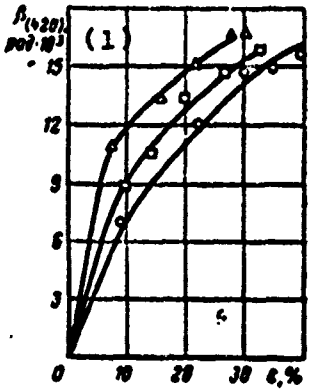

Figure 111. Change in the physical line width (420) of copper as a function of type and degree of deformation. The symbols are the same as on Figure 108.

1. $\beta_{(420)}$, rad·10^3

The harmonic analysis which we made for the shape of the x-ray lines of nichrome [244] and the MA-8 alloy [237] showed a different dependence of the size of the microdeformations on the size of the region of averaging for the quasi-static and dynamic deformations. The gradient of change in the microdeformations is higher during dynamic deformation and the microdeformations are distributed in a smaller volume of the crystal. Thus it is obvious that the fields of microdeformations from the pile-up of dislocations during dynamic deformation act at a smaller distance than during quasi-static. The authors of reference [248] assume that this must correspond to the more uniform distribution of dislocations which they proved on nickel.

There are also data that pulsed deformation facilitates the formation of packing defects. Such results were obtained by us on a magnesium alloy [247], on the alloy Co-Ni-Nb, and also in reference [249] on austenite steel. However this question requires more careful proof.

The data of x-ray structural analysis have been confirmed by electron microscopic investigations. After quasi-static deformation of copper up to ε = 7% (Figure 112) the majority of dislocations lie in the plane (111) of the primary glide system. The dislocations are distributed with small pile-ups - tangles, which are not visible on the original samples. As was shown, up to ε = 7% of the quasi-static deformation, the glide takes place along a single plane. Here no effective barriers are formed to slow down the motion of the dislocations. When $\varepsilon > 7\%$ a tendency is observed for the onset of a cellular structure which corresponds to the beginning of glide in the secondary systems.

Table 28. Results of Measuring the Physical Width of X-Ray Lines (200) and (400) of Copper and Nichrome After Different Types of Deformation.

(The Ratio $\frac{\cos\beta_{200}}{\cos\beta_{400}}$ is Equal to 1.75 for Copper and 1.85 for Nichrome: The Ratio $\frac{\tan\beta_{400}}{\tan\beta_{200}}$ is 3.47 for Copper and 3.7 for Nichrome)

Материал (1)	Штамповка (4)	$\dot{\varepsilon}$, $сек^{-1}$ (11)	ε, %	β_{200}, рад.10^3 (12)	β_{400}, рад.10^3 (13)	$\frac{\tan\beta_{400}}{\tan\beta_{200}}$	$\rho \cdot 10^{-10}$
Медь (2)	Гидростатическая (5)	$0{,}5—5 \cdot 10^{-3}$	9	1,70	4,50	[illegible]	0,36
			30	3,14	8,14	[illegible]	1,05
			41	3,90	10,4	[illegible]	2,05
	Электрогидравлическая (6)	$10—10^2$	10	1,50	4,65	[illegible]	0,78
			20	2,89	8,50	[illegible]	2,54
			32	3,46	10,9	[illegible]	4,50
	Гидровзрывная (7)	$\sim 10^5$	8	2,22	7,40	3,33	2,54
			22	2,81	9,65	3,41	5,02
			38	2,4[illegible]	12,00	3,41	7,56
	Электромагнитная (8)	$5 \cdot 10^4$	7	1,85	6,44	3,47	2,31
			22	2,00	10,5	3,51	5,89
			30	3,42	12,9	3,5	8,02
Нихром (3)	Гидростатическая (9)	$0{,}5—5 \cdot 10^{-3}$	7	—	—	2,4	—
			9	—	—	2,9	—
			11	—	—	3,0	—
	Гидровзрывная (10)	$\sim 10^5$	7	—	—	2,1	—
			[illegible]	—	—	2,9	—
			11	—	—	3,3	—
			13	—	—	3,1	—

1. Material
2. Copper
3. Nichrome
4. Punching
5. Hydrostatic
6. Electrohydraulic
7. Hydrodetonation
8. Electromagnetic
9. Hydrostatic
10. Hydrodetonation
11. $\dot{\varepsilon}$, sec^{-1}
12. β_{200}, rad.10^3
13. β_{400}, rad.10^3

After pulsed deformation of copper already at ε = 5-7% the cellular structure is completely formed (Figure 113). At the walls of the cells the dislocations form complex and irregular configurations and it is not possible to determine to which individual glide planes they belong.

Figure 112. Dislocation structure of copper after hydrostatic deformation: a. ε = 7%; b. ε = 12%; individual pile-ups are visible with no formation of a cellular structure.

The difference in formation of the cellular structure by quasi-static and pulsed punching is determined by the respective deformation mechanism. For the formation of a cellular structure it is necessary that there be an effect from more than one glide system and the greater the effective systems the sooner the cellular structure is formed. Such a relationship was mentioned in reference [214].

Another characteristic of the dislocation structure of copper after pulsed deformation is the decrease in the average size of the cells in comparison with quasi-static deformation. As follows from Table 29, with increase in the

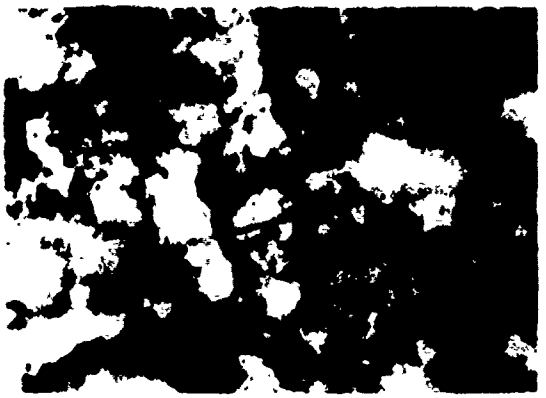

Figure 113. Dislocation structure of copper after hydrodetonation deformation up to $\varepsilon = 8\%$. The cellular structure is fully formed.

Table 29. Dimension of Cells as a Function of Type and Degree of Deformation

Штамповка (1)	Размер исходного зерна, мкм (4)	ε, %	Диаметр ячеек, мкм (5)		
			средней (6)	максимальный (7)	минимальный (8)
(2) Гидростатическая	20	10	0,63	1,57	0,5
		22	0,60	1,43	0,28
		37	0,75	1,30	0,25
	150	10	0,86	1,60	0,40
(3) Гидровзрывная	20	10	0,33	0,65	0,13
		21	0,27	0,46	0,09
		38	0,24	0,44	0,08
	150	10	0,30	0,60	0,15

1. Punching
2. Hydrostatic
3. Hydrodetonation
4. Size of original grain, μm
5. Diameter of cells, μm
6. Average
7. Maximal
8. Minimal

degree of deformation the average size of the cells is decreased both during quasi-static and during pulsed deformation regardless of the size of the original grain. The average diameter of the cells after pulsed deformation is two

to three times less than after quasi-static. This can be explained by the fact that, as a result of the earlier development of multiple glide, the barriers which exert resistance to displacement of the dislocations are found at smaller distances from one another. Such a dislocation structure produces additional strengthening of the copper.

Unlike copper and nickel, no cellular structure is generated [250] in aluminum by impact contraction, which is obviously due to the low melting point of aluminum.

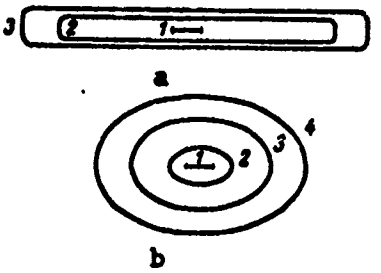

Figure 114. Propagation of dislocation loops in bcc (a) and fcc (b) crystals during deformation by detonation (the ordinal numbers indicate the sequential position of the loops) [252].

Several researchers [251, 106], based on the uniform dislocation structure obtained in alpha-Fe after pulsed deformation, reached the conclusion that at high deformation velocities no dislocation reactions can take place. However the results described above and in references [252, 248] show that during the pulsed deformation of fcc metals a cellular structure is formed, i.e., the interaction between dislocations also takes place at significant deformation velocities. At the same time with the high-velocity deformation of iron and molybdenum, Burgers dislocations are formed but there is no cellular structure. According to Hirsh, the walls of the cells are generated by the interaction between Burgers dislocations arranged along different glide systems as a result of their transverse glide relative to the primary plane.

But as shown in [252] it is namely such a displacement in the crystals with a bcc lattice that is difficult. And with high-velocity and low-temperature deformation (4.2° K) of molybdenum, regular Burgers dislocations are formed that possess significantly lower mobility in comparison with the edge components of the loop (the mobility ratio is 1:40). As a result of this the dislocation loop consists of elongated Burgers components, not suitable for transverse displace-

ment and binding of the cells (Figure 114 a). A large part of the plastic deformation is accomplished because of the movement of the edge dislocations at comparatively large distances.

In fcc metals the Burgers component possesses significantly greater mobility, the dislocation loop has an almost symmetrical shape (Figure 114 b), and the formation of a cellular structure takes place freely.

The dislocation density ϱ during hydrodetonation deformation of copper is one and a half to two tires greater than during hydrostatic, and the grain size does not influence the dependence $\varrho(\delta)$ (Figure 115), which in logarithmic coordinates is linear. Using the method of least squares we found the parameters of this dependence for both types of deformation and obtained the following equations:

$$\varrho = 4.0^{\pm 0.5} \cdot 10^9 \cdot \varepsilon^{0.38 \pm 0.04}$$ (for quasi-static deformation),

$$\varrho = 4.7^{\pm 0.4} \cdot 10^9 \cdot \varepsilon^{0.65 \pm 0.04}$$ (for dydrodetonation deformation).

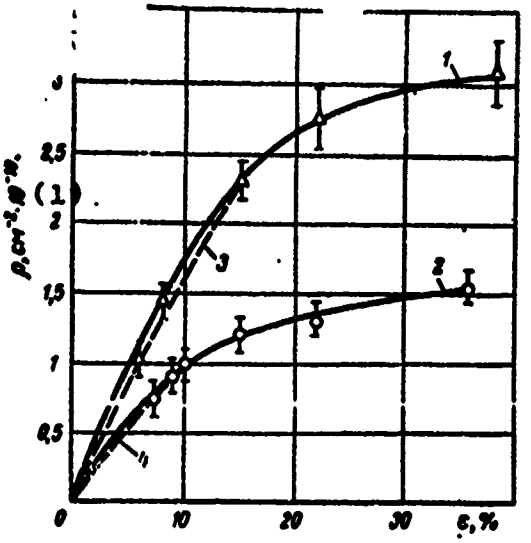

Figure 115. Dependence of dislocation density in copper on degree of deformation during hydrodetonation (1) and hydrostatic (2) loading; the solid lines represent the grain size of about 20 μm; the dotted lines represent those of 150 μm.

1. ϱ, $cm^{-2} \cdot 10^{-10}$

From the equations it follows that the dislocation density with increase in ε during high-velocity deformation, grows significantly more rapidly than during quasi-static. The results obtained coincide with the x-ray data.

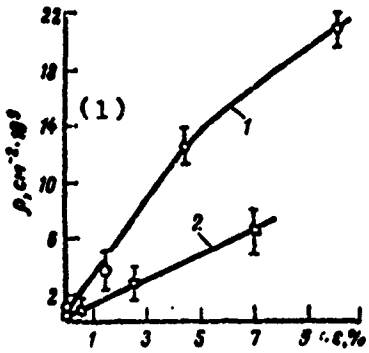

Figure 116. Dependence of dislocation density on degree of deformation of molybdenum [253]: 1. $\dot{\varepsilon} = 2 \cdot 10^{3}$ sec^{-1}; 2. $\dot{\varepsilon} = 2 \cdot 10^{-5}$ sec^{-1}.

1. ρ, cm$^{-2} \cdot 10^{9}$

Analogous measurements on the dislocation density during deformation at a velocity of $2 \cdot 10^{-5}$ and $2 \cdot 10^{3}$ sec^{-1} were carried out on molybdenum [253]. The curves found in this paper for the changes in dislocation density (Figure 116) duplicate our curves obtained for copper quite well.

In formula (66) the total length of the mobile dislocations L may be replaced by the density of the mobile dislocations ρ_m, and ρ_m may differ substantially from the total dislocation density comprising, in individual instances, all of 0.1ρ.

Let us turn our attention to the fact that by changing the deformation velocity by seven to eight orders of magnitude, as in our experiments with copper, and in the experiments of Gilbert et al with molybdenum, the dislocation density is increased altogether by several times.

The authors of reference [253] tentatively estimated [1] the value of the effective cleavage stress for the deformation γ.

[1] γ was computed from formula (23) which does not allow for a precise computation of this value because of variation in the index n in wide ranges.

Carrying out partial differentiation of equation (66) over τ, we find

$$\frac{\partial \lg \dot{\varepsilon}}{\partial \tau} = \frac{\partial \lg \rho_m}{\partial \tau} + \frac{\partial \lg \tilde{v}}{\partial \tau}. \qquad (69)$$

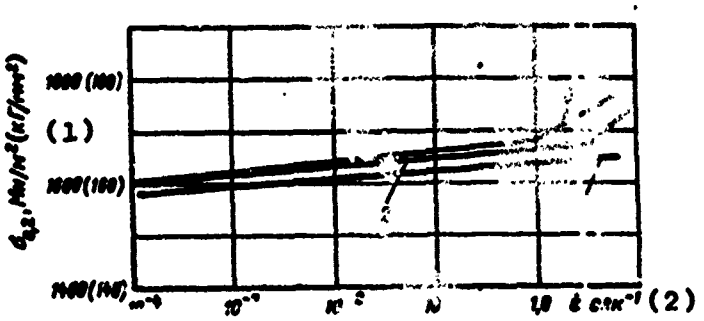

Figure 117. Influence of deformation velocity on yield stress of 4340 steel as a function of original microstructure: 1. fine-grain martensite; 2. coarse-grain martensite; 3. bainite.

1. $\sigma_{0.2}$, Mn/m^2 (kgf/mm^2) 2. $\dot{\varepsilon}$, sec^{-1}

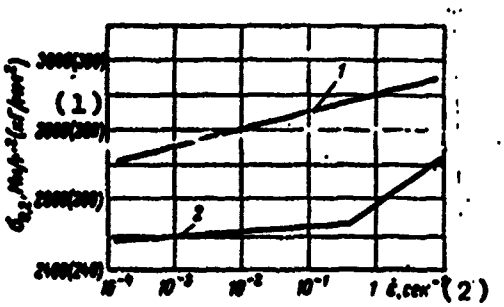

Figure 118. Influence of deformation velocity on yield stress of martensite aged steel (1) and type N-11 steel (2).

1. $\sigma_{0.2}$, Mn/m^2 (kgf/mm^2) 2. $\dot{\varepsilon}$, sec^{-1}

From the results of this work it follows that the basic contribution to increase in deformation velocity is made by the second term, rather than their density. The authors assume that the data obtained indicate a more uniform distribution of the dislocations as a result of which the size of the

path of the dislocations is reduced during transverse gliding. In turn the increase in velocity of the dislocation displacement, as was shown earlier, is due to the increase in resistance of the lattice to their displacement.

The influence of deformation velocity on the properties of the materials is found to be a selective one. The range of velocities in which a significant change is observed in the strength properties depends not only on the metal itself, but also on its original microstructure, and consequently, on the preliminary treatment.

In reference [254] the influence of deformation velocity was studied in the range from 10^{-4} to 10 sec^{-1} on the yield stress $\sigma_{0.2}$ as a function of the original structure of type 4340 steel (0.44% C, 0.75% Mn, 0.3% Si, 1.65% Ni, 0.85% Cr, 0.21% Mo). By quenching this steel from a temperature of 840° C in oil, a fine-grain martensite was produced; by quenching from 930° a coarse-grain martensite was produced, and by quenching from 840° C in a salt bath at t = 315° C, a bainite structure was produced. All three structural states, as is clear from Figure 117, act differently in the range of investigated velocities. In semi-logarithmic coordinates the increase in $\sigma_{0.2}$ of the fine-grain martensite takes place uniformly over the entire range of velocities with a relatively small slope of the line. For the coarse-grain martensite at a velocity of $0.5 \cdot 10$ sec^{-1} a sharp break is seen, after which the influence of deformation velocity is expressed much more. For an initial bainite structure this break appears at a lower velocity.

Martensite aged steel with 18% Ni in the state of quenching from 815° and annealing (480° C) is strengthened more strongly than the others in the entire velocity range (Figure 118). In type N-11 steel (0.4% C, 5% Cr, 1.3% Mo, 0.5% V) the yield stress is increased practically at a deformation velocity greater than 0.5 sec^{-1}.

Thus, from the examples given, it follows that the effectiveness of strengthening by high-velocity deformation to a significant degree is determined by the original microstructure. It is difficult to unambiguously analyze the results cited. One of the possible explanations may be the following. In the fine-needle martensite, where the distribution of defects is most uniform, it is more difficult to produce additional strengthening factors than in the coarse-crystalline martensite which is characterized by a greater heterogeneity in the defect distribution. In such a structure there are fields where the blocking sources are not strong as in the region of the martensite crystal, therefore the effect of deformation velocity also appears earlier.

Table 30. Plastic Properties of Steels Under Quasi-Static and Dynamic Tension [255]

(1) Марка стали	Начало мартенситного превращения °К (9)	Квазистатическое растяжение (10)			Динамическое растяжение (12)				
		δ_1, %	ψ_1, %	количество мартенсита α_1, % (11)	δ_2, %	ψ_2, %	количество мартенсита α_2, % (13)	$\Delta\delta = \delta_2 - \delta_1$	$\Delta\delta = \frac{\delta_2 - \delta_1}{\delta_1} \cdot 100$, %
Н28,5 . . (2).	233—213	42,1	36,4	1,6	51,4	42,1	8,8	+7,2	+22,0
40Н25 . . (3).		41,8	42,6	1,5	40,8	63,1	1,5	0	—2,4
2Х18Н9 . (4).	<77	58,0	79,5	1,0	54,5	65,5	0,5	—0,5	—6,9
67Х7Н7 . (5).	253—238	12,5	11,3	2,7	45,3	40,7	16,6	+13,9	+263
30Х10Г10 * (6).		9,3	10,8	11,6	27,0	22,6	50,0	+38,4	+190
30Х10Г10 ** (7). . . .		23,1	17,1	18,8	46,6	59,0	15,5	—3,3	+102
47Х10Г8 . (8).		7,9	9,7	24,4	30,5	29,8	45,5	+21,1	+286

(14) *: После ковки и охлаждения на воздухе.
(15) **: После двукратной закалки с промежуточным старением.

1. Type of steel
2. N28.5
3. 40N25
4. 2Kh18N9
5. 67Kh7N7
6. 30Kh10G10*
7. 30Kh10G10**
8. 47Kh10G8
9. Onset of martensite transformation
10. Quasi-static tension
11. Amount of martensite α_1, %
12. Dynamic tension
13. Amount of martensite α_2, %
14. * After forging and cooling in air
15. ** After double quenching with intermediate aging

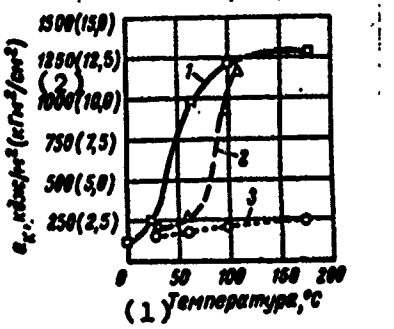

Figure 119. Temperature dependence of the impact strength of steel after different types of treatment: 1. quenching; 2. impact loading at 95 kbar; 3. specific loading at 220 kbar.

1. Temperature, °C 2. a_K, kJ/m^2 (kgfm^2/cm^2)

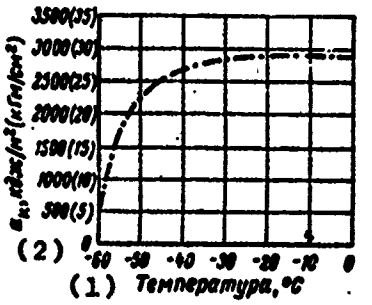

Figure 120. Temperature dependence of impact strength of steel after deformation at a shock wave pressure of 1-2 kbar.

1. Temperature, °C 2. a_K, kJ/m^2 (kgfm/cm^2)

In martensite aged steel a quantitative rather rapid pile-up of dislocations takes place as a result of precipitation of the secondary phase as an effect of deformation aging. This effect does not involve any effect from the new mechanism in the examined range of velocities. We know only that the increase in deformation velocity amplifies the effect of deformation aging [274].

3. Plastic Properties of Metals

It follows to distinguish the plastic properties of metals appearing in the process of dynamic loading and the characteristics of plasticity found in a metal after strengthening treatment.

The plasticity of metals in the process of high-velocity deformation is determined mainly by the deformation mechanism or by those processes which this deformation induces. We know that many hexagonal metals (titanium, magnesium, etcetera) are found to be significantly more plastic under high-velocity loading, new glide and twinning systems come into play which permit increasing the total degree of deformation.

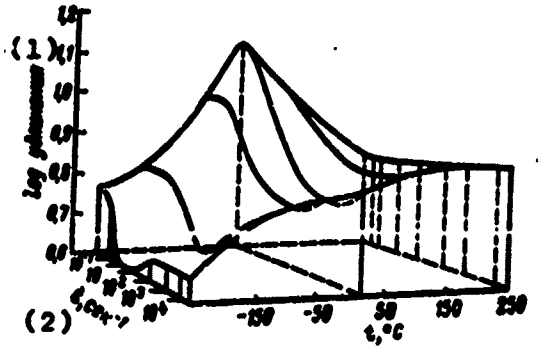

Figure 121. Dependence of plasticity of stainless steel 303 on velocity and temperature of deformation.

1. log expansion 2. $\dot{\varepsilon}$, sec^{-1}

Interesting research was done by Bogachev et al [255] on a group of austenite steels having different points for the onset of martensite transformation. Quasi-static expansion of the samples was done on the IM-4P machine at a constant deformation velocity of 4 mm/min, the dynamic expansion was done on a special device by means of detonating 1.75 g powder. This suspension was found to be sufficient to fracture the samples of all the investigated steels. The velocity of impact (detonation) expansion on the devices of this type was 10-30 m/sec.

Before and after deformation the amount of martensite was determined using the magnetic method.

The plastic properties during quasi-static and dynamic tests are shown on Table 30.

The maximal relative increase in plasticity during the dynamic tests is seen in steels on a chrome-nickel and chrome-manganese base, for which the increase in the martensite phase was maximal. In the opinion of the authors, this effect is determined by the different drop in resistance to

deformation at the moment of the martensite transition. The authors assume that by the dynamic deformation it is possible to have the phase transitions $\gamma \rightarrow \alpha$ and $\gamma \rightarrow \varepsilon$, since as a result of heating produced by dynamic application of the load, the reverse transition $\varepsilon \rightarrow \gamma$ is accomplished. However, formation of the ε-phase is not very probable at such relatively low deformation velocities.

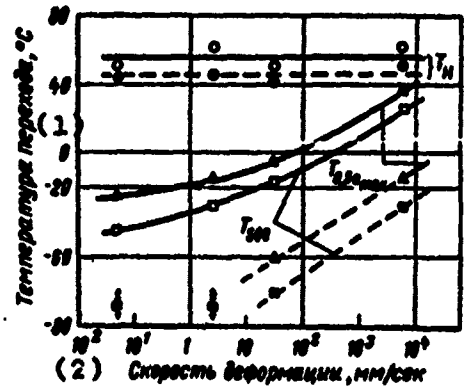

Figure 122. Dependence of temperature of transition to the brittle state during tests for impact strength of steel with 0.14% C on the deformation velocity: T_0 is the temperature of the onset of transition to the brittle state; $T_{0.5a_{max}}$ is the temperature corresponding to the half-value of the maximal impact strength; T_{500} is the temperature corresponding to $a_0 = 500$ kJ/m^2 (5 kgfm/cm^2). The solid lines pertain to the V-shaped notch, the dotted lines to the U-shaped notch.

1. Transition temperature, °C 2. Deformation velocity, mm/sec

Obviously in these experiments also some kind of contribution to the increase in plasticity during high-velocity deformation is made by changing the mechanism of the process itself, which the authors unfortunately did not study. This assumption particularly is confirmed by the authors' experiment on 30Kh10G10 steel in which, by double quenching and intermediate aging, the martensite transformation was delayed. During dynamic expansion this steel gave a double increase in the relative expansion and more than a triple increase in the narrowing of the cross section.

The brittleness of the deformed metal has a different dependence on the conditions of pulsed loading. During contact

detonation, as shown in the work of Dieter [148], the temperature of transition of steel to the ductile state is significantly increased. At a pressure of 25 kbar the temperature of the brittle transition grows by 50° C, in comparison with the quenched one, and at a pressure of 220 kbar the ductile state does not set in before 170° C (Figure 119).

A different picture is found by detonation strengthening through a transmitting medium when the pressure of the wave is 1-2 kbar. As is clear from Figure 120, the temperature of transition from brittle state to ductile is even lowered. But with passage of a certain amount of time, the temperature of transition again is increased which probably is due to deformation aging. In the range of deformation velocities from 10^{-1} to 10^{4} min^{-1} the increase in yield stress of steel, copper, and aluminum is not accompanied by any significant reduction in plasticity [62].

However in a wide temperature range the dependence of plasticity on deformation velocity is not monotonic. On Figure 121 a spatial diagram is given for the dependence of plasticity of stainless steel on deformation velocity and temperature [256]. For this steel a drop in plasticity is seen in the region of deformation velocity of 10 sec^{-1}, and this drop is more abrupt at low temperatures.

Interesting results were found in reference [257], where the authors studied the influence of deformation velocity on impact strength and determined the temperature of the onset of drop in impact strength, the temperature at which the impact strength reached half the maximum, and the temperature at which the impact strength was equal to 500 kJ/m^2 (5 $kgf \cdot m/cm^2$). The results shown on Figure 122 show that the temperature of the half-value a_K and the temperature at which a_K = 500 kJ/m^2 (5 $kgf \cdot m/cm^2$) depend on deformation velocity. The temperature of the onset of transition to the brittle state does not change. Hence, we can obviously make the conclusion that deformation velocity does not influence the formation of cracks but rather influences their propagation.

CHAPTER 5

HIGH-VELOCITY DEFORMATION AND PHASE TRANSITIONS IN METALS

The use of quasi-static methods for producing high pressures has permitted observing phase transitions in various materials [258]; here for a noticeable determination of the transformation several hours are sometimes required. At the same time the phase transitions are noted during passage of shock waves for a time measured in several microseconds. It is interesting to note that using both the quasi-static methods of creating high pressures and in impact loading, reversible and irreversible phase transitions are observed. Tests on impact loading of graphite permitted establishing the possibility of producing diamonds by retaining the given modification of carbon after unloading [191]. However the phase transition of iron under the influence of shock waves has a reversible character and it is not possible to determine the high-pressure phase at atmospheric pressure.

The works of Bancroff et al [192] were the first to show the possibility of observing a phase transition under the influence of shock waves. They observed a bend in the Juygens curve for iron at a shock wave pressure greater than 130 kbar. Then the phase transitions under the influence of the shock wave were determined on bismuth [194], antimony [193], and other materials [259].

The generation of new phases disrupts the monotonic path of the curves for impact contraction. The presence of phase transitions in the process of impact loading is described in the P-V coordinates by the line with the break (Figure 123).

To interpret the results describing similar curves we can briefly examine the structure of the waves induced in the material subjected to impact contraction. If there is no bend on the Huygens curve, then this corresponds to the

case of propagation in a material of a single shock wave with a stable amplitude. A bend on the Huygens curve corresponds to the case when the shock waves in a given pressure range become unstable and several waves are propagated with different amplitudes.

The phase transition begins at point 1 at a pressure P_1 (see Figure 123). Between point 1 and point 3, which lies on the intersection of the adiabatic curve of the secondary phase with the wave line 0-1, a decay takes place in the shock front. A wave of critical amplitude P_1 moves ahead of it, and behind it at lower velocity the wave of the phase transition P_2 is propagated; here $P_2 > P_1$. On the segment 1-1' after passage of the secondary wave there simultaneously exist phases of low and high pressure. The segment of the 1'-4P-V diagram describes the state of the high pressure phase. At point 3 we observe an insignificant bend associated with the weak entropy discontinuity, generated by the disappearance of the two-wave configuration and by the recovery of the single discontinuity surface.

Figure 123. Huygens curve for a material undergoing polymorphous transformation.

The reverse recrystallization of the material when the high pressure is removed leads to a break in the isentrope of broadening and to the appearance of expansion shock waves. From a certain state n on the adiabatic curve of the secondary phase a broadening takes place in the unloading wave along the isentrope mn. Then there may be either a sudden reduction in pressure in the expansion wave converting the material from state n to state k, pas-

through the segment nrk, or an insentropic broadening is observed up to zero values along the curve mnℓ. In the second case the expansion wave is absent. Intermediate variations are also possible.

Phase transitions (including melting and evaporation) may also take place after removing the pressure. In this case the shape of the Huygens curve does not change. The phase transitions may be determined by measuring the velocity of the free surface and by constructing the adiabatic curve P-V. But this involves considerable experimental difficulty.

The phenomenon of polymorphism in the shock waves is determined from the Huygens curve for many metals, salts, and rocks. Below we give the materials for which the phase transition was observed and also show the amount of pressure determining the transition.

Pressure of the shock wave of the phase transition, kbar*:

Antimony	about 115
Bismuth at a temperature, °C	
-28	31.3
19	27.2
236	17.6
Alpha-iron at a temperature, °C	
room	32
195	50
884	19
Nickel and chrome steels	100-180
36% Ni + Fe (invar)	60
30% Ni + Fe	25
Carbon (graphite)	300-400; 600-700
Phosphorous	
red	25-35
yellow	70-80
Sulfur	67-106
Iodine	700
Germanium	about 125
Marble	150
Sandstone	about 70
Quartz:	
melted	250
NaCl <100>	29
KCl <100>	20±0.8
KBr <100>	18.5±0.8
CdS	29-32
InSb	17-20
Barium titanate	8

* Where the temperature is not shown, the material is at the temperature of the surrounding temperature.

The fact of phase transition under the influence of shock waves has also been established repeatedly by x-ray and metallographic investigation.

Iron has been studied most fully. The first systematic investigation of iron fo-lowing impact loading was done by Smith [176] who showed that the microstructure of iron subjected to the effect of a shock wave at presaures greater than 130 kbar, is similar to martensite obtained by abrupt quenching from the gamma-region. The phase transition is accompanied by a sharp increase in hardness (see Figure 98).

The structure of the steel after pulsed loading, producing the phase transition, differs significantly from the structure after deformation. Figure 124 a shows the microstructure of a deformed single crystal of iron after the effect of the shock wave at a pressure less than 130 kbar, where the deformation twins are clearly visible. With loading by shock wave at $P > 130$ kbar along with the twins a ribbon relief reminescent of the martensite structure is formed (Figure 124 b).

Figure 124. Microstructure of single crystals of iron following impact loading [101]: a. $P < 130$ kbar; b. $P > 130$ kbar; X 400.

In this paper the difference in the structure of the crystals deformed at pressures, smaller and greater than the critical, was established radiographically. Figure 125 shows the pole figure (111) for two crystals. The crystal, deformed at $P < P_{cr}$, has a pole figure on which along with the reflections from the planes of the primary orientation there are reflections from the deformation twins (Figure 125 a). The crystal, deformed at $P > P_{cr}$ has no twin reflections on the pole figure; the structure consists of martensite and the pole figure corresponds to an almost ideal Nishiyama orientation (Figure 125 b).

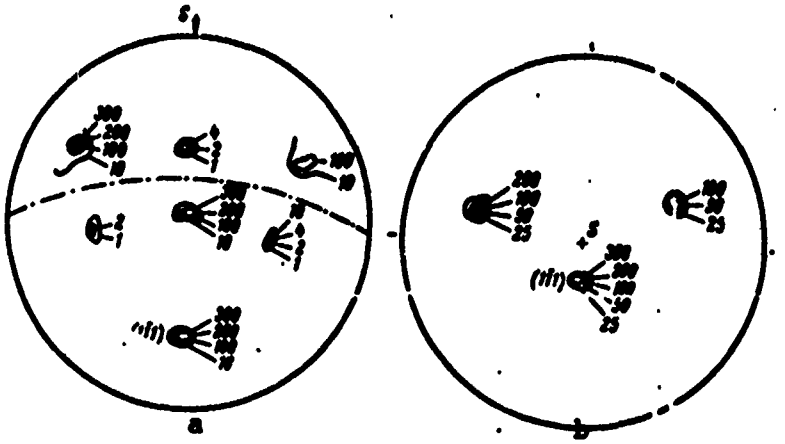

Figure 125. Pole figure (111) of single crystals of Fe+29% Ni, deformed [10]: a. at pressures less than P_{cr}; b. at pressures greater than P_{cr}.

It is important to mention that the composition and temperature of the original metal influences the amount of critical pressure above which the phase transition is observed. Fowler et al [172, 199] studied the dependence of critical pressure on the composition of steel. It was found that doping iron with chrome up to 10% (by mass) changes the value of the critical pressure very little, however with a large amount of chrome, P_{cr} grows and reaches 130 kbar at 20% Cr. Nickel on the other hand slightly reduces the value of P_{cr}.

The temperature dependence of the phase transition in iron induced by detonation, was investigated by Johnston et al [260] in the temperature range from 78 to 1158° K. The results which they found are shown on Table 31.

From Table 31 it follows that by increasing the temperature, the amount of pressure necessary for the transition in iron is lowered. Along with this the authors turned their attention to the fact that the structure of iron at $T > 775°$ K differs sharply from the structure at lower temperatures. After impact loading at temperatures less than 775° K, in the annealed grains of ferrite twin formations appear as observed by Smith.

Above this temperature the transition in iron is accompanied by a sharp reduction in grain size. The average diameter of the grains in the annealed iron was 250 μm and 1.5 μm after the transition. Such a reduction in grain size

may be due to recrystallization, since for the occurence of recrystallization at T < 1100° K, at least one hour is required.

Table 31. Critical Pressure of the Phase Transition in Iron at Various Temperatures

T, °K	(1) $P_{кр}$, кбар	T, °K	(1) $P_{кр}$, кбар
78	150	875	[illegible]
298	130	975	[illegible]
421	124	1073	[illegible]
540	124	1158	[illegible]
773	111		

1. P_{cr}, kbar

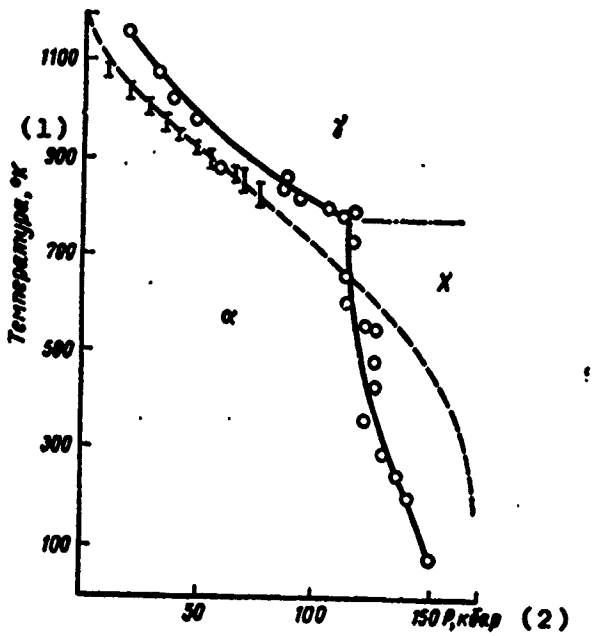

Figure 126. Diagram of the phase state of iron in the coordinates temperature-pressure. The dotted lines show the theoretical computation after Kaufman.

1. Temperature, °K 2. P, kbar

Based on these data the authors assume that a critical point exists at T = 775° K and P = 115 kbar, which separates the region of existence of iron into the various modifications. This can be shown schematically in the form of the diagram given on Figure 126. The authors compared their experimental data with the theoretical computations of Kaufman [261]. The agreement was found to be good for the $\alpha \rightarrow \gamma$-transition. At lower temperatures where discrepancies exist between the experimental and computational data, the alpha-phase transforms into another crystal modification.

In later investigations [262, 263] it was shown that at pressures above P = 130 kbar and T < 770° K, the alpha-Fe transforms into a hexagonal densely-packed lattice (ε-phase) rather than into the fcc lattice. This same phenomenon was detected during the static increase in pressure which permitted better determining the characteristics of the ε-phase [264-266]. Jameson and Lawson [265] were the first to radiographically establish the existence of a hexagonal phase in iron under the effect of hydrostatic pressure.

Belchan and Drichamer [267] measured the critical pressure for the transition of alpha-Fe into the high-pressure phase. According to their research the pressure of the transition was found to be equal to 130 kbar under these conditions as well, which agrees with the data found in the experiments on shock waves. At the moment of transition α-Fe $\rightarrow \varepsilon$-Fe a fourfold increase in electrical resistance is observed.

In reference [266] the lattice constants of the hexagonal densely-packed modification of iron were found and it was shown that up to 300 kbar at room temperature the ratio c/a does not depend on pressure and has a mean value equal to 1.603±0.001. Change in the constant is described by the empirical formula:

$$a_{(hdp)} = 2{,}523\left(1 + \frac{P}{330}\right)^{-0.033}.$$

The constant of the bcc lattice of iron varies as a function of pressure according to the expression

$$a_{(bcc)} = 2{,}866\,(1 + P/275)^{-0.033}.$$

The crystallographic transition of alpha-Fe into the hexagonal modification is accomplished first as a result of the small change in the interatomic spacing in the direction

<001> of the bcc lattice and secondly as a result of the shift in the planes (110) in the direction [1$\bar{1}$0] or [$\bar{1}$10]. The ratio c/a for the hexagonal densely-packed iron is less than for the ideal dense packing, but the interatomic spacing in the hexagonal densely-packed iron is greater than in the alpha-iron. Thus, by such phase transition (as by the way in other cases as well) a growth in the coordination number is accompanied by an increase in the interatomic spacing. Increasing the interatomic spacing $d_{(110)}$ of the bcc lattice being equivalent to $d_{(002)}$ for the hexagonal densely-packed lattice.

In a number of cases a correspondence is noted between the critical pressure of the transition during static and impact loading.

Table 32. Critical Pressure of the Phase Transition in Bismuth by Various Methods of Treatment

(1) Вид испытаний	(5) P, кбар (при 25 °С)	Изменение удельного объема в момент превращения (6)
Ударное нагружение литого поликристалла (2)	25,9±1,2	0,939±0,003
Ударное нагружение предварительно деформированного поликристалла (3)	25,4±0,8	0,940±0,002
Статическое нагружение (4)	25,4±0,1	0,940±0,001

1. Type of tests
2. Impact loading of a molten polycrystal
3. Impact loading of a predeformed polycrystal
4. Static loading
5. P, kbar (at 25°C)
6. Change in specific volume at the moment of the transition

In reference [268] this question was investigated for the phase transition of bismuth. In the opinion of the author, the non-agreement observed in a number of papers is due to strengthening of the metals by impact loading. If the strengthening is taken into account, then the amounts of the critical pressure determined from the dynamic and static data agree rather well (Table 32).

In spite of such agreement, it is difficult to suggest in both cases that the mechanism of the transition is the same. It is not clear how this mechanism ensures a high velocity of the transition for a time less than 10^{-6} sec.

Probably the shock waves create high displacement stresses which are localized in the narrow front of the shock wave.

Quite interesting results were obtained in reference [26], where various materials subjected to impact loading were investigated by the methods of x-ray structural analysis. In the powder-form and molten samples of manganese and cobalt they detected a polymorphous transformation. After the impact effect an irreversible transition of the powder of alpha-Mn (cubic complex lattice: a = 8.9 kX, 58 atoms per cell) into beta-Mn (cubic complex lattice: a = 6.3 kX, 20 atoms per cell) took place and the molten samples assumed a two-phase structure $\alpha+\beta$.

The original mixture, consisting of two modifications of cobalt, alpha (hexagonal densely-packed) and beta (fcc) with predominance of the hexagonal densely-packed phase as a result of the impact effect, had a greater amount of the cubic phase, and in the zone with maximal temperature and pressure (2000° K and 1600 kbar) the alpha-phase disappeared completely.

Under ordinary circumstances the single-phase state of the beta-cobalt can not be determined even with abrupt quenching in water. This gives a basis for assuming that the polymorphous transition observed during detonation loading is not the result of purely temperature changes, generated in the zone of the shock wave, but is due to the effect of high pressures.

An analogous effect is also observed on large-scale samples: when P = 420 kbar and T = 470° K, a significant transition of the α-Co $\rightarrow$ β-Co takes place.

In reference [26] the synthesis of powders in the shock wave was also studied: The composition of powders of iron and vanadium of equiatomic composition under the influence of impact loading converts to the solid solution on the base of the bcc lattice. The lattice constant of the solid solution is equal to 2.90 kX, which according to the literature data, corresponds to a solid solution on a base of iron with 40-50% (atomic) vanadium. Here no lines of the σ-phase, corresponding in the given system to low-temperature equilibrium, were detected.

In the other composition of the equiatomic composition manganese-tungsten, where both components do not interact under ordinary conditions either in the liquid or in the solid state, under the influence of shock waves a solid solution is formed on the base of tungsten (Figure 127). Here along with the solid solution there are the original components.

Evaluation of the lattice constant of the solid solution gives a value of a ≈ 3.14 kX. The decrease in the lattice constant to 0.02 kX the authors believe to be due to the dissolving of about 20% (atomic) Mn.

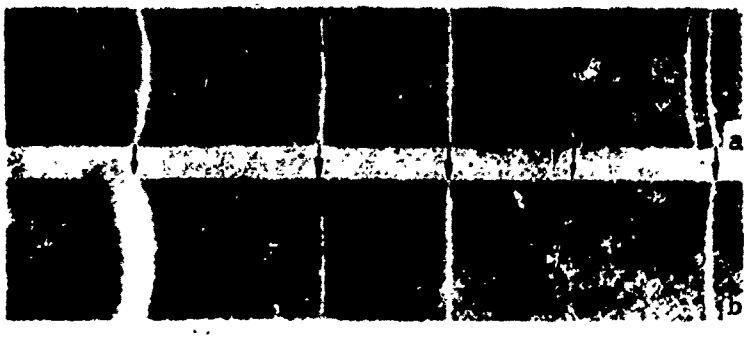

Figure 127. Interaction of manganese and tungsten under the influence of a shock wave: a. radiogram of the mixture prior to testing; b. the same, following testing; the arrows indicate the lines of the solid solution of manganese in the tungsten.

The equiatomic composition in the system iron-silicon corresponds to the chemical compound FeSi which is stable from room temperature to the melting points. X-ray investigation showed that as a result of dynamic loading of the powders of these components an iron silicide FeSi with a cubic lattice (P_{2_13} a = 4.473 kX) and a silicide with a hexagonal primitive lattice (P_{6_3}/mmc, a = 2.69 kX, c = 5.11 kX) are formed. A slight amount of the original components is retained.

The authors of [26] studied also the recrystallization of the solid phase under the influence of shock waves in the system Fe-Mn, where it is usually done by the martensite mechanism. In this system it is possible to produce the ε-phase as a result of heat treatment. The authors investigated an alloy with 24.8% Mn, consisting of two phases $\gamma+\varepsilon$ (alloy 1) and a single-phase (γ) alloy with 39.8% Mn (alloy 2). After loading by the shock wave at a pressure of 800 and 1600 kbar in alloy 1 the amount of the ε-phase was increased and in alloy 2 lines of the ε-phase appeared (Figure 128). Thus, the presence of a phase transition during impact loading was confirmed by direct x-ray structural investigation.

The passage of the shock wave in solid bodies produces a whole series of interesting effects. Without pausing to examine them in detail, let us simply look at several of them.

Figure 128. Formation of the -phase in an alloy of iron and 39.8% Mn: a. radiogram of the sample prior to testing; b. same, following impact loading.

Under the effect of the shock waves, invar and an alloy of iron and 30% Ni, undergo a phase transition of the second kine from the ferromagnetic state to the paramagnetic [200]. In a number of semiconductors and insulators under the effect of impact loads, the electrical conductivity grows sharply. This effect was observed at rather high quasi-static pressures [269].

Shock waves may alter the degree of ordering of the solid solution. In reference [270] the alloy Cu_3Au was investigated. After rolling, recrystallization at 565° C, and slow cooling from 380° C, long-range ordering was determined in the alloy. In this same alloy, but after annealing at 460° C for a period of one hour and quenching in water, the short-range order was established. Investigation of the influence of the shock wave on the structure of the alloy in the two different original states permitted establishing several laws. Beginning from a certain pressure, a disordering of the alloys takes place in both states. Thus, from a pressure of 290 kbar the electrical resistance of the initially ordered alloy grows sharply. When $P > 290$ kbar the specific electrical resistance is decreased in the disordered alloy which is also due to the disruption in short-range order.

Interesting results have been obtained in recent years on the pulsed effect of laser radiation [271]. Irradiation by a laser of a sample of technical iron, on the surface of

which carbon was deposited, leads to a broadening of the x-ray lines of the alpha-phase and to the appearance of lines of the gamma-phase.

Consequently, under these conditions a saturation of iron with carbon up to comparatively high values takes place for a teime of 10^{-3} sec. After such treatment it was possible to metallographically observe segments having a eutectic structure. The hardness on the surface is increased up to 1400 HV, whereas the hardness of the irradiated iron, which melts under the effect of the ray, is only 170 HV.

In several cases after irradiation it was possible to find a martensite fine-needle structure that is characteristic of medium-carbon steel.

The greatest hardness is that of the white layer forming on the surface of the sample similar to the layer of the solid melt in the high-carbon steels and cast irons. Probably the saturation with carbon takes place basically in the molten metal.

BIBLIOGRAPHY

1. Landau, L.D. and Lifshits, Ye.M., Teoriya Uprugosti (Theory of Elasticity), Nauka Publishing House, 1965.

2. Al'tshuler, L.V., "Use of Shock Waves in the Physics of High Pressures," Uspekhi Fiz Nauk (Achievements in the Physical Sciences), Vol 85, No 2, p 197, 1965.

3. McQueen, R.G. and March, S.P., J Appl Phys, Vol 31, pp 1253-1269, 1960.

4. Pashkov, P.O. and Gelunova, Z.M., Deystviye Udarnykh Voln na Zakalennyye Stali. (The Effect of Shock Waves on Quenched Steel), Nizhne-Volzhskoye Knizhnoye Izdatel'stvo (Lower Volga Book Publishing House), 1969.

5. Hobson, G. and Amini, E., Int J Mach Tool Design and Res, Vol 4, No 2, pp 73-90, 1964.

6. Reichardt, J. and Pierson, J., Vzryvnaya Obrabotka Metallov (Detonation Treatment of Metals), Mir Publishing House, 1966.

7. Yedneral, N.V., Kracikov, K.I., Novobratskiy, R.L., Perper, F.A., Umanskiy, Ya.S., and Epshteyn, G.N., Izv Vuzov, Chernaya Metallurgiya (Bulletin of the Higher Educational Institutions, Ferrous Metallurgy), No 9, p 156, 1968.

8. Harris, I.T. et al, Sheet Metal Inds, Vol 39, No 442, pp 383-394, 399-410, 1962.

9. Pikhtovnikov, R.V. and Zav'yalova, V.I., Shtampovka Listovogo Metalla Vzryvom (Punching of Sheet Metal by Detonation), Mashinostroyeniye Publishing House, 1964.

10. Kruver, R.U. et al, In the Collection Vysokoskorostnoye Deformirovaniye Metallov (High-Velocity Deformation of Metals), Mashinostroyeniye Publishing House, p 44, 1966.

11. Portvin, P.A., Mem Scient Rev Metallurgie, Vol 60, No 9, pp 591-608, 1963.

12. Kraft, I.M., Instrumentation for High-Speed Strain Measurement. Response of Metals to High Velocity Deformation, New York-London, p 9, 1961.

13. Gouforz, P.E., In the Collection Vysokoskorostnoye Deformirovaniye Metallov, Mashinostroyeniye Publishing House, p 126, 1966.

14. Shcheglov, B.A., In the Collection Plasticheskoye Formoizmeniye Metallov (Plastic Deformation of Metals), Nauka Publishing House, p 12, 1967.

15. Krasikov, K.I., Umanskiy, Ya.S., Epshteyn, G.N., et al, Fiz-Khim Mekhanika Materialov (Physico-Chemical Mechanics of Materials), Vol 3, No 6, p 702, 1967.

16. Rickert, A., Technik, No 2, pp 99-105, 1965.

17. Ecker, W. and Müller-Akht, F., Werkstatt und Betrieb, Vol 96, No 3, p 163, 1963.

18. DeGroat, G., Amer Machinist -- Metalwork (Manufact), Vol 107, No 2, p 93, 1963.

19. Lipmann, H.J. and Schreiner, H.Z., Metallkunde, Vol 55, p 737, 1964.

20. Svistunov, Ye.P. and Bernshteyn, M.L., Zavodskaya Laboratoriya (Plant Laboratory), No 7, p 904, 1967.

21. Popov, Ye.A. et al, Kuznechno-Shtampovochnoye Proizvodstvo (Forging and Punching Production), No 5, p 1, 1966.

22. Lamar, H., BMnder-Fleche Rohre, Vol 7, No 12, p 843, 1966.

23. Corteville, I. et al, Ann Mines, p 863, Oct-Nov 1966.

24. Bowden, H.G. and Kelly, P.M., Metal Sci J, p 75, May 1967.

25. Barnett, J.D. et al, J Appl Phys, Vol 37, p 875, 1966.

26. Adadurov, G.A. et al, Izv AN SSSR, Metally (Bulletin of the USSR Academy of Sciences, Metals), No 6, p 135, 1968.

27. Gelunova, Z.N. et al, Fizika i Khimiya Obrabotki Metallov (Physics and Chemistry of Treating Metals), No 3, p 269, 1970.

28. Weertman, I., Response of Metals to High-Velocity Deformation, New York-London, p 205, 1961.

29. Gilman, I.I., Australian J Phys, Vol 13, p 327, 1960.

30. Gutmanas, E.Yu et al, FTT (Solid State Physics), Vol 5, p 743, 1963.

31. Lyubov, B.Ya. and Chernizer, G.N., DAN SSSR (Reports of the USSR Academy of Sciences), Vol 161, No 6, p 1324, 1966.

32. Peierls, R., Proc Phys Soc, Vol 52, p 34, 1940.

33. Nabarro, F.R., Adv Phys, Vol 1, p 271, 1952.

34. Huntington, H.B. et al, Phys Rev, Vol 100, p 1117, 1955.

35. Dingley, D.I. and McLean, D., Acta Metallurgica, Vol 15, pp 885-901, 1967.

36. Eshelby, I.D., J Appl Phys, Vol 24, p 176, 1953.

37. Frank, F.C., Proc Phys Soc, Vol 62, p 131, 1950.

38. Chandhuri, A.B. et al, J Appl Phys, Vol 33, p 2736, 1962.

39. Dew-Hughes, D., IBM Journ, Vol 5, p 279, 1961.

40. Schadler, H.W. and Low, I.R., Final Report on Contract, No 0112-2614(00), April, 1962.

41. Frekel, H.L. and Conrad, H., Acta Metallurgica, Vol 15, p 955, 1967.

42. Stein, D.L. and Low, I.R., J Appl Phys, Vol 31, p 362, 1960.

43. Erickson, I.S. J Appl Phys, Vol 33, p 2499, 1962.

44. Johnston, W.G. and Gilman, I.I., J Appl Phys, Vol 30, p 129, 1959.

45. Johnston, W.G., J Appl Phys, Vol 33, p 2716, 1962.

46. Gutmanis, E.Yu. and Nadprornyy, E.N., FTT, Vol 10, p 2284, 1968.

47. Gilman, I.I., J Appl Phys, Vol 36, p 3195, 1965.

48. Lavrent'yev, F.F. and Salita, O.P., FMM (Physics of Metals and Metal Research), Vol 23, No 3, p 548, 1967.

49. Gilman, I.I., Phys Rev Letters, Vol 20, No 4, p 157, 1968.

50. Campbell, I.D. and Hardin, I., Response of Metals to High-Velocity Deformation, New York-London, p 51, 1961.

51. Okawa, A.J., Appl Physics, Japan, Vol 32, No 10, p 1, 1963.

52. Eshelby, I.D., Proc Phys Soc, Vol 69, p 1013, 1956.

53. Hart, E.W., Acta Metallurgica, Vol 2, p 416, 1954.

54. Campbell, I.D. et al, Trans ASME, Vol D28, No 3, p 447, 1961.

55. Seitz, F., Adv Phys, Vol 1, p 43, 1952.

56. Panchenko, Ye.V. et al, Laboratoriya Metallografii (Laboratory of Metallography), Metallurgiya Publishing House, 1965.

57. Yakutovich, M.V. et al, Sb Posvyashchennon 70-Letiyu Akad A.F. Ioffe (Collection Dedicated to the Seventieth Anniversary of Academician A.F. Ioffe), USSR Academy of Sciences Publishing House, p 336, 1950.

58. Klerboro, L.M. and Khargrivs, M.Ye., Usnekhi Fiziki Metallov (Achievements in the Physics of Metals), Vol 5, Metallurgizdat, p 7, 1963.

59. Rozenberg, V.M., Polzuchest' Metallov (Creep of Metals), Metallurgiya Publishing House, 1967.

60. Nader, S., In the Collection Elektronnaya Mikroskoniya i Prochnost' Kristallov (Electron Microscopy and Strength of Crystals), Metallurgiya Publishing House, p 169, 1968.

61. Kuhlman-Wilsdorf, D. and Wilsdorf, H., Acta Metallurgica, Vol 1, p 394, 1953.

62. Tomas, G. and Watting, K., J Inst Met, Vol 86, p 1, 1956-1957.

63. Nader, S. and Seger, A., Acta Metallurgica, Vol 8, p 513, 1960.

64. Jan, J.P., J Appl Phys, Vol 26, p 1291, 1955.

65. Rakin, V.G., Kristallografiya (Crystallography), Vol 10, No 3, p 389, 1965.

66. Brawn, A.F., J Inst Met, Vol 80, p 115, 1951.

67. Ioshida, S. and Hayata, H., Trans Japan Inst Metals, Vol 8, No 28, p 108, 1954.

68. Ioshida, S. and Hayata, H., J Japan Inst Metals, Vol 31, p 444, 1237, 1967.

69. Hader, S. et al, In the Collection Struktura i Mekhanicheskiye Svoystva Kristallov (Structure and Mechanical Properties of Crystals), Metallurgiya Publishing House, p 9, 1967.

70. Bergeran, A. and Fourdeux, A., J Appl Phys, Vol 30, p 1913, 1959.

71. Tomas, G., Elektronnaya Mikroskopiya Metallov (Electron Microscopy of Metals), Foreign Literature Publishing House, 1963.

72. Amelinks, S., Metody Pryamogo Nablyudeniya Dislokatsiy (Methods of Direct Observation of Dislocations), Mir Publishing House, 1968.

73. Khaydenraykh, P., Osnovy Prosvechivayushchey Mikroskopii (Bases of Transmission Microscopy), Mir Publishing House, 1966.

74. Schmid, E. and Boas, V., Plastichnost' Metallov (Plasticity of Metals), GONTI (State United Scientific and Technical Publishing House), 1938.

75. Maddin, R. and Chen, N.K., Uspekhi Fiziki Metallov, Vol 2, Metallurgizdat, 1958.

76. Kaşan, A.S., FMM, Vol 17, No 6, p 917, 1964.

77. Rovinskiy, B.M. and Rybakova, L.M., Izv AN SSSR, Seriya Fizicheskaya (Bulletin of the USSR Academy of Sciences, Physics Series), No 15, p 1, 1961.

78. Kostyukova, Ye.P., Izv AN SSSR, Seriya Fizicheskaya, No 16, p 13, 1962.

79. Hirsh, P.B., Acta Crystallographica, Vol 5, p 172, 1952.

80. Newton, C.J. and Vacher, H.C., J Res National Bur Standards, Vol 65C, p 1, 1961.

81. Epshteyn, G.N., Kaybyshev, O.A., and Kazachkov, I.V., Zavodskaya Laboratoriya, No 5, p 566, 1969.

82. Kaybyshev, O.A., Epshteyn, G.N., and Kazachkov, I.V., Zavodskaya Laboratoriya, No 12, p 1528, 1967.

83. Groves, G.W. and Kelly, A.T., Phil Mag, Vol 8, p 877, 1963.

84. Cox, J.J. et al, Trans AIME, Vol 49, p 118, 1957.

85. Burret, C. and Massalsky, T., The Structure of Metals, McGraw-Hill Co, New York-London, 1967.

86. Allen, N.P. et al, Proc Roy Soc, Vol 234, p 221, 1956.

87. Fridel', J., Dislokatsii (Dislocations), Mir Publishing House, 1967.

88. Low, J.R. and Guard, R.W., Acta Metallurgica, Vol 7, p 171, 1959.

89. Burke, E.C. and Hibbard, W.R., Trans AIME, Vol 194, p 255, 1952.

90. Revnor, G., Metallovedenive Magniva i Yego Splavov (Metal Research on Magnesium and its Alloys), Metallurgizdat, 1964.

91. Tyson, W., Acta Metallurgica, Vol 15, p 574, 1967.

92. Bastein, P. and Poihtu, P., J Nuclear Materials, Vol 5, p 153, 1962.

93. Price, P.B., J Appl Phys, Vol 32, p 1746, 1961.

94. Stoff, N.S. and Gensamer, M., Trans AIME, Vol 22, p 70, 1963.

95. Churchman, A.T., Proc Roy Soc, A, Vol 226, No 1165, p 216, 1954.

96. Ioshida, S. and Nagata, N., International Conf on the Strength of Metals and Alloys, Tokyo, September 1967.

97. Epshteyn, G.N., Izv Vuzov, Tsvetnaya Metallurgiya (Bulletin of the Higher Educational Institutions, Nonferrous Metallurgy), No 1, p 35, 1971.

98. Serer, A. et al, In the Collection Elektronnaya Mikroskopiya i Prochnost' Kristallov (Metallurgiya Publishing House, p 332, 1966.

99. Ferguson, W.G. et al, J Appl Phys, Vol 38, p 1863, 1967.

100. Epshteyn, G.N. and Kazachkov, I.V., FMM, Vol 29, No 1, p 212, 1970.

101. Verbraak, C.A., Metallkunde, Vol 55, p 723, 1964.

102. Kaybyshev, O.A. et al, FMM, Vol 23, No 2, p 324, 1967.

103. Finkel', V.M. et al, FTT, Vol 8, p 2738, 1966.

104. Hu Hsun and Cline, H.S., Trans MSA, Vol 223, No 2, p 310, 1965.

105. Campbell, I.D. and Maiden, C.J., Phil Mag, Vol 3, p 872, 1958.

106. Leslie, W.C. et al, J Iron and Steel Inst, Vol 200, p 622, 1962.

107. Odinokova, L.I. and Borachev, I.N., Tsvetnyye Metally (Nonferrous Metals), No 2, p 71, 1965.

108. Kaybyshev, O.A., Krayukhin, V.I., Umanskiy, Ya.S., and Epshteyn, G.N., FMM, Vol 4, No 3, p 353, 1967.

109. Kaybyshev, O.A., Umanskiy, Ya.S., and Epshteyn, G.N., DAN SSSR, Vol 177, No 3, p 562, 1967.

110. Klien, M. and Edington, J., Phil Mag, Vol 14, p 21, 1966.

111. Kaybyshev, O.A., FMM, Vol 26, No 2, p 900, 1968.

112. Borachev, I.N. and Filinov, N.A., Izv Vuzov, Tsvetnaya Metallurgiya, No 5, p 118, 1966.

113. Rosenhain, W. and Hanfrey, J.C.W., J Iron and Steel Inst, Vol 87, p 219, 1913.

114. Pearson, C.E., J Inst Metals, Vol 54, p 111, 1934.

115. Gindin, I.A. and Staroduvob, Ya.D., FTT, Vol 1, p 1642, 1959.

116. Toar, H.W. and Ripling, E.J., Trans AIME, Vol 206, p 930, 1956.

117. Mises, R.Z., Angew Math Mech, Vol 8, p 161, 1928.

118. Taylor, G.I., J Inst Metals, Vol 62, p 307, 1938.

119. Chalmers, B., Proc Roy Soc, A, Vol 162, p 120, 1937.

120. Ke, T.S., Phys Rev, Vol 20, p 274, 1949.

121. Voloshina, L.A. and Rozenberg, V.M., FMM, Vol 12, p 118, 1961.

122. Rhines, F.N. et al, Trans ASM, Vol 48, p 919, 1956.

123. Crussard, C. and Fridel, I., Symposium on Creep and Fracture in Metals at High Temperatures, London, p 243, 1956.

124. Leak, G.M., Proc Phys Soc, Vol 78, p 1520, 1961.

125. Fazon, C.M. et al, Trans AIME, Vol 200, p 919, 1954.

126. Hauser, F.E. et al, Trans ASM, Vol 47, p 102, 1955.

127. Yoshinaga, H., Kinzoku Butsuri, Vol 10, No 3, p 91, 1964.

128. McLean, D., J Inst Metals, Vol 81, p 133, 1952-1953.

129. Rachinger, W.A., J Inst Metals, Vol 81, p 415, 1952-1953.

130. Klassen-Neklyudova, M.V., Mekhanicheskoye Dvoynikovaniye Kristallov (Mechanical Twinning of Crystals), USSR Academy of Sciences Publishing House, 1960.

131. Schmid, E. and Boas, W., Plasticity of Crystals, London, 1950.

132. Cottrell, A.H. and Bilby, B.A., Phil Mag, Vol 42, No 329, p 573, 1951.

133. Venables, I.A., Phil Mag, Vol 6, p 379, 1961.

134. Venables, I.A., Deformation Twinning, New York-London, p 77, 1964.

135. Williams, D.F., Metal Sci J, Vol 1, p 94, May 1967.

136. Leslie, W.C. et al, High-Strength Materials, Berkely Inst Metals Conf. 2-nd Proc, p 382, Jun 1964.

137. Peissker, E., Z Metallkunde, Vol 56, No 3, p 155, 1965.

138. Cullity, B.D., Elements of X-Ray Diffraction, Massachusetts, 1956.

139. Wertlake, D.G., Deformation Twinning, New York-London, p 29, 1964.

140. Reed-Hill, R.E., Trans AIME, Vol 218, p 554, 1960.

141. Couling, S.L. et al, Trans ASM, Vol 51, p 94, 1959.

142. Gahn, R.W., Deformation Twinning Mat Soc Conf, New York, Vol 25, p 3, 1969.

143. Price, P.B., Proc Roy Soc, A, Vol 260, p 251, 1961.

144. Chuchman, T.N., In the Collection Prochnost' i Nadezhnost' Metallov i Splavov, Ch 2 (Strength and Reliability of Metals and Alloys, Part 2), Leningrad House of Scientific and Technical Propaganda, 1965.

145. Davidenkov, N.N. et al, ZhETF (Journal of Experimental and Theoretical Physics), No 3, p 350, 1933.

146. Mil'man, Yu.V. et al, Mekhanizm Plasticheskoy Deformatsii Metallov (Mechanism of Plastic Deformation of Metals), Naukova Dumka Publishing House, Vol 2, p 29, 1965.

147. Bochvar, A.A. et al, DAN SSSR, Vol 164, No 2, p 305.

148. Dieter, I., Strengthening Mechanism in Solids, Amer Soc Metals, Cleveland, p 279, 1962.

149. Marcinkowski, M.I. and Lipstitt, H.A., Acta Metallurgica, Vol 10, p 95, 1962.

150. Reid, C.N. et al, Deformation Twinning, New York-London, p 386, 1964.

151. Takenchi, T.J., Phys Soc Japan, Vol 21, p 2616, 1966.

152. Bunshah, R.F., Deformation Twinning, New York-London, p 320, 1964.

153. Joshinaga, H. and Morinchi, R., Trans JIM, Vol 3, p 220, 1962.

154. Kuhlman-Wilsdorf, D., Z Metallkunde, Vol 5, p 324, 1962.

155. Reed-Hill, R.E., Deformation Twinning, New York-London, p 205, 1964.

156. Iohari, O. and Thomas, G., Acta Metallurgica, Vol 12, p 1153, 1964.

157. Severdenko, V.P. et al, In the Collection Plastichnost' i Obrabotka Metallov Davleniyem (Plasticity and Pressure Treatment of Metals), Minsk, Nauka i Tekhnika Publishing House, p 85, 1966.

158. Severdenko, V.P. et al, DAN BSSR (Reports of the Byelorussian SSR Academy of Sciences), Vol 10, No 12, p 941, 1966.

159. Odinokova, L.P., Izv AN SSSR, Metally, No 1, p 134, 1967.

160. Ul'yanov, B.A. and Moskalenko, V.A., Metalloved i Term Obrabotka Metallov (Metal Research and Heat Treatment of Metals), No 10, p 48, 1966.

161. Bykov, L.A. et al, Zavodskaya Laboratoriya, No 9, p 1137, 1966.

162. Startsev, V.I. et al, Kristallografiya, No 4, p 425, 1956.

163. Rosenthal, D. and Woolsey, C.G.J., Welding J, Vol 31, No 10, p 475, 1952.

164. Reed-Hill, R.E. and Buchman, E.R., Acta Metallurgica, Vol 11, No 1, p 73, 1963.

165. Knizhnik, G.S., Izv Vuzov, Chernaya Metallurgiya, No 1, p 154, 1966.

166. Rosi, F.D. et al, J Metals, Sect 2, Vol 5, No 2, Supplement, 1953.

167. Reed-Hill, R.E., Acta Metallurgica, Vol 5, p 728, 1957.

168. Williams, D.N. and Ennelsheimer, D.S., J Inst Met, Vol 81, p 553, 1952-1953.

169. McHargue, C.I. et al, Trans AIME, Vol 197, p 1199, 1953.

170. Suzuki, H. and Barrett, C.S., Acta Metallurgica, Vol 6, p 156, 1958.

171. Blewitt, T.H. et al, J Appl Phys, Vol 28, p 651, 1957.

172. Zukas, E.G. et al, Trans AIME, Vol 227, p 746, 1963.

173. Holder, R.L. and Thomas, G., Acta Met, Vol 11, p 994, 1963.

174. DeAngelies, R.I. and Cohen, I., Deformation Twinning, New York-London, p 430, 1964.

175. Smith, C.S. and Fowler, C.M., Response of Metals to High-Velocity Deformation, New York-London, p 309, 1961.

176. Smith, C.S., Trans Met Soc AIME, Vol 214, p 574, 1958.

177. Dieter, G.E., Response of Metals to High-Velocity Deformation, New York-London, p 409, 1961.

178. Pogrebnoy, E.N. and Zhak, K.M., FMM, Vol 23, No 1, p 106, 1967.

179. Grechnyy, Ya.V. et al, In the Collection Fizicheskaya Priroda Plasticheskoy Deformatsii (Physical Nature of Plastic Deformation), Naukova Dumka Publishing House, No 13, p 111, 1966.

180. Worthington, P.E. and Smith, E., Acta Metallurgica, Vol 14, p 35, 1966.

181. Tardif, H.P. et al, Response of Metals to High Velocity Deformation, New York-London, p 389, 1961.

182. Shekhtman, V.Sh et al, FMM, Vol 31, No 1, p 48, 1971.

183. Davidenkov, N.N., ZhTF (Journal of Technical Physics), Vol 28, p 2502, 1958.

184. Zukas, E.G. and Fowler, C.M., Response of Metals to High-Velocity Deformation, New York-London, p 343, 1961.

185. Bowden, H.G. and Kelly, P.M., Acta Metallurgica, Vol 15, p 105, 1967.

186. Mehl, R.F., J Iron and Steel Inst, Vol 159, p 113, 1948.

187. Hirsh, P. et al, Elektronnaya Mikroskopiya Tonkikh Plenok. (Electron Microscopy of Thin Films), Mir Publishing House, 1968.

188. Dieter, G.E., In the Collection Mekhanizm Uprochneniya Tverdykh Tel (Mechanism of Strengthening Solids), Metallurgiya Publishing House, p 245, 1965.

189. Appleton, A.S. et al, Trans AIME, Vol 221, p 90, 1961.

190. LaRocca, E.W. and Burkhardt, K.A., Bull Amer Phys Soc, Vol 2, p 263, 1957.

191. DeCarli, P.S. and Jamieson, I.C., Science, Vol 133, p 1821, 1961.

192. Bancroff, D. et al, J Appl Phys, Vol 27, pp 291-298, 1956.

193. Katz, S. et al, J Appl Phys, Vol 30, p 568, 1959.

194. Duff, R.E. and Minshall, F.S., Phys Rev, Vol 108, p 1207, 1957.

195. Graham, R.A. et al, J Appl Phys, Vol 36, p 3955, 1965.

196. Holtzman, A. and Cowan, G.R., Response of Metals to High-Velocity Deformation, New York-London, p 447, 1961.

197. Parker, E.R. and Smith, E.A., Trans AIME, Vol 156, p 142, 1944.

198. Minshall, F.S., Response of Metals to High-Velocity Deformation, New York-London, p 249, 1961.

199. Fowler, C.M., Response of Metals to High-Velocity Deformation, New York-London, p 275, 1961.

200. Curran, D.R., J Appl Phys, Vol 32, p 1181, 1961.

201. Rosi, F.D., Trans AIME, Vol 200, p 1009, 1954.

202. Andrade, E.N. and Aboav, D.A., Proc Roy Soc, A, Vol 240, p 304, 1957.

203. Davis, K.G., Can J Phys, Vol 41, p 1963, 1963.

204. Schweinghofer, A. and Marsh, W., Phys Stat Solidi, Vol 25, No 2, p 91, 1968.

205. Adams, M.A. and Cottrell, A.H., Phil Mag, Vol 40, p 1187, 1955.

206. Andrade, E.N. and Henderson, C., Phil Trans, Vol 244, p 177, 1951.

207. Boas, W. and Schmid, E., Z Phys, Vol 61, p 767, 1930.

208. Lücke, K. et al, Z Metallkunde, Vol 46, p 792, 1955.

209. Lindholm, U.S. and Jeakley, L.M., J Mech Phys Solids, Vol 13, p 41, 1965.

210. Hirsh, P. et al, In the Collection Struktura i Mekhanicheskiye Svoystva Metallov (Structure and Mechanical Properties of Metals), Metallurgiya Publishing House, p 42, 1967.

211. Seger, A. et al, Phil Mag, Vol 2, p 323, 1957.

212. Sokolov, L.D., FMM, Vol 26, No 1, p 170, 1968.

?. Seger, A. et al, Z Physik, Vol 155, p 247, 1959.

214. Rol' Dislokatsiy v Uprochnenii i Razrushenii Metallov (The Role of Dislocations in the Strengthening and Fracture of Metals), Edited by V.S. Ivanova, Nauka Publishing House, p 64, 1965.

215. Sokolov, L.D., Soprotivleniye Metallov Plasticheskoy Deformatsii (Resistance of Metals to Plastic Deformation), Metallurgizdat, 1963.

216. Rao, N.R. et al, J Mater, Vol 1, No 1, p 241, 1966.

217. Kolesnikov, G.N. et al, ZhTF, Vol 19, No 1, p 62, 1949.

218. Wessel, E.T., J Metals, No 9, p 930, 1957.

219. Pond, R.B. and Glass, C.M., Response of Metals to High-Velocity Deformation, New York-London, p 145, 1961.

220. Yada, H. and Mimura, H., J Phys Soc Japan, Vol 24, p 1269, 1968.

221. Yamada, I. and Koterazawa, K., J Soc Mater Sci Japan, Vol 15, No 153, p 425, 1966.

2?. Sakui, S. et al, J Japan Inst Met, Vol 31, No 2, p 204, 1967.

223. Pearson, I. and Hayes, G., Amer Soc Tool and Manuf Eng Techn Paper, (SP62-07), 1962.

224. Cottrell, A.H., In the Collection Struktura i Mekhanicheskiye Svoystva Metallov (Structure and Mechanical Properties of Metals), p 210, 1967.

225. Govorkov, V.G. et al, FTT, Vol 6, No 4, p 1039, 1964.

226. Imai, S. and Hashiwara, U., J Japan Inst Metals, Vol 29, No 1, p 7, 1965.

227. Baron, H.G., Sheet Metal Ind, Vol 39, No 420, p 257, 1962.

228. Bowden, H.G. and Kelly, P.M., Metal Sci J, p 75, May 1967.

229. Doran, D.G. and Linde, R.K., Solid State Physics, Vol 19, p 229, 1966.

230. Gubkin, S.I., Teoriya Plasticheskoy Deformatsii Metallov (Theory of the Plastic Deformation of Metals), Metallurgizdat, 1947.

231. Baron, H.G., J Iron and Steel Inst, Vol 182, p 354, 1956.

232. Davidenkov, N.N. and Chuchman, T.N., FMM, Vol 9, No 5, p 740, 1960.

233. MacDonald, R.I. et al, Amer Soc for Testing Mater Proc, Vol 56, p 704, 1956.

234. Ohmori, M. and Yochinaga, Y., J Japan Inst Metals, Vol 31, No 4, p 433, 1967.

235. Cottrell, A.H. and Stokes, R.I., Proc Roy Soc, A, Vol 233, No 1192, p 17, 1956.

236. Dorn, I.E. et al, Trans AIME, Vol 188, p 205, 1950.

237. McLean, D., Mekhanicheskiye Svoystva Metallov (Mechanical Properties of Metals), Metallurgiya Publishing House, 1965.

238. Basinski, Z.S., Phil Mag, Vol 4, No 40, p 393, 1959.

239. Basinski, Z.S. and Christian, I., Austrialian J Phys, Vol 13, p 229, 190.

240. Conrad, H. and Schoeck, G., Acta Metallurgica, Vol 8, p 791, 1960.

241. Haasen, P., Phil Mag, Vol 3, p 384, 1958.

242. Pearson, J., In the Collection Vysokoskorostnoye Deformirovaniye Metallov (High-Velocity Deformation of Metals), Mashinostroyeniye Publishing House, p 29, 1966.

243. Nishiyama, U. and Tanimura, S., Trans Japan Soc Mech Eng, Vol 33, No 246, p 182, 1967.

244. Krasikov, K.I. et al, Fiz-Khim Mekhanika Materialov, Vol 3, No 6, p 702, 1967.

245. Krivoglaz, M.A. and Ryaboshapka, K.P., FMM, Vol 16, No 5, p 64, 1963.

246. Krivoglaz, M.A. and Ryaboshapka, K.P., FMM, Vol 15, No 1, p 18, 1963.

247. Kaybyshev, O.A., Kryukhin, V.I., Umanskiy, Ya.S., and Enshteyn, G.N., Tekhnologiya Legkikh Splavov (Technology of Light Alloys), Scientific and Technical Bulletin of the All-Union Institute of Light Alloys, No 3, p 9, 1967.

248. Nodler, H.L. and Thomas, G., Acta Met, Vol 12, p 227, 1964.

249. Jewett, R. and Jacobs, A., Electron Microscopy, Tokyo, Vol 1, p 317, 1966.

250. Rose, M.F. and Berger, L.T., Phil Mag, Vol 17, No 150, p 1121, 1968.

251. Low, J.R., Iron and its Dilute Solid Solution, p 217, 1963.

252. Kressel, H. and Brown, N., Acta Metallurgica, Vol 14, p 1860, 1966.

253. Gilbert, A. et al, Phil Mag, Vol 12, No 117, p 649, 1965.

254. Kendall, D.P. and Davidson, T.F., Paper Amer Soc Mech Engr, M-WA/Met-8, p 1, 1965.

255. Bogachev, I.N. et al, FMM, Vol 21, No 3, p 472, 1966.

256. Form, G.W. and Baldwin, W.M., Trans Amer Soc Metals, Vol 48, p 474, 1956.

257. Yochinaga, Y. and Ohmori, M., J Japan Inst Metals, Vol 30, No 8, p 795, 1966.

258. Gscheider, K.A. et al, Metallurgy at High Pressures and Temperatures, Gordon Breach, New York, 1963.

259. Al'tshuller, L.V. et al, ZhETF, Vol 52, No 2, 400, 1967.

260. Johnson, P.C. et al, J Appl Phys, Vol 33, p 557, 1962.

261. Kaufman, L. et al, Progress in Very High Pressure Research, New York, p 90, 1961.

262. Clendon, R.L. and Drickamer, H.G., J Phys Chem Solids, Vol 25, p 85, 1964.

263. Takahashi, K. and Basett, W.A., Science, Vol 145, p 483, 1964.

264. Voronov, F.F. and Vereshchagin, L.F., FMM, Vol 11, p 443, 1961.

265. Jameson, I.C. and Lawson, H., J Appl Phys, Vol 33, p 780, 1962.

266. Ho-Kwang Mao et al, J Appl Phys, Vol 38, p 272, 1967.

267. Belchan, A. and Drickamer, H.G., Rev Sci Inst, Vol 32, pp 308-318, 1961.

268. Larson, D.B., J Appl Phys, Vol 38, p 1541, 1967.

269. Drickamer, H., Phys and Chem of High Pressure, New York-London, p 122, 1963.

270. Beardmore, P. et al, Trans AIME, Vol 230, p 4, 1964.

271. Mirkin, L.I., DAN SSSR, Vol 186, No 2, p 305, 1969.

272. Fisher, E.S. and Renken, C.J., Phys Rev, No A482, p 135, 1964.

273. Atroshchenko, L.S. et al, FMM, Vol 19, p 797, 1965.

274. Sukhovarov, V.F. et al, Fiz-Khim Mekhanika Materialov, Vol 3, No 2, p 210, 1967.

-END-

11 734
CSO: R-14244-N